Modeling, Simulation and Experimental Studies on Downdraft Biomass Gasifier

THESIS

Submitted in partial fulfillment
of the requirements for the degree of
DOCTOR OF PHILOSOPHY

By

PRATIK N SHETH

Under the supervision of
Prof. B. V. Babu

BIRLA INSTITUTE OF TECHNOLOGY AND SCIENCE
PILANI (RAJASTHAN) INDIA
2009

Modeling, Simulation and Experimental Studies on Downdraft Biomass Gasifier

THESIS

Submitted in partial fulfillment

of the requirements for the degree of

DOCTOR OF PHILOSOPHY

By

PRATIK N SHETH

Under the supervision of

Prof. B. V. Babu

BIRLA INSTITUTE OF TECHNOLOGY AND SCIENCE

PILANI (RAJASTHAN) INDIA

2009

BIRLA INSTITUTE OF TECHNOLOGY AND SCIENCE

PILANI, RAJASTHAN, INDIA

CERTIFICATE

This is to certify that the thesis entitled **"Modeling, Simulation and Experimental Studies on Downdraft Biomass Gasifier"** and submitted by **Pratik N Sheth** ID. No. **2003PHXF009P** for the award of PhD Degree of the Institute embodies the original work done by him under my supervision.

Signature in full of the Supervisor _____

Name in capital block letters **Prof B V BABU**

Designation Dean-Educational Hardware Division
Professor-Chemical Engineering Group
BITS-Pilani, India

Date:

DEDICATED

TO

MY PARENTS

ACKNOWLEDGEMENTS

It gives me a deep sense of gratitude and an immense pleasure to sincerely thank my guide **Prof (Dr) B V Babu**, Dean-Educational Hardware Division and Professor-Chemical Engineering Group for his constant encouragement, constructive & valuable suggestions, and moral support throughout the period of this research work. It has been a privilege for me to work under his valuable guidance.

I thank the members of Doctoral Advisory Committee, Dr Arvind Kumar Sharma, Assistant Professor and Dr Suresh Gupta, Assistant Professor, Chemical Engineering Group for their support and suggestions to carry out this work effectively.

My sincere thanks go to Prof L K Maheshwari, Vice-Chancellor, BITS Pilani for giving me the opportunity to carry out the PhD. work in BITS. I am thankful to Prof V S Rao, Director (Hyderabad Campus), Prof K E Raman, Director (Goa Campus), Prof G Raghurama, Deputy Director (Academics), Prof R K Mittal, Deputy Director (Administration) and Prof Ravi Prakash, Dean-Research and Consultancy Division for providing the necessary facility and infrastructure to carry out this work.

I extend my special thanks to Prof B R Natarajan, Dr Bharat Bhushan Gulyani, Dr Harekrishna Mohanta, Mr Ashish M Gujrathi, Mr Sushil Kumar, Mr Nikhil Prakash, Mrs. Smita Raghuvanshi, Mr Amit Jain, Mr Dipaloy Dutta and other members of chemical engineering group for their valuable advice and moral support throughout the work. My special thanks and appreciation to Mr Gaurav Mishra for his help, suggestions, and encouragement throughout the work. My sincere thanks to Prof R P Vaid and Prof H S Moondra for their affectionate enquiries about the status of my PhD work. I also thank Dr Ashish Chaurasia, Dr S D Manjare, Dr Rakesh Angira and Dr Basudeb Munshi for providing me all the support during start of PhD work. I would also like to thank Mr Nitin Maheshwari, Mr Amit Gaikwad, Ms Sonny Sachdeva, and Mr Nipen Shah for their help in getting scientific literature and support throughout the work. I also thank to Dr Sajeev Chandran and Dr Girish Bhinde for providing help in understanding the operation of gas chromatograph. I also thank my other colleagues having created a good environment to carry out the work.

Besides all the faculty members and other friends, I would also take this opportunity to thank Mr Ashok Saini and Mr Jeevan Verma for their extended help in carrying out the experimental work. Thanks are also due to Mr Babu Lal Saini and Shri Jangvirji for their cooperation during my PhD work. I also wish to acknowledge Mr V N Sharma, Mr Suresh Saini, Mr Mahendra Saini, Mr Vikas Sharma and Mr Kamlesh Pipalwa for their help and cooperation. I express my thanks to Dr K S Sangwan and his office personnels, Shri Banwarilalji, Shri Ramavtar Soni, Shri Banwarilal Saini, and Shri Madanji for their help in the fabrication of biomass gasifier and getting biomass ready in appropriate sizes.

I also would like to acknowledge the ‘‘K K Birla Academy, India” for providing financial support through a sponsored research project.

This work could not have been completed without the moral support I got from my loving parents – Shri Nitinchandra D Sheth and Smt Anjana N Sheth and my loving wife – Hiral. Their unconditional love, constant encouragement, moral support and their immense confidence in me made this work possible.

Last but not the least, I pray and thank to ALMIGHTY GOD for showering HIS blessings and giving me an inner strength and patience.

PRATIK N SHETH

ABSTRACT

Energy is the most important requirement to sustain life for any living organism in the biosphere. The finite energy resources will not only get consumed in the near future due to tremendous demand, but their impacts on health and air pollution are also of serious concerns. The effects on global and environmental air quality of pollutants released into the atmosphere from fossil fuels provide strong arguments for the substitution of fossil fuels with renewable energy resources. Bioenergy is essentially renewable or carbon neutral. Carbon dioxide released during the combustion of fuels derived from biomass circulates through the biosphere, and is reabsorbed in equivalent stores of biomass through photosynthesis.

The direct combustion of biomass leads to an incomplete and inconsistent combustion, which may produce organic particulate matter, carbon monoxide and other organic gases. Hence, biomass is required to be upgraded in terms of more easily handled fuels, namely gases, liquids, and charcoal using various technologies such as pyrolysis, gasification, carbonization, digestion, fermentation, etc. Although fermentation or digestion as a process is successfully used to produce ethanol, it is feedstock limited, time consuming and results in low yields. Biomass gasification is one of the promising routes amongst the renewable energy options of future energy. Gasification is a process of conversion of solid biomass into combustible gas, known as producer gas, by partial oxidation.

In the present study, a combined transient single particle and fuel bed model is formulated by incorporating the mass, momentum and energy balances. The developed model takes into account of the kinetics of chemical reactions, heat and mass transfer between solid and gaseous phases and transport of volatiles produced. To validate the combined transport and kinetic model, experimental study is carried out using wood waste as biomass to generate producer gas using an Imbert downdraft gasifier. The developed model is also validated with the experimental data reported in the literature. To compare the results predicted by combined transport and kinetic model with those of the equilibrium model, the latter model is also formulated in the present study. The present study also comprises of the estimation of kinetic parameters for the proposed kinetic scheme based on two competing reactions using differential evolution, a nontraditional evolutionary algorithm.

The developed model is divided into three parts according to three different zones developed: (1) pyrolysis, (2) oxidation, and (3) reduction. Pyrolysis bed is modeled as a stack of particles in one dimension. To consider the temperature gradient both in the bed and also inside the single particles, the entire bed is divided into two subsystems, i.e., gas phase inside the bed and the individual particles. The volatile products generated in the pyrolysis zone flow downwards and enter into the oxidation zone where a part of the volatiles gets oxidized. In the reduction zone, the gaseous mixture passes through the hot porous charcoal bed resting above the grate. The endothermic reactions are carried out where the degree of temperature drop depends upon the extents of reactions. The extent

of reaction in turn depends upon the reactivity of char, which is represented by Char Reactivity Factor (*CRF*) value. In the present model on reduction zone, the exponential variation of *CRF* along the reduction zone of downdraft biomass gasifier is proposed. To study the kinetics of pyrolysis, the kinetic scheme based on the two competing reactions is proposed. Four different models are proposed based on different possible relations of the activity of biomass with the normalized conversion. The corresponding kinetic parameters of the above models are estimated by minimizing the square of the error between the reported non isothermal experimental data of thermogravimetry of hazelnut shell and the simulated model predicted values of residual weight fraction using population based search algorithm as optimization routines (Differential Evolution and Logarithmic Differential Evolution algorithms).

To validate the simulation results, experimental study is carried out covering a wide range of operating parameters. Dalbergia sisoo, generally known as sesame wood or rose wood is used as a biomass material in the present gasification studies. An Imbert downdraft biomass gasifier is used to carry out the gasification experiments with the waste generated while making furniture using sesame wood in the carpentry section of the institute's workshop. The producer gas generated in the downdraft gasifier is sampled using airtight syringes and analyzed using a gas chromatograph (NUCON 5765) with thermal conductivity detector (TCD). The effects of air flow rate and moisture content on biomass consumption rate and quality of the producer gas generated are studied by performing experiments covering a wide range of operating conditions. The performance of the biomass gasifier system is evaluated in terms of equivalence ratio, producer gas composition, calorific value of the producer gas, gas production rate, zone temperatures and cold gas efficiency. Material balance is carried out to examine the reliability of the results generated. The experimental results are compared with those reported in the literature.

The experiments are carried out covering a wide range of air flow rates and biomass moisture content. The rate of biomass consumption is found to vary from 1.0 to 3.63 kg/h for an air flow rate ranging from 1.85 to 3.39 m^3/h. The moisture content is varied from 0.0254 to 0.164 wt fraction on wet basis. The biomass consumption rate is found decreasing for increase in the moisture content and also for decrease in the air flow rate. The optimum operating conditions are found by varying the equivalence ratio, which gives producer gas with the highest calorific value. The calorific value, pyrolysis zone temperature and the oxidation zone temperature are maximum at an equivalence ratio of 0.205. The proposed combined transport and kinetic model is validated with the experimental data reported in the literature and those obtained in the present experimental study. The model predicted composition of producer gas matches very well with the experimental data reported in the literature and those obtained in the present study in comparison to the equilibrium model predictions. The proposed kinetic model represents the thermogravimetry results better than the apparent decomposition rate expression.

Keywords: *Bioenergy; Biomass; Dalbergia Sisoo; Pyrolysis; Combustion; Gasification; Downdraft gasifier; Producer gas; Reaction kinetics; Mathematical model; Kinetic parameter estimation; Char reactivity factor; Equivalence ratio; Simulation; Differential Evolution.*

TABLE OF CONTENTS

LIST OF FIGURES

LIST OF PLATES

LIST OF TABLES

NOMENCLATURE

a	Specific surface area (m^2/m^3)
A	Area (m^2)
A_1, A_2, A_3	Frequency factors, (1/s)
b	Geometry factor (slab=1, cylinder=2, sphere=3)
B	Virgin biomass
C_1	$(Char)_1$
C_2	$(Char)_2$
C_B	Concentration of B (kg/m^3)
C_{G1}	Concentration of G_1 (kg/m^3)
C_{C1}	Concentration of C_1 (kg/m^3)
C_{G2}	Concentration of G_2 (kg/m^3)
C_{C2}	Concentration of C_2 (kg/m^3)
$C_{p,i}$	Specific heat of any species i (kJ/kg K)
D	Diffusivity (m^2/s).
E	Activation Energy (kJ/mol)
f_p	Fraction of Pyrolysis (-)
G_1	$(Gases\ and\ volatiles)_1$
G_2	$(Gases\ and\ volatiles)_2$
h	Convective heat transfer coefficient (W/m^2 K)
HR	Heating Rate (K/s)
H_f^0	Heat of formation of any species i (J/mol)
k_i	Rate Constant (reaction i)
k	Thermal conductivity (W/mk)
k_{mG1}	Mass transfer coefficient of $(gases\ and\ volatiles)_1$ across the film (m/s)
K	Equilibrium constant (-)

L_n	Normalized length (-)
L_{in}	Initial normalized length at which 85 % of the total composition change
m	Kmol of oxygen per kmol of wood (-)
$\dot{m}$	Rate of mass transfer from particle to the gas phase(kg/m^2 s)
MW	Molecular weight (kg/kmol)
n_i	Molar rate of species *i* (mol/m^{3}h)
n_1, n_2, n_3	Orders of reactions
Q	Heat of reaction number, m^3/kg
p	Gas pressure (N/m^2)
r	Radial distance (m)
r_i	Rate of reaction *i*
R	Radius for cylinder and sphere; half thickness for slab (m)
R_c	Universal gas constant (J/mol)
t	Time (s)
T	Temperature (K)
v	Gas velocity (m/sec)
w	Kmol of water per kmol of wood (-)
W	Residual weight fraction (-)
x	Coefficients of constituents of the producer gas
z	Dimensionless conversion (-)

Greek Symbols

α	Thermal diffusivity (m^2/s)
β	Deactivation rate constant (-)
ΔH	Heat of reaction (J/kg)
$\Delta\tau$	Axial grid length (m)
Δx	Radial grid distance (m)
ε	Porosity (-)
η	Reaction progress variable
θ	Normalized temperature (-)
μ	Viscosity (kg/m s)

ρ	Density (kg/m^3)
σ	Stefan Boltzmann constant (W/m^{2}K^4)
τ	Dimensionless time (-)
Φ	Equivalence ratio
ϕ	Permeability (m^2)

Subscripts

0	Initial condition
bed	Bed
calc	Calculated
eff	Effective
exp	Experimental
g	Gas phase
i	Any species N_2, CO_2, CO, CH_4, H_2O, H_2, tar
o	Optimum
p	Of particle

Abbreviations

CRF	Char reactivity factor
DE	Differential evolution
FC	Fixed carbon
GC	Gas chromatography
HHV	Higher heating value
LIDE	Logarithmic initialization with simple DE
LDE	Logarithmic DE
MC	Moisture content
MW	Molecular weight
NP	Number of population
TDMA	Tri-diagonal matrix algorithm
VM	Volatile matter

CHAPTER – 1

INTRODUCTION

1.1 Energy Resources

All living organisms rely on an external source of energy to grow and to reproduce. The principal perpetual energy resources are solar energy, wind power and bioenergy, all of which ultimately depend on an extra-terrestrial source, namely the Sun. Most of the world's energy resources are from the sun's rays hitting earth – some of that energy has been preserved as fossil energy, some is directly or indirectly usable, e.g., via wind, hydro or wave power, some is interspersed in the biomass as a chemical energy via photosynthesis process. Prehistoric plants stored the Sun's energy in their leaves, branches and roots, and when they died and eventually converted to fossil fuel, the energy from which releases upon burning. Sun warms our atmosphere and the resulting heated air tends to rise and forms winds and waves. These energy resources may be categorized into two groups: finite (e.g. minerals) and perpetual (renewable resources such as solar, wind, tidal, etc.). Whilst each major energy source has its own characteristics, applications, advantages and disadvantages, the fundamental distinction among these is between those that are finite and those that are, on any human scale, effectively perpetual or everlasting. The finite resources comprise a number of organically-based substances such as coal, crude oil, oil shale, natural bitumen & extra-

heavy oil, and natural gas, together with the metallic elements such as uranium and thorium. And the principal perpetual resources are solar energy, wind energy and bioenergy. Other perpetual resources are various forms of marine energy – tidal energy, wave energy and ocean thermal energy conversion (OTEC). There are other energy resource such as peat and geothermal energy, which are, to some extent intermediate in nature, with both finite and perpetual elements in their make-up. Bioenergy is arguably the one truly renewable energy resource, in that each new crop or harvest represents a partial renewal of its resource base, which itself is subject to constant depletion through its use as a fuel or feedstock. All the remaining perpetual energy resources are available on a continuing, although varying basis, are not depleted by the utilization of their energy content, and are therefore not subject to renewal (Caillé, 2007).

The world's primary energy consumption is about 400 EJ/year as per estimates reported by Fridleifsson (2003) and is mostly provided by fossil fuels (80%). The effects on global and environmental air quality of pollutants released into the atmosphere from fossil fuels provide strong arguments for the substitution of these fossil fuels with renewable energy resources. Clean, domestic and renewable energy is commonly accepted as the key for future life. The renewable sources collectively provide 14% of the primary energy, in the form of traditional biomass (10%), large (>10 MW capacity) hydropower stations (2%), and the "new renewable sources" (2%). Nuclear energy constitutes 6% of the total energy. The World Energy Council (London, UK) expects the world primary energy consumption to have grown by 50–275% in 2050, depending on different scenarios. The renewable energy sources are expected to provide 20–40% of the primary energy in 2050 and 30–80% in 2100. The technical potential of the renewable

sources is estimated at 7600 EJ/year, and thus certainly sufficiently large to meet future world energy requirements (Fridleifsson, 2003).

1.2 Bioenergy

Biomass is a term used to describe all biologically produced matter and it is the name given to all earth's living matter. It is a general term for material derived from growing plants or from animal manure (which is effectively a processed form of plant material). The chemical energy contained in the biomass is derived from solar energy using the process of photosynthesis. This is the process by which plants take in carbon dioxide and water from their surroundings and, using the energy from sunlight, convert them into sugars, starches, cellulose, lignin, etc. which make up vegetable matter loosely termed carbohydrates (and shown for simplicity as $[CH_2O]$) and oxygen.

$$CO_2 + 2H_2O \longrightarrow [CH_2O] + H_2O + O_2 \qquad (1.1)$$

Biomass energy is derived from the plant sources, such as wood from natural forests, waste from agricultural and forestry processes and industrial, human or animal wastes. The stored energy in the plants and animals (that eat the plants and other animals), or the waste that they produce is called biomass energy or bioenergy. It is a natural process that the entire biomass ultimately decomposes to its molecules with the release of heat. And the combustion of biomass imitates the natural process. So the energy obtained from biomass is a form of renewable energy and it does not add carbon dioxide to the environment in contrast to the fossil fuels (Twidell, 1998). Of all the renewable energy sources, biomass is unique in that it effectively stores solar energy inherently.

Furthermore, it is the only renewable energy source of carbon and is able to convert into convenient solid, liquid and gaseous fuels (Demirbas, 2001).

Bioenergy is essentially renewable or carbon neutral. Carbon dioxide released during the energy conversion of biomass (such as combustion, gasification, pyrolysis, anaerobic digestion or fermentation) circulates through the biosphere, and is reabsorbed in equivalent stores of biomass through photosynthesis. Fig. 1.1 shows the combustion of wood and thereby CO_2 generation. It also depicts that net CO_2 generation is zero as new biomass could be developed photosynthetically for the growth of which this CO_2 is utilized. Biomass energy is a renewable and unique form of solar energy. Of the massive 178,000 x 10^{12} Watts of solar energy that falls on the Earth's surface, some 0.02% or around 40 x 10^{12} Watts is captured by plants via photosynthesis and is available as biomass energy. This translates into the production of some 220 billion 'dry' tonnes of biomass per year, which as an energy source represents some ten times the world's total current energy use. Currently some 15 percent of the planet's energy requirements are met from biomass, mainly for cooking and heating in developing countries. Biomass is also supplied as a fuel in a growing number of large scale, modern biomass energy plants in industrialized countries. By comparison, the world population consumes around 10 EJ/year of energy in the form of food, which of course is a biomass energy resource in itself (Stucley et al., 2004).

1.3 Biomass Conversion Technologies

Conventionally biomass was used in a similar way to fossil fuels, by burning it at a constant rate in a boiler furnace to heat water for producing steam. This steam passes

through the multiple blades of turbine, spinning the shaft. The turbine shaft drives an electricity generator which produces an alternating current for local use or to supply the national grid. Wood is still a predominant fuel in many non-OPEC (Organization of the Petroleum Exporting Countries), tropical, developing countries and it will continue to be used for many years. It competes well with fossil fuels, because it is renewable, and with soft energies (solar and wind), on account of its energy storage capability. It is being used in the domestic sector (for cooking and water heating), commercial sector (water heating) and industrial sector (for water heating and process heat); and also in rural industries, such as brick kilns, potteries etc. (Demirbas, 2000). In nature, biomass is not concentrated, and so, the use of naturally occurring biomass requires transportation, which increases the cost and reduces the net energy production. Biomass has a low bulk density, which makes transportation and handling more difficult and costly. Apart from transportation, incomplete combustion of biomass generates a concern among the environmentalists, as it may produce organic particulate matter, carbon monoxide and other organic gases. If high temperature combustion is used, oxides of nitrogen would be produced. The health impact of air pollution is a significant problem in developing countries, where fuel wood is burnt inefficiently in open fires for domestic cooking and space heating (Demirbas, 2001). The conversion technologies for utilizing biomass can be separated into three basic categories: direct combustion processes, thermochemical processes and biochemical processes. Direct combustion deals mainly with primary fuels, e.g., the form in which it is available in nature or after some form of processing (drying, sizing, briquetting, etc.). In the other two processes the primary fuel is converted into a secondary fuel (solid, gas and/or liquid form) by processes such as pyrolysis, gasification,

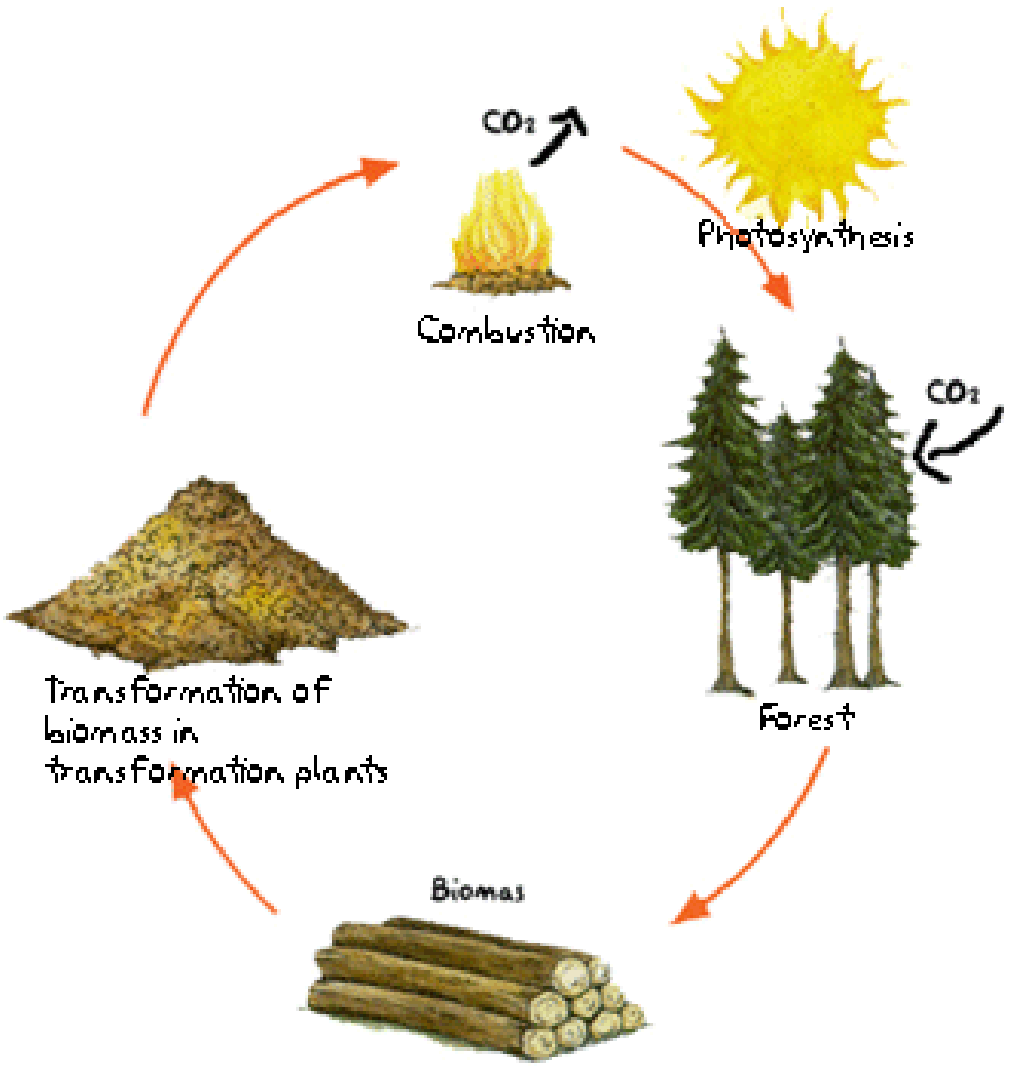

Fig. 1.1 Lifecycle of forest biomass
(Source: http://www.paisatge.net/SapreRenovables/ENG/eSproj.htm)

carbonization, digestion, fermentation, etc. The secondary fuels obtained from the conversion process can be used directly for various end-use activities for further processing (Babu, 2008a).

Direct combustion is used to convert biomass into a useful energy. The heat and/or steam produced during this process are/is used to provide process heat for domestic cooking and industrial processes or to generate electricity. Biomass-fired power plants have been installed in a number of countries in Asia. The main disadvantage of this process is the incomplete and inconsistent combustion of solid fuel. Direct combustion of biomass materials usually results in smoke and ash pollution unless special filtering equipment is used. Biochemical processes make use of the biochemistry of the raw materials, and the action of microbial organisms, to produce gaseous and liquid fuels like biogas, ethanol and methanol. Digestion is the biochemical conversion of organic material to biogas, which mainly consists of methane and carbon dioxide. Anaerobic reactors are generally used for the production of biogas from manure and crop residues. Fermentation is another example of biochemical process in which micro-organisms (usually yeast) break down sugars to produce ethanol. Ethanol is produced from certain biomass materials that contain sugars, starch or cellulose. It is regarded as an important potential alternative source of liquid fuels for the transport sector. Ethanol blended with conventional fuel like petrol or diesel is widely used now-a-days. Although fermentation is successfully used to produce ethanol, it is feedstock limited, time consuming and low yield process. There has been an increasing interest for thermochemical conversion of biomass and urban wastes for upgrading the energy in terms of more easily handled fuels, namely gases, liquids, and charcoal in the past decade. The thermochemical conversion

of biomass (pyrolysis, gasification, combustion) is one of the promising routes amongst the renewable energy options of future energy. It is renewable form with many ecological advantages (Babu, 2008a).

Thermochemical conversion processes can be subdivided into gasification, pyrolysis, and direct liquefaction. Gasification is a process of conversion of solid carbonaceous fuel into combustible gas by partial combustion. The resulting gas, known as producer gas, is a mixture of carbon monoxide, hydrogen, methane, carbon dioxide and nitrogen. The producer gas is more versatile than the original solid biomass. It is burnt to produce process heat and steam or used in gas turbines to produce electricity. In both pyrolysis and liquefaction processes, feed stock organic compounds are converted into liquid products. In case of liquefaction, the macromolecules of feedstock compounds are decomposed into fragments of light molecules in the presence of a suitable catalyst. These unstable and highly reactive fragments repolymerize into heavy compounds having high molecular weights. Whereas in pyrolysis, catalyst is not used and light decomposed fragments are converted to oily compounds through homogeneous reactions in the gas phase. The difference in operating conditions for liquefaction and pyrolysis are shown in Table-1.1 (Demirbas, 2000). In the pyrolysis process, biomass gets decomposed by heat in the absence of oxygen, which results in the production of various organic gaseous products, charcoal and tar. The study of pyrolysis is attracting researchers, as it is not only an independent process, but also a first step in the gasification or the combustion process (Babu and Chaurasia, 2003a-b).

Table 1.1 Comparison of liquefaction and pyrolysis

Process	**Temperature (°C)**	**Pressure (MPa)**	**Drying**
Liquefaction	525-600	5-20	Unnecessary
Pyrolysis	650-800	0.1-0.5	Necessary

1.4 Biomass Gasification

Gasification was discovered independently in both France and England in 1798. By 1850 the technology had been developed to the point that it was possible to light much of London with the manufactured gas or "town gas" from coal (Singer, 1958). During World War I and II wood gas generators, called Gasogene, were used when fuel supply was not enough but after a few years, a more reliable and cheap technology was developed that runs on petroleum; and gradually the use of gas produced by biomass was reduced. Due to the energy crisis in most of the countries and towering cost of petroleum, biomass based gasification process is again in focus in the recent past (Reed and Das, 1988). Gasification of biomass is one of the majorly used processes to increase the efficiency of energy harnessing from biomass. Gasification is a process that takes carbonaceous materials as its feed, such as coal, petroleum, or biomass, and converts into carbon monoxide and hydrogen. The raw material reacts with a controlled amount of oxygen and/or steam at high temperatures (Reed and Das, 1988). It is also a very efficient method for extracting energy from many different types of organic materials, and also has applications as a clean waste disposal technique. Moreover the usage of producer gas is potentially more efficient than direct combustion of the original fuel because it can be combusted at higher temperatures. The typical composition of hydrogen in producer gas varies from 5-25% depending upon moisture content of the fuel. After separation and purification, it can be utilized in fuel cell and biomass gasification process can be considered as a one of the prominent process for biohyrogen production (Babu, 2008b). There are mainly two techniques available for gasification of biomass, viz., fixed bed mode and fluidized bed mode (Bhave, 2001). The three main configurations of fixed bed

gasifiers include Updraft, Downdraft, and Crossdraft mode of operations. In the updraft gasifiers, biomass moves down vertically and comes in contact with an upward moving product gas stream counter-currently. The updraft gasifier is easy to build and operate but product gas is very dirty with high amount of tar. It also has a high thermal efficiency as gases from the combustion zone passes upwards through incoming fuel, which preheat it (Bridgwater, 2002). In the downdraft gasifier biomass moves slowly downwards and air is introduced cocurrently and reacts at a throat that supports the gasifying biomass. They are cheap and easy to make. A relatively clean gas is produced with low tar and usually with high carbon conversion. In the cross draft gasifier, air is introduced on one side of the gasifier and the gas outlet is on the opposite side. Normally an air inlet nozzle is extended to the center of the combustion zone. The main advantages of the crossdraft gasifiers are: (1) its rapid response to change in load, (2) its simple construction and (3) its lightweight. Cross draft gasifiers are best suited for clean fuel like charcoal (Reed and Das, 1988). Out of different configuration of reactors for biomass gasification, a survey of gasifier manufacturers have reported that 75% of gasifiers offered commercially were downdraft, 20% were fluid beds [including circulation fluid beds], 2.5% were updraft, and 2.5% were of other types (Bridgwater, 2002).

Fig.1.2 is a schematic diagram of the down draft biomass gasifier. The nozzle and constricted hearth downdraft gasifier is sometimes called an “Imbert” gasifier, named after its entrepreneurial inventor, Jacques Imbert (Reed and Das, 1988). It may be divided into four distinct zones: (1) Drying/Preheating zone (2) Pyrolysis/Devolatilization zone (3) Combustion zone and (4) Reduction/Gasification zone. The description of these four zones is given in the subsequent sections.

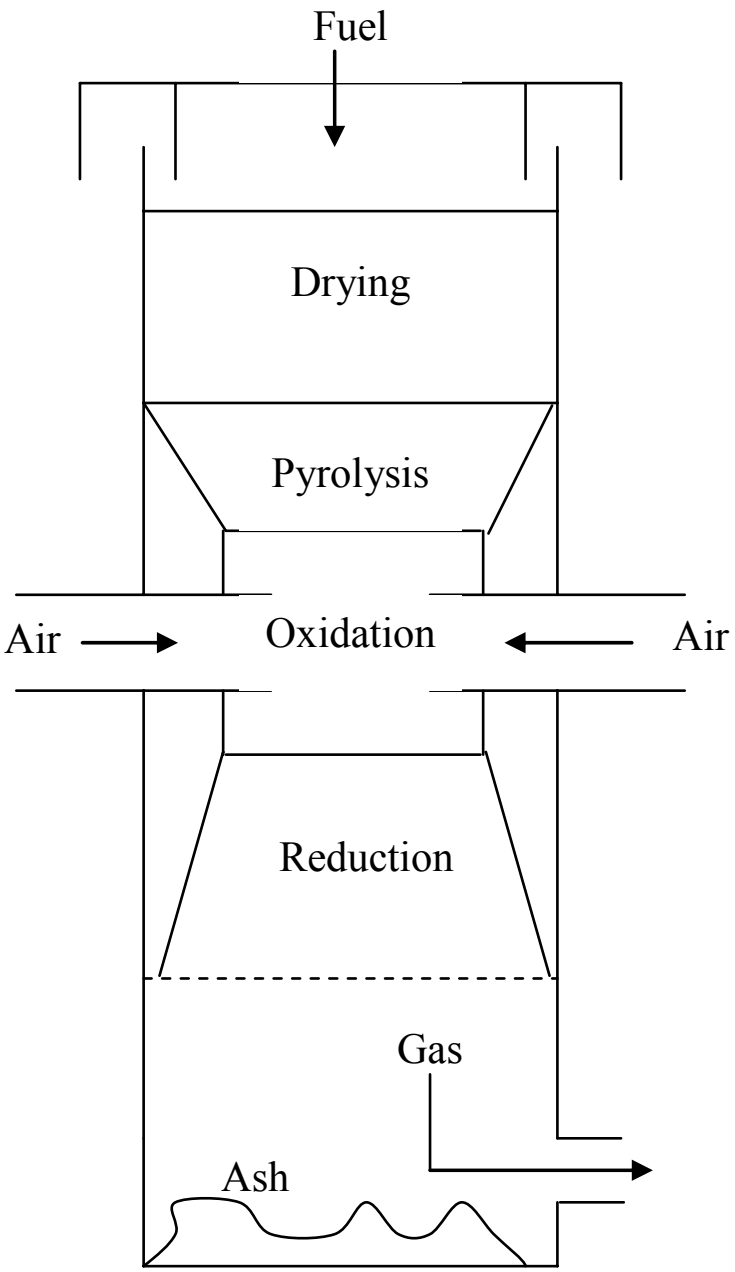

Fig.1.2 Schematic diagram of an Imbert downdraft biomass gasifier

1.4.1 Drying

The first zone in which the feed comes in contact in biomass gasifier is the drying zone. Basically drying is a mass transfer operation resulting in the removal of water moisture by evaporation from a solid or semi-solid. To achieve this, there must be a source of heat, and a sink of the vapor thus produced. This process should ideally take place at a temperature of around 160ºC using waste heat from the conversion process. In the drying zone, feed descend into the gasifier and moisture is removed using the heat generated in the zones below by evaporation. The water vapor flows downward in the gasifier. Part of it may be reduced to hydrogen in the reduction zone and the rest will end up as moisture in the gas. The rate of drying depends on the surface area of the fuel, the temperature difference between the feed and the hot gases, the re-circulation velocity, relative humidity of these gases, and the internal diffusivity of moisture within the fuel (Dogru et al., 2002). In this zone, no chemical reaction takes place and only the water removal is carried out.

1.4.2 Pyrolysis

The pyrolysis of biomass is a promising route for the production of solid (charcoal), liquid (tar and other organics such as acetic acid, acetone and methanol) and gaseous products (H_2, CO_2, CO). These products are of interest as they are possible alternate sources of energy. Pyrolysis is a process by which a biomass feedstock is thermally degraded in the absence of oxygen/air. The basic phenomena that take place during pyrolysis are: (1) heat transfer from a heat source, leading to an increase in temperature inside the fuel; (2) initiation of pyrolysis reactions due to this increased temperature, leading to the release of volatiles and the formation of char; (3) outflow of volatiles,

resulting in heat transfer between the hot volatiles and cooler unpyrolysed fuel; (4) condensation of some of the volatiles in the cooler parts of the fuel to produce tar; and (5) autocatalytic secondary pyrolysis reactions due to these interactions (Babu, 2008a; Babu and Chaurasia, 2004a-d; Chaurasia and Babu, 2004). Pyrolysis can also be used as an independent process for the production of useful energy (fuels) and/or chemicals. The overall process of pyrolysis can be classified into primary and secondary stages. When a solid particle of biomass is heated in an inert atmosphere the following phenomena occur. Heat is first transferred to the particle surface by radiation and/or convection and then to the inside of the particle. The temperature inside the particle increases, causing (1) removal of moisture that is present in the biomass particle, (2) the pyrolysis reactions to occur. The heat changes due to the chemical reactions, and phase changes contribute to a temperature gradient as a function of time, which is nonlinear. Volatiles and gaseous products flow through the pores of the particle and participate in the heat transfer process. The pyrolysis reactions proceed with a rate depending upon the local temperature. During the pyrolysis process, the pores of the solid are enlarged, and the solid particle merely becomes more porous because the biomass converts into gases (Curtis and Miller, 1988). According to Anthony and Howard (1976), the enlarged pores of the pyrolyzing solid offer many reaction sites to the volatile and gaseous products of pyrolysis and favor their interaction with the hot solid. Inside the pyrolyzing particle, heat is transmitted by the following mechanisms: (a) conduction inside the solid particle; (b) convection inside the particle pores; and (c) convection and radiation from the surface of the pellet.

Depending upon the operating conditions, the pyrolysis process can be divided into three subclasses: conventional pyrolysis (carbonization), fast pyrolysis, and flash

pyrolysis. The ranges of the main operating parameters for pyrolysis processes are given in Table-1.2. Conventional pyrolysis is defined as the pyrolysis that occurs under a slow heating rate. This condition permits the production of solid, liquid, and gaseous pyrolysis products in significant portions. The first stage of biomass decomposition occurs between 395 and 475 K and is called pre-pyrolysis. During this stage, some internal rearrangement such as water elimination, bond breakage, appearance of free radicals, and formation of carbonyl, carboxyl, and hydroperoxide groups takes place (Shafizadeh, 1982). The second stage of solid decomposition corresponds to the main pyrolysis process. It proceeds with a high rate and leads to the formation of the pyrolysis products. During the third stage, the char decomposes at a very slow rate and carbon-rich residual solid forms. If the objective is to the produce mainly liquid and/or gaseous products, a fast pyrolysis is recommended. The achievement of fast heating rates requires high operating temperatures, very short contact times, and very fine particles. Flash pyrolysis differs strongly from that of conventional pyrolysis, which is performed slowly with relatively massive pieces of wood. Flash pyrolysis gives mostly gaseous products due to high heating rate and very small particle size (Demirbas, 2002). Hydropyrolysis (pyrolysis in a hydrogen atmosphere) is also considered to have a potential application in the conversion of biomass to liquids enriched in hydrocarbons (Barth, 1999). Most biomass materials are chemically and physically heterogeneous, and their components have different reactivities and yield different products. Biomass is mainly composed of three constituents which are hemicellulose, cellulose, and lignin. It also contains minor amounts of extractives. Each component of biomass pyrolyzes at different rates and by different mechanisms and pathways.

Table 1.2 Ranges of main operating parameters for pyrolysis processes

Parameters	**Conventional Pyrolysis**	**Fast Pyrolysis**	**Flash Pyrolysis**
Pyrolysis Temperature (K)	550-950	850-1250	1050-1300
Heating rate (K/s)	0.1-1.0	10-200	>1000
Particle size (mm)	5-50	<1	<0.2
Solid residence time (s)	450-550	0.5 -10	<0.5

It is believed that as reaction progresses the carbon becomes less reactive and forms stable chemical structures, and consequently the activation energy increases as the conversion level of biomass increases. Cellulose and hemicellulose decompose over a very narrow temperature range as compared to lignin. The rate and extent of degradation of each of these components depend on the process parameters such as reactor type, temperature, particle size, heating rates and pressure (Bridgwater, 1999). The hemicellulose breaks down first, at a temperature of 470 to 530 K, and cellulose follows in the temperature range 510 to 620 K, with lignin being the last component to pyrolyze at temperatures of 550 to 770 K (Demirbas, 1999).

1.4.3 Combustion

In the oxidation or combustion zone, biomass along with the volatile products of pyrolysis are oxidized resulting in a rapid rise in temperature up to 1200°C due to highly exothermic reactions. The heat generated is used to drive the drying and pyrolysis of the fuel and the gasification reactions. The oxidation reactions of volatiles are very rapid and the oxygen is consumed before it can diffuse to the surface of the char. Therefore, no combustion of solid char can take place. Oxidation of the condensable organic fraction to form lower molecular weight products is important in reducing the amount of tar produced by a gasifier (Dogru et al., 2002). Biomass combustion is more complex than either pyrolysis or gasification since the biomass must first pyrolysed, then be partially combusted (gasified) before it is fully combusted. However, the overall global reaction of biomass oxidation can be represented by Eq. (1.2) (Reed and Das, 1988).

$$CH_{1.4}O_{0.6} + 1.05O_2 + 3.95N_2 \longrightarrow CO_2 + 0.7H_2O + 3.95N_2 \qquad (1.2)$$

where $CH_{1.4}O_{0.6}$ is an average formula for woody biomass.

1.4.4 Reduction

The gaseous mixture leaving the combustion zone mainly containing carbon dioxide, water vapor, inert nitrogen, and some amount of low molecular weight hydrocarbons such as methane, ethane, ethylene etc., passes over the hot charcoal in the reduction zone, which is often referred as gasification zone. The principal reaction in the reduction zone is that of carbon dioxide with hot carbon to produce carbon monoxide. This is an endothermic process. It is referred to as the 'Boudouard' reaction (Eq. (1.3)).

$$C + CO_2 \longrightarrow 2CO \qquad \Delta H = 1{,}72{,}600 \text{ J/mol} \qquad (1.3)$$

Another important reaction occurs between water vapor and carbon resulting in the formation of carbon monoxide and hydrogen as given by Eq. (1.4).

$$C + H_2O \longrightarrow CO + H_2 \qquad \Delta H = 1{,}31{,}400 \text{ J/mol} \qquad (1.4)$$

Reaction (1.4) is called the water gas reaction. This is also an endothermic reaction and takes place between 600°C and 950°C. As the reactions (1.3) and (1.4) are endothermic, gas stream loses heat and the temperature drops in the reduction zone progressively. If excess water is present in the reduction zone the so-called water shift reaction can also takes place (Reaction (1.5)).

$$CO + H_2O \longrightarrow CO_2 + H_2 \qquad \Delta H = -41{,}200 \text{ J/mol} \qquad (1.5)$$

This is an exothermic reaction and is undesirable as it reduces the calorific value of gas. So the excess moisture in the fuel is to be avoided. Most of the hydrogen that is produced in the reduction zone remains free. However, a portion of it can combine with carbon to form small amounts (about 3 to 5%) of methane as given by reaction (1.6).

$$C + 2H_2 \longrightarrow CH_4 \qquad \Delta H = -75{,}000 \text{ J/mol} \qquad (1.6)$$

The gaseous mixture leaving the biomass gasifier mainly contains carbon monoxide, hydrogen, carbon dioxide, nitrogen and water vapor. It may also contain some amount of hydrocarbons such as CH_4, C_2H_2 and C_2H_6, the amount of each may depend upon the configuration of the gasifier. Producer gas is also loaded with dust, tar and water vapor.

1.5 Modeling of Biomass Gasification

In view of the considerable interest in the gasification process worldwide, it is necessary to model and predict the performance of the gasifier, *a priori*. Modeling of biomass gasification implies the representation of chemical and physical phenomena constituting drying, pyrolysis, combustion, and reduction in the mathematical form. In other words, whole process is to be represented as the system of equations which taken together can provide valuable quantitative information about the process. Downdraft biomass gasification models can be categorized into two groups: (1) Equilibrium models and (2) Combined transport and kinetic models. The equilibrium model assumes that all the reactions are in thermodynamic equilibrium in biomass gasifier. Many researchers (Chern et al., 1991; Zainal et al., 2001; Mathieu and Dubuisson, 2002 and Altafini et al., 2003; Melgar et al., 2007; Sharma, 2008) have developed and/or modified the equilibrium models for biomass gasification. Chern et al. (1991) developed a basic model based on thermodynamic equilibrium of the C-H-O-inert system and mass and energy balances, and applied to the air-blown downdraft gasification of wood. Zainal et al. (2001) formulated the equilibrium model and represented the gasification process as a single reaction. The elemental balances and the equilibrium ratio between the species are used to find the composition of producer gas. Zainal et al. (2001) incorporated enthalpy

balance of the reactions involved and found the effect of temperature of reaction on the calorific value of gases. The effects of initial moisture content in wood and the temperature in gasification zone on the calorific value of gas have been investigated. In addition to wood, the predictions are also made for peddy husk, paper and municipal waste. Mathieu and Dubuisson (2002) used ASPEN PLUS process simulator to study the performance of biomass gasifier. Altafini et al. (2003) also used an equilibrium model based on minimization of Gibb's free energy to predict the fuel gas compositions. Sensitivity study for the effects of sawdust moisture content at certain reaction temperatures on gasification characteristics has been studied in their work (Altafini et al., 2003). Melgar et al. (2007) discussed the combined effect of various parameters related to chemical equilibrium and the thermodynamic equilibrium of global reaction, predicting the final composition of the producer gas as well as its reaction temperature. Most comprehensive equilibrium model for the down draft biomass gasifier is developed by Sharma (2008). He modified the basic equilibrium model by incorporating the stoichiometric equilibrium approach for all the possible reactions (water gas shift reaction, steam reforming reaction, Boudouard reaction, water gas primary reaction and methanation reaction).

Kinetics-free, equilibrium models can predict the exit gas composition, given the solid composition and the equilibrium temperature, but they cannot be used for reactor design (Di Blasi, 2000). An equilibrium model can not predict the concentration or temperature profiles across the gasifier axis and hence results generated using an equilibrium model would give the same final composition for different lengths of reduction zone of biomass gasifier. Di Blasi (2000) developed a one-dimensional

unsteady model for biomass gasification in a stratified concurrent (downdraft) reactor. Heat and mass transfer across the bed are coupled with moisture evaporation, biomass pyrolysis, char combustion and gasification, gas-phase combustion and thermal cracking of tars. Wurzenberger et al. (2002) developed a model for crosscurrent moving bed furnace of biomass. A combined transient single particle and fuel bed model is formulated by incorporating the mass, momentum and energy balances. However, for an Imbert downdraft biomass gasifier, a complete model including pyrolysis, combustion and reduction has not yet been reported in the literature. Taking into account of the importance of downdraft biomass gasifier and its varied applications, it is essential to have a complete model for such configuration. The present study is an attempt to meet this objective.

1.6 Objectives

Thus, the following objectives of the present study are formulated based on the background on this subject till date:

1. Understanding of physical aspects of pyrolysis and reduction in the modeling of biomass gasification.
2. Improvement of the existing models by considering reaction kinetics of gasification and including secondary reactions of pyrolysis for fixed bed biomass gasifier.
3. Obtaining data by conducting experiments on gasifier and also from the literature sources.

4. Validating the proposed models with the actual experimental data obtained from the above sources.

The above mentioned objectives are achieved by initially carrying out an exhaustive literature survey for modeling and simulation of biomass gasification which is given in Chapter-2. The improvement in the existing mathematical models for fixed-bed biomass gasification is proposed in Chapter-3. It also includes simulation methodology for the proposed model for the downdraft biomass gasifier. To obtain the data on gasifier for model validation, experiments are carried out and the details of experimental setup and its procedures are elaborated in Chapter-4. The obtained experimental data are discussed and analyzed in detail in Chapter-5. It also includes the validation of proposed mathematical model with the obtained experimental data and the data available in the literature. Chapter-6 deals with the summary of the work and important conclusions drawn from the present study.

CHAPTER – 2

LITERATURE REVIEW

Various studies reported in literature on theoretical and experimental investigations of downdraft fixed bed biomass gasifier are discussed in detail in section 2.1 and 2.2 respectively below.

2.1 Theoretical Studies on Biomass Gasification

Theoretical studies on downdraft fixed bed biomass gasification include the modeling and simulation of various zones such as drying, pyrolysis, combustion and reduction of the biomass gasifier. Pyrolysis, thermal degradation of biomass in the absence of oxygen/air, is carried out independently also for the production of useful energy (fuels) and/or chemicals. It is necessary to understand the kinetics of pyrolysis in order to design a suitable biomass gasifier. In order to prepare the comprehensive model of biomass gasifier, it is important to incorporate models describing the kinetics and the governing mechanisms of pyrolysis. Various studies reported in the literature describing the modeling of pyrolysis are discussed in section 2.1.1. Downdraft biomass gasification models can be categorized into two groups: (1) Equilibrium models and (2) Combined transport and kinetic models. The equilibrium model assumes that all the reactions are in thermodynamic equilibrium in biomass gasifier. Various equilibrium models and

combined transport and kinetic models reported in the literature on downdraft biomass gasification are discussed in section 2.1.2 and section 2.1.3 respectively.

2.1.1 Modeling of Pyrolysis

Shafizadeh and Chin (1977) suggested the pyrolysis mechanism as shown in Fig. 2.1. According to this mechanism wood gets pyrolysed into gas, tar and char as per three parallel reactions (reaction 1, 2, and 3), called primary reactions. The tar gets decomposed into two parallel reactions (reaction 4 and 5), called secondary reactions. Numerous products are formed during pyrolysis and they were lumped together as three different products to simplify the analysis.

Thurner and Mann (1981) applied a kinetic scheme of wood pyrolysis established by Shafizadeh and Chin (1977) for the pyrolysis of oak saw dust. Thurner and Mann (1981) designed the experiments to accomplish the removal of the tar from the reaction zone as it gets formed. However, secondary reactions are essentially occurring in the pyrolysis zone of the biomass gasifier. Thus, secondary reactions were not included in their kinetic model. Each primary reaction was assumed as first-order reaction. The activation energies for these reactions were found to be 88.6, 112.7, and 106.5 kJ/mol, respectively, and their frequency factors were reported as 8.61×10^5, 2.47×10^8, and 4.43×10^7 min^{-1}. The developed model was validated with the experimental data.

Shafizadeh (1982) studied the pyrolysis of cellulose and developed a kinetic model based on a two-step mechanism. Active cellulose formed as a first step, which subsequently decomposes by two competitive first-order reactions, one yielding volatile anhydrosugars and the other yielding char and a gaseous fraction (Fig. 2.2).

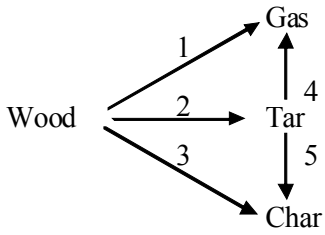

Fig. 2.1 Mechanism of wood pyrolysis

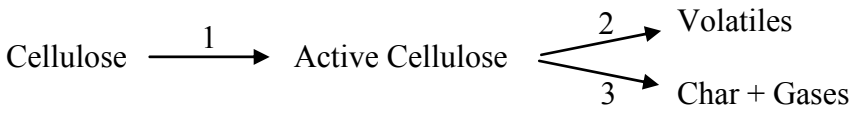

Fig.2.2 Pyrolysis mechanism for cellulose

Shafizadeh (1982) performed experimental study to validate the model and concluded that the pyrolysis at lower temperatures (below 300 °C) favored the production of char, water, CO_2 and CO, whereas heating at higher temperatures (300-500°C) favored the production of tar, containing anhydrosugars, oligosaccharides and some pyran and furan dehydration products.

Pyle and Zaror (1984) assumed a single-step mechanism, and the pyrolysis to follow the first-order kinetics. Kinetic model based on first-order kinetics was combined with heat transfer model to predict the rate of pyrolysis of a single biomass particle. It was assumed that the heat transfer to solid from the surrounding gas and furnace is by a combination of convection and radiation. It was shown that the relative importance of internal and external heat transfer and of intrinsic pyrolysis kinetics could be determined from the Biot number (*Bi*). The developed model was validated with the measurements of decomposition and temperature distribution in pyrolysing wood cylinders with diameters ranging from 0.6 to 2.2 cm in the temperature ranging from 380 to 500°C.

Koufopanos et al. (1989; 1991) studied the kinetics of pyrolysis of fine particles (less than 1 mm size) and also of coarse particles (2 – 20 mm) of lignocellulosic materials with a view of providing simple kinetic models. Koufopanos et al. (1989) represented the overall rate of pyrolysis as a sum of the corresponding rates of all the main biomass components (cellulose, hemicellulose and lignin). The kinetic models of each of these biomass components were simulated to predict the pyrolysis rate and the final weight loss for various heating conditions (5 K/min to 80 K/min). It was concluded that the pyrolysis of fine particles of lignocellulosic particles was kinetically controlled and the possible effects of heat and mass transfer phenomena were drastically reduced. Koufopanos et al.

(1991) presented the model coupling heat transport with chemical kinetics for a pyrolysis of a single particle. The kinetics of pyrolysis was simulated by a scheme consisting of two parallel reactions and a third reaction for the secondary interactions between charcoal and volatiles [Fig. (2.3)]. It was reported that as the particle size and pyrolysis temperature increase, the relative importance of heat transfer and secondary reactions also increase.

Bilbao et al. (1993) studied the thermal decomposition of large particles of pine wood. A mathematical model was used to calculate the temperature and solid conversion at different points in the particle undergoing pyrolysis. The kinetic model was combined with heat balance in the solid particle to predict the rate of volatile release and charcoal formation. The kinetic equations of the thermal decomposition were of the first-order. It was assumed that there was no mass transfer resistance inside the solid particle. A good agreement with experimental results was obtained for particles up to 4 cm in diameter. It was found that for larger particles the mass transfer resistance inside the solid and the existence of secondary reactions might acquire an appreciable importance. The influence of moisture content on the thermal decomposition of wood was analyzed by Bilbao et al. (1996). A mathematical model was used to calculate the temperature at different points in the biomass particle and the average total solid conversion. The experimental results were compared with those calculated by the model and an acceptable agreement was achieved.

The coupled effects of particle size and the external heating conditions on cellulose pyrolysis were investigated by means of a model accounting for all main transport phenomena, variable thermophysical properties, and secondary reaction processes by Di Blasi (1996a). She developed a pyrolysis model for cellulose pyrolysis

through a semi-global, multi-step scheme based on lumping of different products into three groups: gas, tar and char, which is shown in Fig. 2.4. The dynamics of particle conversion are predicted and the final product distribution was favorably compared with the experimental measurements. Di Blasi (1996a) constructed a map in terms of particle size as a function of reactor temperature, to identify the transition from a kinetically controlled conversion (thermally thin regime) to a heat transferred controlled conversion (thermally thick regime). In her subsequent study, Di Blasi (1996b) coupled the chemical process with an unsteady, one-dimensional, variable property model of transport phenomena including heat convection, conduction and radiation, volatile tar and gas transport by diffusion and convection and momentum transfer. It was reported that for typical cellulosic material permeabilities, product distribution and process dynamics were not significantly influenced by pressure variations. In another study, Di Blasi (1996c) used a pyrolysis scheme introduced by Shafizadeh and Chin (1977). The virgin material was considered as a homogeneous single species, wood and reaction products were grouped into a few main components such as gas, tar and char. Primary reactions were assumed to be adequately represented as first-order in the mass of pyrolyzable material. She included the effect of particle shrinkage on rate of pyrolysis. Larger tar yields were predicted for shrinking particles because of the lager temperatures at the primary reaction front and the reduced volatile residence times.

Srivastava et al. (1996) used a kinetic scheme developed by Koufopanos et al. (1991). The concentration profiles of pyrolysis of different lignocellulosic materials in the isothermal and non-isothermal conditions were predicted. The ordinary differential

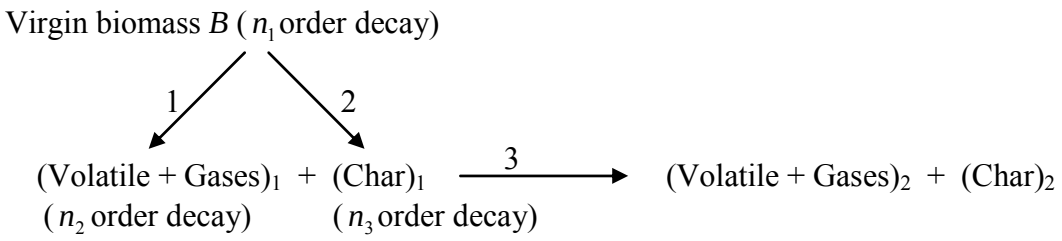

Fig. 2.3 Kinetic scheme of biomass decomposition

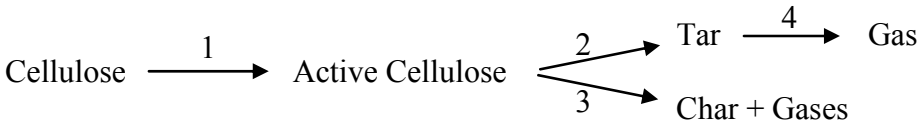

Fig. 2.4 Two-step mechanism of cellulose pyrolysis

equations describing the mass change of the biomass and secondary reactions of products were solved numerically using a fourth-order Runge-Kutta Predictor-Corrector method.

The thermal decomposition of lignocellulosic biomass materials and their major components was discussed by Varhegyi et al. (1997). The kinetic scheme developed by Shafizadeh et al. (1982) was employed in the modeling to predict the weight loss of the biomass sample. Thermogravimetric curves at different temperature heating conditions were evaluated by the method of least squares. Pseudo-first-order models, parallel, successive and competitive reaction schemes and complex reaction networks were employed in the modeling. Thermal decomposition of cellulose at low (2°C min^{-1}) and high (50-80°C min^{-1}) heating rates were studied. Thermal decomposition of cellulose, xylan, lignin and lignocellulosic plant were performed.

Green et al. (1997) developed a decay model based on the first-order kinetics that gives analytical time and temperature dependencies for cellulose, activated cellulose, tar, and total gas. The impact of heating rates and heat transfer upon the pyrolysis of cellulose using slow pyrolysis data obtained by thermogravimetric analysis were also examined.

Di Blasi (1997) performed the parametric study on biomass devolatilization characteristics using the model developed in their previous studies (Di Blasi, 1996a-c). For conversion in thermally thick regime, it was found that variations in the physical properties mainly affect the activity of secondary reactions of tar vapors and the conversion time. It was concluded that the maximum sensitivity was associated with the biomass density and char thermal conductivity.

Demirbas (1998) conducted hazelnut shell pyrolysis under a variety of experimental conditions resulting in the production of char, a tarry material, an aqueous

fraction and gaseous products. The kinetic parameters such as activation energy, rate constant, and order of reaction were found using first-order kinetics. It was found that both the temperature and heating rate strongly affect the pyrolysis products and kinetic parameters. The influence of the main reaction parameters, such as temperature, particle size, catalyst and heating rate, on the yields from pyrolysis had been studied and the results were analyzed. The effect of a catalyst (K_2CO_3) on the yield of pyrolysis was also incorporated.

Rao and Sharma (1998) proposed a model by which pyrolysis rates of biomass materials could be predicted from the species compositions in terms of the basic constituents (cellulose, hemicellulose and lignin) and their individual kinetic parameters. It was assumed that biomass components decomposed by first-order kinetics. The activation energies, frequency factors and reaction orders for cellulose, hemicellulose and lignin were determined on the basis of best-fit criteria between experimental and predicted results. The measured rates of pyrolysis of different biomass species (hazelnut, wood, olive husk and rice husk) agreed well with the literature data.

Liliedahl and Sjöström (1998) developed a theory for deriving the pyrolysis rate of different geometries of biomass particles (single infinite slab, infinite cylinder, sphere, etc.) in a constant temperature furnace. In analogy with the shrinking-core model a pyrolysis propagation front velocity was defined. The velocity was subsequently used in a compartment-model approach for deriving a set of ordinary differential equations for solving the burn-off over time. A comparison of model prediction with the experimental data was reported.

Di Blasi (1998a) presented a transport model for the drying of wooden particles exposed to the convective/radiative heating in an inert environment. She assumed that the moisture transport includes water vapor convection and diffusion, capillary water convection in the pores of the particle, and bound water diffusion in solid wood. In the model, local thermodynamic equilibrium was assumed to exist. Di Blasi (1998b) simulated a lumped parameter kinetic model for two-dimensional porous, anisotropic, variable property biomass sample. The kinetic scheme developed in her earlier study was used (Di Blasi, 1996a). The dynamics of particle degradation were found to be strongly affected by the grain structure of the solid.

Janse et al. (2000) designed a reactor for flash pyrolysis of biomass to maximize the yield of bio-oil, at the expense of the by-products (gas and char). To understand the effect of chemical and physical factors on the yield of bio-oil, the flash pyrolysis of a cylindrical wood particle simulated by solving the governing equations for mass, enthalpy and momentum conservation for the reactant and products. The kinetic scheme developed by Shafizadeh et al. (1982) was employed in the one-dimensional modeling. It was reported that the bio-oil yield was not affected by the particle size (200–1000 mm diameter). The heating of a particle was notably delayed by the outflow of vapors. It was concluded that an extensive description of internal mass transport phenomena in flash-pyrolysis modeling was not necessary, while accurate knowledge of the reaction kinetics and heat transfer parameters was crucial.

Mousqués et al. (2001) developed two models of solid particle pyrolysis which were used to simulate reaction schemes of varying complexity. The one model was for a homogeneous solid particle and another was for heterogeneous biomass particle. The

temperature, composition, velocity and pressure gradients inside the particle were found. Both models were tested with the data from literature concerning wood and Poly Vinyl Chloride (PVC). Experimental kinetic and thermophysical data were obtained to complement the model, and validate it over the operating range.

Bryden et al. (2002) developed a general model of the pyrolysis of a wood slab and validated with experimental data. The model was applied to particle half-thicknesses from 5 μm to 5 cm, temperatures from 800 to 2000 K, and moisture contents from 0% to 30%. Internal temperatures, pyrolysis rates and yields of tar, hydrocarbons and char were presented. Four pyrolysis regimes were identified, depending on external temperature and particle size: thermally thin (kinetically limited), thermally thin (heat transfer limited), thermally thick, and thermal wave regimes. Hagge and Bryden (2002) incorporated the shrinkage of biomass particle in the developed model. It was concluded that the shrinkage has a negligible effect on pyrolysis in the thermally thin (Bi <0.2) and the thermally thick (0.2< Bi <10) pyrolysis regimes. However, in the thermal wave pyrolysis regime (Bi >10), shrinkage affected both the pyrolysis time and the pyrolysis products. It was also found that char shrinkage affected the pyrolysis process in several ways. Due to char shrinkage and higher mass flux of the pyrolysis products, the pyrolysis reaction region thinned, the pyrolysis temperatures increased, the residence time of the gases within the particle reduced, and the char layer got cooled. Bryden and Hagge (2003) included the effect of moisture on the rate of pyrolysis. It was concluded that coupling between moisture content and shrinkage was found to result in longer pyrolysis times than if they were considered separately. Coupling between moisture content and shrinkage increased

tar yield and decreased light hydrocarbon yield compared to considering moisture and shrinkage separately.

Babu and Chaurasia (2002 a-b; 2003 a-b; 2004 a-d) carried out extensive modeling and simulation studies on pyrolysis. The kinetic scheme proposed by Koufopanos et al. (1989, 1991) for the pyrolysis of biomass based on the two-stage model was used by them for validating the experimental data. Babu and Chaurasia (2002a) carried out the pyrolysis study on single solid particle for a wide range of temperature from 303-2700 K and of particle diameter from 0.0005-0.026 m. It was found that upon the increase of particle size, the time required for completion of pyrolysis at a certain pyrolysis temperature and the effect of secondary reactions increased. It was observed that, for particle sizes below 1mm, the process was controlled by the primary pyrolysis reactions and, possibly, by the external heat transfer. For particles greater than 1mm, heat transfer, primary pyrolysis and secondary pyrolysis control the pyrolysis process. Babu and Chaurasia (2003a) estimated the optimum parameters in the pyrolysis of biomass for both nonisothermal and isothermal conditions. The modeling equations were solved numerically using the fourth-order Runge–Kutta fourth-order method over a wide range of heating rates (25–360 K/s) and temperatures (773–1773K). The simulated results were compared with those reported in the literature and found to be in good agreement qualitatively in the range of operating conditions covered. It was found that the final pyrolysis time first decreased at lower values of net heating rate or temperature and then increased at higher values of net heating rate or temperature, providing an optimum value of net heating rate or temperature at which final pyrolysis time was minimum (2003a). The mathematical model to describe the pyrolysis of a single solid

particle of biomass was modified by incorporating the heat transfer equation with the chemical kinetics equations in the subsequent study carried out by Babu and Chaurasia (2003b). The dependence of convective heat transfer coefficient on Reynolds number and Prandtl number was incorporated in the model. A finite difference method using a pure implicit scheme was used for solving the heat transfer equation and the Runge–Kutta fourth-order method for the chemical kinetics equations. The model equation was solved for cylindrical pellets, spheres and slab geometries of equivalent radius ranging from 0.00025 to 0.013 m and temperature ranging from 303 to 1000K. The simulated results obtained using this modified model, were in excellent agreement with the experimental data, much better than the agreement with the earlier models reported by Pyle and Zaror (1984). Babu and Chaurasia (2004a) studied the effect of convective heat transfer and orders of reactions on pyrolysis of biomass particle using the model developed in their previous studies (2003a-b). The wide ranges of temperature (303-2700 K) and pellet diameters (0.0005-0.026 m) were considered. It was found that the pyrolysis was faster for zeroth-order as compared to first-order of reaction 1 (Fig. 2.3), as the rates were independent of initial biomass concentration for zeroth-order. The effects of the parameters such as thermal conductivity, reactor temperature and particle size on product concentrations were analyzed (Chaurasia and Babu, 2003a-b; 2005).

To describe the chemical process of the pyrolysis completely, an unsteady state, one dimensional, variable property model of transport phenomena, including heat convection, conduction and radiation, volatiles and gas transport diffusion and convection and momentum transfer was required. This generalized reference model was developed by Babu and Chaurasia (2004c) in their subsequent study of pyrolysis. A finite difference

pure implicit scheme utilizing a Tri-Diagonal Matrix Algorithm (TDMA) was employed for solving the heat transfer and mass transfer model equations. A Runge–Kutta fourth-order method was used for the chemical kinetics model equations. Simulations were performed considering different geometries of equivalent radius ranging from 0.0001 to 0.017 m and temperatures ranging from 303 to 2800 K. The results obtained using these improved models were in excellent agreement with the experimental data of Pyle and Zaror (1984), much better than the agreement with earlier models reported in the literature (Bamford et al., 1946; Jalan and Srivastava, 1999). The effects of the heat of reaction on the biomass conversion, concentration, and temperature profile in the particle had been analyzed based on the improved model. The variation in temperature profile and concentration profile for exothermic and endothermic pyrolysis reaction was explained by using heat of reaction number (Babu and Chaurasia, 2003c). Effects of the most important thermal and thermodynamic properties (thermal conductivity, heat transfer coefficient, emissivity and heat of reaction number) of the feedstock on the convective-radiant pyrolysis of biomass fuels were also carried out by Babu and Chaurasia (2004a). Sensitivity analysis was conducted to find the most important properties affecting the pyrolysis and found that the highest sensitivity is associated with the emissivity and thermal conductivity of the biomass (Babu and Chaurasia, 2004a). Simulations were carried out for different geometries considering the equivalent radius ranging from 0.0000125 m to 0.011 m, and the temperature ranging from 303 K to 2100 K (Babu and Chaurasia, 2004b). Effects of heating conditions, density of biomass, product yields and conversion on pyrolysis of biomass fuels were studied and found that the yield of $(char)_l$ increases while the yield of (volatile & gases)$_l$ decreased as the particle thickness was

increased. There was no effect of density of biomass on both the primary and secondary reaction products. The conversion time did not depend on density of biomass and was nearly constant for complete conversion. Complete conversion of pyrolysis occured at successively shorter times as the heating rate was increased. The time required for complete conversion of pyrolysis was the highest for the slab geometry and lowest for the sphere geometry of biomass particles (Chaurasia and Babu, 2003b, 2004). The numerical model was used to predict the effects of the dominant design variables such as thermal conductivity, heat transfer coefficient, emissivity, reactor temperature and heat of reaction number (Babu and Chaurasia, 2004b).

The impact of shrinkage on pyrolysis of biomass particles was studied employing a kinetic model coupled with heat transfer model using a practically significant kinetic scheme consisting of physically measurable parameters (Babu and Chaurasia, 2004d). The numerical model was used to examine the impact of shrinkage on particle size, pyrolysis time, product yields, specific heat capacity and Biot number considering the cylindrical geometry. Simulations were carried out for radius ranging from 0.0000125 to 0.05 m, temperature ranging from 303 to 900 K and shrinkage factors ranging from 0.0 to 1.0 (Babu and Chaurasia, 2004d). It was found that the temperature profile of the particle changes due to increased density and decreased distance across the pyrolysis region. The magnitude of the temperature gradient was more for shrinking particle as compared to non-shrinking particle. Shrinkage affected the pyrolysis time in thermally thick regime. Pyrolysis conversion process was fast for shrinking particle as compared to nonshrinking particle (Babu and Chaurasia, 2003d). The modeling and simulation of the above process was coupled with the optimization of a non-linear function using Differential Evolution

to find optimal time of pyrolysis and heating rate under the restriction on concentration of biomass. It served as the input to the coupled ordinary differential equations to find the optimum values of volatiles and char using Runge-Kutta fourth-order method (Babu and Chaurasia, 2003e).

Branca and Di Blasi (2003) developed a kinetic model based on semi-global reaction mechanism as given by Fig. 2.5. Experimental tests were carried out without significant interferences of transport phenomena and for temperatures of 528–708 K. The kinetic constants (activation energies and pre-exponential factors) were estimated by means of analytical solution of the mass conservation equations. It was concluded that three reaction zones exist in pyrolysis: the first (degradation of extractives and the most reactive fractions of hemicellulose), the second (degradation of cellulose and part of lignin and hemicellulose) and the third (lignin and small fractions of cellulose and hemicellulose).

Peters and Bruch (2003) developed a flexible and stable numerical method to predict the thermal decomposition of large wood particles due to drying and pyrolysis. The model was applied to each particle of a packed bed and the entire packed bed process was represented as a sum of individual particle processes. The various processes such as heat-up, drying and pyrolysis were described by a set of one dimensional and transient conservation equations for mass and energy. A comparison between measurements and predictions of drying models yielded satisfactory agreement only for the constant evaporation temperature model and thus, indicated that the drying process was transport limited by heat transfer for large wood particles.

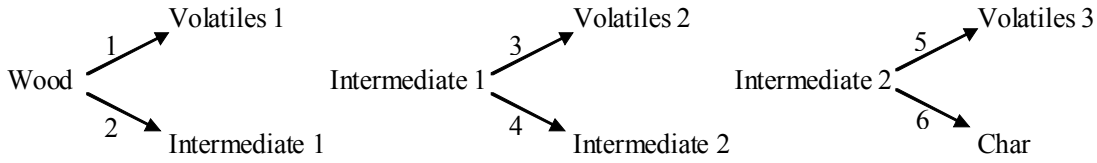

Fig. 2.5 Semi-global reaction mechanism of wood pyrolysis

Galgano and Di Blasi (2004) modeled decomposition of moist wood using the shrinking unreacted-core approximation for a finite rate of reaction and the assumption of a thermally controlled evaporation of moisture across an infinitely thin front at constant temperature. The one-dimensional, quasi-steady (along the char layer) equations were presented which took into account of convective, conductive, and radiative heat transfer and different physical properties for char, dry wood, and moist wood. An acceptable agreement between predicted and measured weight losses for 0.04-m-thick beech wood particles (external radiative heat fluxes between 40 and 80 kW/m^2 and initial moisture contents between 0 and 47 wt% on a dry basis) were found. A parametric analysis indicated that, apart from a linear dependence on moisture content, the characteristic times were especially affected by water evaporation in case of thick samples. It was also found that assuming a coincident front for both wood decomposition and moisture evaporation could be applied with sufficient accuracy only for thick samples with high moisture contents and subjected to severe thermal heating.

Radmanesh et al. (2006) used a three-independent-parallel-reactions scheme to model kinetics of total devolatilization. The composition of condensable vapors (tar and H_2O) and non-condensable gases (H_2, CH_4, CO and CO_2) were found using gas chromatography technique. It was shown that upon an increase of the heating rate, the final total yield of gases increased and those of tar decreased. A kinetic model based on first-order kinetics was proposed and the corresponding parameters were calculated, which could predict the change of the gas yields at different heating rates. The performance of the kinetic models was evaluated with the experimental data available in the literature and also by exposing the biomass to different heating programs.

Shen et al. (2007) proposed a one-dimensional pyrolysis model to examine the influence of heat flux, species and moisture content on the process of thermal decomposition of wet wood. Temperature profiles at different points and solid conversion were calculated and compared with the experimental data. There was good agreement between the experimental and model predicted results.

Song et al. (2007) studied the slow pyrolysis of six types of biomasses available in China by thermogravimetric experiments. Non-linear square fitting method was used to calculate Differential Thermogravimetry data. It was concluded that one-step model with different mechanisms was not representing the biomass pyrolysis exactly. Three-pseudocomponent model was used to simulate the biomass pyrolysis. It was found that the three-pseudocomponent model with *n*-order kinetics was more accurate than the model with first-order kinetics. It was shown that the model with *n*-order kinetics yields the better simulation results, especially with respect to the pyrolysis of the first pseudocomponent (hemicellulose) and the last one (lignin).

Zabaniotou and Damartzis (2007) developed a mathematical model for the pyrolysis of a single solid olive kernel particle and predicted the fast pyrolysis product yields. The kinetic model was coupled with the heat transfer model. The global degradation of biomass was based on the mechanism proposed by Koufopanos et al. (1989, 1991). The analysis was focused on the primary degradation of a small particle. Simulations were carried out for a spherical particle with a radius of 175μm. The model was validated with the laboratory experiments of wire mesh reactor, for a temperature range from 573 K to 873 K and a heating rate of 200 K/s. The results of the simulation were in good agreement with the experimental data, regarding temperature, conversion

histories and product distribution of olive kernel fast pyrolysis. The numerical method applied was finite difference for the heat transfer model and Runge-Kutta fourth-order method for chemical kinetics model equations.

Yuen et al. (2007) developed a three-dimensional mathematical model for the pyrolysis of wet wood with detailed consideration of moisture evaporation, anisotropic and variable properties, and pressure driven internal convection of gases. Multiple competing reactions were formulated; however, a single first-order Arrhenius reaction was applied. Transient pyrolysis of a beech wood cube with different initial moisture contents was investigated under various furnace temperatures. Influences of anisotropic properties due to the grain structure on heat and mass transfer were discussed.

Chaurasia and Kulkarni (2007) suggested the most sensitive parameters in pyrolysis of shrinking biomass particle. The impact of shrinking and non-shrinking biomass particles on pyrolysis was studied employing a kinetic model coupled with a heat transfer model using a practically significant kinetic scheme consisting of physically measurable parameters. The numerical model was used to predict the effects of the most important physical and thermal properties (thermal conductivity, heat transfer coefficient, emissivity, reactor temperature and heat of reaction number) considering cylindrical geometry. It was established that the reactor temperature and exothermic reaction were the most dominant design variable.

Sand et al. (2008) performed numerical simulation of the pyrolysis process of a dry and wet birch wood log in a cylindrical heating chamber. The model included the flow inside and outside the porous wood log and accounts for convective, conductive and radiative heat transfer. A two-step pyrolysis reaction scheme was used to model the

conversion from wood to tar, gas and char (Fig. 2.1). The results of the simulations compared well with the experimental data which were presented in terms of radial temperature distribution and mass reduction, for both dry and wet cases. The transient simulations provided the detailed flow field inside and outside the wood log.

Zhengqi et al. (2008) studied the thermal decomposition of corn straw samples (corn stalks skins, corn stalks cores, corn bracts and corn leaves) using thermogravimetric analysis. Two different three-pseudocomponent models were used to simulate the corn straw pyrolysis assuming the addition of three independent parallel reactions, corresponding to three pseudocomponents linked to the hemicellulose, cellulose and lignin. It was found that the three-pseudocomponent model with *n*-order kinetics was more accurate than the model with first-order kinetics in most cases. It showed that the model with *n*-order kinetics was more accurate to describe the pyrolysis of the hemicellulose.

Sadhukhan et al. (2008) developed a fully transient analysis involving a kinetic model coupled with heat transfer model. The kinetic model consisted of both primary and secondary pyrolysis reactions while the heat transfer model included diffusive, convective and radiative modes of heat transfer. Fourth-order Runge–Kutta–Gill method was used to solve the kinetic model, while implicit Finite Volume Method (FVM) with Tri-Diagonal Matrix Algorithm (TDMA) was employed to solve the heat transfer model. The kinetic parameters and heat of reaction were estimated by Levenberg Marquardt nonlinear optimization technique. A general-purpose FORTRAN program was developed to solve the model equations and estimation of parameters. Experimental investigations were carried out for wood fines and cylinders in an electrically heated reactor. The model

predictions for temperature and mass loss histories were in good agreement with the experimental results.

2.1.2 Equilibrium Models of Biomass Gasification

Chern et al. (1991a) developed a basic model based on thermodynamic equilibrium of the C-H-O-inert system and mass and energy balances, and applied to the air-blown downdraft gasification of wood. The air blown gasification process, based on dry ash free feed, was represented by overall stoichiometry as given by Eq. (2.1).

$$CH_aO_bN_c + n_wH_2O + n_a\,(0.21O_2 + 0.79N_2) = n_cC + n_G\,(x_1H_2 + x_2CO + x_3CO_2 + x_4H_2O + x_5CH_4 + x_6\,N_2) \qquad (2.1)$$

The model predicts the temperature, gas composition and char yield at the exit of the gasifier for a specified set of heat loss and input conditions. A parametric study was conducted through simulations for finding the influences of the air-to-feed mass ratio and moisture-to-feed mass ratio on the performance of gasifier. The model predictions were compared with a comprehensive set of experimental data obtained from the gasification of wood in a commercial-scale downdraft gasifier; the air-to-feed ratios range from 1.1 to 2.1 and the moisture to feed ratios ranging from 0.05 to 0.3. The predicted trends for variations in the operating parameters were in general in good agreement with the experimental data. In their subsequent studies, Chern et al. (1991b) applied the equilibrium model to the flaming pyrolysis (FP) zone. The temperature, gas composition and char yield at the exit of the FP zone for a set of specified fuel material, heat loss and input conditions were predicted. Based on the parametric study, the influence of air-to-feed ratio on the performance of the flaming pyrolysis zone was determined. It was concluded that the minimum value of air-to-feed ratio was 1.2 to completely pyrolyze the biomass fuel in the FP zone. It was found that high moisture content to feed ratio resulted

in a low temperature in the FP zone, which in turn might prevent the biomass fuel from being completely pyrolysed. The biomass fuel with very low volatile content might result in an excessively high temperature in the FP zone and hence might lead to the melt-down of the gasifier.

Ruggiero and Manfrida (1999) used an equilibrium model and carried out the simulations of biomass gasification process using gaseous phase equilibrium reactions. A set of non-linear equations describing the conservation of chemical species (C, O, H, N and S) and the additional equations for thermal equilibrium of the independent reactions were incorporated to predict the output under given compositions of the reactants and operating conditions. The model predictions were validated with published experimental data. An exergy analysis was also carried out to estimate the overall irreversibility of the process transforming biomass feed stock into a hot synthetic fuel gas stream.

Zainal et al. (2001) formulated an equilibrium model and represented the gasification process as a single reaction. The elemental balances and the equilibrium ratio between the species were used to find the composition of producer gas. Zainal et al. (2001) incorporated enthalpy balance of the reactions involved and found the effect of temperature of reaction on the calorific value of gases. The effect of initial moisture content in wood and the temperature in gasification zone on the calorific value of gas was investigated. In addition to wood, the predictions were also made for peddy husk, paper and municipal waste. The model simulations predicted the composition and the calorific value of the producer gas for any biomass with known ultimate analysis. The predicted calorific values were compared with the literature and found in good agreement. The

content of hydrogen in the producer gas was found decreasing almost in a linear fashion with increase in the moisture content of the biomass.

Schuster et al. (2001) developed a model for steam gasification of biomass by applying thermodynamic equilibrium conditions. With this model, the simulation of a decentralized combined heat and power station based on a dual fluidized-bed steam gasifier was carried out. The effects of gasification temperature ranging from 650 °C to 1050 °C and water content in biomass varying from 10% to 66% on product gas composition were found. Fuel composition was varied in terms of carbon to hydrogen ratio (0-100) and fuel oxygen content (0-60 wt%) to study their effects on the lower heating value of the producer gas and chemical efficiency of the gasifier. Their influences on amount, composition, and heating value of product gas and process efficiencies were evaluated. It was shown that the accuracy of an equilibrium model for the gas composition was sufficient for thermodynamic considerations. Sensitivity analysis showed that gasification temperature and fuel oxygen content were the most significant parameters determining the chemical efficiency of the gasification.

Mathieu and Dubuisson (2002) used ASPEN PLUS process simulator to study the performance of a biomass gasifier. The modeling of biomass gasification process and more particularly the wood gasification was presented. The model based on the minimization of the Gibbs free energy was performed in the ASPEN PLUS process simulator. The entire gasification process was divided into five simulation modules (pyrolysis, combustion, Boudouard reaction, gasification and equilibrium reactor) and the corresponding results were presented. The sensitivity analysis with respect to oxygen factor, air temperature, oxygen content in air, operating pressure and injection of steam

were presented. The existence of a critical air temperature was found, above which the preheating was no longer efficient. The oxygen enrichment of air found to play an important role under a value of 30%, beyond that there was little effect on the gasification efficiency. The operating pressure had only a slight positive effect on process efficiency.

Altafini et al. (2003) also used an equilibrium model based on minimization of Gibb's free energy to predict the fuel gas compositions. The equilibrium model predictions were validated with the gasification experimental data of Pinus Elliotis sawdust. Sensitivity studies for the effects of moisture content in sawdust at a reaction temperature of 800 °C on gasification characteristics were studied. It was reported that although the equilibrium models do not represent the reactions that occur at relatively high temperatures (800 °C) very well, these models could be useful to show some tendencies on the variations of working parameter of a gasifier.

Melgar et al. (2007) discussed the combined effect of various parameters related to chemical equilibrium and the thermodynamic equilibrium of global reaction, predicting the final composition of producer gas and its reaction temperature. The cold gas efficiency of gasifier, the amount of dissociated water in the process and the heating value and engine fuel quality of the gas were found out. The model was validated with experimental data. The parametric study was carried out to find the influence of the relative air-to-fuel ratio and moisture content of biomass on the characteristics of the process and the producer gas composition. The model predicted the behavior of different biomass types and was a useful tool for optimizing the design and operation of downdraft biomass gasifiers.

Sharma (2008) modified the basic equilibrium model by incorporating the stoichiometric equilibrium approach for all the possible reactions (water gas shift reaction, steam reforming reaction, Boudouard reaction, water gas primary reaction and methanation reaction). He proposed a full equilibrium model of global reduction reactions for a downdraft biomass gasifier in order to predict the accurate distribution of various gas species, unconverted char and reaction temperature. Model predictions for equilibrium constants for reduction reactions and dry gas composition were validated by comparing the experimental data collected from the literature. Simulations were carried out to find the influences of moisture content in feedstocks, pressure, equivalence ratio and initial temperature input on dry gas composition, unconverted char, calorific value of gas, gasification efficiency, outlet gas temperature and endothermic heat released in the char bed. It was found that for optimal energy conversion of Douglas fir bark, the range of moisture content and equivalence ratio should be limited to 10-20% and 0.3-0.45 respectively, while the initial temperature in the reduction reaction zone should not be less than 1200 K.

2.1.3 Combined Transport and Kinetic Models of Biomass Gasification

Di Blasi (2000) formulated a one-dimensional unsteady model for biomass gasification in a stratified concurrent (downdraft) reactor. Heat and mass transfer across the bed were coupled with moisture evaporation, biomass pyrolysis, char combustion and gasification, gas-phase combustion and thermal cracking of tars. Numerical simulations were carried out to predict the influence of kinetic parameters and operational variables on process dynamics, structure of the reaction front and quality of the producer gas. In particular, two different stabilization modes of the reaction front were determined. It was found that

for high values of the air-to-fuel ratio and of the primary pyrolysis rate; the process was top-stabilized, resulted in a high conversion efficiency and good gas quality. As the air flow was decreased below a critical limit value, the reaction front found to become grate-stabilized. The two different configurations were largely determined by the gas-phase combustion of volatile pyrolysis products. It was reported that the predictions of the gas composition and the axial temperature profiles were in agreement with the experimental data.

Wurzenberger et al. (2002) presented a combined transient single particle and fuel bed model. A representative particle in each layer was chosen to discretize the fuel bed in axial direction, which was individually discretized in a radial direction at each grid point. Mass, momentum and energy balances were solved for the entire system. Drying was modeled using an equilibrium approach and primary pyrolysis was described by independent parallel reactions. Secondary tar cracking, homogeneous gas reactions and heterogeneous char reactions were modeled using kinetic data from the literature. Simulated results were validated with the experimental data.

Giltrap et al. (2003) developed a phenomenological model of downdraft gasification under steady state operation based on the reaction kinetics in the reduction zone. The pyrolysis and cracking reactions were not considered in the model due to the complexity of pyrolysis models. It was assumed that all the oxygen from air was combusted to CO_2 and that the pyrolysis products were completely cracked. Solid carbon in the form of char was assumed to be present throughout the reduction zone. The model predictions of gas compositions were found in good agreement with experimental data. However, the model over-predicted the methane concentration. The accuracy of the

model was limited by the availability of data on the initial conditions at the top of the reduction zone.

Jayah et al. (2003) formulated a program consisting of two sub-models of the pyrolysis and gasification zones. The pyrolysis sub-model was used to determine the maximum temperature and the composition of the gas entering the gasification zone. The gasification zone sub-model was calibrated using the data gathered from experiments. Flaming pyrolysis zone model was used to calculate the composition of the product gas entering the gasification zone in terms of CO, H_2, CO_2, H_2O, CH_4 and N_2 and the maximum temperature in the zone. The calculated concentration and temperature profiles predicted by the Flaming pyrolysis zone sub-model were then used as inputs to the gasification zone sub-model. In the gasification zone sub-model, it was assumed that a single char particle moved vertically downwards along the vertical axis of the gasifier. The description of the physical and chemical processes, flow equations, transport phenomena and conservation principles were included in the gasification sub-model. FORTRAN based computer program was written to calculate the characteristic profiles of temperature, gas concentration and conversion efficiency along the reactor axis. Simulations were carried out to study the effects of various operating and design parameters such as chip size, air inlet temperature, moisture content and throat angle on the conversion efficiency.

A fluid flow and heat transfer model was developed for the reactive, porous bed of a biomass gasifier to simulate pressure drop, temperature profile in the bed and flow rates by Sharma (2007). The conservation equations, momentum equation and energy equation were used to describe the fluid and heat transport in a porous gasifier bed. The

model was accounted for drag at wall, and the effect of radial as well as axial variation in bed porosity to predict pressure drop in the bed. Heat transfer was modeled using the effective thermal conductivity approach. Model predictions were validated with experimental, while effective thermal conductivity values were tested qualitatively using models available in the literature. Parametric analysis was carried out to investigate the effect of various parameters on bed temperature profile and pressure drop in the gasifier. The temperature profile was found to be very sensitive to gas flow rate, and heat generation in oxidation zone, while high bed temperature, gas flow rate and the reduction in feedstock particle size were found to cause a marked increase in pressure drop across the gasifier. The temperatures of the down stream zones were more sensitive to any change in heat generation in the bed as compared to the upstream zone.

Ningbo and Aimin (2008) simulated the behavior of a global fixed bed biomass gasification reactor. The pyrolysis zone and reduction zone models were combined to simulate the global process of biomass gasification. The volatiles and gases released from the pyrolysis zone were assumed to crack into equivalent amounts of CO, CH_4 and H_2O. It was considered that the volatiles and gases leaving the pyrolysis zone instantaneously entered into the reduction zone. The numerical method applied was a Runge–Kutta fourth-order method for solution of the pyrolysis zone model and finite differences for the reduction zone model to solve the coupled ordinary differential equations. Simulations were performed for varying pyrolysis temperature with a heating rate of 25 K/min. The constant temperature of 1400 K as the initial reduction zone temperature was assumed. The simulations results for temperature and concentrations of the gaseous species were in good agreement with the published experimental data.

2.2. Experimental Studies on Biomass Gasification

Sheng (1989) introduced the properties of biomass gasifier and the gasifying reaction processes. Various fuels usually considered unusable or low-value wastes, such as sawdust, wood chips, corn cobs, nut shells, rice hulls, etc, were used in the biomass gasifier to produce a high calorific value gas. It was found that gas could replace conventional energy sources, such as fuel oil, electricity and natural gas for crop drying, space heating, and industrial boilers. It was concluded that the gas produced by down-draft gasifiers is tar-free and could be used directly to drive most of the internal combustion engines.

Maschio et al. (1994) studied the influence of the operating conditions on gasification of biomass at a pilot plant scale. The entire process of pyrolysis and gasification was carried out using two reactors in series. The first step of the process, a conventional pyrolysis, was carried out in an indirectly heated continuous-screw reactor at a temperature ranging from 400 to 600°C. The second step, gasification, was carried out in a tubular coiled entrained-bed reactor mounted in a furnace at an operating temperature ranging from 700 to 950°C. The stream leaving the entrained-bed reactor was first cooled in a heat exchanger followed by quenching. Experimental results concerning thermal and catalytic runs were presented. They concluded that it was possible to produce syngas with different compositions. It was found that upon increase of moisture content, gas richer in hydrogen could be produced. The use of a catalyst permitted a decrease in the operating temperature and a drastic reduction in the production of tar.

Rice husk was successfully used as a biomass material in a downdraft biomass gasifier by Chowdhury et al. (1994). Experiments were carried out by varying air velocity in the range of 0.032-0.099 m/s, and gasification rate in the range $1.8x10^{-2}$ - $4.3x10^{-2}$ kg/m^2s. The temperature profile across the gasifier and the outlet gas compositions were measured. The calorific value of producer gas obtained from the gasifier was found in the range of 3240-4382 kJ/m^3. A set of theoretical kinetic equations, on the assumption of non-equilibrium conditions, were developed and solved numerically. The simulated temperature profile and outlet gas compositions were compared with those obtained from the experimental runs. It was reported that the model developed from a mechanistic approach was found to explain the behavior of the system appreciably within the range of variables studied.

Jorapur and Rajvanshi (1995) developed a gasifier running on chopped sugarcane leaves (1 – 10 cm). The experimental system consisted of a throatless cylindrical gasifier, a gas conditioning system and a diesel-powered generator along with its control panel. The gas conditioning system consisted of a cyclone, an impact filter, an indirect-contact heat exchanger, a centrifugal scrubber and a bubbling-cum-packed bed filter. A 15 kVA diesel generator set was operated for over 200 h using the gasifier. The gas flow rate was varied in the range of 3-4 Nm^3/hr. The gas compositions, calorific values and cold gas efficiency were found. The calorific value of the producer gas obtained was 3.5 to 5.0 MJ $/Nm^3$. The cold gas efficiency found to be 35-60% over the entire range of loads tested (3.5-11.3 kW). About 15-28% by weight of the fuel was converted into char with a calorific value of 19 MJ kg^{-1}. This char was mixed with a suitable binder and briquetted, which resulted in an excellent fuel for wood stoves. It was concluded based on the

economic analysis using the Levelised Annual Cost (LAC) method that such gasifier was more suited for direct heat applications than for shaft power applications. Jorapur and Rajvanshi (1997) in their subsequent study reported the development of a commercial-scale (1080 MJ/h) gasification system using low-density biomass such as sugarcane leaves, bajra stalks, sweet sorghum stalks and bagasse for thermal applications. The system was tested for higher than 700 h of operations under laboratory conditions at 288–1080 MJ/h output levels. The calorific value of the gas was reported as 3.56–4.82 MJ/m^3. After successful laboratory trial, the system was tested at a metallurgical company, where it was retrofitted to an oil-fired furnace for baking speciality ceramics. The furnace was operated exclusively on the gasification system and the product quality was at par with, if not better than, that obtained during oil-fired operation. The economics of the system were also presented.

Di Blasi et al (1999) designed a laboratory scale countercurrent fixed-bed gasification plant and constructed to produce data for process modeling and to compare the gasification characteristics of several biomass materials such as beechwood, nutshells, olive husks, and grape residues. The composition of producer gas and spatial temperature profiles were measured for biomass gasification at different air flow rates. It was found that the gas heating value reached a maximum with a variation of air-to-fuel ratio. The gas heating values were in the range of 5 – 5.5 MJ/Nm^3 with 28-30% CO, 5-7% CO_2, 6-8% H_2, 1-2% CH_4, and small amounts of C_2-hydrocarbons (apart from nitrogen). It was reported that the gasification of agricultural residues was more difficult because of bed transport, partial ash sintering, non uniform flow distribution and the presence of muddy phase in the effluents, which might require proper pretreatments.

Zainal et al. (2002) carried out an experimental investigation of a downdraft biomass gasifier using furniture wood and wood chips. The effect of equivalence ratio on gas composition, calorific value and the gas production rate was presented. It was found that the calorific value of producer gas increased with equivalence ratio initially, attained a peak and then decreased with an increase in equivalence ratio. The gas flow rate per unit weight of the fuel was found increasing linearly with equivalence ratio. It was also observed that the complete conversion of carbon to gaseous fuel did not occur even for the optimum equivalence ratio.

Dogru et al. (2002) used a pilot scale downdraft gasifier to investigate the gasification potential of hazelnut shells. A full mass balance was used including the tar production rate. The effect of feed rate on composition of product gas and the gasifier zone temperatures were determined. The temperatures were recorded throughout the main zones of the gasifier, at the gasifier outlet and gas cleaning zones. Pressure drop was measured across the gasifier and the gas cleaning system. The quality of product gas was found to depend on the smooth flow of the fuel and the uniformity of pyrolysis. The optimum value of air-to-fuel ratio found to be ranging from 1.44 to 1.47 Nm^3/kg. At the optimum air-fuel-ratio, the volumetric flow rate of the producer gas was found to be 8.5 Nm^3/h with a calorific value of about 5 MJ/m^3. It was reported that the hazelnut shells could be easily gasified in a downdraft gasifier to produce good quality gas with a minimum of polluting by-products. It was suggested that, in view of the ease of operation, small-scale gasifier could make an important contribution to the economy of rural areas where the residues of nuts were abundantly available.

Jayah et al. (2003) carried out experimental studies on a gasifier, which was fabricated in Sri Lanka for tea industry, to examine the effect of certain key operating parameters and design features on its performance. It was found that wood chips of size 3–5 cm with a moisture content below 15% (dry basis) should be used in this gasifier. Air flow was measured at the exit side of blower, and pressure measurements were made either side of the orifice plate using a manometer. Axial temperatures in the gasification zone and the outer surface of the gasifier were measured using K- and T-type thermocouples.

Wander et al. (2004) analyzed the sawmill residues as an energy source to offer the best technical, economic and environmental alternative. The characterization (quantity, type, chemical and energetic analysis) of the residues generated, in addition to the energy needs of sawmills, was supportive to find the suitable technology. It was found that the technology of wood gasification could produce a gas that is able to burn in an internal combustion engine after appropriate cleaning. In order to assess the performance of the wood residues gasification process, a small, fixed bed, downdraft, stratified and open top gasifier was built. The gasifier capacity was around 12 kg/h. An internal gas recirculation was introduced, in which part of the produced gas was burnt to raise the gasification reaction temperature. The mass and energy balances of the gasifier were carried out and its cold gas, global and mass conversion efficiencies were found out using several parameters measured in the experiments.

Hanaoka et al. (2005) studied the effect of woody biomass components on air-steam gasification using a downdraft fixed bed gasifier operated at 1173 K and at atmospheric pressure. Cellulose, xylan, and lignin as model compounds of woody

biomass components, and Japanese oak and Japanese red pine bark as woody biomass were employed as feedstock. The gasification conversions in cellulose, xylan, and lignin were 97.9%, 92.2%, and 52.8% on a carbon basis, respectively. In each run, the main components of the gas phase were CO, CO_2, H_2, and CH_4. The product gas composition in cellulose was 35.5% CO, 27.0% CO_2, and 28.7% H_2. It was found that the mole fraction of CO was higher than that of CO_2 or H_2. In contrast, the product gas compositions in xylan and lignin were approximately 25 mol% CO, 36 mol% CO_2, and 32 mol% H_2. These results suggest that the fundamental information obtained in the gasification of each component could possibly be used to predict the composition of product gas generated in air-steam gasification of woody biomass.

Sharma (2007) used an open top downdraft biomass gasifier of capacity 20 kWe to validate the model developed in his earlier studies (Sharma, 2006). Steady state temperatures at different locations inside the reactor were measured using K – type thermocouples at various values of pressure and air flow rate.

2.3 Existing Gaps of Research

The existing literature on pyrolysis modeling suggests that great strides have been made in understanding the modeling aspects of pyrolysis in the last three decades. However, the studies on modeling of fixed bed pyrolyser are scarce. The secondary reactions in pyrolysis play an important role in the pyrolysis of large size particles. A fixed bed pyrolysis zone exists in the gasification of large size wood waste particles in a downdraft biomass gasifier. Thus, secondary reactions must be included in the kinetic modeling of pyrolysis in biomass gasifier. In the existing literature, many researchers used first-order

kinetics for biomass pyrolysis. A few researchers used the models based on secondary reactions, but model predictions are validated with experimental data of small size particles and thus secondary reaction effects are neglected. There is a need to carry out the modeling of pyrolysis considering chemical reaction kinetics model including the secondary reactions, heat transfer model and mass transfer mechanisms for the fixed bed pyrolysis zone of the downdraft biomass gasifier.

The chemical reaction kinetics and transport phenomena have not been properly coupled to model the conventional fixed bed gasifier. Many researchers developed and/or modified the equilibrium model for biomass gasifier, which assumes that all the reactions are in thermodynamic equilibrium. It is expected that the pyrolysis products burn and achieve equilibrium in the reaction zone before leaving the gasifier. This implies that residence time is long enough to allow the chemical reaction to reach an equilibrium state. Kinetics-free equilibrium models can be used to predict the exit gas composition, given the solid composition and the equilibrium temperature, but they can not be used for the reactor design. The prediction of concentration or temperature profiles across the gasifier axis is not possible by an equilibrium model and hence results generated using an equilibrium model would give same final composition for different length of reduction zone of a biomass gasifier. There is a need to develop a model which takes into account of the kinetics of homogeneous and heterogeneous chemical reactions, transport of volatiles produced, heat and mass transfer between solid and gaseous phase and pyrolysis reactions.

Various models that have been reported for various gasifier configurations include: (1) unsteady one-dimensional model for stratified downdraft gasification, (2)

transient single particle and fuel bed model for crosscurrent moving bed furnace, (3) steady-state reduction zone model for downdraft gasification and (4) steady state fluid flow and heat transfer model for open top throat-less downdraft gasification. However, for throated close-top downdraft biomass gasifier, commonly known as an Imbert downdraft gasifier, a complete model including pyrolysis, combustion and reduction zones has not yet been reported in the literature. A survey report of gasifier manufacturers states that 75% of gasifiers offered commercially were downdraft, 20% were fluid beds (including circulation fluid beds), 2.5% were updraft, and 2.5% were of other types (Bridgwater, 2002). Taking into account of the importance of downdraft biomass gasifier and its wide applications in industry, it is necessary to have a complete model for such a configuration. Furthermore, it should be based on unsteady state modeling of heat and mass transfer, which may allow the prediction of dynamic behavior of the conventional fixed bed biomass gasifier. This would help in understanding different modes of stabilization of the reaction front.

2.4 Scope of Work

A generalized mathematical model for throated close-top down draft biomass gasifier is developed which takes into account of the limitations of the earlier studies. The developed model accounts for the pyrolysis, secondary tar reactions, homogeneous gas reactions and heterogeneous combustion/ gasification reactions. In the gas phase, eight species (O_2, N_2, CO_2, CO, H_2O, H_2, CH_4 and tar) are considered. The solid phase is biomass in the pyrolysis and combustion/ oxidation zone, whereas charcoal in the reduction zone. The pyrolysis model presented here considers gradients both in the bed

and inside single particles. Thus the entire bed is divided into the two subsystems, i.e., gas phase inside the bed and the individual particles. To validate the proposed mathematical model, experiments are carried out covering wide range of operating parameters. The wood waste is used as a biomass material in the biomass gasification experiments. Various operating parameters such as air flow rate, biomass moisture content, biomass consumption rate, etc. are varied to study their effects on the performance of the gasifier.

CHAPTER – 3

MATHEMATICAL MODELING AND SIMULATION

Modeling of biomass gasification implies the representation of chemical and physical phenomena constituting all the four zones of the gasifier (pyrolysis, combustion, reduction, and drying) in the mathematical form. In other words, whole process is to be represented as a system of equations which taken together can provide valuable quantitative information about the entire process. The models of downdraft biomass gasification can be categorized into two groups: (1) Equilibrium models and (2) Combined transport and kinetic models. Equilibrium models are important in order to predict the thermodynamic limits of chemical reactions describing the gasification process. The equilibrium model assumes that all the reactions are in thermodynamic equilibrium in biomass gasifier. Many researchers (Chern et al., 1991; Zainal et al., 2001; Mathieu and Dubuisson, 2002 and Altafini et al., 2003; Melgar et al., 2007) have developed and/or modified the equilibrium models for biomass gasification. It is observed that most of the stoichiometric equilibrium models of biomass gasification developed till now describe the equilibria of reduction reactions, viz. methane–carbon reaction (heterogeneous reaction) and water gas shift reaction (homogeneous reaction) assuming: (1) the drying, pyrolysis and gasification processes are lumped together into a

single zone, (2) residence time for reactants is sufficiently high in order to establish chemical equilibrium, and (3) all the carbon available in biomass is gasified. Kinetics-free equilibrium models can predict the exit gas composition, given the solid composition and the equilibrium temperature, but they cannot be used for reactor design (Di Blasi, 2000). An equilibrium model can not predict the concentration or temperature profiles across the axis of gasifier and hence results generated using an equilibrium model would give the same final composition for different lengths of reduction zone of biomass gasifier. Hence, there is a need to develop a combined transport and kinetic model which takes into account of the kinetics of homogeneous and heterogeneous chemical reactions, transport of volatiles produced, heat and mass transfer between solid and gaseous phase and pyrolysis reactions. Various models that have been reported for different gasifier configurations include: (1) unsteady one-dimensional model for stratified downdraft gasification (Di Blasi, 2000), (2) transient single particle and fuel bed model for crosscurrent moving bed furnace (Wurzenberger et al., 2002), (3) steady-state reduction zone model for downdraft gasification (Giltrap et al., 2003) and (4) steady state fluid flow and heat transfer model for open top throat-less downdraft gasification (Sharma, 2007). However, for throated close-top downdraft biomass gasifier, commonly known as an Imbert downdraft gasifier, a complete model including pyrolysis, combustion and reduction zones has not been reported in the literature. In a survey of gasifier manufacturers, it is reported that 75% of gasifiers offered commercially were downdraft, 20% were fluid beds (including circulation fluid beds), 2.5% were updraft, and 2.5% were of other types (Bridgwater, 2002). Taking into account of the importance of

downdraft biomass gasifier and its commercial applications, it is essential to have a complete model for such a configuration.

In the present study, a combined transport and kinetic model which takes into account of the kinetics of chemical reactions, heat and mass transfer between solid and gaseous phases and transport of volatiles produced is developed. To validate the combined transport and kinetic model, experimental data is generated in the present study. To compare the results predicted by combined transport and kinetic model with those of the equilibrium model, the latter model is also formulated in the present study. Hence, the mathematical modeling of a downdraft biomass gasifier is carried out by two approaches: (1) developing an equilibrium model which represents the entire gasification process by a single reaction, (2) developing a combined transport and kinetic model which takes into account of the kinetics of chemical reactions, heat and mass transfer between solid and gaseous phases and transport of volatiles produced. These two approaches are discussed in detail in section 3.1 and 3.2 respectively.

3.1 Equilibrium Model

The equilibrium model assumes that all the reactions are in thermodynamic equilibrium with each other in the biomass gasifier. This model represents the gasification process as a single reaction. It is expected that the pyrolysis products get burnt and achieve equilibrium in the reduction zone of the gasifier before exiting from the gasifier. This implies that the residence time is long enough to allow the chemical reaction to reach an equilibrium state. The elemental balances and the equilibrium ratio between the species are used to find the composition of the producer gas. Equilibrium model does not

represent the reactions that occur at relatively high temperatures (800 °C) in the biomass gasifier very well. However, it is useful to predict the exit gas composition, given the solid composition and the equilibrium temperature. It is used to estimate the trend of a biomass gasifier output with variations in working parameters.

The typical chemical formula of woody material, based on a single atom of carbon, is CH_aO_b. The amounts of hydrogen and oxygen atoms (*a* and *b*) can be found out from the biomass composition. The global gasification reaction can be written as shown by Eq. (3.1).

$$CH_aO_b + wH_2O + mO_2 + 3.76mN_2 = x_1H_2 + x_2CO + x_3CO_2 + x_4H_2O + x_5CH_4 + 3.76mN_2 \quad (3.1)$$

where *w* is the kmol of water per kmol of wood, *m* is the kmol of oxygen per kmol of wood, x_1 to x_5 are the coefficients of constituents of the products, and 3.76 represents the molar ratio of N_2 to O_2 (i.e. $^{79}/_{21}$). The methane generation and water gas shift reactions are included in the equilibrium model and are given by Eq. (3.2) and Eq. (3.3) respectively.

$$C + 2H_2 \longleftrightarrow CH_4 \qquad \Delta H = -75{,}000 \text{ J/mol} \quad (3.2)$$

$$CO + H_2O \longleftrightarrow CO_2 + H_2 \qquad \Delta H = -41{,}200 \text{ J/mol} \quad (3.3)$$

The equilibrium constant for methane generation (K_1) is given by Eq. (3.4).

$$K_1 = \frac{x_5}{x_1^2} \quad (3.4)$$

The equilibrium constant for water gas shift reaction (K_2) is given by Eq. (3.5).

$$K_2 = \frac{x_1 x_3}{x_2 x_4} \quad (3.5)$$

For a known value of moisture content, the value of w becomes a constant and m can be found out from the airflow rate per kmol of wood. From the global gasification reaction [Eq. (3.1)], there are six unknowns x_1 to x_5, and T, representing the five unknown species of the product and the temperature of the reaction. Thus, six equations are required to find their values, which are obtained from the three elemental molar balances (carbon, hydrogen and nitrogen), energy balance, and two equilibrium constant relations [Eq. (3.4) and Eq. (3.5)].

Carbon Balance:

$$1 = x_2 + x_3 + x_5 \tag{3.6}$$

Hydrogen Balance:

$$2w + a = 2x_1 + 2x_4 + 4x_5 \tag{3.7}$$

Oxygen Balance:

$$w + b + 2m = \mathrm{x}_2 + 2x_3 + x_4 \tag{3.8}$$

The energy balance for gasification process (assumed to be adiabatic) is:

$$\begin{bmatrix} H^0_{fwood} + w\left(H^0_{fH_2O(l)} + H_{(vap)}\right) + \\ mH^0_{fO_2} + 3.76mH^0_{fN_2} \\ + \Delta T'\left(mC_{pO_2} + 3.76mC_{pN_2}\right) \end{bmatrix} = \begin{bmatrix} x_1H^0_{fH_2} + x_2H^0_{fCO} + x_3H^0_{fCO_2} \\ + x_4H^0_{fH_2O(vap)} + x_5H^0_{fCH_4} + \Delta T(x_1C_{pH_2} + \\ x_2C_{pCO} + x_3C_{pCO_2} + x_4C_{pH_2O(vap)} + x_5C_{pCH_4} \\ + 3.76\, mC_{pN_2}) \end{bmatrix} \tag{3.9}$$

where ΔT and $\Delta T'$ are $(T_2 - T_1)$ and $(T_2' - T_1)$ respectively. T_1 is the ambient temperature, T_2 is the temperature of reduction zone, T_2' is the air inlet temperature, $H^0_{f,i}$ is the heat of formation of any species i, and $C_{p,i}$ is the specific heat of any species i.

Eqs. (3.4-3.9) represent a system of six equations with six unknowns, out of which two of them [Eq. (3.4) and Eq. (3.5)] are nonlinear and rest four are linear. The above system of

six equations are reduced to a set of four equations as given by Eqs. (3.13-3.16), by carrying out the algebraic manipulations as shown below.

From Eq. (3.6)

$$x_5 = 1 - x_2 - x_3 \tag{3.10}$$

From Eq. (3.7)

$$x_4 = w + \left(\frac{a}{2}\right) - x_1 - 2x_5 \tag{3.11}$$

Substituting the value of x_5 from the Eq. (3.10) into Eq. (3.11)

$$x_4 = -x_1 + 2x_2 + 2x_3 + w + \left(\frac{a}{2}\right) - 2 \tag{3.12}$$

From Eq. (3.4) and Eq. (3.10)

$$x_1^2 K_1 = 1 - x_2 - x_3 \tag{3.13}$$

Substituting the value of x_4 from the Eq. (3.12) into Eq. (3.8)

$$-x_1 + 3x_2 + 4x_3 = 2m + b - \frac{a}{2} + 2 \tag{3.14}$$

Substituting the value of x_4 from the Eq. (3.12) into Eq. (3.5)

$$x_1 x_3 = K_2 x_2 \left(-x_1 + 2x_2 + 2x_3 + w + \left(\frac{a}{2}\right) - 2\right) \tag{3.15}$$

From Eq. (3.9)

$$T_2 = T_1 + \frac{\left[\begin{array}{l} H^0_{fwood} + w\left(H^0_{fH_2O(l)} + H_{(vap)}\right) + H^0_{fO_2} + 3.76mH^0_{fN_2} + \Delta T'\left(mC_{pO_2} + 3.76mC_{pN_2}\right) \\ - x_1 H^0_{fH_2} + x_2 H^0_{fCO} + x_3 H^0_{fCO_2} + x_4 H^0_{fH_2O(vap)} + x_5 H^0_{fCH_4} \end{array}\right]}{\left(x_1 C_{pH_2} + x_2 C_{pCO} + x_3 C_{pCO_2} + x_4 C_{pH_2O(vap)} + x_5 C_{pCH_4} + 3.76mC_{pN_2}\right)} \tag{3.16}$$

The general equations for K_1 and K_2, reported by Zainal et al. (2001), are represented as Eqs. (3.17-3.18).

$$\ln K_1 = \left[\frac{7082.848}{T} + (-6.567)\ln T + \frac{7.466\times10^{-3}}{2}T + \frac{-2.164\times10^{-6}}{6}T^2 + \frac{0.701\times10^{-5}}{2(T)^2} + 32.541 \right] \tag{3.17}$$

$$\ln K_2 = \left[\frac{5870.53}{T} + 1.86\ln T - 2.7\times10^{-4}T - \frac{58200}{(T)^2} - 18.007 \right] \tag{3.18}$$

The above set of 9 equations [Eqs. (3.10 - 3.18)] is solved using the following algorithm (steps 1-9):

1. Specify the value of *m*, *w*, *a*, and *b*.
2. Assume temperature T_2, and find K_1 & K_2 using Eq. (3.17) and Eq. (3.18) respectively.
3. Assume the value of x_1, x_2, and x_3.
4. Find the new values of x_1 and x_2 using Eq. (3.13) and Eq. (3.15) by Newton-Raphson method of nonlinear equations.
5. Find new value of x_3 using Eq. (3.14).
6. Repeat steps 3-5 (again apply the Newton-Raphson method with new set of values), until the successive values of x_1, x_2, and x_3 remain constant.
7. Find x_4 and x_5 using Eq. (3.12) & Eq. (3.10) sequentially.
8. Calculate the new value of T_2 using Eq. (3.16).
9. Repeat the steps 2-7, until successive value of T_2 becomes constant.

In case of steam gasification, elemental balance equations for hydrogen and oxygen, and the energy balance equations are required to be modified to take into account of the steam added. The modified elemental balance equations for hydrogen and oxygen are given by Eq. (3.19) and Eq. (3.20) respectively.

$$2(w + s) + a = 2x_1 + 2x_4 + 4x_5 \tag{3.19}$$

$$w + s + b + 2m = x_2 + 2x_3 + x_4 \tag{3.20}$$

The modified energy balance equation is given by Eq. (3.21).

$$\begin{bmatrix} H^0_{fwood} + w\left(H^0_{fH_2O(l)} + H_{(vap)}\right) + mH^0_{fO_2} \\ +3.76mH^0_{fN_2} + s\begin{pmatrix} H^0_{fH_2O(g)} \\ +\Delta T'' C_{pH_2O(vap)} \end{pmatrix} \\ +\Delta T'\left(mC_{pO_2} + 3.76mC_{pN_2}\right) \end{bmatrix} = \begin{bmatrix} x_1H^0_{fH_2} + x_2H^0_{fCO} + x_3H^0_{fCO_2} \\ +x_4H^0_{fH_2O(vap)} + x_5H^0_{fCH_4} + \Delta T(x_1C_{pH_2} + \\ x_2C_{pCO} + x_3C_{pCO_2} + x_4C_{pH_2O(vap)} + x_5C_{pCH_4} \\ +3.76\, mC_{pN_2}) \end{bmatrix} \tag{3.21}$$

where ΔT" is (T_2" − T_1"), s is kmol of steam per kmol of wood, T_2" is the steam temperature, and T_1" is the ambient temperature.

3.2 Combined Transport and Kinetic Model

A transient one dimensional model is developed for the throated close-top downdraft biomass gasifier. The model takes into account of the pyrolysis, secondary tar reactions, homogeneous gas reactions and heterogeneous combustion/gasification reactions. Eight gaseous species namely O_2, N_2, CO_2, CO, H_2O, H_2, CH_4 and tar are considered in the gas phase. In the pyrolysis and combustion zone, the solid phase is a biomass, whereas in the reduction zone it is a charcoal. The developed model is divided into three parts according to three different zones formed: (1) pyrolysis, (2) oxidation, and (3) reduction.

3.2.1 Pyrolysis

Pyrolysis is a process by which a biomass feedstock is thermally degraded in the absence of oxygen/air to produce solid (charcoal), liquid (tar and other organics) and gaseous (H_2, CO_2, CO, etc.) products. Released volatiles from each biomass particle flow downward in packed pyrolysis bed. Rate of volatiles release depends on the particle size and temperature within a single particle. Pyrolysis bed is modeled as a stack of particles in

one dimension. The model presented here considers temperature gradient both in the bed and also inside the single particles. Thus the entire bed is divided into two subsystems, i.e., gas phase inside the bed and the individual particles. The assumptions made in this model are: (1) the volatiles released from biomass particles flow downward, (2) unsteady state operation, (3) released volatiles is a mixture of CO, CH_4, CO_2, H_2, H_2O and tar, (4) velocity varies along the bed, (5) solid biomass does not move downward during the operation, and (6) porosity of the bed remains constant.

3.2.1.1 Transport Model for Gas Phase in Pyrolysis Zone

The continuity equation for the gas phase in a packed bed is given by Eq. (3.22).

$$\frac{\partial\, \varepsilon_{g,bed}\rho_{g,bed}}{\partial t} = -\frac{\partial}{\partial z}\left[\varepsilon_{g,bed}\rho_{g,bed}v_{g,bed}\right] + a_p\dot{m}_p \tag{3.22}$$

where, $\varepsilon_{g,bed}$ is the porosity of the bed, $v_{g,bed}$ is the gas velocity (m/s), $\rho_{g,bed}$ is the density of the gas phase (kg/m^3), $\dot{m}_p$ is the mass transfer rate from particle to the gas phase (kg/m^2 s), and a_p is the specific surface area of particle (m^2/m^3).

The species conservation equation is given by Eq. (3.23).

$$\begin{aligned}\varepsilon_{g,bed}\frac{\partial\, \rho_{ig,bed}}{\partial t} = -\varepsilon_{g,bed}\left[v_{g,bed}\frac{\partial\rho_{ig,bed}}{\partial z} + \rho_{ig,bed}\frac{\partial v_{g,bed}}{\partial z}\right] \\ + \frac{\partial}{\partial z}\left[\varepsilon_{g,bed}D_{i,eff,bed}\frac{\partial\rho_{ig,bed}}{\partial z}\right] + a_p\dot{m}_{i,p}\end{aligned} \tag{3.23}$$

where, $\rho_{ig,\,bed}$ is the density of the species *i* in packed bed gas phase, $D_{i,eff,bed}$ is the effective diffusivity of species *i* in packed bed gas phase, and $\dot{m}_{i,p}$ is the mass transfer rate of species *i* from particle to the gas phase (kg/m^2 s).

The initial and boundary conditions are given below by Eq. (3.24) and Eq. (3.25) respectively.

Initial Conditions:

at $t = 0$; $\rho_{ig,\,bed} = 0$; $v_{g,\,bed} = 0$ (3.24)

Boundary Conditions:

at $z = 0$; $\rho_{ig,\,bed} = 0$; $v_{g,\,bed} = 0$ for all $t > 0$ (3.25a)

at $z = L$; $\frac{\partial \rho_{ig,bed}}{\partial z} = 0$ for all $t > 0$ (3.25b)

Pyrolysed gas generated from the biomass particle flows downward and its velocity is computed using Eq. (3.26).

$$v_{g,bed} = \left(\frac{\text{Flow rate}}{\text{Area}}\right) = \left(\frac{\rho_{g,bed} A \Delta z}{\text{Density of gaseous mixture}}\right)\left(\frac{1}{\Delta t}\right)\left(\frac{1}{\text{Area}}\right) \quad (3.26)$$

The numerator of the first term on RHS of Eq. (3.26), i.e., $\rho_{g,bed} A \Delta z$, represents the multiplication of the total concentration of the gas with elemental volume under consideration which gives the amount of gas within that elemental volume. The term $\rho_{g,bed} A \Delta z$ is divided with density which results in the volume of the gas and further divided by time interval to get the flow rate. Velocity of the gas is found by dividing the flow rate by area of the packed bed.

3.2.1.2 Single Particle

To describe the chemical process of pyrolysis in a single solid particle, an unsteady state one dimensional variable property model of transport phenomena is required. It should include heat (conductive, convective and radiative modes), mass (diffusive and convective modes) and momentum transport of the products formed within the solid (volatiles and gases). Babu and Chaurasia (2002 a-b; 2003 a-e; 2004 a-d) carried out exhaustive modeling and simulation studies on the pyrolysis of single solid particle. The model developed and modified by Babu and Chaurasia (2003 a-b; 2004 a-d) uses

physically measurable parameters and practically explainable kinetic scheme, incorporating the convective and diffusion effects. Babu and Chaurasia (2004c) proposed three models for the pyrolysis of biomass under two categories namely, (1) Generalized reference model (Model-I), and (2) Simplified models (Model-II & Model-III). In most practical situations of industrial pyrolysis reactions, the contributions of the bulk motion of gases inside the pores of the particle are insignificant. Because the resistance offered by the pores in the solid particle is so high, the transport of these gases would take place essentially by a diffusion mechanism but not by bulk motion (i.e. convection). Taking this situation into consideration, Model –II is used in the present study, which is based on the assumption that there is no bulk motion contribution (i.e. convective transport is neglected) to the temperature profile and the product yield predictions. This model incorporates all the possible effects of kinetics, heat transfer, mass transfer and momentum transfer. The assumptions made in developing this model are as follows:

(1) The thermal and transport properties (porosity, thermal conductivity, specific heat, mass diffusivity) vary with the conversion level.
(2) Heat transfer occurs by all three modes (i.e. conduction, convection and radiation).
(3) Gas phase processes occur under unsteady state conditions.
(4) Transport of mass takes place by diffusion of volatile species.
(5) Pressure and velocity vary along the porous sample.
(6) Local thermal equilibrium exists between the solid matrix and the flowing gases.
(7) The system is one dimensional.
(8) There is no moisture content and no particle shrinkage.

The equations of the Model-II are presented in Table-3.1 and are expressed in dimensionless form with the help of dimensionless groups presented in Table-3.2. Notation of the variables used in the particle pyrolysis model is shown in Table-3.3.

The total amount of released volatiles from the biomass particle is given by the product of concentration gradient of volatiles at particle boundary $\left.\frac{\partial C_{G1}}{\partial x}\right|_R$ and effective diffusivity D_{eG1} in the particle [Eq. (3.53)].

$$\dot{m}_p = D_{eG1}\left.\frac{\partial C_{G1}}{\partial x}\right|_R \tag{3.53}$$

To solve species conservation equation [Eq. (3.23)], the individual amount ($\dot{m}_{i,p}$) of each species (CO, CH_4, CO_2, H_2, H_2O and tar) is required.

Sharma et al. (2006) formulated a model to find pyrolysis product composition at low heating rates (< 100 °C/min) for woody biomass materials. A model developed by Sharma et al. (2006) is based on the elemental balance equations and on the experimental findings of Boroson et al. (1989) and Thunman et al. (2001). Complete elemental balances along with data from the literature (Boroson et al., 1989) on CO/CO_2, H_2O/CO_2 and light hydrocarbon/CO_2 ratios have been used for determining the product composition as a function of temperature. Boroson et al. (1989) considered the charcoal yield reported by Tillman et al. (1981) in the elemental balance equations. In the present study, the model developed by Sharma et al. (2006) is modified by incorporating the charcoal yield based on the particle pyrolysis model.

Table 3.1 Mathematical model of single solid particle pyrolysis

Koufopanos et al. (1991) mechanism

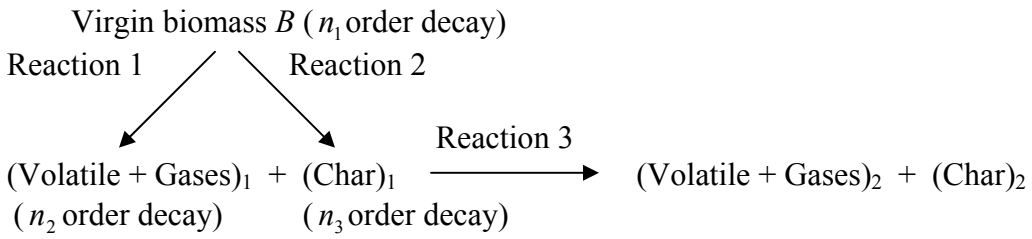

Particle model

Mass conservation for biomass, (gases and volatiles)$_1$ (char)$_1$, (gases and volatiles)$_2$ and (char)$_2$:

$$\frac{\partial C_B}{\partial t} = -k_1 C_B^{n_1} - k_2 C_B^{n_1} \tag{3.27}$$

$$\frac{\partial (C_{G1}\varepsilon")}{\partial t} = D_{eG1}\left(\frac{b-1}{r}\frac{\partial C_{G1}}{\partial r} + \frac{\partial^2 C_{G1}}{\partial r^2}\right) + k_1 C_B^{n_1} - \varepsilon" k_3 C_{G1}^{n_2} C_{C1}^{n_3} \tag{3.28}$$

$$\frac{\partial C_{C1}}{\partial t} = k_2 C_B^{n_1} - k_3 C_{G1}^{n_2} C_{C1}^{n_3} \tag{3.29}$$

$$\frac{\partial C_{G2}}{\partial t} = k_3 C_{G1}^{n_2} C_{C1}^{n_3} \tag{3.30}$$

$$\frac{\partial C_{C2}}{\partial t} = k_3 C_{G1}^{n_2} C_{C1}^{n_3} \tag{3.31}$$

Enthalpy:

$$\frac{\partial}{\partial t}\left(C_p \rho T\right) = k\left(\frac{b-1}{r}\frac{\partial T}{\partial r} + \frac{\partial^2 T}{\partial r^2}\right) - \left(D_{eG1}\frac{\partial C_{G1}}{\partial r}\right) C_{pG1}\frac{\partial T}{\partial r} + \left(-\Delta H\right)\left(-\frac{\partial \rho}{\partial t}\right) \tag{3.32}$$

Initial conditions:

$$t = 0; \quad C_B = C_{B0},\ C_{G1} = C_{C1} = C_{G2} = C_{C2} = 0,\ T(r,0) = T_0 \tag{3.33}$$

Particle boundary conditions:

$$t > 0; \quad r = 0, \qquad \frac{\partial C_{G1}}{\partial r} = 0, \qquad \left(\frac{\partial T}{\partial r}\right)_{r=0} = 0 \tag{3.34)-(3.35}$$

$$t > 0; \quad r = R, \qquad D_{eG1}\left(\frac{\partial C_{G1}}{\partial r}\right) = k_{mG1}(C_{G10} - C_{G1}) \tag{3.36}$$

$$t > 0; \quad r = R, \qquad k\left(\frac{\partial T}{\partial r}\right)_{r=R} = h\left(T_f - T\right) + \sigma\varepsilon\left(T_f^4 - T^4\right) \tag{3.37}$$

(Contd…)

Table 3.1 Mathematical model of single solid particle pyrolysis (continued)

Dimensionless forms of Eqs. (3.27-3.37):

$$\frac{\partial \overline{C}_B}{\partial t} = -k_1 \overline{C}_B^{n_1} - k_2 \overline{C}_B^{n_1} \tag{3.38}$$

$$\varepsilon'' \frac{\partial \overline{C}_{G1}}{\partial \tau} = \frac{\overline{D}_{G1}}{Le}\left(\frac{b-1}{x}\frac{\partial \overline{C}_{G1}}{\partial x} + \frac{\partial^2 \overline{C}_{G1}}{\partial x^2} \right) + \frac{R^2 k_1 \overline{C}_B^{n_1}}{\alpha} - \frac{\varepsilon'' R^2 k_3 \overline{C}_{G1}^{n_2} \overline{C}_{C1}^{n_3}}{\alpha} \tag{3.39}$$

$$\frac{\partial \overline{C}_{C1}}{\partial t} = k_2 \overline{C}_B^{n_1} - k_3 \overline{C}_{G1}^{n_2} \overline{C}_{C1}^{n_3} \tag{3.40}$$

$$\frac{\partial \overline{C}_{G2}}{\partial t} = k_3 \overline{C}_{G1}^{n_2} \overline{C}_{C1}^{n_3} \tag{3.41}$$

$$\frac{\partial \overline{C}_{C2}}{\partial t} = k_3 \overline{C}_{G1}^{n_2} \overline{C}_{C1}^{n_3} \tag{3.42}$$

$$\frac{\partial \theta}{\partial \tau} = \frac{b-1}{x}\frac{\partial \theta}{\partial x} + \frac{\partial^2 \theta}{\partial x^2} + \frac{Q'' R^2 k_1}{\alpha} + \frac{1}{Le}\left(\overline{D}_{G1} \frac{\partial \overline{C}_{G1}}{\partial x} \right) \overline{C}_{pG1} \overline{C}_{B0} \frac{\partial \theta}{\partial x} \tag{3.43}$$

$$\tau = 0; \quad \overline{C}_B = 1, \ \overline{C}_{G1} = \overline{C}_{C1} = \overline{C}_{G2} = \overline{C}_{C2} = 0, \ \theta(x,0) = 1 \tag{3.44}$$

$$\tau > 0; \quad x = 0, \qquad \frac{\partial \overline{C}_{G1}}{\partial x} = 0, \qquad \frac{\partial \theta}{\partial x} = 0 \tag{3.45)-(3.46}$$

$$\tau > 0; \quad x = 1, \qquad \overline{D}_{G1}\left(\frac{\partial \overline{C}_{G1}}{\partial x} \right) = Sh(\overline{C}_{G10} - \overline{C}_{G1}) \tag{3.47}$$

$$\tau > 0; \quad x = 1, \qquad \frac{\partial \theta}{\partial x} = -\theta \, Bi_M \tag{3.48}$$

Koufopanos et al. (1991) correlation:

$$h = 0.322(k/l) Pr^{1/3} Re^{0.5} \tag{3.49}$$

Other relations:

$$\varepsilon'' = \varepsilon_0'' + \gamma \ (1 - \overline{C}_B), \ \phi = \eta \phi_B + (1-\eta)\phi_{C1}, \ \eta = C_B / C_{B0} \tag{3.50)-(3.51}$$

Conversion of biomass:

$$X = \frac{\overline{C}_{B_0} - \left[\left(\sum_{i=1}^{M} \overline{C}_B \right) \Big/ (M+1) \right]}{\overline{C}_{B_0}} \tag{3.52}$$

Table 3.2 Dimensionless groups used in the particle pyrolysis model

Thermal Diffusivity, $\alpha = k/\rho C_P$

Dimensionless Radial Distance, $x = r/R$

Dimensionless Time, $\tau = \alpha t/R^2$

Dimensionless Temperature, $\theta = \left(T - T_f\right)/\left(T_0 - T_f\right)$

Modified Biot Number, $B_{i,M} = \left(R/k\right)\left[h + \varepsilon\sigma\left(T^3 + T^2 T_f + T_f^2 T + T_f^3\right)\right]$

Heat of Reaction Number, $Q = \left(-\Delta H + C_P T\right)/\left[\rho C_P\left(T_0 - T_f\right)\right]$

Heat of Reaction Number, $Q'' = QC_B^{n_1}$

Dimensionless Concentration of B, $\overline{C}_B = C_B/C_{B0}$

Dimensionless Initial Concentration of B, $\overline{C}_{B0} = C_{B0}/\rho_0$

Dimensionless Concentration of G_1, $\overline{C}_{G_1} = C_{G_1}/C_{B0}$.

Dimensionless Initial Concentration of G_1, $\overline{C}_{G_1 0} = C_{G_1 0}/C_{B0}$

Dimensionless Concentration of C_1, $\overline{C}_{C_1} = C_{C_1}/C_{B0}$

Dimensionless Concentration of G_2, $\overline{C}_{G_2} = C_{G_2}/C_{B0}$

Dimensionless Concentration of C_2, $\overline{C}_{C_2} = C_{C_2}/C_{B0}$

Dimensionless Heat Capacity of (gases and volatiles)$_1$, $\overline{C}_{pG_1} = C_{pG_1}/C_{pG_1 0}$

Dimensionless Effective Diffusivity of (gases and volatiles)$_1$, $\overline{D}_{eG_1} = D_{eG_1}/D_{eG_1 0}$

Lewis Number, $Le = k/\left(\rho_0 C_{pG_1 0} D_{eG_1 0}\right)$

Sherwood Number, $Sh = \left(k_{mG_1} R\right)/D_{eG_1 0}$

Table 3.3 Notations used in the particle pyrolysis model

A_1, A_2, A_3	frequency factor, 1/s
b	geometry factor (slab=1, cylinder=2, sphere=3)
B	virgin biomass
G_1	$(\text{gases and volatiles})_1$
C_1	$(\text{char})_1$
G_2	$(\text{gases and volatiles})_2$
C_2	$(\text{char})_2$
C_B	concentration of B, C_{B0} at initial condition, kg/m^3
C_{G1}	concentration of G_1, C_{G10} at initial condition, kg/m^3
C_{C1}	concentration of C_1, C_{C10} at initial condition, kg/m^3
C_{G2}	concentration of G_2, C_{G20} at initial condition, kg/m^3
C_{C2}	concentration of C_2, C_{C20} at initial condition, kg/m^3
C_p	specific heat capacity, J/kg K
C_{pG1}	heat capacity of $(\text{gases and volatiles})_1$
C_{pG10}	heat capacity of $(\text{gases and volatiles})_1$ at initial condition, J/mol K
D_1, D_2	constants defined by expressions of k_1 and k_2 respectively, K
D_{eG1}	effective diffusivity of $(\text{gases and volatiles})_1$, D_{eG10} for initial effective diffusivity, m^2/s
E_3	activation energy defined by expression of k_3, J/mol
h	convective heat transfer coefficient, W/m^2 K
k	thermal conductivity, W/m K
k_{mG1}	mass transfer coefficient of $(\text{gases and volatiles})_1$ across the film, m/s
k_1, k_2, k_3	rate constants, 1/s
L_1, L_2	constants defined by expressions of k_1 and k_2 respectively, K^2
M	total number of equations used in the simulation of the model
n_1, n_2, n_3	orders of reactions
p	gas pressure, N/m^2
P_1, P_2	variation constants of the parameters defined
Q	heat of reaction number, m^3/kg
r	radial distance, m
R	radius for cylinder and sphere; half thickness for slab, m
R_c	universal gas constant, J/mol
t	time, s
T	temperature, K
W_i	molecular weight of species *i*, kg/mol
x	dimensionless radial distance
X	conversion of biomass

Table 3.3 Notations used in the particle pyrolysis model (continued)

Greek letters	
α	thermal diffusivity, m^2/s
ΔH	heat of reaction, J/kg
$\Delta\tau$	axial grid length
Δx	radial grid distance
ε	emissivity coefficient
ε"	void fraction of particle as defined by Eq. (3.50), ε_0" at initial condition
η	reaction progress variable
θ	normalized temperature
μ	viscosity, kg/m s
ρ	density, ρ_0 at initial condition, kg/m
σ	Stefan Boltzmann constant, $W/m^2 K^4$
τ	dimensionless time
γ	constant defined by Eq. (3.50)
ϕ	permeability, m^2
Dimensionless numbers	
Bi_M	Modified Biot number
Le	Lewis number
Pr	Prandtl number
Q"	Heat of reaction number
Re	Reynolds number
Sh	Sherwood number
Subscripts	
0	initial
B	wood
g	gas
f	final
m	mean
L	light hydrocarbons
V	water vapor

The fraction of each species in the pyrolysed gas depends upon the wood species considered. The pyrolytic decomposition of any wood species is given by Eq. (3.54).

$$C_6H_{HB}O_{OB} \longrightarrow n_{char}C + n_{CO}CO + n_{CO_2}CO_2 + n_{H_2}H_2 + n_{H_2O}H_2O + n_{CH_4}CH_4 + n_{TAR}C_6H_{6.2}O_{0.2} \quad (3.54)$$

$C_6H_{HB}O_{OB}$ is the chemical formula of the dry and ash-free biomass and *n* represents the number of moles of a given species involved in the process. The chemical formula of any biomass species is obtained from its cellulose, hemi-cellulose and lignin contents, using the chemical formulae of these constituents as given in Table-3.4.

The elemental balances of Eq. (3.54) are described through Eqs. (3.55-3.57).

Carbon Balance:

$$6 = n_{char} + n_{CO} + n_{CO_2} + n_{CH_4} + 6n_{tar} \quad (3.55)$$

Hydrogen Balance:

$$HB = 2n_{H_2} + 2n_{H_2O} + 4n_{CH_4} + 6.2n_{tar} \quad (3.56)$$

Oxygen Balance:

$$OB = n_{CO} + 2n_{CO_2} + n_{H_2O} + 0.2n_{tar} \quad (3.57)$$

Eqs. (3.55-3.57) include seven unknown variables ($n_{char}, n_{CO}, n_{CO_2}, n_{CH_4}, n_{tar}, n_{H_2}$ and n_{H_2O}) and to solve them, three more equation are required. Based on the experimental data presented in the form of plots by Boroson et al. (1989), the correlations as given by Eqs. (3.58-3.60) proposed for the product ratios (CO/CO_2, H_2O/CO_2 and light hydrocarbon/CO_2) and reported by Sharma et al. (2006) are used in the present study.

$$\frac{n_{CO}}{n_{CO_2}} = \left(\frac{MW_{CO_2}}{MW_{CO}}\right) e^{-1.845 + \frac{7730.3}{T} - \frac{5019898}{T^2}} \quad (3.58)$$

Table 3.4 Chemical formulas of the biomass constituents (Grobski et al., 1981)

Biomass Constituent	Cellulose	Hemicellulose	Lignin
Chemical Formula	$C_6H_{10}O_5$	$C_6H_{10}O_5$	$C_9H_{7.95}O_{2.4}(OCH_3)_{0.92}$

$$\frac{n_{CO_2}}{n_{H_2O}} = \left(\frac{MW_{H_2O}}{MW_{CO_2}} \right) \; 1.0 \tag{3.59}$$

$$\frac{n_{CH_4}}{n_{CO_2}} = \left(\frac{MW_{CO_2}}{MW_{CH_4}} \right) \; 5.0 \text{ x } 10^{-16} \, T^{5.06} \tag{3.60}$$

Eq. (3.58) gives the molar ratio of carbon monoxide to carbon dioxide variation with absolute temperature in the pyrolysed gas mixture. The mass ratio of water vapor to carbon dioxide [Eq. (3.59)] is taken as unity as suggested by Thunman et al. (2001). The variation of molar ratio of methane to carbon dioxide with absolute temperature in the pyrolysed gas mixture is represented by Eq. (3.60). The molar amount of charcoal production (n_{char}) per mole of biomass is found from the particle pyrolysis model by accounting the average value across the particle radius. Eqs. (3.55-3.60) are solved to get the molar fraction of the species considered (CO, CH_4, CO_2, H_2, H_2O and tar) in the pyrolysed gas.

3.2.1.3 Kinetic Parameter Estimation

The kinetics of pyrolysis plays an important role in the modeling of downdraft biomass gasifier. In the comprehensive model of biomass gasifier, the kinetic scheme based on the mechanism proposed by Koufopanos et al. (1991) is used and described below.

Virgin biomass B (n_1 order decay)

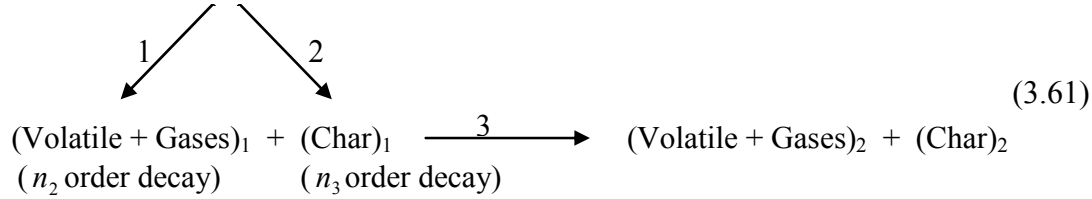

(3.61)

This kinetic scheme assumes that biomass decomposes to volatiles, gases and char. The volatiles and gases may further react with char to produce different types of volatiles, gases and char where the compositions are different. As particle size increases, the

residence time of the volatiles inside the biomass increases and the effects of secondary reactions also increase. The kinetic parameters (activation energy and frequency factors) of the proposed kinetic scheme are found by minimizing the square of the error between the experimental data of thermogravimetry and predicted values of the kinetic model. The kinetic equations for the scheme considered are represented by Eqs. (3.62-3.64).

$$r_1 = k_1 B^{n_1} \tag{3.62}$$

$$r_2 = k_2 B^{n_1} \tag{3.63}$$

$$r_3 = k_3 G_1^{n_2} C_1^{n_3} \tag{3.64}$$

where r_i and k_i are the rate and the kinetic constant of i^{th} reaction, B is the biomass concentration, C_1 is the concentration of Charcoal_1 , and G_1 is the concentration of $(\text{Gas + Volatiles})_1$.

Thermogravimetry data for a biomass sample at any heating rate are commonly reported as % weight loss versus temperature or in terms of residual weight fraction. Generally a small amount (20-500 mg) of the biomass sample is taken in the thermogravimetry experiments. Thus, the secondary reaction [reaction 3 of Eq. (3.61)] can be neglected as the released volatiles would not interact with either char or unreacted biomass. The residual weight fraction in the thermogravimetry experiments is defined as given by Eq. (3.65)

$$\text{Residual Weight Fraction } (W_{\exp}) = \frac{(\text{Residual Weight})}{(\text{Initial Weight})} \tag{3.65}$$

Theoretically, the residual weight fraction is calculated using Eq. (3.66).

$$W_{\text{calc}} = B + C_1 \tag{3.66}$$

The order of reactions 1 and 2 are taken as 1.0. Then, Eqs. (3.62) and (3.63) reduce to Eqs. (3.67) and (3.68) respectively.

$$\frac{dB}{dt} = -(k_1 + k_2)B \tag{3.67}$$

$$\frac{dC_1}{dt} = k_1 B \tag{3.68}$$

The change of residual weight fraction with time [Eq. (3.69)] is obtained by adding Eqs. (3.67) and (3.68).

$$\frac{dW_{\text{calc}}}{dt} = -k_1 B \tag{3.69}$$

To find temperature (T) at a particular time (t), Eq. (3.70) is used.

$$T = (HR)t + T_0 \tag{3.70}$$

where, HR is the heating rate, t is time, and T_0 is the intitial temperature.

Differentiating Eq. (3.70) results in Eq. (3.71).

$$dT = (HR)dt \tag{3.71}$$

Using Eq. (3.69) and Eq. (3.71), the relations of change of residual weight fraction with temperature can be found, which is given by Eq. (3.72).

$$\frac{dW_{\text{cal}}}{dT} = -k_1 B \frac{1}{HR} \tag{3.72}$$

Using Eq. (3.67) and Eq. (3.71), the relation of change of biomass weight fraction with temperature can be found, which is given by Eq. (3.73).

$$\frac{dB}{dT} = -(k_1 + k_2)B \frac{1}{HR} \tag{3.73}$$

Arrhenius relation is given by Eq. (3.74) for reactions 1 & 2 of Eq. (3.61):

$$k_i = A_i \exp\left(\frac{-E_i}{RT}\right) \qquad i = 1, 2 \text{ for reactions 1 \& 2 respectively} \tag{3.74}$$

where, A_i and E_i are frequency factor and activation energy of i^{th} reaction.

Values of the frequency factor and activation energy of both reactions are found by minimizing the objective function as given by Eq. (3.75).

$$F\left(A_{1,}E_1,A_2,E_2\right)=\sum_{j=1}^{n}\left(W_{\exp,j}-W_{\text{cal},j}\right)^2 \tag{3.75}$$

In the model described by Eqs. (3.66-3.75), change of activity with respect to conversion is assumed to be negligible. Thus, activity is taken as unity throughout the pyrolysis. Let us denote it as *Model-KPE1*, which is given below:

Model-KPE1: Rate constants are taken as a function of temperature (Arrhenius relation of kinetic constant with temperature) only, which is represented by Eq. (3.74).

The activity of solid reactant is expected to decrease with the extent of reaction due to the changes in chemical and pore structure of solid. Based on these observations, various other models are proposed in which activity decreases as a function of either conversion or activity itself, which are described by *Model-KPE2 to KPE4.*

Model-KPE2: In this model, the rate of change of activity with respect to normalized conversion $\left(\frac{-da}{dz}\right)$ is expressed as a function of normalized conversion $\left(z=\frac{1-W}{1-W_{\text{final}}}\right)$ as given by Eq. (3.76).

$$\frac{-da}{dz}=\beta\ \ z^n \tag{3.76}$$

where, β is the deactivation rate constant.

Decrease of activity of solid with conversion is obtained by integration of Eq. (3.76) taking activity to be unity when z =0 and is shown by Eq. (3.77).

$$a = 1 - \left(\frac{\beta}{n+1} \right) z^{n+1} \tag{3.77}$$

Activity approaches to zero when dimensionless conversion (z) goes to unity. So variation of reaction rate constants with conversion is obtained, and is given by Eq. (3.78).

$$k_i = A_i \left(1 - z^{n+1}\right) \exp\left(\frac{-E_i}{RT} \right) \qquad i = 1, 2 \text{ for reactions 1 \& 2 respectively} \tag{3.78}$$

The implication of this model is a decrease of frequency factor of pyrolysis rate constants with conversion.

Model-KPE3: In this model, the deactivation process is considered to be directly proportional to activity itself, as given by Eq. (3.79).

$$\frac{-da}{dz} = \beta \quad a \tag{3.79}$$

Integration of Eq. (3.79) and considering the activity to be unity when $z = 0$, yields the reaction rate constants as given by Eq. (3.80):

$$k_i = A_i \exp\left[-E_i \left(\frac{1 + \beta' Tz}{RT} \right) \right] \qquad i = 1, 2 \text{ for reactions 1 \& 2 respectively} \tag{3.80}$$

where $\beta' = \dfrac{\beta R}{E}$ (3.81)

This model predicts an increase of activation energy of pyrolysis with conversion.

Model-KPE4: For further improvement of *Model-KPE3* to incorporate the non-linear variation, change of activity is expressed as given by Eq. (3.82)

$$\frac{-da}{dz} = \beta \quad a \quad z^n \tag{3.82}$$

From this model, the variation of apparent rate constant is found using Eq. (3.83).

$$k_i = A_i \exp\left[-E_i\left(\frac{1+\beta' T z^{n+1}}{RT}\right)\right] \qquad i = 1, 2 \text{ for reactions 1 \& 2 respectively} \qquad (3.83)$$

where $\beta' = \left(\frac{\beta}{n+1}\right)\frac{R}{E}$ (3.84)

This model also predicts an increase in activation energy with fractional conversion. For a special case of n=0, *Model-KPE4* reduces to *Model-KPE3*. Values of the frequency factors (A_1 and A_2), activation energies (E_1 and E_2), deactivation rate constant (β) and power of fractional conversion (n) of both reactions are found by minimizing the objective function as given by Eq. (3.85).

$$F(A_1, E_1, A_2, E_2, \beta, n) = \sum_{j=1}^{n}\left(W_{\exp,j} - W_{cal,j}\right)^2 \qquad (3.85)$$

It may be noted that Eq. (3.85) is a modified and an improved version of Eq. (3.75), which takes into account of the changes that are incorporated in *Models KPE2-4*.

3.2.2 Combustion

The biomass present in the oxidation zone reacts with oxygen to form carbon dioxide, which provides heat for the subsequent gasification reactions. In complete combustion, carbon present in biomass is completely converted to carbon dioxide while hydrogen is converted to water vapor. It is an exothermic reaction and yields temperatures in the range of 1000 °C to 1500 °C. In the present model, complete combustion of biomass is assumed which can be ensured by supplying excess air (usually around 20%) than stoichiometrical requirement. The combustion reaction therefore is represented as given by Eq. (3.86)

$$C_6H_{HB}O_{OB} + \left(6 + \frac{HB}{4} - \frac{OB}{2}\right)\ O_2 \longrightarrow 6CO_2 + \frac{HB}{2}H_2O \qquad (3.86)$$

The volatile products generated in the pyrolysis zone flow downwards and enter into the oxidation zone where a part of volatiles gets oxidized. It is assumed that the tar present in the pyrolysed gas mixture completely gets decomposed due to very high temperature present in the oxidation zone. The tar decomposition is represented by Eq. (3.87).

$$C_6H_{6.2}O_{0.2} + 7.45O_2 \longrightarrow 6CO_2 + 3.1H_2O \quad (3.87)$$

3.2.3 Reduction

The main components of the gaseous mixture leaving the combustion zone are carbon dioxide, water vapor, inert nitrogen, carbon monoxide, hydrogen and some amount of low molecular weight hydrocarbons such as methane, ethane, ethylene etc. In the reduction zone, the gaseous mixture passes through the hot porous charcoal bed resting above the grate. The reduction zone is often referred as gasification zone. Giltrap et al. (2003) developed a model of reduction zone of downdraft biomass gasifier to predict the composition of producer gas under steady state operation. The accuracy of the model is limited by the availability of data on the initial conditions at the top of the reduction zone. Moreover they assumed that the char reactivity factor (*CRF*) which represents the reactivity of char and the key variable in simulation is constant throughout the reduction zone. In this study, Giltrap's model (2003) is modified by incorporating the variation of *CRF* along the reduction zone of downdraft biomass gasifier. It is assumed that *CRF* is exponentially increasing along the bed length of the reduction zone. Solid carbon in the form of char is assumed to be present throughout the reduction zone. The model proposed in this study uses the reaction kinetic parameters developed by Wang and Kinoshita (1993) and the adopted reaction scheme as given by Eqs. (3.88-3.91).

$$C + CO_2 \longleftrightarrow 2CO \qquad \Delta H = 1{,}72{,}600 \text{ J/mol} \quad (3.88)$$

$$C + H_2O \longleftrightarrow CO + H_2 \qquad \Delta H = 1{,}31{,}400 \text{ J/mol} \quad (3.89)$$

$$C + 2H_2 \longleftrightarrow CH_4 \qquad \Delta H = -75{,}000 \text{ J/mol} \tag{3.90}$$

$$CH_4 + H_2O \longleftrightarrow CO + 3H_2 \qquad \Delta H = 2{,}06{,}400 \text{ J/mol} \tag{3.91}$$

The model assumes a cylindrical gasifier bed of uniform cross-sectional area *A* with negligible radial variation in the properties of both the bed and gas. The molar balance and energy balance yield in a set of equations [Eqs. (3.92-3.100)] as given in Table-3.5. The species considered here are nitrogen, carbon dioxide, carbon monoxide, methane, water vapor and hydrogen. Table-3.6 shows the notations used in the reduction model equations.

3.2.4 Numerical Solution and Simulation

The mathematical model [Eqs. (3.22-3.100)] is simulated to predict the outlet composition of the producer gas. The algorithm, described in the following sections, involves the simulation of pyrolysis zone followed by combustion and reduction zones.

3.2.4.1 Simulation of Particle Model

Eqs. (3.39) and (3.43) are discretized by a finite difference method using a pure implicit scheme. The pure implicit scheme is an unconditionally stable scheme, i.e. there is no restriction on time step in sharp contrast with the Euler and Crank-Nicholson method discussed by Ghoshdastidar (1998). The discretized form of Eqs. (3.39) and (3.43) are solved by the Tri-Diagonal Matrix Algorithm (TDMA) also known as the Thomas Algorithm (Carnahan et al., 1969). The initial and boundary conditions represented by Eqs. (3.44-3.48) are applied to solve them numerically. Eqs. (3.38-3.43) are solved simultaneously. Eqs. (3.38) and (3.40-3.43) are solved by finite difference explicit method. The values of the various parameters employed for the simulation of particle model are listed in Tables-3.7 and 3.8.

Table 3.5 Reduction model equations

Type	Model Equation	Eq No
Molar Balance	$\frac{dn_x}{dz} = \frac{1}{v}\left(R_x - n_x \frac{dv}{dz}\right)$	(3.92)
Energy Balance	$\frac{dT}{dz} = \frac{1}{v\sum_x n_x c_x}\left(-\sum_i r_i \Delta H_i - v\frac{dP}{dz} - P\frac{dv}{dz} - \sum_x R_x c_x T\right)$	(3.93)
Velocity Variation	$\frac{dv}{dz} = \frac{1}{\sum_x n_x c_x + nR}\left(\frac{\sum_x n_x c_x \sum_x R_x}{n} - \frac{\sum_i r_i \Delta H_i}{T} - \frac{dP}{dz}\left(\frac{v}{T} + \frac{v\sum_x n_x c_x}{P}\right) - \sum_x R_x c_x\right)$	(3.94)
Pressure Gradient	$\frac{dP}{dz} = 1183\left(\rho_{\text{gas}} \frac{v^2}{\rho_{\text{air}}}\right) + 388.19\, v - 79.896$	(3.95)
Rate Equations for the Proposed Reaction scheme	$r_1 = n\, CRF\, A_1 \exp\left(\frac{-E_1}{RT}\right)\cdot\left(P_{CO_2} - \frac{P_{CO}^2}{K_1}\right)$ $A_1 = 3.616\text{x}10^{1}\text{s}^{-1}$; $E_1 = 77.39$ kJ/mol	(3.96)
	$r_2 = n\, CRF\, A_2 \exp\left(\frac{-E_2}{RT}\right)\cdot\left(P_{H_2O} - \frac{P_{CO}\cdot P_{H_2}}{K_2}\right)$ $A_2 = 1.517\text{x}10^{4}\text{s}^{-1}$; $E_2 = 121.62$ kJ/mol	(3.97)
	$r_3 = n\, CRF\, A_3 \exp\left(\frac{-E_3}{RT}\right)\cdot\left(P_{H_2}^2 - \frac{P_{CH_4}}{K_3}\right)$ $A_3 = 4.189\text{x}10^{-3}\text{s}^{-1}$; $E_3 = 19.21$ kJ/mol	(3.98)
	$r_4 = n\, CRF\, A_4 \exp\left(\frac{-E_4}{RT}\right)\cdot\left(P_{CH_4}\cdot P_{H_2O} - \frac{P_{CO}\cdot P_{H_2}^3}{K_4}\right)$ $A_4 = 7.301\text{x}10^{-2}\text{s}^{-1}$; $E_4 = 36.15$ kJ/mol	(3.99)
Equation of CRF Variation	$CRF = A\, e^{Bx}$ where A = 1, B = 0.0037 and x = reduction zone bed length	(3.100)

Table 3.6 Notations used in the reduction model equations

A	Cylindrical bed area (m^2)
A_i	Frequency Factor for reaction i (1/s)
c_x	Molar heat capacity (J/mol K)
CRF	Char reactivity factor
E_i	Activation Energy of reaction i (Joules /mol K)
f_p	Fraction of pyrolysis
K_i	Equilibrium constant of reaction i
L_n	Normalized length
L_{in}	Initial normalized length at which 85% of the total composition change
n_x	Molar density of species x (mol/m^3)
n	Summation of n_x of all species
P_x	Partial pressure of gaseous species x (Pa)
r_i	Rate of reaction i (mol/m^3 s)
R_x	Rate of formation of species x (mol/m^3 s)
R	Gas constant (J/mol K)
T	Temperature (K)
v	Superficial gas velocity (m/s)
z	Axial distance (m)

Greek Letters

ρ	Density (kg/m^3)

Subscript

i	Reaction number
x	Species N_2, CO_2, CO, CH_4, H_2O, H_2

Table 3.7 Values of parameters used in the numerical solution of the model

Property	Value	Source
Convective heat transfer coefficient	$h = 8.4$ W/m^2 K	Pyle and Zaror (1984)
Wood specific heat	$C_p = 1112.0 + 4.85(T - 273)$, J/kg K	Koufopanos et al. (1991)
Char specific heat	$C_p = 1003.2 + 2.09(T - 273)$, J/kg K	Koufopanos et al. (1991)
Wood thermal conductivity	$k = 0.13 + 0.0003(T - 273)$, W/m K	Koufopanos et al. (1991)
Char thermal conductivity	$k = 0.08 - 0.0001(T - 273)$, W/m K	Koufopanos et al. (1991)
Heat of reaction	$\Delta H = -255000$ J/kg	Koufopanos et al. (1991)
Initial thermal diffusivity of wood	$\alpha = 1.79 \times 10^{-7}$ m^2/s	Jalan and Srivastava (1999)
Rate constant of reaction 1	$k_1 = A_1 \exp[(D_1 / T) + (L_1 / T^2)]$ where $A_1 = 9.973 \times 10^{-5}\ s^{-1}$; $D_1 = 17254.4$ K $L_1 = -9061227$ K^2;	Koufopanos et al. (1991)
Rate constant of reaction 2	$k_2 = A_2 \exp[(D_2 / T) + (L_2 / T^2)]$ where $A_2 = 1.068 \times 10^{-3}\ s^{-1}$; $D_2 = 10224.4$ K $L_2 = -6123081$ K^2	Koufopanos et al. (1991)
Rate constant of reaction 3	$k_3 = A_3 \exp[(-E_3 / RT)]$ $A_3 = 5.7 \times 10^5\ s^{-1}$ $E_3 = 81$ kJ/mol	Koufopanos et al. (1991)
Heat capacity of (gases and volatiles)$_1$	$\overline{C}_{PG_1} = 1 + P_1(\theta - 1); P_1 = 0.001$	Fan et al. (1977)
Effective diffusivity of (gases and volatiles)$_1$	$\overline{D}_{G_1} = (\theta)^{P_1} \exp\{P_2(1 - \overline{C}_B)\}; P_1 = 1.5; P_2 = 1.0$	Fan et al. (1977)
Sherwood number	$Sh = P_1(\theta)^{P_3}; P_1 = 50{,}000; P_2 = 0.75$	Fan et al. (1977)
Lewis nuber	$Le = 2.0$	Fan et al. (1977)

Table 3.8 Nominal values of parameters employed in the present study

Parameters	Values
Geometry factor	b =1, dimensionless
Order of reaction 1	n_1=0, dimensionless
Order of reaction 2	n_2 =1.5, dimensionless
Order of reaction 3	n_3=1.5, dimensionless
Particle radius range	R =0.0127 m
Emissivity coefficient	ε =0.95, dimensionless
Stefan Boltzmann constant	$\sigma = 5.67 \times 10^{-8}$ W/m^2 K^4
Initial density of wood	$\rho_0 = 1170$ kg/m^3

Eqs. (3.55-3.60) are solved to find the molar fraction of the species considered (CO, CH_4, CO_2, H_2, H_2O and tar) in the pyrolysed gas.

3.2.4.2 Simulation of Transport Model for Gas Phase in Pyrolysis Zone

Eq. (3.23) is solved numerically by a finite difference method using a pure implicit scheme. The initial and boundary conditions given by Eqs. (3.24-3.25) are used. The discretized form of Eq. (3.23) is solved by the Tri-Diagonal Matrix Algorithm (TDMA). Eq. (3.26) is solved simultaneously to find the velocity of gaseous mixture in the packed bed pyrolysis zone of the downdraft biomass gasifier.

3.2.4.3 Simulation of Combustion Model

Based on the amount of air supplied in combustion zone and the tar present in pyrolysed gas, the amount of CO_2 produced stoichiometrically is found using combustion reactions given by Eqs. (3.86) and (3.87). Inert N_2, produced CO_2 and H_2O are assumed to mix completely with the pyrolysed gas leaving the pyrolysis zone.

3.2.4.4 Simulation of Reduction Model

The initial position in this model is the top of the reduction zone and the end of the oxidation zone. Gases leaving the oxidation zone are a mixture of pyrolyzed gas, incombustible CO_2 and inert N_2. Eqs. (3.92-3.100) are solved simultaneously using the finite difference explicit method. The results (temperature, velocity, and molar flow rate of each component) obtained from the simulation of combustion model are used as the input data for simulation of reduction model.

3.2.4.5 Simulation for Estimation of Kinetic Parameters

The objective functions [Eq. (3.75) and Eq. (3.85)] are highly nonlinear and complex in nature, having local optima (non-concave). Most of the traditional optimization

algorithms based on gradient methods have the possibility of getting trapped at local optimum depending upon the degree of non-linearity and initial guess (Babu, 2004). In the recent past, nontraditional search and optimization techniques (evolutionary computation) based on natural phenomenon such as genetic algorithms (GAs), differential evolution (DE), etc. (Goldberg, 1989; Price and Storn, 1997; Babu and Sastry, 1999; Ownubolu and Babu, 2004) have been developed to overcome these problems. One such population based search algorithm, DE, which is simple & robust and has proven successful record, is applied. The details of DE algorithm and pseudo code are available in literature (Angira and Babu, 2006; Babu, 2004; Babu and Angira, 2004, 2005; Babu et al. 2005; Babu and Munavar, 2007; Ownubolu and Babu, 2004). The key parameters of control in DE are: *NP*- the population size, *CR*-the cross over constant, and *F* the weight applied to random differential (scaling factor). These parameters are problem dependent. However, certain guidelines and heuristics are available for the choice of these parameters (Babu, 2004; Price and Storn, 1997). Based on these heuristics, the values of DE key parameters for the present problem are set as NP = 40, 80, 200, 300; CR = 0.9; F = 0.5. To find the theoretical value of the residual weight fraction (W_{calc}), forward finite difference technique (Ghoshdastidar, 1998; Gerald and Wheatley, 1994) is applied to Eqs. (3.72-3.74) with the following initial conditions.

At time $t = 0$; $T_0 = 325$ K; $B = 1.0$; $C_1 = 0.0$; $G_1 = 0.0$.

The results generated by simulation of the entire biomass gasification model are discussed in chapter 5 (results and discussion). In order to validate this model, the experiments are performed, the details of which are discussed in the next chapter (Experimental Studies).

CHAPTER – 4

EXPERIMENTAL STUDIES

In this chapter, the detailed description of experimental work, carried out for validating the model developed in this study (Chapter 3) and the effective utilization of wood waste as a biomass in a downdraft gasifier, is described.

4.1 Experimental Setup

The main equipment of the experimental set up is an Imbert downdraft biomass gasifier. An Imbert downdraft biomass gasifier is the one, which has throated combustion zone and different diameter for pyrolysis and reduction zones unlike stratified downdraft biomass gasifier in which diameter of the gasifier is uniform through out (Reed and Das, 1988). Biomass is fed from top of the gasifier and air is introduced through nozzle in the combustion zone. The downdraft gasifier converts the solid biomass into a combustible gas, generally known as a producer gas. Biomass undergoes pyrolysis and gets oxidized in the combustion zone near air inlet. The pyrolysed gas mixture and the gases produced due to combustion passes over the charcoal bed resting above the grate and generate producer gas. The details of the gasification are given in the section 4.1.1. The schematic diagram of the experimental setup is shown in the Fig. 4.1 and photograph of the same is shown in Plate-4.1. A rotameter and a pressure gauge are used to measure the flow rate

and pressure respectively of air. Provisions are made to measure the temperature inside the gasifier at various locations along the axial length of the gasifier. Plate-4.1 shows temperature indicators used to measure the temperature inside the gasifier. The details of the temperature measurement are discussed in section 4.1.2.

The producer gas generated in the downdraft biomass gasifier is sampled using airtight syringes (100 ml) and analyzed using gas chromatograph (NUCON 5765) with thermal conductivity detector (TCD). The photograph of gas chromatograph showing carrier gas cylinder, oven, temperature control unit, TCD and FID (flame ionization detector) modules, data station, and a desktop computer is displayed in Plate-4.2.

4.1.1 Details of Gasification

The downdraft gasifier has four distinct reaction zones: (1) drying, (2) pyrolysis, (3) oxidation and (4) reduction. The schematic diagram of the Imbert downdraft biomass gasifier used in the study is shown in Fig.4.2a. In downdraft gasifiers, pyrolysed gas and moisture generated in pyrolysis and drying zone respectively flow downwards. The pyrolysis gases pass through a combustion zone followed by a hot bed of char which is supported by a grate. Biomass is fed to the gasifier and oxidized in the zone where continuous air is supplied from two air nozzles. The heat generated in the combustion zone gets transferred to the pyrolysis, drying and reduction zones. The released heat from biomass combustion raises the temperature of the biomass particles resting above the oxidation zone and thus they get pyrolysed. The biomass particles are decomposed into volatiles and charcoal in the pyrolysis zone. The released volatiles from each of the biomass particles flow downward in the packed pyrolysis bed.

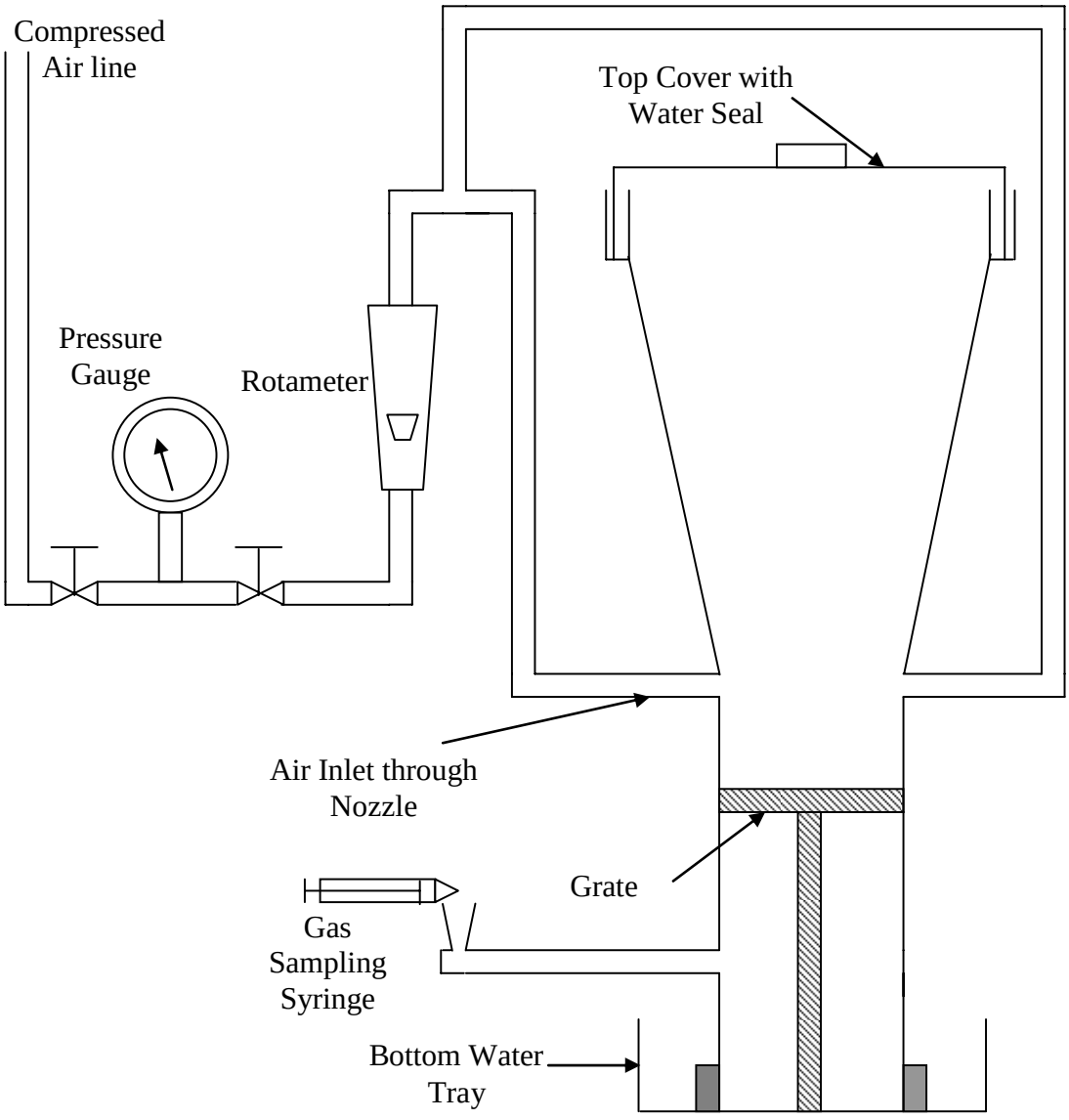

Fig. 4.1 Schematic of the gasification experimental setup

Plate-4.1 Photograph of the downdraft biomass gasifier

.

Plate-4.2 Photograph of the gas chromatograph

The rate of volatiles release depends on particle size and temperature within the particle. Due to the high temperature of combustion zone, tar of the pyrolysed gas mixture cracks into non-condensable gases and water. The cracked pyrolysed gas mixes with the carbon dioxide generated due to combustion and the inert nitrogen present in the air. This hot gaseous mixture passes over the bed of charcoal and undergoes endothermic reduction reactions. The producer gas, leaving the grate placed below the reduction zone, is sent to a burner via a gas line. Water tray is placed below the gasifier to make sure that there is no leakage of producer gas. Water seal is also provided at the top of the gasifier to direct the flow downwards.

The total height of the gasifier is 1.1 m. The diameter at the pyrolysis zone is 0.31 m and the diameter at the reduction zone is 0.15 m. The height of the reduction zone is 0.1 m and that of oxidation zone is approximately 0.053 m. The height of the pyrolysis zone depends upon the biomass loading. The charcoal in the reduction zone is supported by a movable grate at the bottom of the gasifier. The ash produced during gasification is removed by rotating the grate using the lever arrangement provided to unclog the grate. By moving the grate, grate clogging and bridging of the biomass can be avoided thereby ensuring a continuous gasification of biomass.

4.1.2 Temperature Measurement

Thermocouples are placed at various locations along the axial length of the gasifier to measure the temperature of various zones in the gasifier, and a digital multi channel temperature indicator (Make: Thermotech, Model: TH 046, L3001) with auto scan facility is used to display the temperature. Five pairs of chromel-alumel and one pair of platinum-rhodium thermocouples are used. Each pair is placed at different heights along

the axial length of the gasifier (Fig. 4.2b) so as to cover all the zones. In each pair, one thermocouple is placed at the center of the gasifier ($r = 0$) while the other is placed at a half radius distance ($r = R/2$). Two pairs of thermocouples are placed in the reduction zone of the gasifier, one at the end of the reduction zone that is close to the grate and one at a height of 0.046 m from the grate. One pair of thermocouples is placed in the oxidation zone present at the level of the air inlet nozzles. Three pairs of the thermocouples are placed in the pyrolysis zone at different heights of 0.237 m, 0.328 m, and 0.428 m from the grate respectively in the biomass gasifier. Plate-4.3 is a photograph of the inside view of the biomass gasifier, which shows thermocouples sheathed in the stainless steel tubes at different heights in the gasifier.

4.2 Materials

The biomass used in the present study is the waste generated in furniture making, collected from the carpentry section of the workshop at Birla institute of Technology and Science, Pilani. Mainly two wood species are used to make furniture in the workshop namely *Dalbergia sisoo,* commonly known as sesame wood or rose wood and teak wood. Teak wood is costlier in comparison to sesame wood and also not easily available. Generally the furniture waste is used either for direct combustion or sold to pottery makers at a very cheap rate. Wastage generated during furniture preparation of sesame wood is collected and cut into appropriate sizes to feed the downdraft biomass gasifier. Plate 4.4 shows the photograph of the biomass material used in the gasification studies. Table-4.1 lists the physical properties, the proximate analyses, ultimate analyses and chemical analyses of *dalbergia sisoo*.

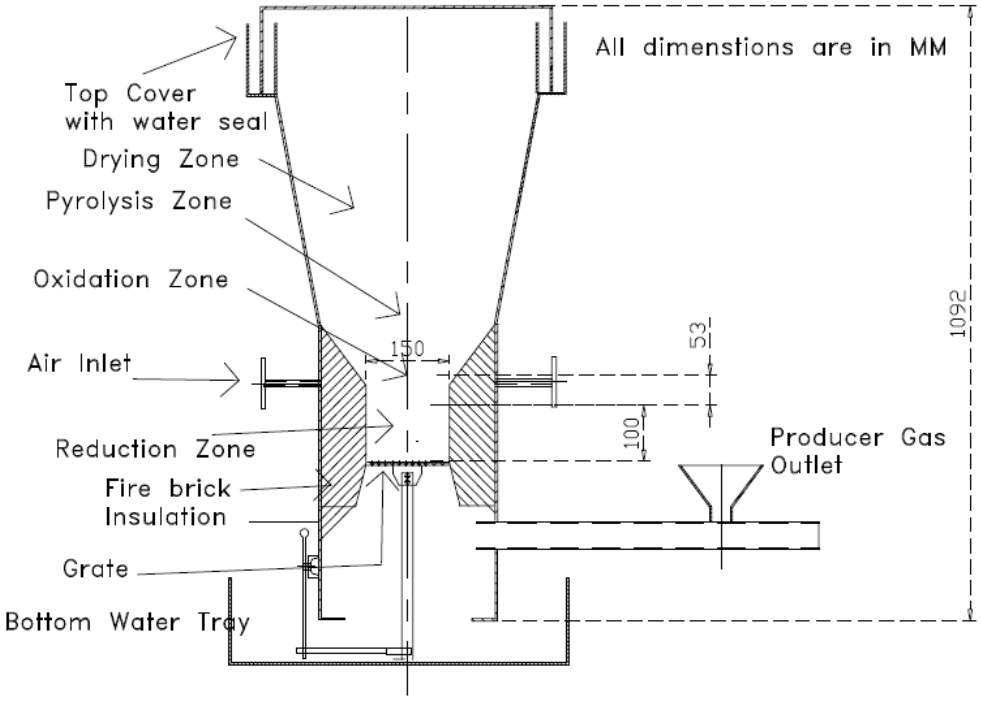

(a) Various parts, zones and dimensions of the unit

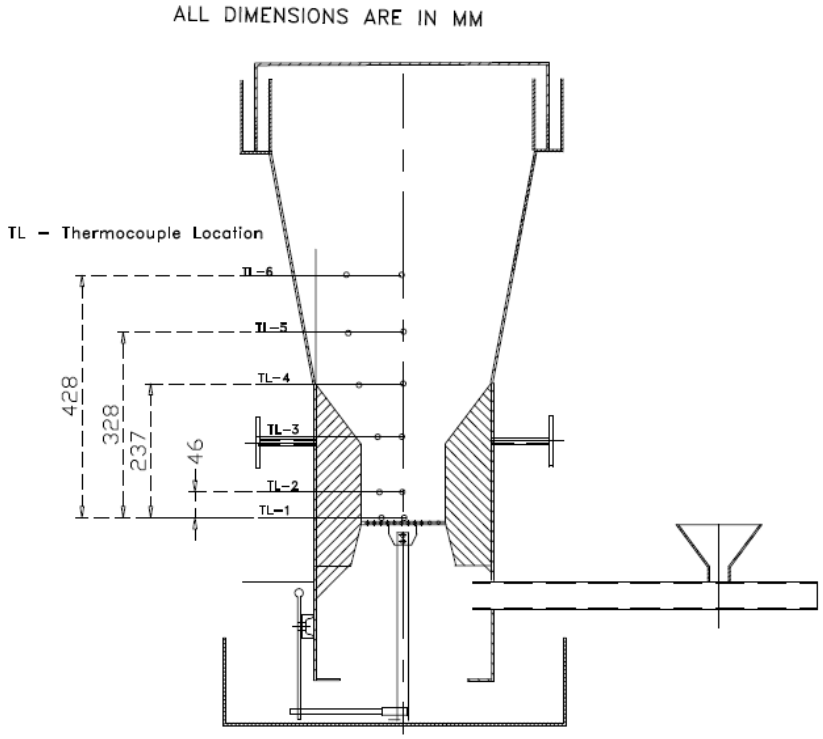

(b) Location of thermocouples

Fig. 4.2 Schematic diagram of Imbert downdraft biomass gasifier used in the experiments

Plate 4.3 Photograph of the inside view of the biomass gasifier

Plate 4.4 Photograph of the wood waste (size: approx. 1 inch cube)

Table 4.1 Characteristics of *Dalbergia sisoo*

Physical Properties			
Size (mm^3)	Absolute Density (kg/m^3)	Bulk Density (kg/m^3)	
25.4 x 25.4 x 25.4	1170	605	
Proximate Analysis (% by wt. dry basis)*			
Fixed Carbon (FC)	Volatile Matter (VM)	ASH	Calculated HHV (MJ/kg)
15.70	80.40	3.90	18.06
Ultimate Analysis (% by wt. dry basis)*			
Carbon	Hydrogen	Oxygen	Nitrogen
48.6	6.2	44.87	0.33
Chemical Analysis (% by wt.)*			
Cellulose	Hemi cellulose	Lignin	Extractives
36.75	11.30	43.65	8.30

*Source: Bhave (2001)

Higher heating value (HHV) of the biomass used in this study is computed using the empirical formula given by Eq. (4.1) reported in the literature (Parikh et al., 2005).

$$HHV\ (MJ/kg) = 0.3536\ FC + 0.1559\ VM - 0.0078\ ASH \quad (4.1)$$

4.3 Experimental Procedure

Biomass gasification experiments are carried out covering a wide range of flow rates. During a particular experiment, pressure and flow rate of air are maintained constant. Measurements of temperatures are carried out at various locations in the gasifier and producer gas sample is collected at different time intervals. Subsequently the collected sample is analyzed with Gas chromatography. The experimental procedure is divided in two parts: (1) Gasification, and (2) Producer gas analysis. Both processes are discussed in sections 4.3.1 and 4.3.2 respectively.

4.3.1 Gasification

Water is filled in the container placed below the gasifier and also in the circular trough at the top of the gasifier which acts as a seal and hence it prevents the gas from escaping out of the gasifier. 500 g of charcoal (collected from the residue of the wood based furnace, used for mass cooking locally) is dumped as a heap into the reduction zone of the gasifier above the grate. The initial charcoal used in the present experimentation is of the same quality as that generated in the gasification experiments by pyrolysis of wood. The air is introduced into the biomass gasifier through nozzles and its flow rate, which is maintained constant through a gate valve, is measured using a rotameter. Biomass is dumped into the oxidation zone of the biomass gasifier and around 25 ml of diesel is poured to aid the combustion of biomass. Once combustion starts properly and spread

across the oxidation zone which generally takes about 3 to 4 minutes, additional 3 kg of biomass is dumped inside the gasifier and it is closed from the top by a cover. It is observed that by the time combustion starts properly in the oxidation zone, most of the diesel gets combusted due to the volatility of diesel and a very high temperature is generated in the oxidation zone. The time at which the cover is closed, is taken to be the starting time of the experiment. Temperatures are recorded at each location (as described in Section 4.1.2) after every five minutes. The samples of producer gas leaving the gas burner are collected in the syringes at an interval of five minutes. Sampled gas is analyzed using a gas chromatograph (NUCON 5765) with thermal conductivity detector, the details of which are discussed in Section 4.3.2. Each experimental run is carried out for duration of 25 to 40 min. At the end of an experiment, the leftover biomass and charcoal, if any, is removed from the gasifier. The details of the range of parameters varied in these experiments are shown in Table-4.2. The rate of biomass consumption is found to vary from 1.0 to 3.6 kg/h for an air flow rate varying from 1.85 to 3.4 m^3/h respectively. Moisture content is varied from 0.0254 to 0.164 wt fraction on wet basis.

4.3.2 Producer Gas Analysis

The sampled producer gas is analyzed using a gas chromatograph (NUCON 5765) with thermal conductivity detector (TCD). The gas chromatography, carrier gas selection, and selection of operating parameters such as oven temperature, carrier gas flow rate, etc. are described in subsequent sections.

4.3.2.1 Gas Chromatography

Chromatography is a technique for separating the components of a mixture on the basis of differences in their affinity towards stationary and mobile phase. Gas chromatography

Table 4.2 Details of the biomass gasification experiments

Biomass Species	Run No	Initial moisture content (wt fraction, wet basis)	Air flow rate (Nm^3/h)	Biomass consumption rate (kg/h)
Dalbergia sisoo ($CH_{1.531}O_{0.693}$)	1	0.1145	2.7765	2.10
	2	0.0437	3.3935	3.63
	3	0.0437	1.8510	2.12
	4	0.0437	2.7765	2.67
	5	0.073	2.7765	2.59
	6	0.10	1.8510	1.00
	7	0.1518	2.7765	2.20
	8	0.07	2.1595	1.488
	9	0.044	2.1595	2.12
	10	0.1167	2.1595	1.1626
	11	0.164	2.1595	1.0424

(GC) is a type of chromatography in which there is a mobile phase and a stationary phase. The mobile phase is a carrier gas, usually an inert gas such as helium or an unreactive gas such as nitrogen. The stationary phase is a microscopic layer of liquid or polymer on an inert solid support, inside glass or metal tubing, called a column. The instrument used to perform gas chromatographic separations is called a gas chromatograph. The injected sample gets vaporized in the injector port and travels through the column in a gas state. The interactions of these gaseous analytes with the walls of the column coated with stationary phase causes different compounds to elute at different times called retention time or residence time. The comparison of these retention times is the analytical power of GC.

In a GC analysis, a known volume of gaseous or liquid analyte is injected at the entrance (head) of the column, usually using a micro-syringe or solid phase micro-extraction fibers or a gas source switching system. As the carrier gas sweeps the analyte molecules through the column, this motion is inhibited by the adsorption of the analyte molecules either onto the column walls or onto packing materials in the column. The rate at which the molecules progress along the column depends on the strength of adsorption, which in turn depends on the type of molecule and on the materials of stationary phase. Since each type of molecule has a different rate of progression, the various components of the analyte mixture are separated as they progress along the column and reach the end of the column at different times (retention time). A detector is used to monitor the outlet stream from the column; thus, the time at which each component reaches the outlet and the amount of that component can be determined. Generally, substances are identified

(qualitatively) by the order in which they emerge (elute) from the column and by the retention time of the analyte in the column.

The purpose of a detector is to monitor the carrier gas as it emerges from the column and to generate a signal in response to variation in its composition due to eluted components. Detection devices for GC must respond rapidly to minute concentration of solutes as they exit the column. The speed of response decides the sensitivity of detection device. Other desirable properties of a detector are linear response, good stability, ease of operation, and uniform response to a wide variety of chemical species or, alternately predictable and selective response to one or more classes of solutes. The thermal conductivity detector (TCD) is a non destructive universal detector. It is widely used in gas chromatography for its high reliability, simplicity and ease of operation. The TCD measures the difference in thermal conductivity between the carrier gas flowing through a reference and a sample component mixture flowing through a measuring cell.

4.3.2.2 Carrier Gas Selection

The choice of carrier gas (mobile phase) is important, with hydrogen being the most efficient and providing the best separation. However, helium has a larger range of flowrates that are comparable to hydrogen in efficiency, with the added advantage that helium is non-flammable, and works with a greater number of detectors. Therefore, helium is the most common carrier gas used. Typical carrier gases include helium, nitrogen, argon, hydrogen and air. The carrier gas is usually determined by the detector being used. However, the carrier gas is selected based on the sample's matrix while analyzing gas samples. Safety and availability can also influence carrier selection, for example, hydrogen is flammable, and high-purity helium can be difficult to obtain in

some areas of the world. The purity of the carrier gas is also frequently determined by the detector, though the level of sensitivity needed can also play a significant role. Typically, the purities up to a level of 99.995% or higher are used in the analysis.

Producer gas sample contains mainly CO, CO_2, CH_4, H_2 and N_2. As the mixture contains H_2 and N_2, flame ionization detector can not be used. For quantitative analysis of the producer gas mixture with a TCD, the thermal conductivity difference between carrier gas and the other gases in the sample should be high. Fig. 4.3 shows the variation of thermal conductivity with temperature of various gases with reference to that of air. It shows that thermal conductivity of helium and hydrogen is higher than that of many of the components so any of them can be used as a carrier gas. Helium would be the right choice as a carrier gas as hydrogen may not detect itself while taking it as a carrier gas. However, thermal conductivity difference of hydrogen and helium is very less, and hence detection of hydrogen with helium as a carrier gas would be very difficult. Moreover, the thermal conductivity of hydrogen is higher than that of helium, and so detection of hydrogen with helium as a carrier gas results in a negative peak in comparison to other components such as N_2, CO_2, CO and CH_4. Therefore nitrogen as a carrier gas is used to determine the content of hydrogen while helium is used to determine the amounts of rest of the components.

4.3.2.3 Operating Parameter Selection

The carrier gas flow rate and the oven temperature are the main parameters which are required to be controlled to achieve the separation of gaseous mixture and the analysis of the same. The anylates take less time in passing through the column when carrier gas flow rate is high. It results in a less retention time for the components to be analyzed.

When the number of components in the gaseous mixture is more than one, the difference between retention times of all the components should be high enough to avoid the overlap. The higher flow rate results in a faster analysis, but at the cost of a lower separation between analytes and that leads to a poor analysis. The flow rate selection therefore is the compromise between the level of separation and analysis time. The actual flow rate is measured at the outlet of the column or the detector with a soap bubble flow meter. The temperature of the oven is another important controlling parameter. The higher oven temperature results in a less adsorption of the analyte molecules either onto the column walls or onto packing materials in the column. The increment in temperature, therefore, leads to the same effect as that of increment in flow rate.

To perform the quantitative and qualitative analysis of producer gas, it is essential to know the order in which compound leaves the column and reaches TCD. Thus, the retention time for each component of the producer gas is required to be found. The components get detected by TCD as it passes through it and the chromatograph shows a peak. The area under the peak of is a measure of the amount of the component. The difference of retention time between every two components of the ordered list, should be sufficiently large so that the individual component only reaches TCD at a time and gets detected without any overlapping. A series of experimental runs are conducted to choose the operating conditions for producer gas analysis, which gives effective separation of each component of gaseous mixture in a column and noticeable response by the detector. For the experimental detection of N_2, CO, CO_2, and CH_4 of gaseous mixture, Helium is used as a carrier gas and to detect H_2 in gaseous mixture, Nitrogen is used as a carrier gas.

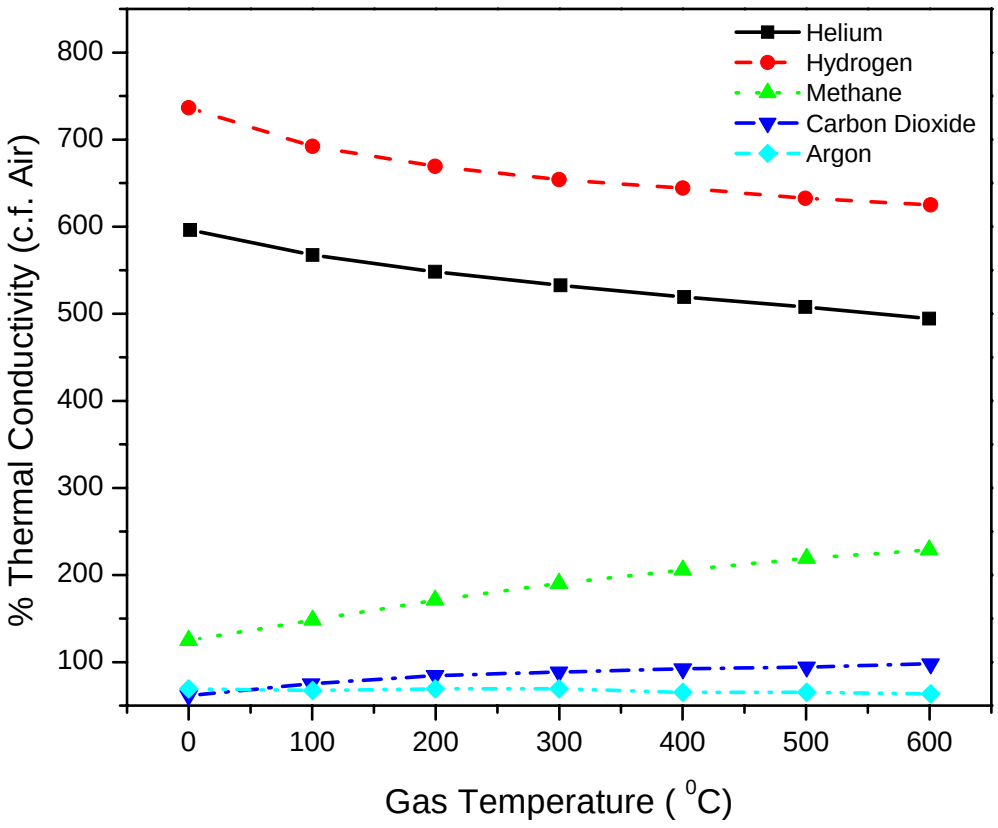

Fig. 4.3 Variation of thermal conductivity with temperature of various gases with reference to that of air [Source: Pellistor (2008)]

Table-4.3 shows the details of operating parameters and settings of the gas chromatography for the experiments carried out to detect N_2, CO, CO_2, and CH_4 of gaseous mixture. The attenuator of TCD module is maintained at 1X position and the polarity button is kept in pressed condition. The first run is carried out with pure CO_2 as a sample to find its retention time. Fig. 4.4 shows the chromatograph displaying the peak of carbon dioxide. The oven is kept at 50 °C and the carrier gas flow rate is fixed at 7.12 ml/min. The retention time of CO_2 is 34 minutes and 42 seconds, as shown in Table-4.3. An additional peak at 6 minute and 37 second is also observed which may be due to the presence of some impurity in the sample.

The second run is carried out with the mixture of N_2 and CO_2 maintaining the same operating conditions used in the experimental run 1. Fig. 4.5 shows the chromatograph displaying the peaks of nitrogen and carbon dioxide. From the value of retention time, it is concluded that the first peak at 6 min 56 seconds is of nitrogen and the second peak is of carbon dioxide. As the retention time of carbon dioxide is very high, carrier gas flow rate is increased to 20.42 ml/min in the third experimental run. The mixture of nitrogen, carbon monoxide and carbon dioxide is injected to find the order in which they leave the column. Fig. 4.6 shows the chromatograph displaying the peaks of N_2, CO and CO_2. The retention time of N_2, CO and CO_2 are 2 min 12 seconds, 3 min 8 seconds and 16 min 36 seconds respectively (Table-4.3). It clearly indicates that CO_2 is taking almost half the time than that it took with the settings of the second run. Nitrogen and carbon monoxide are separated well as shown in Fig. 4.6 although their retention times are very close.

Table 4.3 Experimental details for the selection of operating parameters of GC for the detection of N_2, CO, CH_4, and CO_2

Expt Run No	Carrier gas (He) flow rate (ml/min)	Oven temperature (°C)	Sample loop (ml)	Sample species	Sample injection time (mm:s)	Peak timing (mm:s)	Retention time (mm:s)
1	7.12	50	1	CO_2	0:48	35:30	34:42
2	7.12	50	1	Mixture of N_2 & CO_2	2:02	6:56 40:08	4:54 38:06
3	20.42	50	1	Mixture of N_2 & CO	2:46	4:58	2:12
						5:54	3:08
				CO_2	15:56	32:32	16:36
4	32.26	70	1	Mixture of H_2, N_2, CO, CO_2 & CH_4	0:30	2:06	1:36
						2:38	2:08
						4:37	4:07
						9:49	9:19
5	32.26	70	2.55	Producer gas	0:35	1:25	0:50
						1:53	1:18
						2:25	1:50
						5:16	4:41
						10:00	9:25
					13:20	14:36	1:16
						22:39	9:19
6	14.18	45	1	Mixture of N_2, CO, CO_2	0:44	3:36	2:52
						4:58	4:14
						27:34	26:50

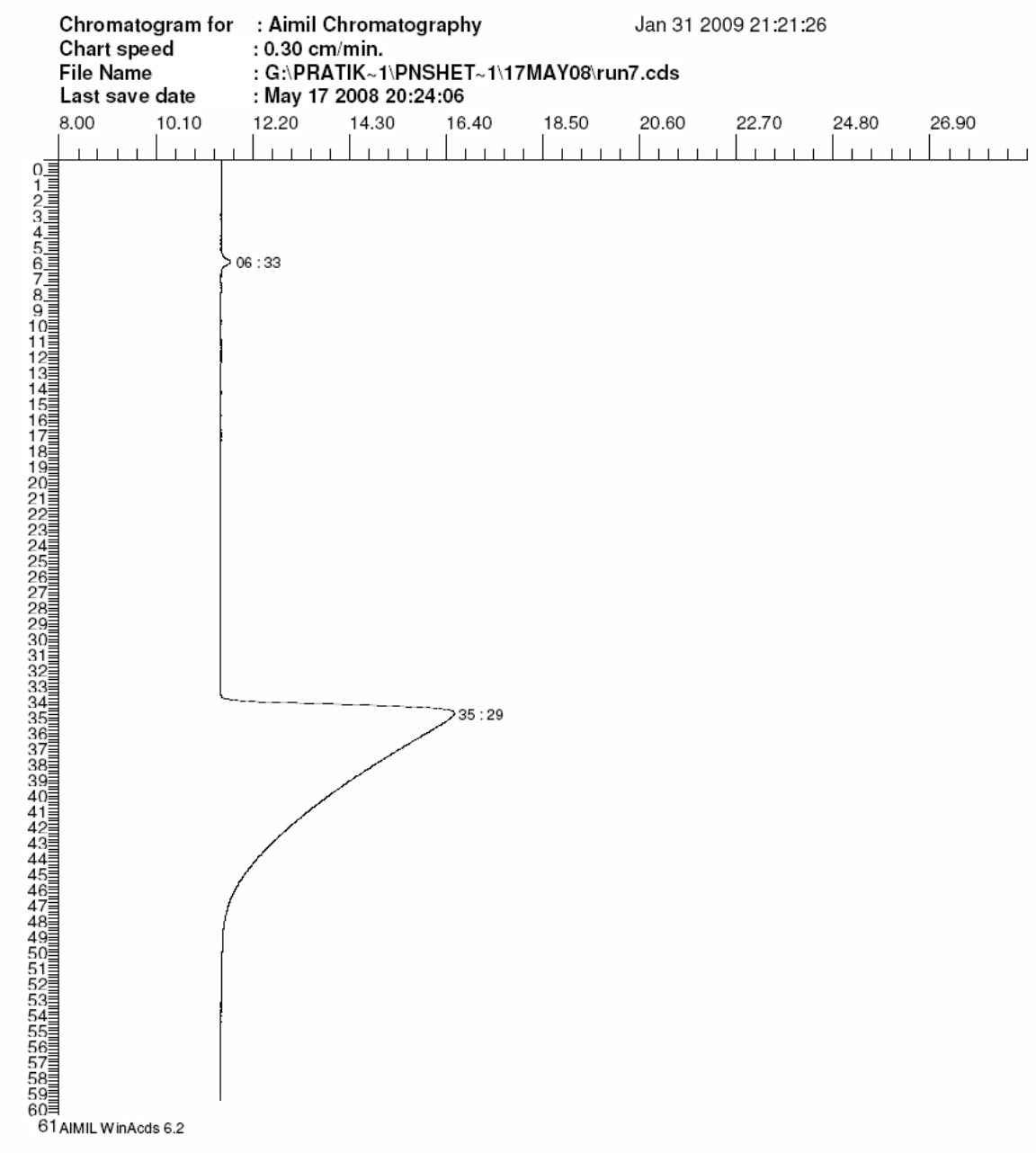

Fig. 4.4 Chromatograph displaying the peak of CO_2 (Run No 1)

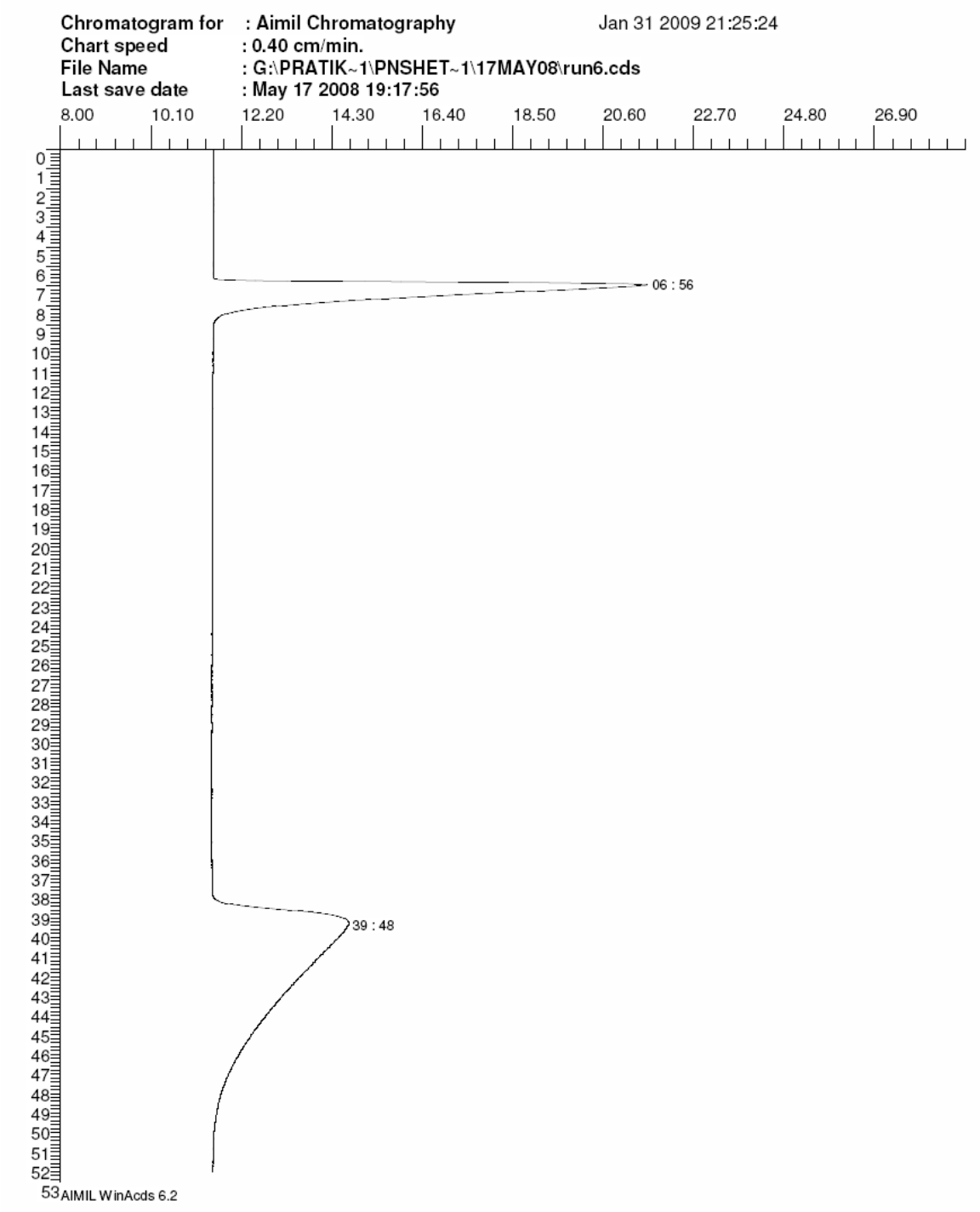

Fig. 4.5 Chromatograph displaying the peaks of N_2 and CO_2 (Run No 2)

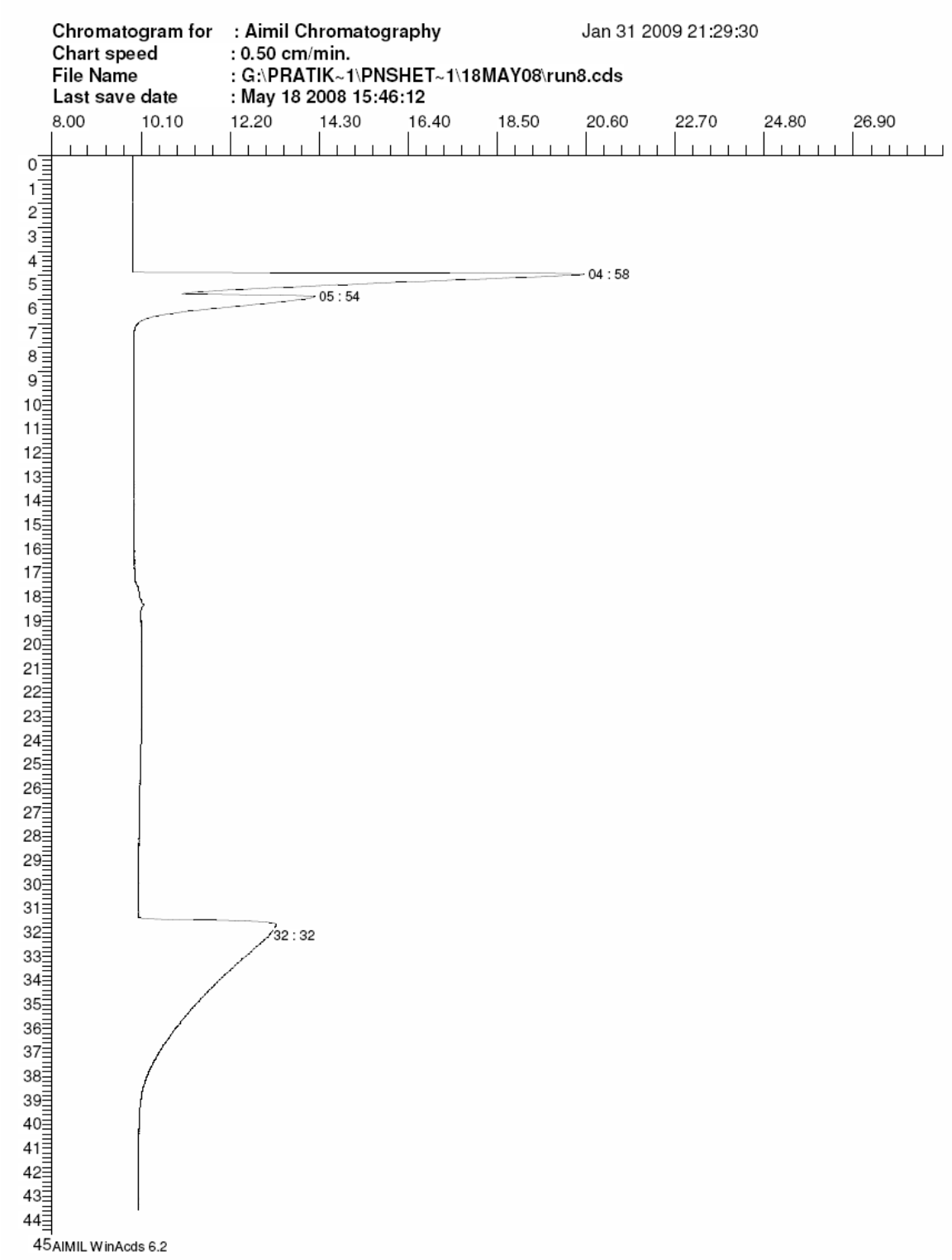

Fig. 4.6 Chromatograph displaying the peaks of N_2, CO and CO_2 (Run No 3)

The fourth run is carried out with a higher flow rate and a higher oven temperature to complete the analysis in a lesser time. A flow rate of 32.26 ml/min and an oven temperature of 70 °C are used in the fourth run. The resulting chromatograph having four peaks is shown in Fig. 4.7. As the thermal conductivity of hydrogen is higher than that of helium, a negative peak is expected. However the H_2 peak is not detected in the chromatograph. And it is concluded that the four peaks correspond to nitrogen, carbon monoxide, methane and carbon dioxide in that order. The analysis gets over within 14 minutes and a clear N_2 and CO separation is obtained without any overlapping.

Hydrogen is not detected by the gas chromatograph with the settings of experimental run 4. To detect the H_2, fifth run is carried out with the same settings as those of the fourth run except higher amount of sample injection. A sample loop of 2.55 ml (loop available in the laboratory with maximum volume) is used in the fifth run. The producer gas sample is collected in a syringe and injected twice by gas sampling valve in an injector at 35 seconds and at 13 min 20 seconds from the start of the experiment. Fig. 4.8 shows the chromatograph displaying a negative peak of H_2 at 1 min 25 seconds and positive peaks of nitrogen, carbon monoxide, methane and carbon dioxide in that order at 1min 53 seconds, 2min 25 seconds, 5 min 16 seconds, and 10 min respectively. In the second injection of producer gas, only two peaks are found, one at 14 min 39 seconds and another at 22 min 39 seconds. It does not show a negative peak of H_2 and moreover the peaks of N_2 and CO gets merged possibly due to a higher concentration of nitrogen. There is no peak of CH_4, may be due to its very low concentration. Thus there is a need to revive the section of operating parameters to incorporate the detection of H_2 and better separation of N_2 and CO.

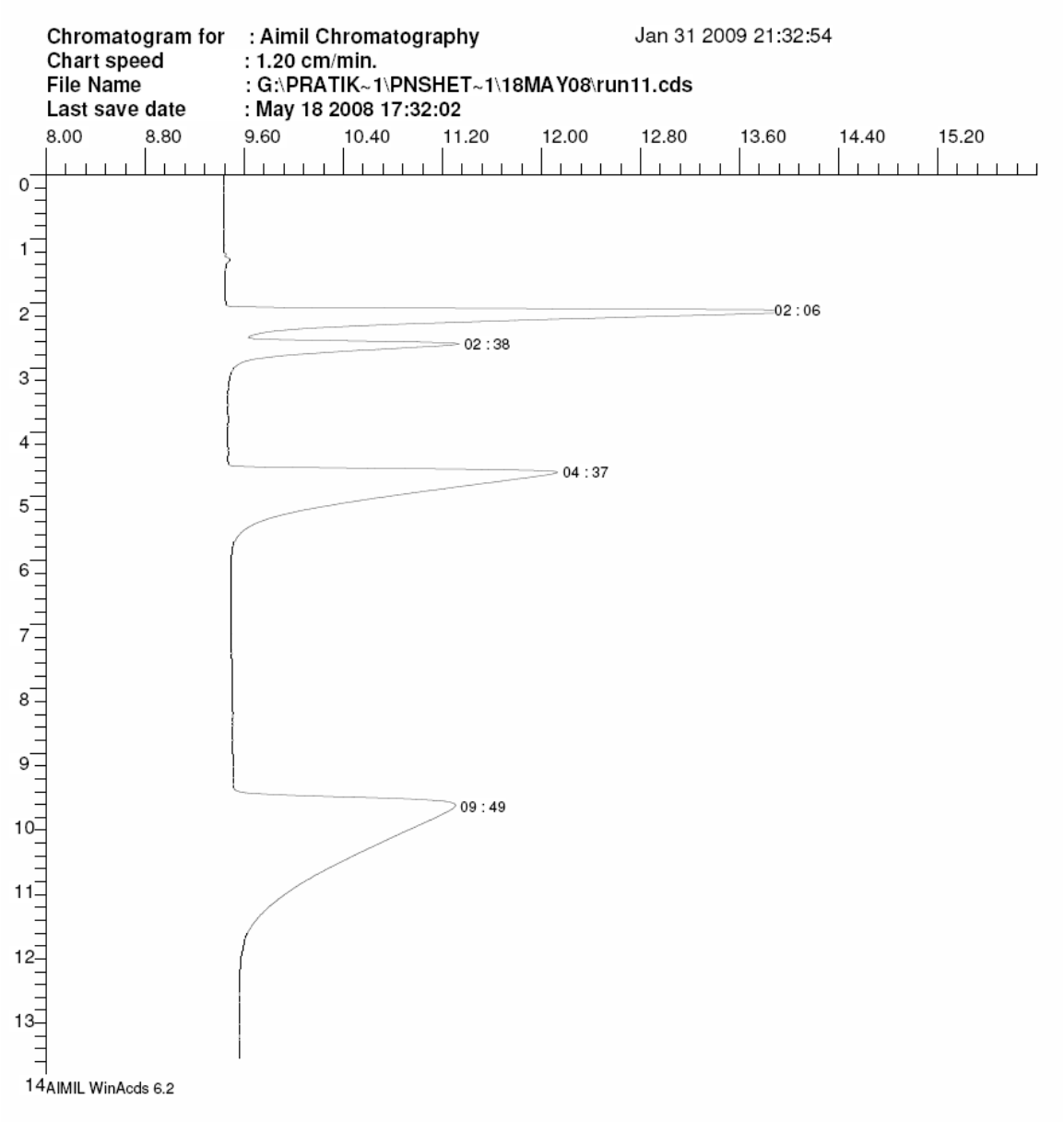

Fig. 4.7 Chromatograph displaying the peaks of N_2, CO, CH_4 and CO_2 (Run No 4)

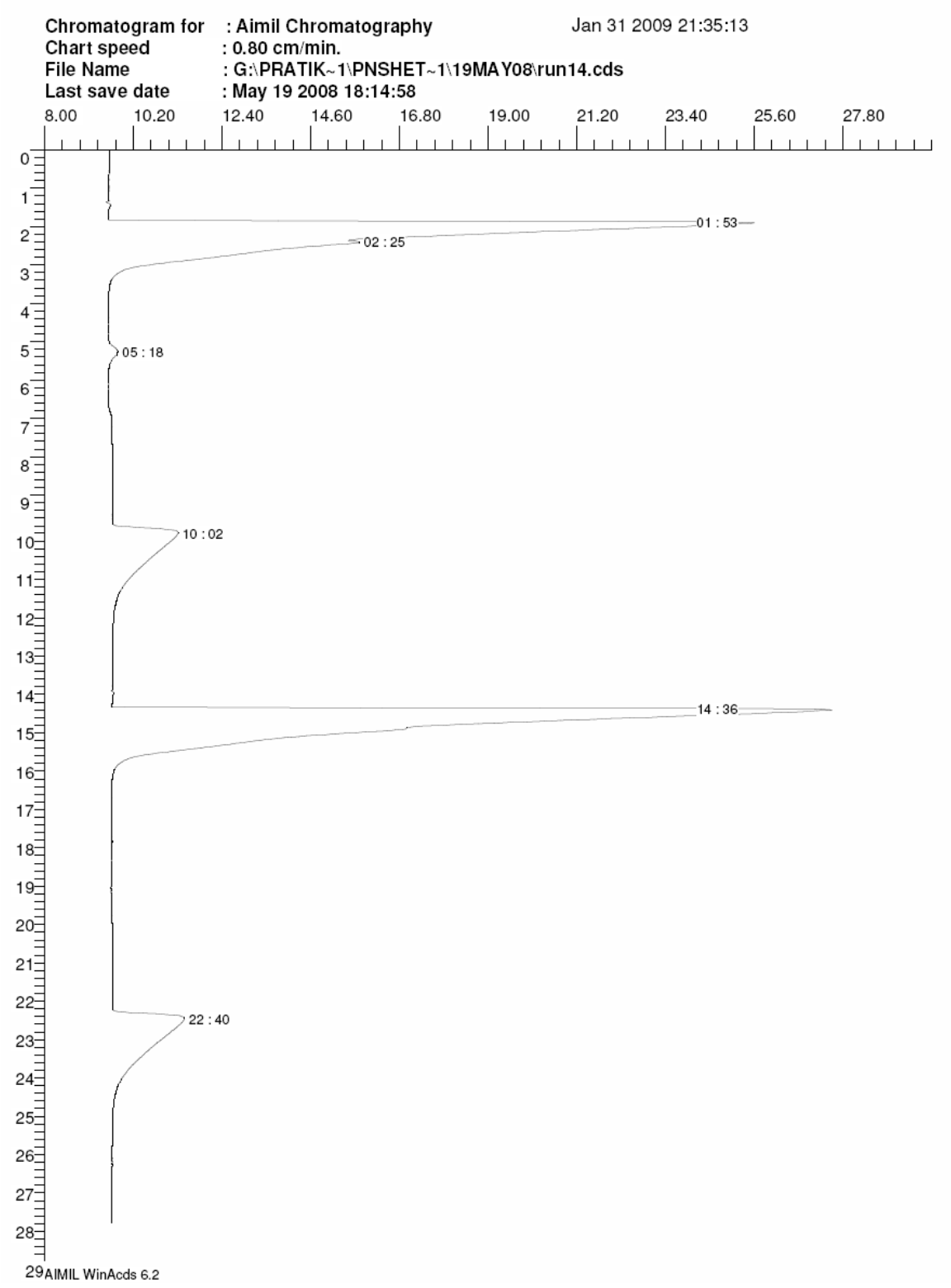

Fig. 4.8 Chromatograph displaying the peaks of N_2, CO, CH_4 and CO_2 (Run No 5)

A wide range of carrier gas flow rates and oven temperatures are tried to perform the detection of hydrogen with helium. It is concluded that detection of hydrogen in a producer gas sample is not possible with helium due to the poor thermal conductivity difference between hydrogen and helium. Based on the results obtained from five experimental runs, carrier gas flow rate of 14.18 ml/min and an oven temperature of 45 °C are proposed as optimum settings (Run No. 6 in Table-4.3) of gas chromatograph to detect N_2, CO, CH_4 and CO_2. Fig. 4.9 shows the resulting chromatograph with the injection of mixture of nitrogen, carbon monoxide and carbon dioxide (Run No. 6).

To detect hydrogen in the producer gas sample, nitrogen as a carrier gas is used. The experiments, the details of which are shown in Table-4.4, are carried out to find the operating parameters of the gas chromatograph to analyze hydrogen. In the first run for hydrogen detection (Run No. 7), carrier gas flow rate is maintained at 14.18 ml/min and an oven temperature is maintained at 80 °C. To find the retention time, hydrogen, carbon dioxide and methane are injected individually into gas chromatograph. Fig. 4.10 shows the chromatograph displaying two peaks of hydrogen and one peak each of carbon dioxide and methane. As can be seen from Fig. 4.10, hydrogen and methane give positive peaks although the thermal conductivity of both hydrogen and methane is higher than that of nitrogen. The positive peaks of hydrogen and methane are due to un-pressed condition of the polarity button in the TCD module. To check the repeatability, hydrogen is injected twice at 1 min 46 seconds and 7 min 16 seconds respectively. The averaged retention time of hydrogen is 2 min 12.5 seconds. It is observed that carbon dioxide gives a negative peak as the thermal conductivity of CO_2 is less than that of nitrogen. The retention time of CO_2 is 9 min 40 seconds.

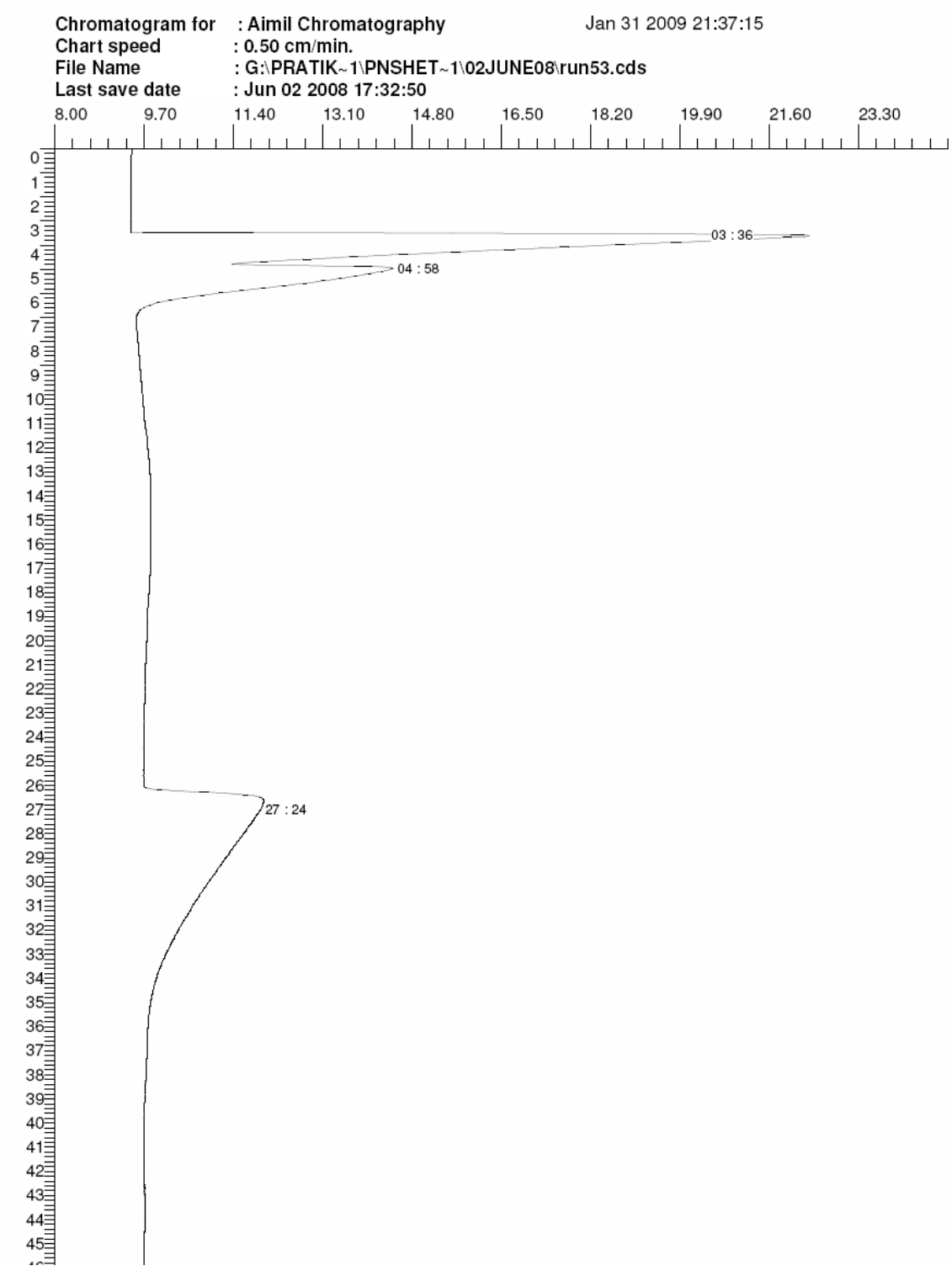

Fig. 4.9 Chromatograph displaying the peaks of N_2, CO and CO_2 (Run No 6)

Table 4.4 Experimental details for the selection of operating parameter of GC for the detection of H_2

Expt Run No	Carrier gas (N_2) flow rate (ml/min)	Oven temperature (°C)	Sample loop (ml)	Sample species	Sample injection time (mm:s)	Peak timing (mm:s)	Retention time (mm:s)
7	14.18	80	2.55	H_2	1:46	3:57	2:11
				H_2	7:16	9:30	2:14
				CO_2	11:50	21:30	9:40
				CH_4	30:36	35:06	4:30
8	14.18	120	2.55	Mixture of H_2, CO, CH_4 & CO_2	0:37	2:25	1:48
						3:00	2:23
						4:37	4:00
						7:20	6:43
9	14.18	110	1.0	Mixture of H_2 and CO	1:54	3:30	1:36
						4:11	2:17

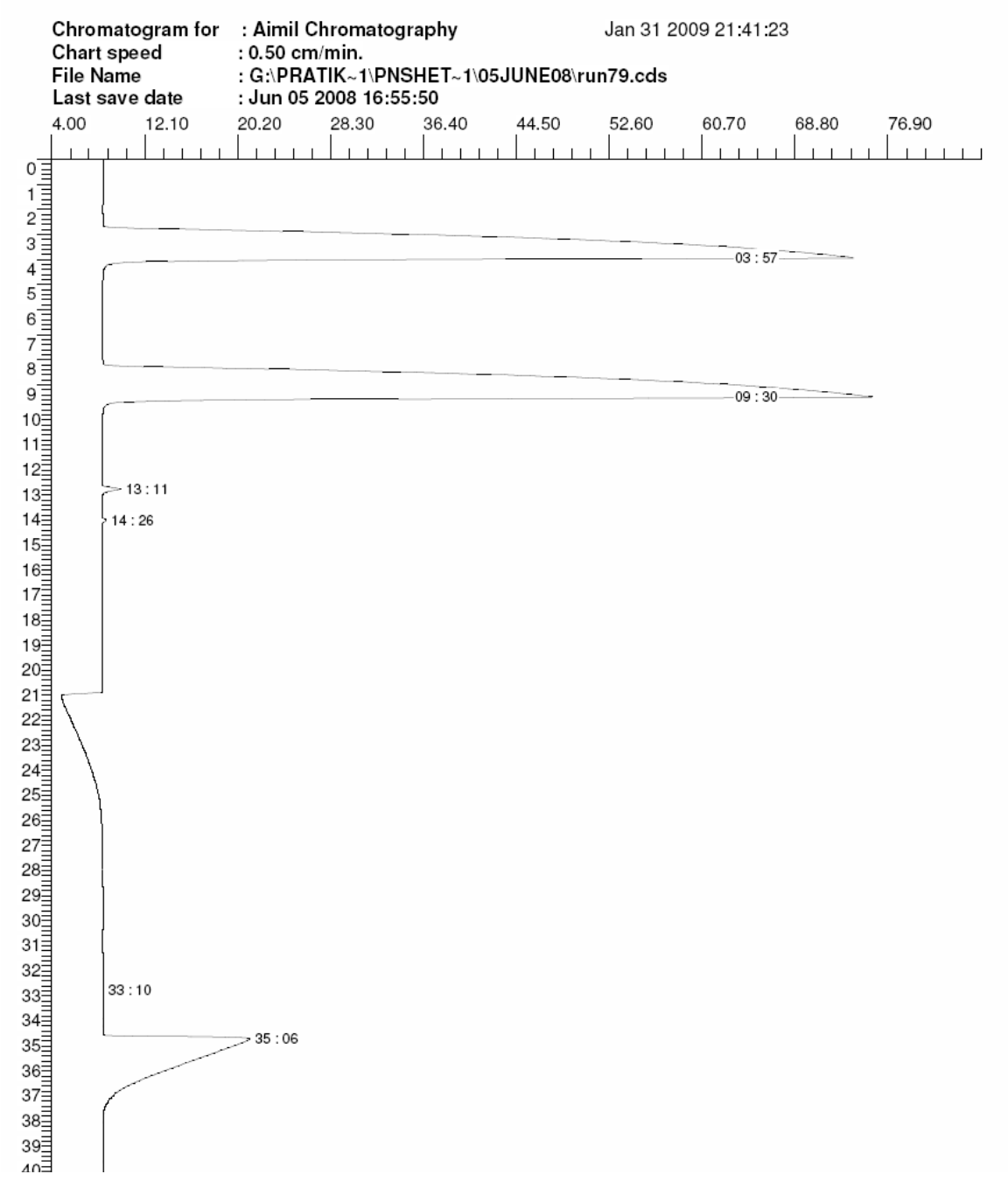

Fig. 4.10 Chromatograph displaying the peaks of H_2, CO_2 and CH_4 (Run No 7)

To reduce the retention time of carbon dioxide, oven temperature is increased to 120 °C and the eighth experimental run is conducted with a carrier gas flow rate of 14.18 ml/min. The gaseous mixture of H_2, CO, CO_2 & CH_4 is injected at 37 seconds from the start of the experiment. Fig. 4.11 shows the chromatograph displaying the peaks of all four components. From the retention time analysis it is found that second negative peak (at 3:00 in Fig. 4.11) is of carbon monoxide. At 80 °C (Run No 8) the retention time of carbon dioxide is 9: 40 whereas at 120 °C (Run No 9) the retention time of CO_2 is 6:43 (Table-4.4). But the difference in retention time between H_2 and CO is very less. Based on these two experiments, it is found that the decrease in temperature results in an increase in the retention time. Hence, the mixture of hydrogen and carbon monoxide is detected at an oven temperature of 110 °C with a flow rate of 14.18 ml/min. Fig. 4.12 shows the chromatograph displaying the clearly separated peaks of hydrogen and carbon monoxide. Hence in the subsequent analysis, the oven temperature and a N_2 flow rate are fixed at 110 °C and 14.18 ml/min respectively for the detection of hydrogen.

4.3.2.4 Calibration

For the quantitative analysis of the gaseous mixture, the amount of each component of the gaseous mixture is required to be found out. To determine the composition of the gaseous mixture, it is essential to find the response of the detector for each and every compound of the gaseous mixture. TCD gives its response for every component present in the mixture in terms of peak and the retention time. Based on the retention time analysis of the pure components, each peak of the chromatograph corresponds to a particular component of gaseous mixture that can be identified. The number of peaks of chromatograph depends upon the number of components present in the gaseous mixture.

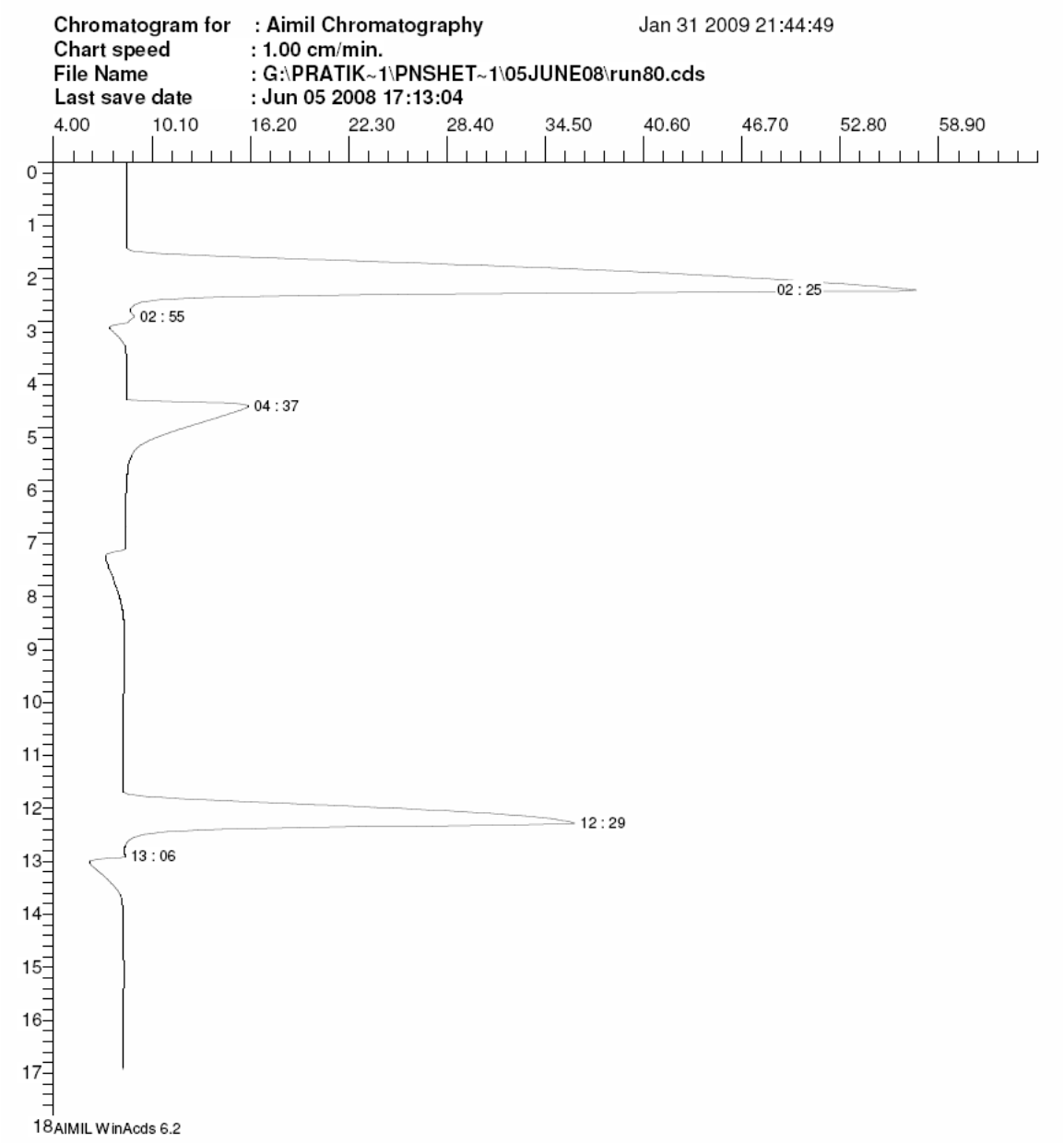

Fig. 4.11 Chromatograph displaying the peaks of H_2, CO, CO_2 and CH_4 (Run No 8)

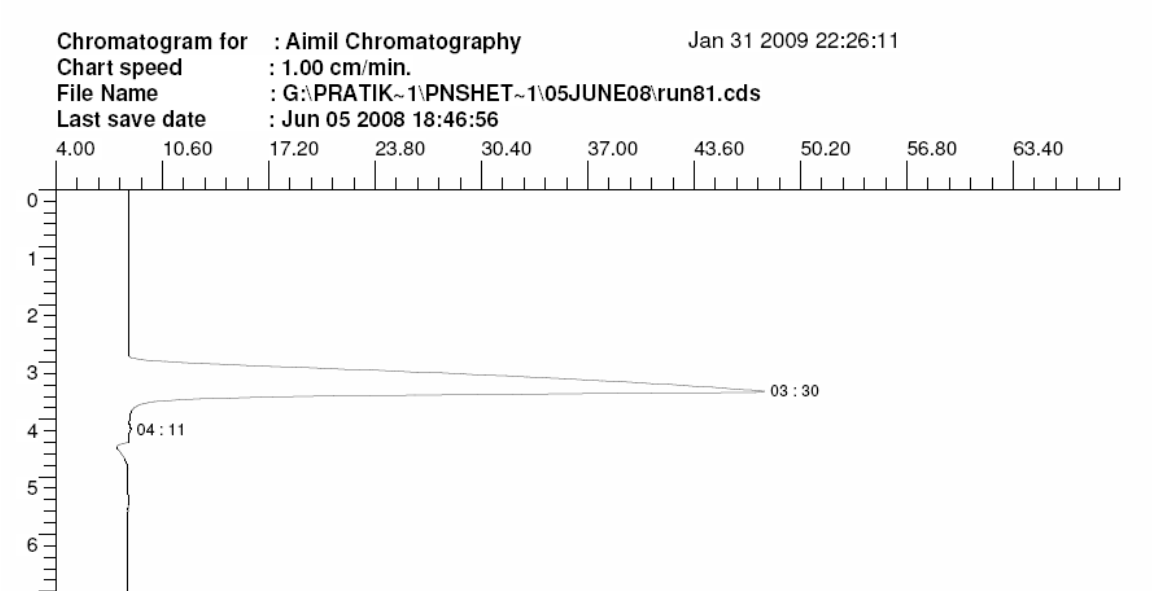

Fig. 4.12 Chromatograph displaying the peaks of H_2 and CO (Run No 9)

For equimolar gaseous mixture, TCD gives different peaks with different areas under them for different components of the gaseous mixture. The area under every peak is to be transformed into an amount of the respective component and the corresponding composition of the gaseous mixture can be found out. The amounts of components in the gaseous mixture are calibrated using the peaks and areas under them. The calibration of gas chromatograph is carried out by injecting a standard gaseous mixture with different sampling loops. The calibration curve is obtained by plotting the peak area of the standard component on the ordinate and the amounts of the standard component on the abscissa. Fig. 4.13 shows the calibration curves for different components of the producer gas. The calibration equations obtained by fitting the curves of Fig. 4.13 by linear regression are shown in Table-4.5.

The results of the present gasification studies are analyzed and discussed in the chapter 5.

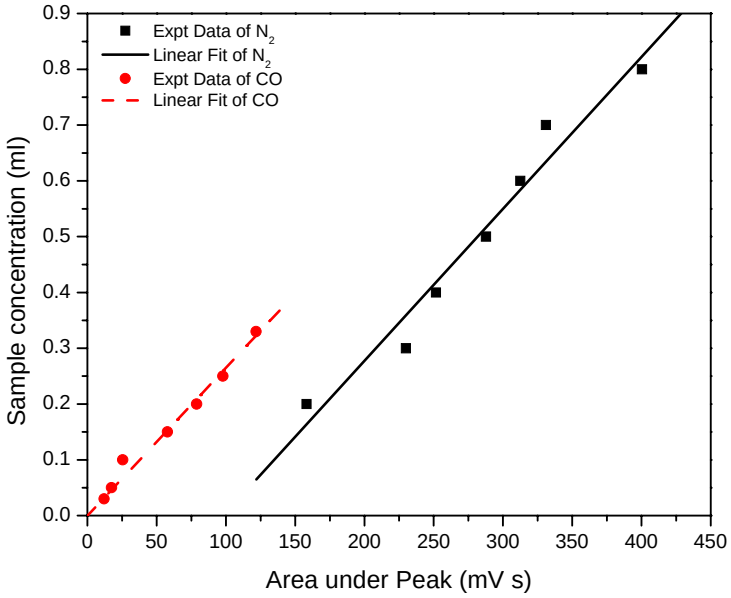

(a) Nitrogen and Carbon monoxide

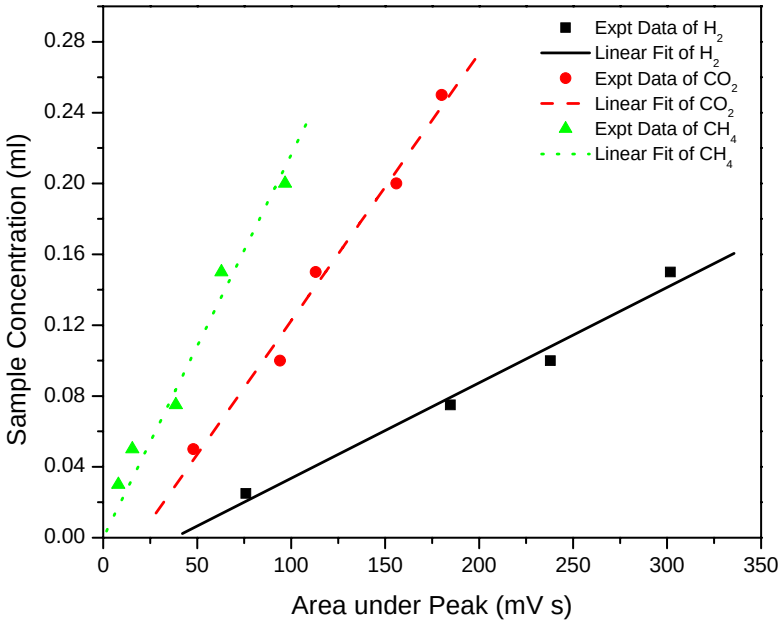

(b) Hydrogen, Carbon dioxide, and Methane

Fig. 4.13 Calibration curve for the components of producer gas

Table 4.5 Calibration equations for the components of the producer gas

Sample component	**Calibration equations (*Y* - Sample concentration (ml) & *X* - Area under peak (mV s))**
H_2	$Y = -0.02034 + 5.38962E\text{-}4\ X$
N_2	$Y = -0.2672 + 0.00272\ X$
CO	$Y = 0.00265\ X$
CH_4	$Y = 0.00216\ X$
CO_2	$Y = -0.02855 + 0.00151\ X$

CHAPTER – 5

RESULTS AND DISCUSSION

This chapter presents the experimental and simulation results obtained for the gasification of wood waste using the Imbert biomass gasifier. In this study, mathematical model is developed (Chapter 3) and to validate it, experiments are carried out (Chapter 4). The results of the experimental study are discussed in Section 5.1. The simulation results of the mathematical model are presented and discussed in Section 5.2.

5.1 Experimental Studies

Biomass gasification experiments are carried out with wood waste as biomass covering a wide range of air flow rates and biomass moisture content. The details of the range of parameters varied in the present experimental study are shown in Table-5.1. The rate of biomass consumption is found to vary from 1.0 to 3.63 kg/h for an air flow rate ranging from 1.85 to 3.39 m^3/h. The moisture content is varied from 0.0254 to 0.164 wt fraction on wet basis. In order to reduce the number of parameters on which the performance of the biomass gasifier depends, an equivalence ratio is defined to reflect the combined effect of air flow rate, rate of wood supply and duration of the run. The equivalence ratio (Φ) for each run is calculated by Eq. (5.1) (Reed and Das, 1988) and reported in Table-5.1.

Table 5.1 Details of the experimental runs for biomass gasification

Experimental No	**Air flow rate (m^3/h)**	**Initial moisture content (wt fraction, wet basis)**	**Biomass consumption Rate (kg/h)**	**Equivalence ratio(Φ)**
1	2.7765	0.1145	2.10	0.2533
2	3.3935	0.0437	3.63	0.1791
3	1.8510	0.0437	2.12	0.1673
4	2.7765	0.0437	2.67	0.1992
5	2.7765	0.073	2.59	0.2054
6	1.8510	0.10	1.00	0.3546
7	2.7765	0.1518	2.20	0.2418
8	2.1595	0.07	1.488	0.278
9	2.1595	0.044	2.12	0.1951
10	2.1595	0.1167	1.1626	0.3558
11	2.1595	0.164	1.0424	0.3968

$$\Phi = \frac{\left(\text{Air Flow Rate} \big/ \text{Biomass Consumption Rate}\right)}{\left(\text{Air Flow Rate} \big/ \text{Biomass Consumption Rate}\right)\Big|_{\text{Stoichiometric}}} \tag{5.1}$$

The stoichiometric ratio of air flow rate to the rate of biomass consumption is 5.22 m^3 air/kg of wood (Zainal et al., 2002).

Material balance is carried out to examine the reliability of the results generated. The total mass input includes biomass consumption, air and total water input. The total mass output comprises of the charcoal and producer gas produced. It is observed that the ash generated in reduction zone of the gasifier and some small pieces of charcoal pass through grate and drop into the water tray kept at the bottom of the gasifier (Fig. 4.1). As the wet ash and small charcoal pieces are insignificantly small, they are not considered in the analysis. The usual method to quantify the discrepancies in the mass balance is the closure of the mass balance which is defined as the percentage ratio of the total output mass to that of the total input mass (Dogru et al., 2002). Table-5.2 shows the detailed mass input, mass output and the mass closure for all the experimental runs. The average mass balance closure is found to be 94% in the eleven experimental runs carried out in this study.

5.1.1 Effect of Moisture Content

The moisture content in biomass greatly effects both the operation of gasifier and the quality of product gas. The constraints in terms of the upper limit on moisture content for gasifier fuels are dependent on the type of gasifier used. Higher values of moisture content could be used in updraft systems but the upper limit acceptable for a downdraft reactor is generally considered to be around 28% on wet basis (Dogru et al., 2002). The effect of moisture content on the rate of biomass consumption is shown in Fig. 5.1.

Table 5.2 Material balance

Run	Equivalence ratio (Φ)	Air flow rate (N m^3/h)	Total input (kg/h)		Total output (kg/h)			Mass balance closure (%)
			Air flow rate (kg/h)	Biomass consumption rate (kg/h)	Producer gas flow rate (Nm^3/h)	Producer gas flow rate (kg/h)	Char produced (kg/h)	
1	0.2533	2.7765	4.91441	2.10	3.83296	6.1634	0.312	92.316
2	0.1791	3.3935	6.0065	3.63	4.75711	7.64944	0.288	82.369
3	0.1673	1.8510	3.27627	2.12	2.37097	3.81251	0.3	76.21
4	0.1992	2.7765	4.91441	2.67	4.05672	6.5232	0.24	89.172
5	0.2054	2.7765	4.91441	2.59	4.19383	6.74368	0.24	93.061
6	0.3546	1.8510	3.27627	1.00	2.51031	4.03658	0.324	99.727
7	0.2418	2.7765	4.91441	2.20	4.3854	7.051723	0.18	101.6489
8	0.278	2.1595	3.82232	1.488	2.9775	4.78782	0.34	96.5633
9	0.1951	2.1595	3.82232	2.12	3.79586	6.103743	0.2	106.0822
10	0.3558	2.1595	3.82232	1.1626	2.8789	4.629271	0.24	97.68
11	0.3968	2.1595	3.82232	1.0424	2.753	4.426824	0.3	97.1654

It is found that with an increase in moisture content fraction, the rate of biomass consumption decreases. Upon an increase in the moisture content of biomass, the energy requirement for drying of biomass increases. The thermal energy requirement for pyrolysis and drying is fulfilled by combustion of biomass. Due to a higher moisture content, the amount of biomass undergoing pyrolysis decreases as a large amount of the thermal energy produced by combustion gets consumed in the drying of biomass particles. Fig. 5.1 shows the experimental findings for two different flow rates (2.7765 and 2.1595 m^3/h). For the air flow rate of 2.1595 m^3/h, the rate of biomass consumption varies from 1.0 to 2.12 kg/h for variation of moisture content ranging between 0.044 and 0.165. The variation of rate of biomass consumption is 2.12 to 2.67 kg/h for the fraction of moisture content ranging between 0.044 and 0.165 for the air flow rate of 2.7765 m^3/h. Also, the biomass consumption rate is more for a higher flow rate of air in comparison to a lower flow rate of air for the same moisture content fraction. This is observed for the entire range of moisture content fraction (0.04 – 0.16). This is because of the fact that a higher flow rate leads to the combustion of more amounts of biomass thereby producing more thermal energy, which leads to a higher rate of biomass consumption.

5.1.2 Effect of Air Flow Rate

The effect of air flow rate on the rate of biomass consumption is shown in Fig. 5.2. For three different values of moisture content fraction (0.04, 0.07 and 0.11), the effects of air flow rate on biomass consumption rate are studied. It is found that with an increase in the air flow rate, the rate of biomass consumption increases for a particular value of moisture content fraction. The increase in air flow rate provides more oxygen to get combusted and a higher amount of biomass gets consumed. The energy released will increase the

rate of drying and the rate of pyrolysis. The rate of biomass consumption increases not only due to a higher combustion rate, but also due to the enhanced pyrolysis and drying rate. It is also observed that for a particular air flow rate, the rate of biomass consumption is low for a higher moisture content fraction value. It is found that the difference between biomass consumption rate for the moisture content fraction values of 0.04 and 0.11 is 1.12 kg/h for an air flow rate of 1.851 m^3/h. The difference of biomass consumption rate is 0.57 kg/h for the same variation of moisture content fraction (0.04 to 0.11) at an air flow rate of 2.7765 m^3/h. This is due to the fact that the energy required to dry the biomass due to an increase in moisture content is little in comparison to the increment in the production of thermal energy due to a higher air flow rate.

5.1.3 Temperature Profiles

For each experimental run, the temperatures are measured at regular intervals using thermocouples placed at different locations along the axis of the gasifier. Fig. 5.3 and Fig. 5.4 show the temperature variation with time for an equivalence ratio of 0.2533 at various distances from the grate covering all four zones of the gasifier. The variation of temperature with time at various axial locations at the center (r = 0) of the gasifier is shown in Fig. 5.3. At the start of the experiment, the temperature of oxidation zone (100-153 mm from the grate) is 725 °C, and temperature at the reduction zone outlet is 70 °C. The pyrolysis zone (153-350 mm from the grate) and drying zone (350-530 mm from the grate) are at an ambient temperature in the beginning. After five minutes from the start of the experiment, the temperature of the oxidation zone reaches to a value around 1100 °C and the heat liberated due to combustion spreads across the gasifier, resulting in the increase of temperature in reduction, pyrolysis, and drying zones.

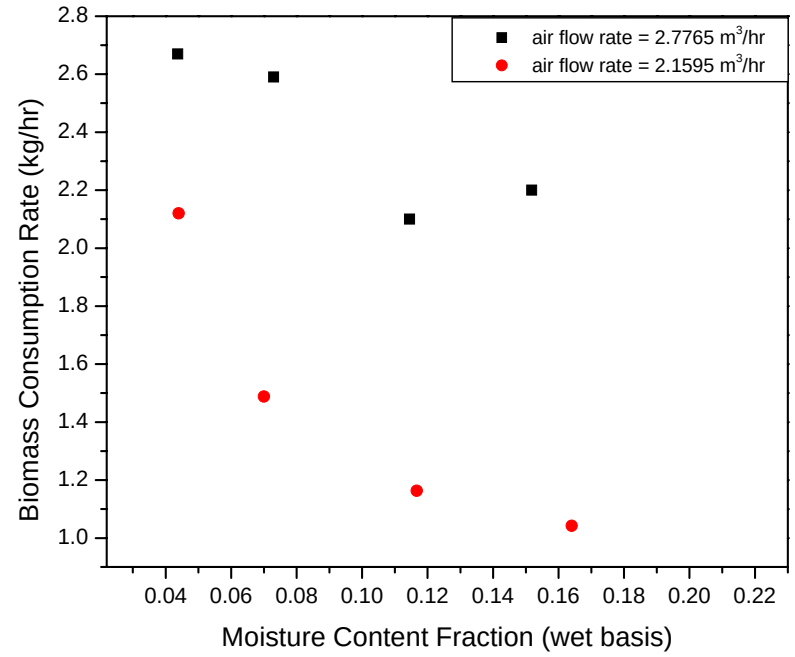

Fig. 5.1 Effect of moisture content on rate of biomass consumption

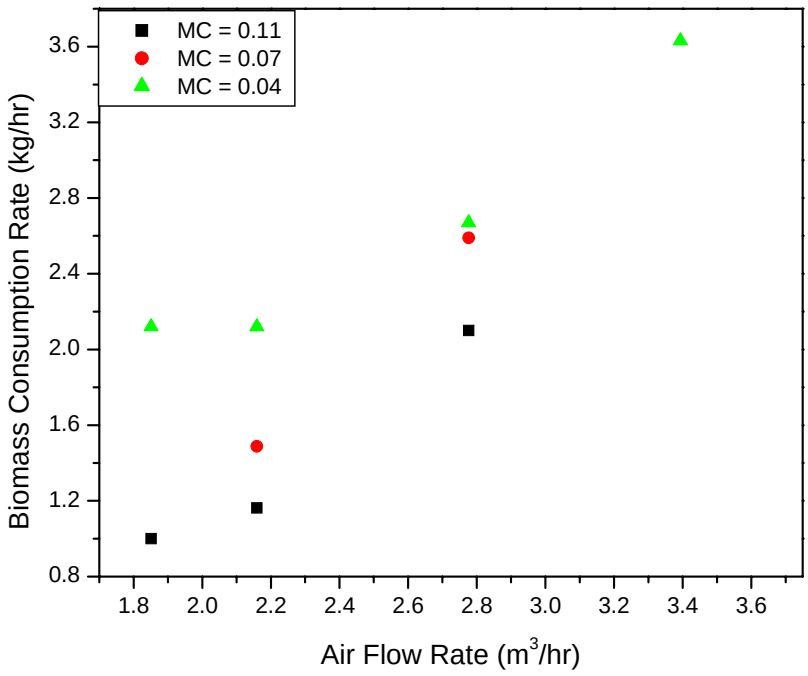

Fig. 5.2 Effect of air flow rate on rate of biomass consumption

The hot gaseous mixture leaving the oxidation zone flows downwards and a significant increase in temperature is observed in the reduction zone (0-100 mm from the grate). The temperature at the outlet of reduction zone reaches 725 °C after ten minutes from the start of the experiment. Afterwards, the temperature of reduction zone ranges between 750 and 900 °C. The temperature of pyrolysis zone varies from 120 °C to 350 °C and that of drying zone varies between 70 °C and 120 °C. Fig. 5.4 shows the variation of temperature with time at a half radial distance ($r = R/2$) at various axial locations in the gasifier. The temperatures at the half radial distances are lower in each zone as compared to those at the centre of gasifier. Similar results are obtained for other experimental runs also. Figs. 5.5-5.14 show the temperature profile at the centre and at a half radial distance for different values of equivalence ratio ranging between 0.1673 and 0.3968.

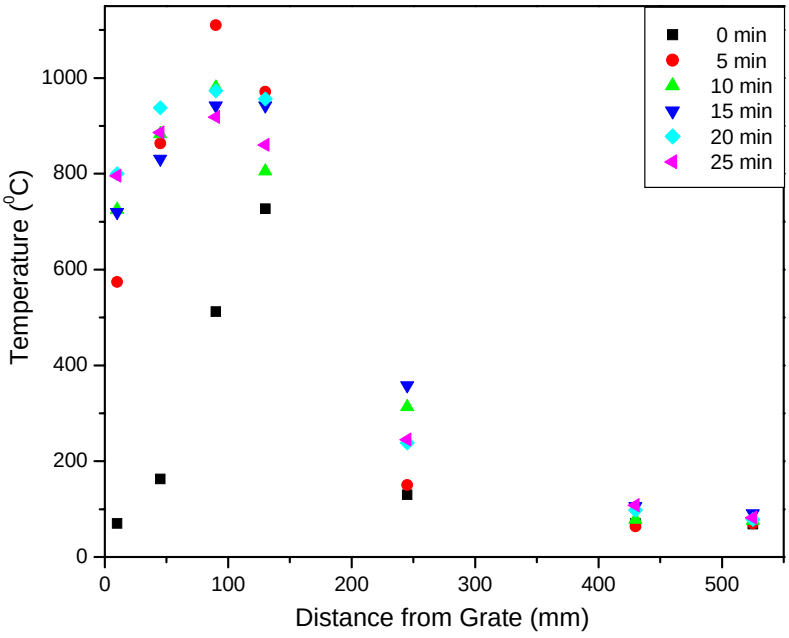

Fig. 5.3 Temperature profile across the gasifier at center (*r* = 0) for equivalence ratio of 0.2533

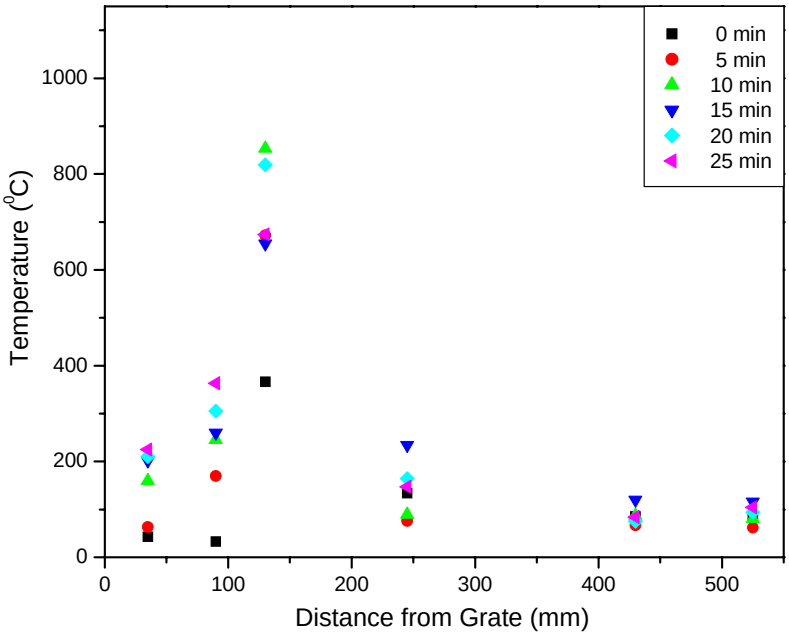

Fig. 5.4 Temperature profile across the gasifier at half radial distance (*r* = *R*/2) for equivalence ratio of 0.2533

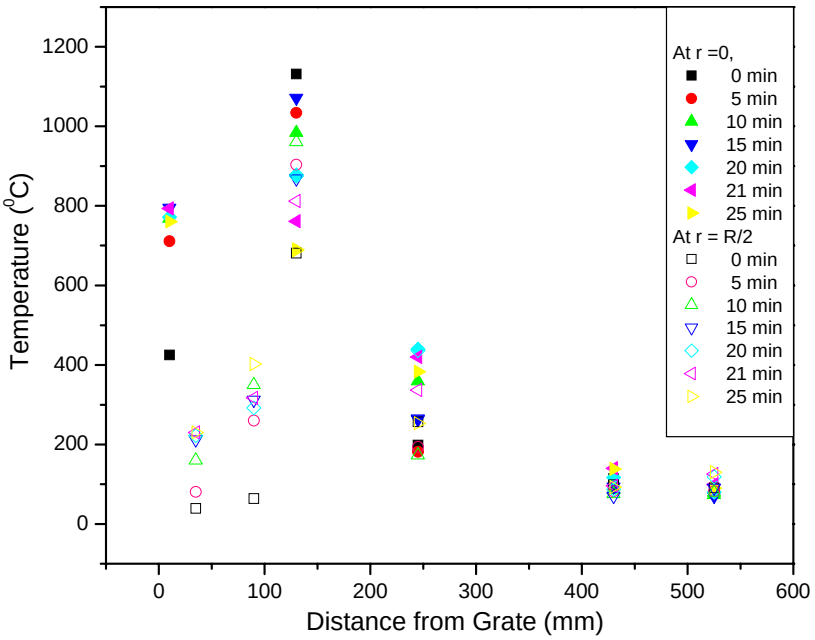

Fig. 5.5 Temperature profile across the gasifier at the centre (r = 0) and at half radial distance (r = R/2) for equivalence ratio of 0.1791

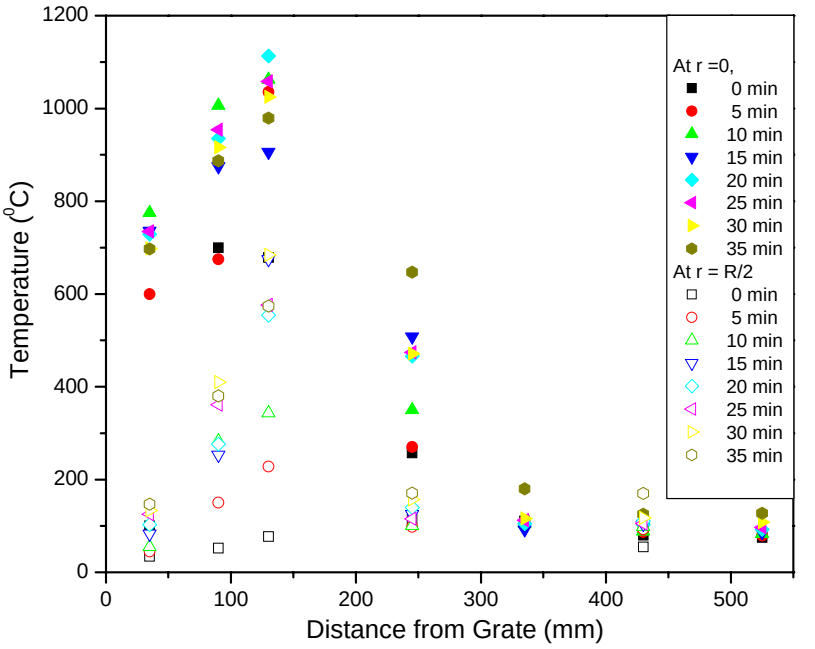

Fig. 5.6 Temperature profile across the gasifier at the centre (r = 0) and at half radial distance (r = R/2) for equivalence ratio of 0.1673

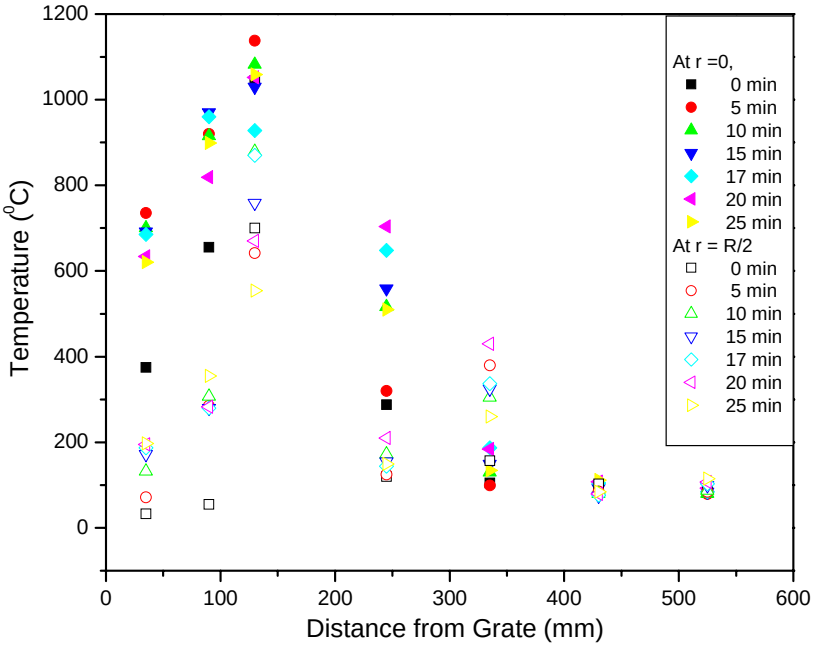

Fig. 5.7 Temperature profile across the gasifier at the centre (r = 0) and at half radial distance (r = R/2) for equivalence ratio of 0.1992

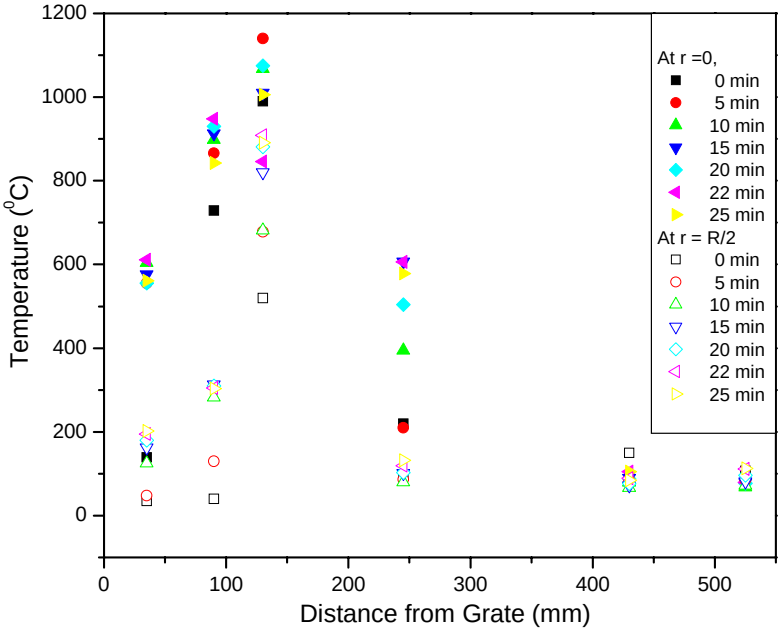

Fig. 5.8 Temperature profile across the gasifier at the centre (r = 0) and at half radial distance (r = R/2) for equivalence ratio of 0.2054

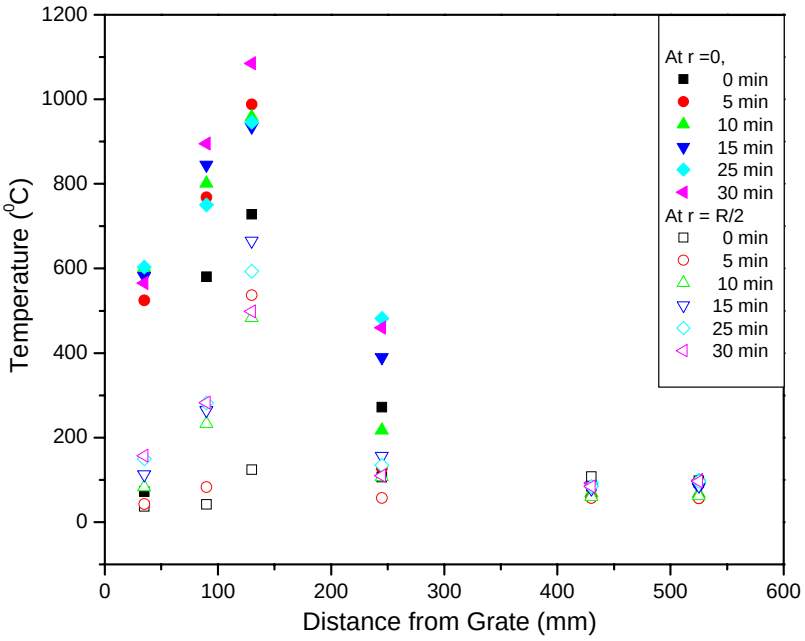

Fig. 5.9 Temperature profile across the gasifier at the centre (r = 0) and at half radial distance (r = R/2) for equivalence ratio of 0.3546

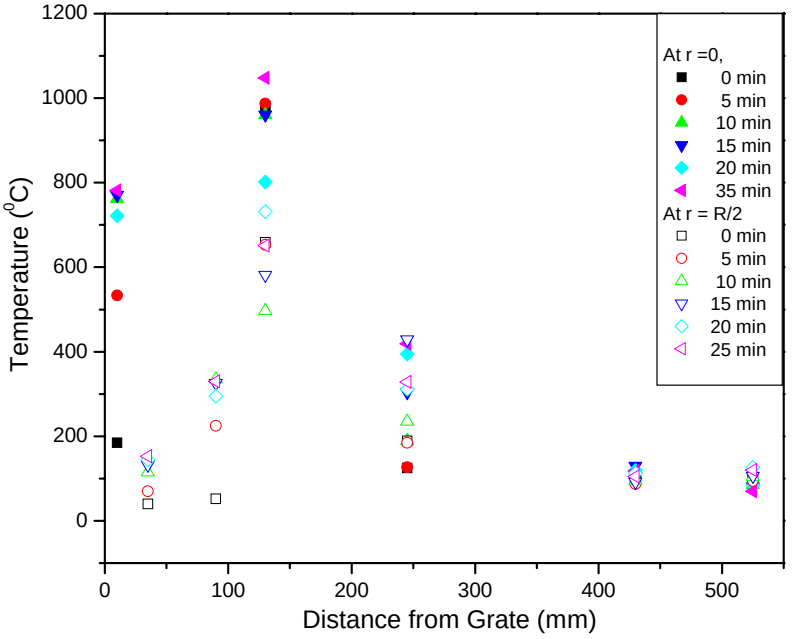

Fig. 5.10 Temperature profile across the gasifier at the centre (r = 0) and at half radial distance (r = R/2) for equivalence ratio of 0.2418

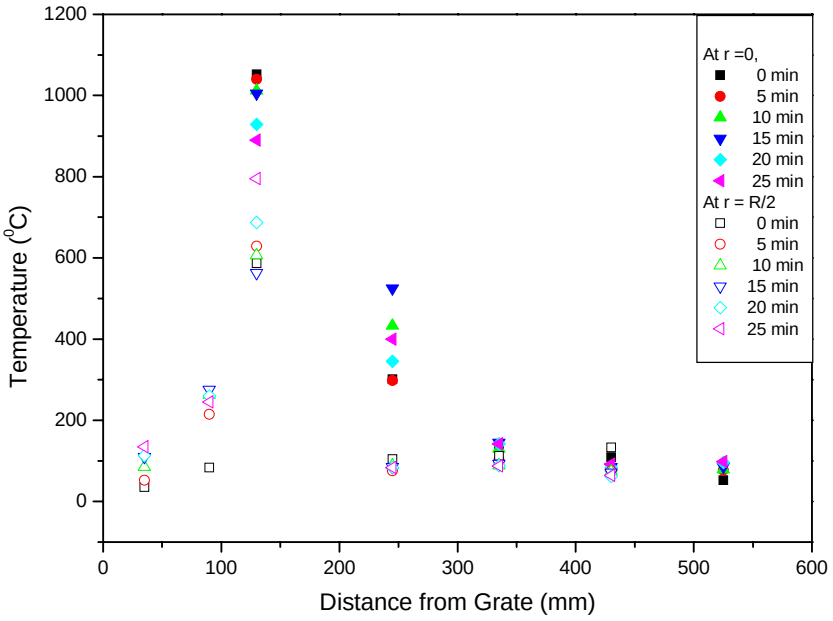

Fig. 5.11 Temperature profile across the gasifier at the centre (r = 0) and at half radial distance (r = R/2) for equivalence ratio of 0.278

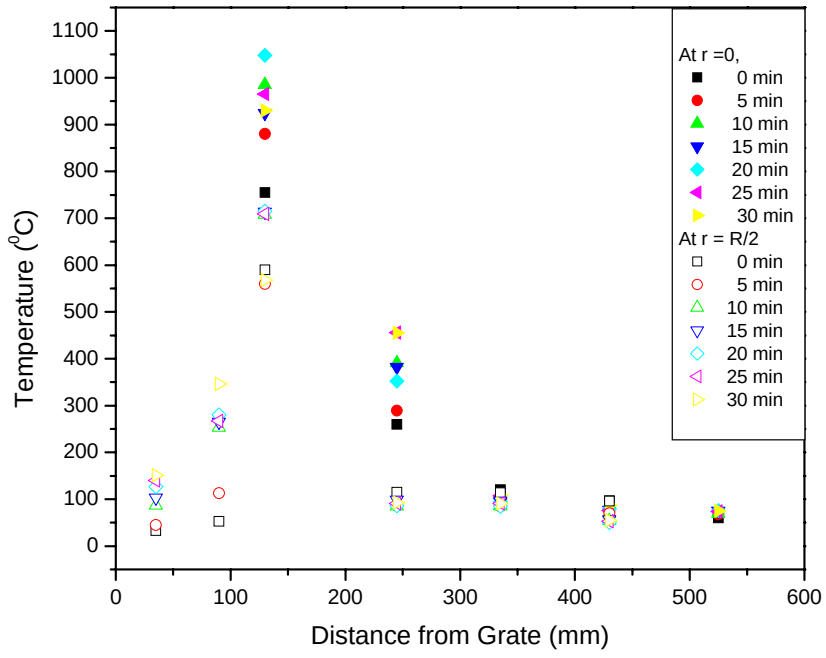

Fig. 5.12 Temperature profile across the gasifier at the centre (r = 0) and at half radial distance (r = R/2) for equivalence ratio of 0.1951

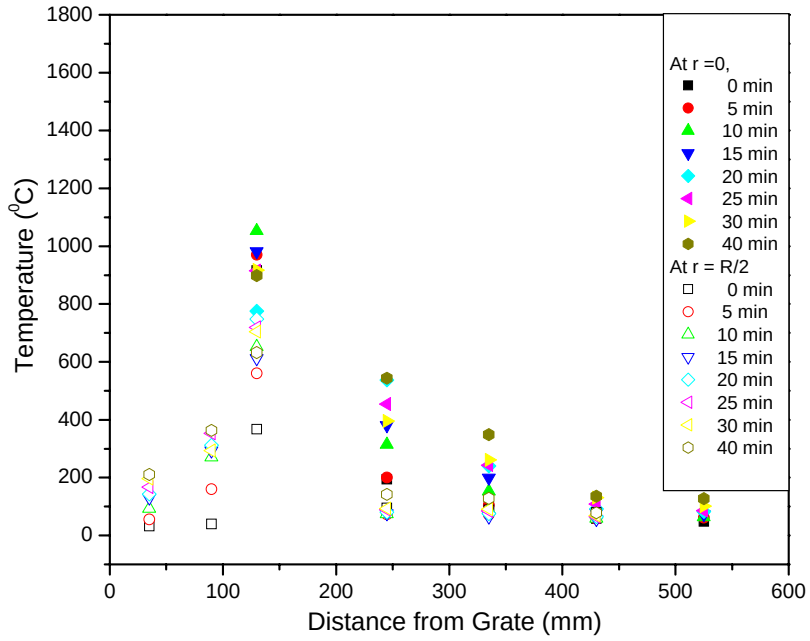

Fig. 5.13 Temperature profile across the gasifier at the centre (*r* = 0) and at half radial distance (*r* = *R*/2) for equivalence ratio of 0.3558

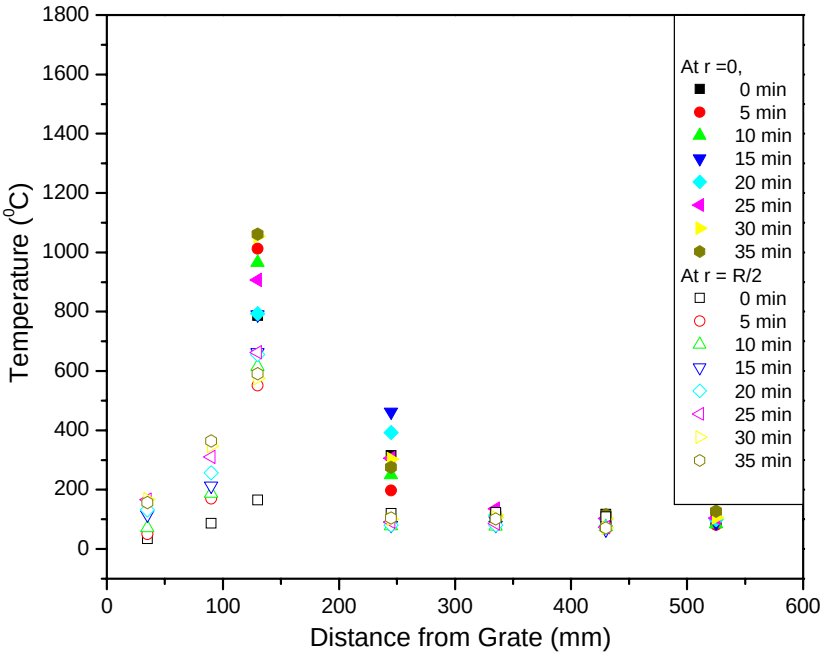

Fig. 5.14 Temperature profile across the gasifier at the centre (*r* = 0) and at half radial distance (*r* = *R*/2) for equivalence ratio of 0.3968

5.1.4 Producer Gas Composition

The composition of producer gas sampled at five minutes interval during gasification experiments is found using a gas chromatograph (NUCON 5765) with thermal conductivity detector. The details of the analysis of producer gas were discussed in chapter 4. Fig. 5.15 shows the variation of the molar composition of the producer gas with time for the experimental run having an equivalence ratio of 0.2533. The composition of nitrogen varies from 0.62 to 0.69 and that of hydrogen varies from 0.12 to 0.08. As nitrogen being an inert component, for a fixed flow rate of air the amount of nitrogen does not vary. However, the molar fraction of nitrogen varies because of the generation and depletion of other gases during the gasification reactions. It is found that the composition of carbon monoxide decreases and that of carbon dioxide increases with time. However, the composition of methane is minute and remains constant around 0.01. The molar fraction of carbon monoxide is 0.23 at five minutes from the start of the experiment and the same is 0.16 at the end of the experiment. The maximum value of the molar fraction of carbon dioxide in producer gas is 0.07 at 25 minutes after the start of the experiment. Similar results are obtained for other experimental runs as well. The variation of molar composition with time during the experimental run having an equivalence ratio of 0.1791 is shown in Fig. 5.16. The molar fraction of carbon monoxide decreases with time and that of carbon dioxide increases with time. The molar fraction of hydrogen ranges between 0.17 and 0.1 and that of nitrogen varies from 0.55 to 0.7. Fig. 5.17 to Fig. 5.25 show the variation of the molar composition of producer gas with time for the other experimental runs covering the equivalence ratio in the range of 0.1673 to 0.3968.

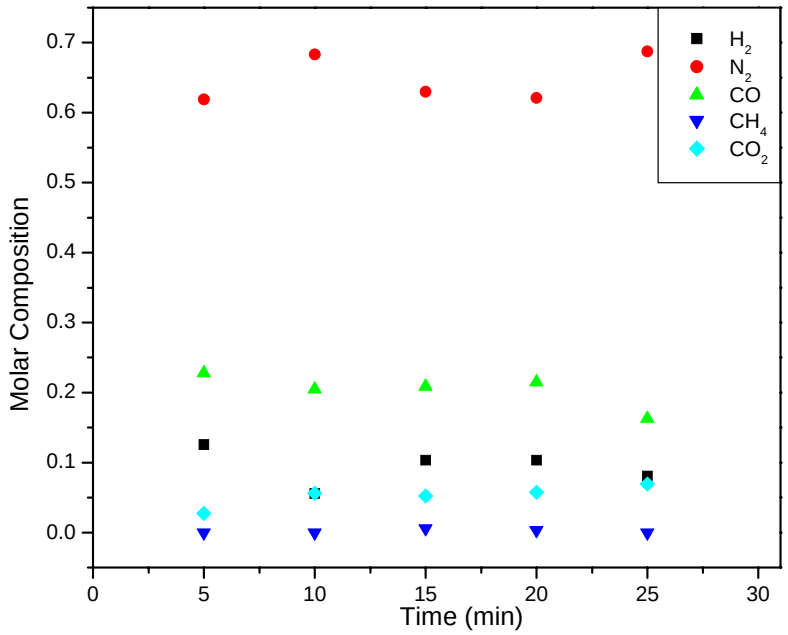

Fig. 5.15 Variation of producer gas composition with time for Φ = 0.2533

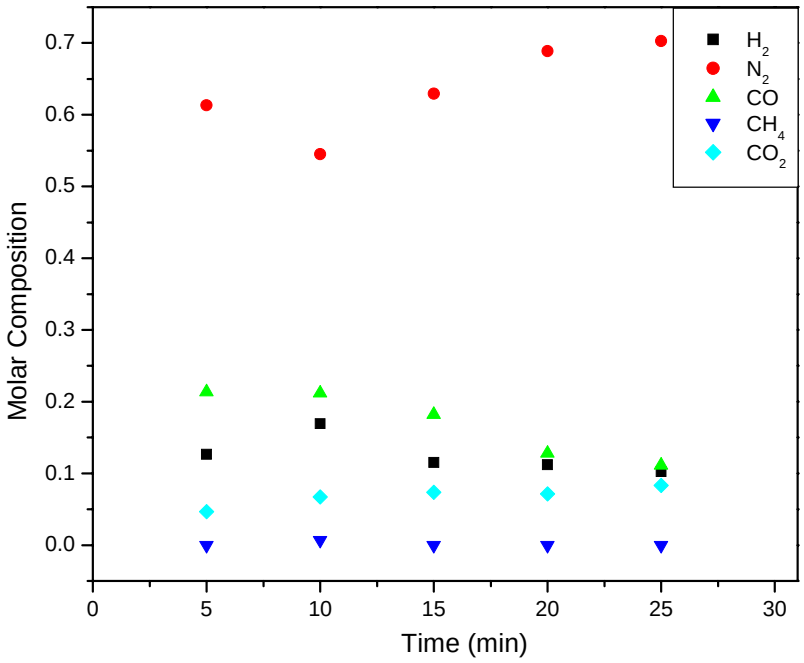

Fig. 5.16 Variation of producer gas composition with time for Φ = 0.1791

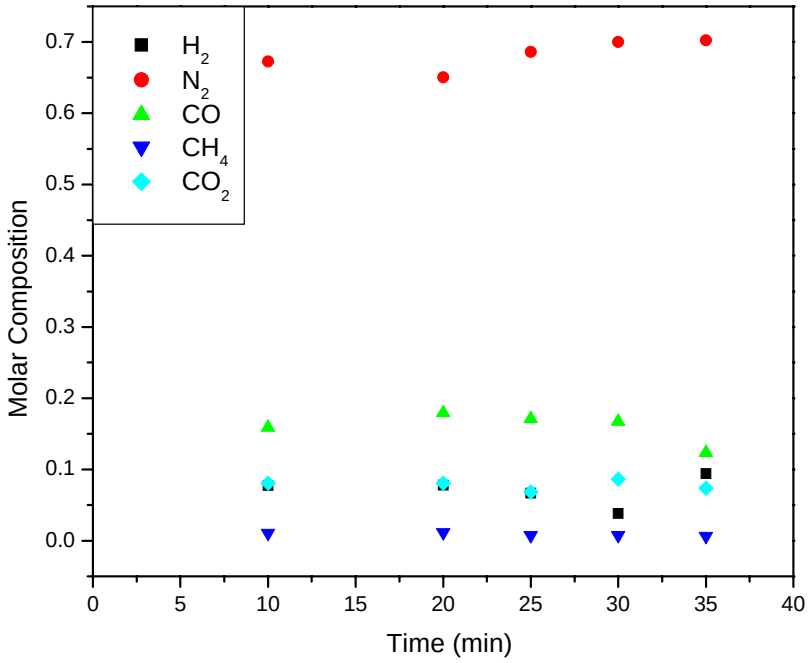

Fig. 5.17 Variation of producer gas composition with time for Φ = 0.1673

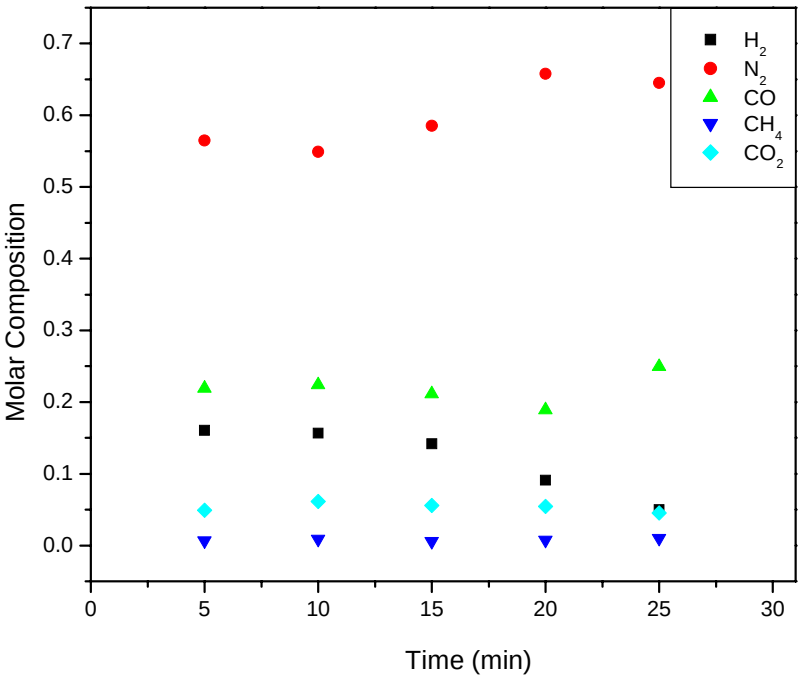

Fig. 5.18 Variation of producer gas composition with time for Φ = 0.1992

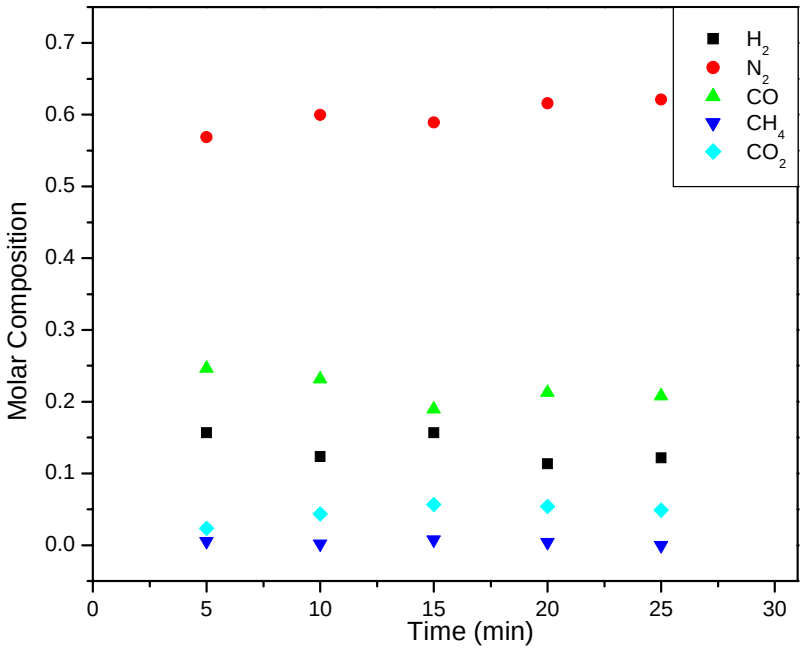

Fig. 5.19 Variation of producer gas composition with time for Φ = 0.2054

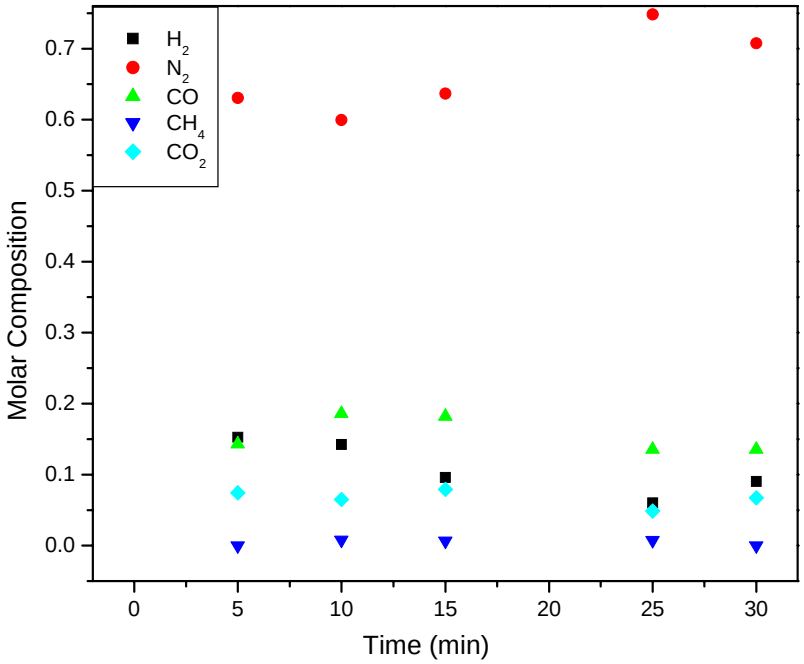

Fig. 5.20 Variation of producer gas composition with time for Φ = 0.3546

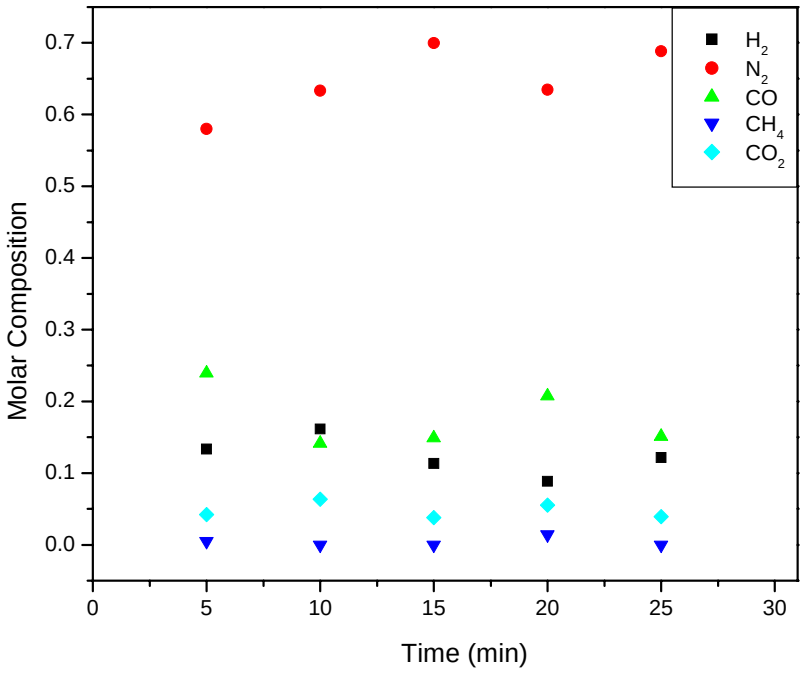

Fig. 5.21 Variation of producer gas composition with time for Φ = 0.2418

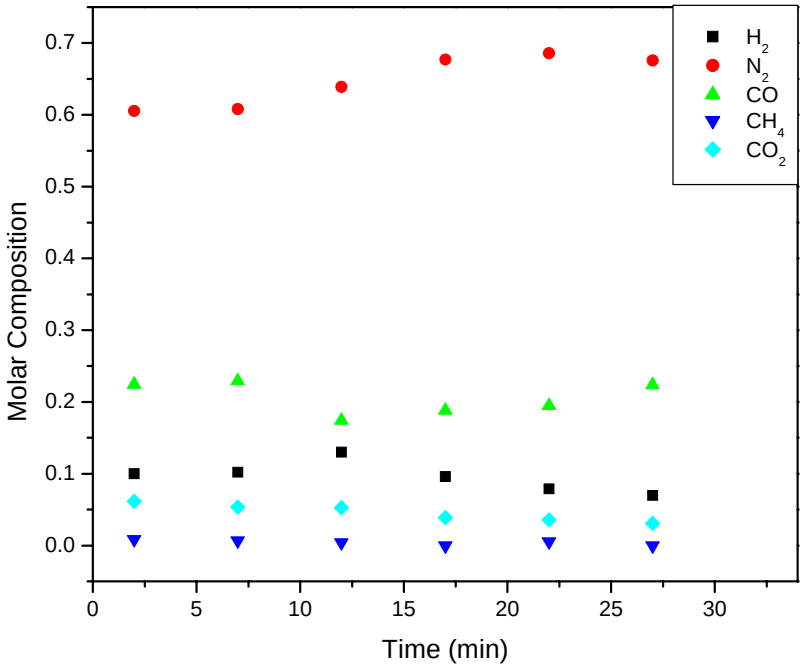

Fig. 5.22 Variation of producer gas composition with time for Φ = 0.278

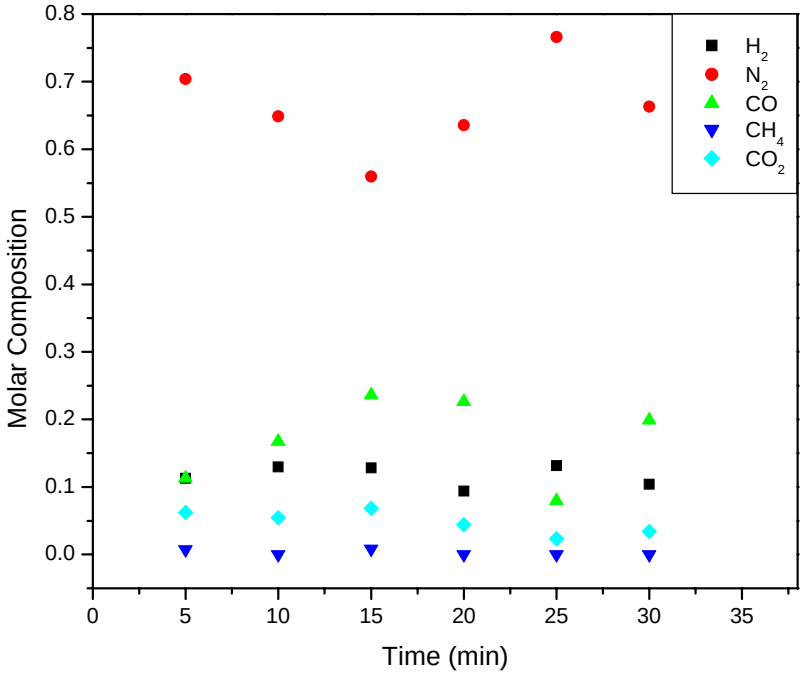

Fig. 5.23 Variation of producer gas composition with time for Φ = 0.1951

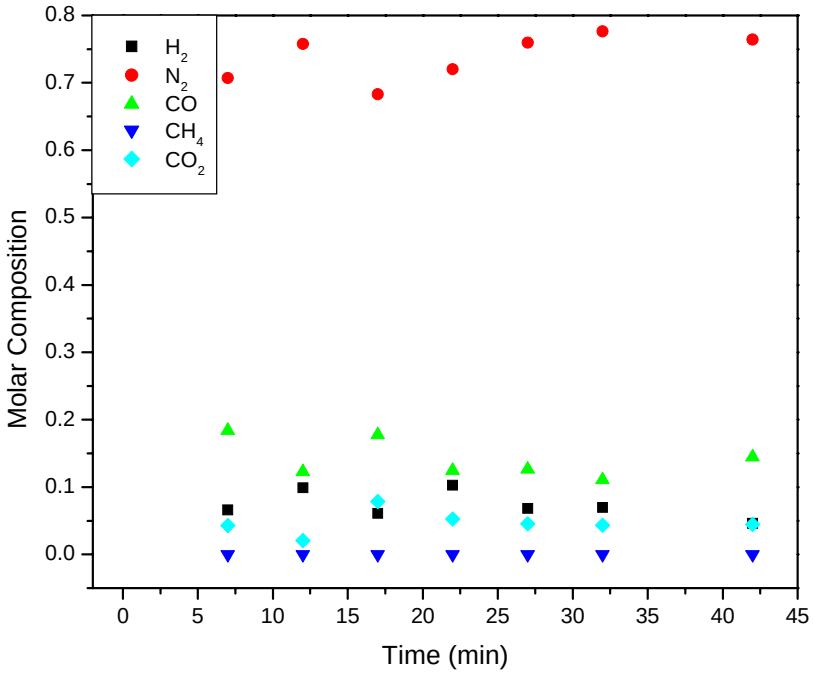

Fig. 5.24 Variation of producer gas composition with time for Φ = 0.3558

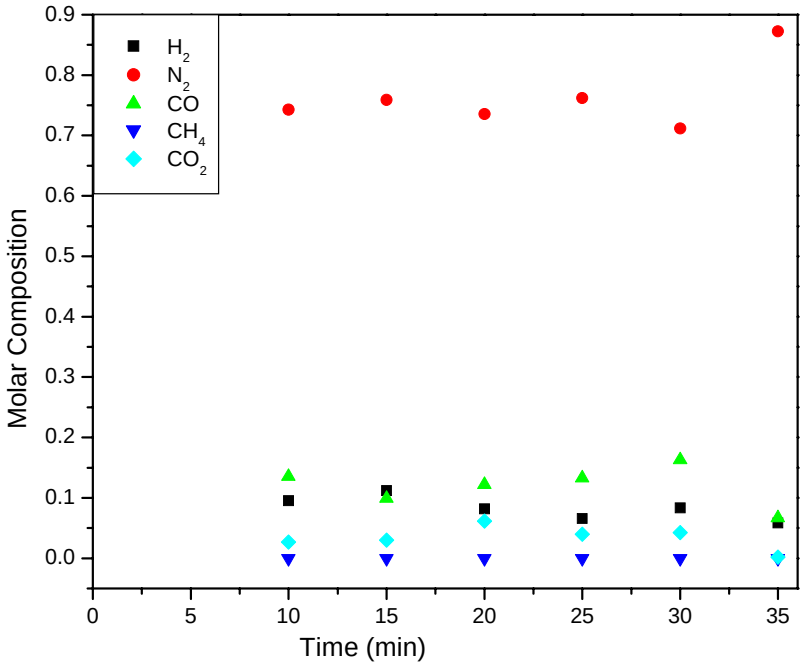

Fig. 5.25 Variation of producer gas composition with time for Φ = 0.3968

5.1.5 Performance Evaluation of Biomass Gasifier

The performance of the biomass gasifier system is evaluated in terms of the producer gas composition, the calorific value of producer gas, gas generation rate, zone temperatures and cold gas efficiency.

5.1.5.1 Producer Gas Composition

To study the effect of equivalence ratio on the producer gas composition, the averaged gas composition for each experimental run is plotted against the equivalence ratio of the same experimental run and shown in Fig. 5.26. The molar fractions of nitrogen and carbon dioxide decrease with an increase in Φ upto a value of Φ = 0.205 and for higher values of Φ, the molar fractions of N_2 and CO_2 are found to increase. The fractions of carbon monoxide and hydrogen show an increasing and decreasing trend just opposite to that of nitrogen and carbon dioxide. A higher value of Φ represents a higher air flow rate for a specific biomass consumption rate which leads to a more amount of CO_2 production in combustion zone and a more amount of N_2 entry along with air flow. The conversion of CO_2 to CO depends upon two factors: (1) the rate of reactions occurring in the reduction zone, and (2) the length of the reduction zone. With an increase in Φ from 0.16 to 0.205, an increased amount of CO_2 is converted into carbon monoxide and hydrogen, and thereby the fractions of CO and H_2 increase with Φ till a value of Φ = 0.205 and subsequently the values decrease. The increase in CO_2 fraction and decrease in CO & H_2 fractions for an equivalence ratio higher than 0.205 represent that CO_2 produced in combustion zone is in excess to that of the conversion capacity of reduction bed. The increase in N_2 fraction for an Φ value ranging from 0.205 to 0.36 is due to an increased amount of N_2 entry along with the air flow.

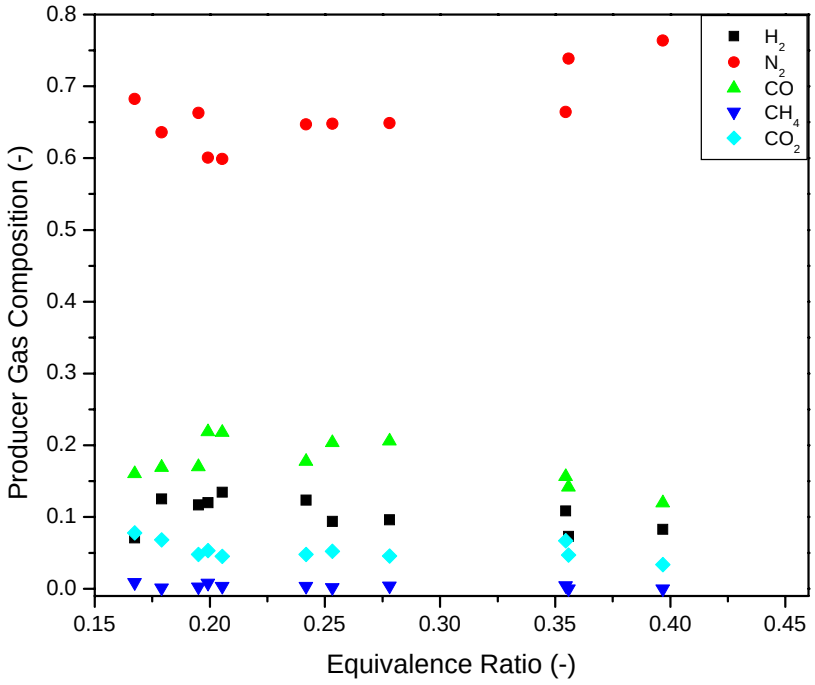

Fig. 5.26 Effect of equivalence ratio on producer gas composition

5.1.5.2 Zone Temperatures

Fig. 5.27 shows the variation of the average temperature (of pyrolysis and oxidation zones) in the downdraft biomass gasifier with the equivalence ratio. The temperature of oxidation zone varies from 900 °C to 1050 °C and that of pyrolysis zone between 280 °C and 550 °C. It clearly indicates that both the temperature profiles pass through a maximum at an equivalence ratio of 0.205. The temperature of oxidation zone depends upon the heat released due to the biomass combustion and air flow rate. As air flow rate increases, it provides more oxygen to oxidize but also brings inert N_2, which acts as a heat carrier and reduces the temperatures of the oxidation and pyrolysis zones. The maximum value of temperature in the pyrolysis and oxidation zones represents the existence of an optimum amount of equivalence ratio. Fig. 5.26 also supports that at an optimum equivalence ratio ($\Phi_{opt} = 0.205$) the fractions of carbon monoxide and hydrogen are the maximum and the fraction of carbon dioxide is the minimum.

5.1.5.3 Calorific Value of Gas

The variation of calorific value of the producer gas with equivalence ratio is presented in Fig. 5.28. The calorific value is calculated using the composition of the producer gas. Carbon monoxide and hydrogen are the main components of the producer gas and are responsible for higher calorific value. The calorific values of hydrogen, carbon monoxide and methane are taken as 285.84, 282.99 and 890.36 MJ/kmol respectively. It is found that at an equivalence ratio of 0.17, the calorific value is 4.5 MJ/Nm^3. With an increase in the equivalence ratio from $\Phi = 0.17$ to $\Phi = 0.205$, the calorific value reaches to a maximum of 6.34 MJ/Nm^3. For the equivalence ratio value higher than 0.205, the calorific value steadily decreases with a further increase in the equivalence ratio. The

increasing and decreasing trend of calorific value is exactly same as that of carbon monoxide and hydrogen variation with equivalence ratio as shown in Fig. 5.26.

5.1.5.4 Gas Production Rate

Fig. 5.29 shows the effect of equivalence ratio on the production rate of producer gas per unit weight of biomass (Nm^3/kg). It clearly shows that with an increase in the equivalence ratio (Φ), the production rate of producer gas continuously increases. Higher values of Φ signify a higher air flow rate for a specific biomass consumption rate. Hence although after a certain value of the equivalence ratio, the calorific value of the producer gas deteriorates due to higher amounts of carbon dioxide as depicted in Figs. 5.26 & 5.28, the production rate of producer gas continues to increase.

5.1.5.5 Cold Gas Efficiency

Cold gas efficiency is defined as the ratio of energy of the producer gas per kg of biomass to the higher heating value (HHV) of the biomass material (Eq. (5.2)).

$$\text{Cold gas efficiency} = \frac{(\text{Calorific value})(\text{Gas production per weight of biomass})}{\text{Higher heating value of the biomass}} \qquad (5.2)$$

The variation of cold gas efficiency with the equivalence ratio is shown in Fig. 5.30. As given in Eq. (5.2), the cold gas efficiency depends upon the calorific value and the amount of producer gas released at a constant HHV of biomass. The amount of producer gas increases continuously and the calorific value passes through a maximum with an increase in the equivalence ratio. Cold gas efficiency is at the lowest value of 0.25 for an equivalence ratio value of 0.17. The value of cold gas efficiency becomes almost double with a small increase in the equivalence ratio at Φ = 0.205. The effect of equivalence ratio on cold gas efficiency is comparatively lower for its higher values. Cold gas efficiency increases from 0.5 to 0.6 for a change in the equivalence ratio from 0.2 to 0.35.

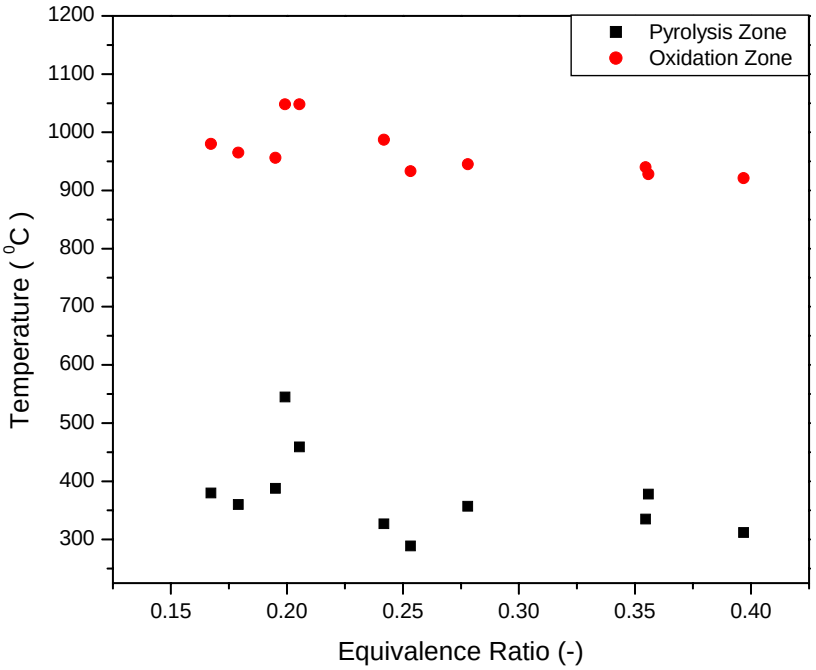

Fig. 5.27 Effect of equivalence ratio on zone temperatures

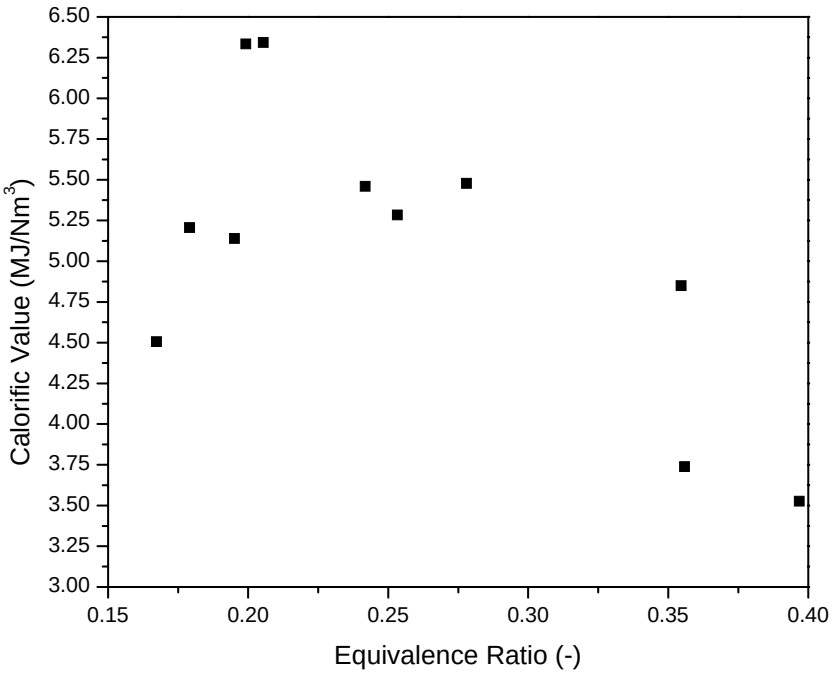

Fig. 5.28 Effect of the equivalence ration on the calorific value of the gas

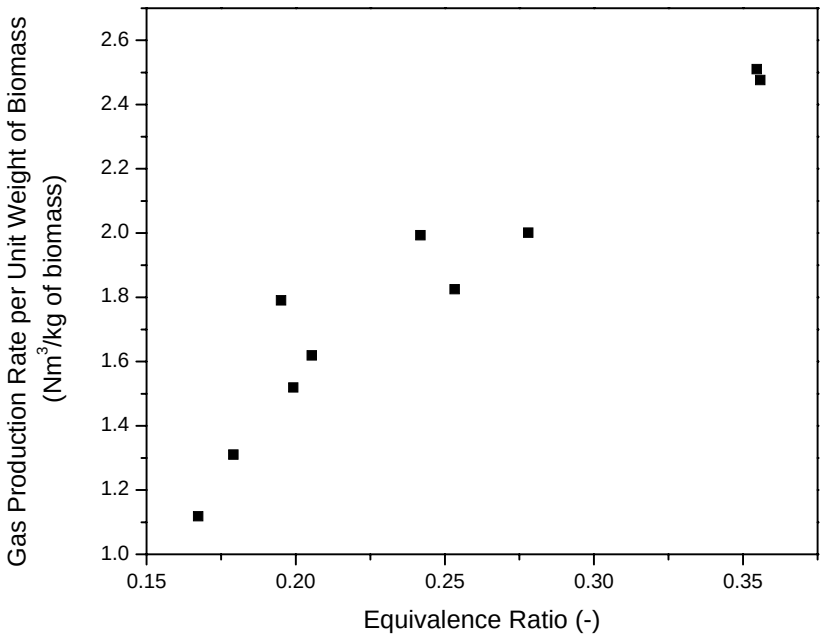

Fig. 5.29 Effect of equivalence ratio on producer gas production rate per unit weight of biomass

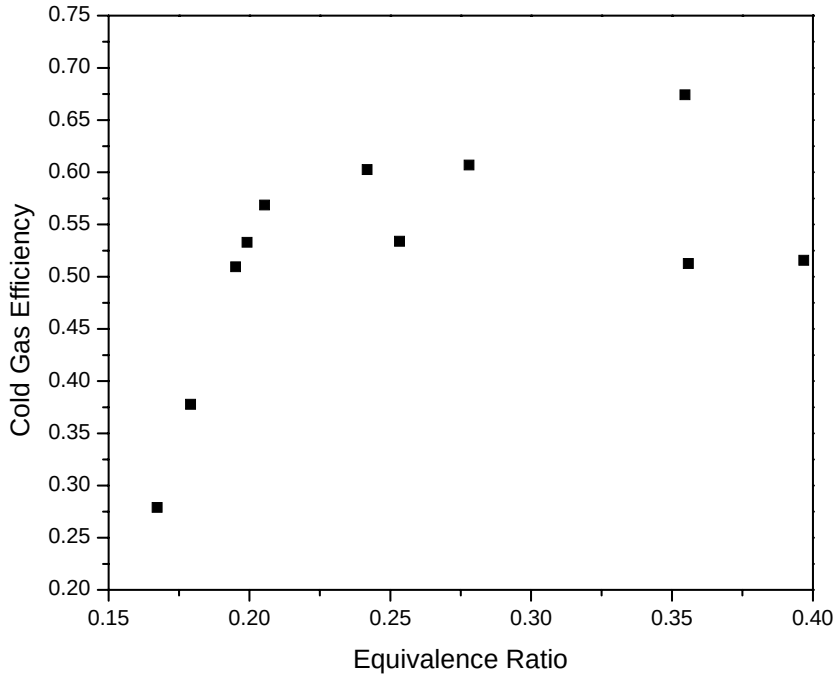

Fig. 5.30 Effect of equivalence ratio on cold gas efficiency

5.1.6 Comparison of Results with the Literature Data

The experimental results are compared with those reported in the literature. Hazelnutshell as a biomass is used in the gasification studies carried out by Dogru et al. (2000). The range of air-to-fuel ratio they varied is 1.37-1.64 Nm^3/kg and that of the equivalence ratio they varied is 0.262-0.314. The optimum operation of the gasifier is found to be between 1.44 Nm^3/kg and 1.47 Nm^3/kg of air-to-fuel ratio at the values of wet feed rate of 4.06 and 4.48 kg/h respectively, which produces the producer gas with a calorific value of about 5 MJ/m^3. Zainal et al. (2002) performed an experimental study on a downdraft biomass gasifier using wood chips and charcoal. Zainal et al. (2002) varied the equivalence ratio from 0.259 to 0.46. It is found that the calorific value increases with equivalence ratio and reaches a peak value of 0.388, for which the calorific value is reported to be 5.34 MJ/Nm^3. Table-5.3 shows the comparison of experimental results obtained corresponding to the optimum equivalence ratio or air-to-fuel ratio in the present work with those reported by Dogru et al. (2000) and Zainal et al. (2002). It shows that the gas produced in the present study, has the highest calorific value.

Table 5.3 Comparison of the experimental results obtained in this study with those reported the literature

Research group	**Biomass species used**	**Optimum equivalence ratio**	**Calorific value (MJ/Nm^3)**	**Gas production rate per unit weight of biomass (Nm^3/kg)**	**Cold gas efficiency (%)**
Dogru et al. (2000)	hazelnut shell	0.276	5.15	2.73	80.91
Zainal et al. (2002)	Furniture wood +charcoal	0.388	5.62	1.08	33.72
Present Study	Furniture waste of *dalbergia sisoo*	0.205	6.34	1.62	56.87

5.2 Mathematical Modeling and Simulation

The mathematical modeling of a downdraft biomass gasifier is carried out by two approaches: (1) developing an equilibrium model, (2) developing a combined transport and kinetic model. The modeling equations with initial and boundary conditions, and numerical solution and simulation of these two approaches were discussed in detail in Chapter 3. In the present section, the simulation results of equilibrium modeling and of combined transport and kinetic modeling are discussed and reported in section 5.2.1 and 5.2.2 respectively. The kinetic parameter estimation, the details of which were discussed in section 3.2.1.3 of Chapter 3, is also carried out in the present study. The simulated results of the same are discussed in section 5.2.3.

5.2.1 Equilibrium Model

The equilibrium model assumes that the pyrolysis products get burnt and achieve equilibrium in the reduction zone before leaving the gasifier. It predicts the steady state exit gas composition, given the solid composition of biomass and the equilibrium temperature of the gasifier. The equilibrium model is validated with the experimental data obtained in the present study and also with those reported in the literature.

5.2.1.1 Validation with Experimental Data

The experimental data reported by Dogru et al. (2002) and those of present study are used to validate the simulation results of the equilibrium model. The initial moisture content fraction, air-to-fuel ratio, equilibrium temperature, and chemical formula of the biomass are required as input data for the simulation model. The equilibrium model is validated using the parametric values shown in Table-5.4.

Table 5.4 Experimental data used for the validation of equilibrium model

Reference	Biomass species	Run No	Initial moisture content (wt fraction, wet basis)	Air to fuel ratio (m^3/kg)	Oxidation zone temperature (°C)	Reduction zone temperature (°C)	*m* (kmol of oxygen per kmol of biomass)
Dogru et al. (2002)	Hazelnutshell ($CH_{1.48}O_{0.735}$)	1	0.1245	1.63	821	621	0.527528
		2	0.1245	1.64	833	633	0.530764
		3	0.1245	1.52	846	646	0.491928
		4	0.1245	1.38	869	669	0.446619
		5	0.1245	1.51	1025	825	0.488691
		6	0.1245	1.46	1015	815	0.472509
		7	0.1245	1.47	1020	820	0.475746
		8	0.1245	1.44	1130	930	0.466037
		9	0.1245	1.37	1206	1006	0.443382
		10	0.1245	1.48	1110	910	0.478982
		11	0.1245	1.50	1021	821	0.485455
Present Study	*Dalbergia sisoo* ($CH_{1.531}O_{0.693}$)	1	0.1145	1.322226	933	801	0.417392
		2	0.0437	0.934902	965	767	0.295124
		3	0.0437	0.873306	980	780	0.27568
		4	0.0437	1.039824	1048	795	0.328245
		5	0.073	1.072188	1048	738	0.338462
		6	0.10	1.851012	940	693	0.584316
		7	0.1518	1.262196	987	714	0.398442
		8	0.07	1.45116	945	745	0.458093
		9	0.044	1.018422	956	756	0.321489
		10	0.1167	1.857276	928	728	0.586294
		11	0.164	2.071296	921	721	0.653854

Dogru et al. (2002) performed the experiments with hazelnutshell. The chemical formula of hazelnutshell is $CH_{1.48}O_{0.735}$, which is obtained from the values of ultimate analysis reported by Dogru et al. (2002). The value of *m* (kmol of oxygen per kmol of biomass) is calculated using Eq. (5.3) and the results are reported in Table-5.4.

$$m = \left(\frac{\text{Air to Fuel Ratio} \left(\text{Nm}^3 / \text{kg} \right)}{4.76} \right) \left(\text{Air Density} \left(\text{kg/Nm}^3 \right) \right) \left(\frac{\text{Mol wt of Biomass}}{\text{Mol wt of Air}} \right) \quad (5.3)$$

The average temperature at the inlet and outlet of the reduction zone is considered as the equilibrium temperature. Dogru et al. (2002) reported averaged values of temperatures of various zones of biomass gasifier excepting for the reduction zone. In the present study, it is observed that the reduction zone temperature is approximately 150 – 250 °C less than the combustion zone temperature. In addition to that the literature also supports the claim that this is valid for other biomasses also. Zainal et al. (2002) performed an experimental study with wood chips and a mixture of furniture wood and charcoal and reported the temperature profile of the various zones. In their study also, the difference between the temperature of reduction zone and combustion zone is observed to be around 150 – 250 °C. Hence in the present simulation studies, while validating the model with experimental data of Dogru et al. (2002), the reduction zone temperature is taken as 200 °C less than the throat temperature.

Figs. 5.31 to 5.36 show the comparison of the equilibrium model predicted composition, flow rate and calorific value of producer gas with experimental data reported by Dogru et al. (2002) and those of present study. The comparison of model predicted composition of producer gas with that of experimental values reported by Dogru et al. (2002) and of present study is shown in Fig. 5.31 and Fig. 5.32 respectively. Fig. 5.31 shows that the simulated model predictions differ a lot from the experimental

values for molar fraction of carbon monoxide and carbon dioxide, whereas the predicted molar fraction values of nitrogen, hydrogen and methane are found to be matching with experimental data. Fig. 5.32 shows that the predicted values of molar fraction match well with experimental data for hydrogen and methane. The predicted molar fraction of carbon monoxide, carbon dioxide and nitrogen does not match with experimental data of the present study (Fig. 5.32). However, the qualitative trend of composition variation with equivalence ratio is predicted well by simulation results for the present experimental study. Fig. 5.32 shows that the predicted molar fraction of carbon dioxide decreases with an increase in Φ up to a value of $\Phi = 0.21$ and for higher values of Φ, molar fraction of nitrogen and carbon dioxide increases. The fraction of carbon monoxide and hydrogen shows an increasing and decreasing trend just opposite to that of nitrogen and carbon dioxide. A higher value of Φ represents a higher air flow rate for a specific biomass consumption rate which leads to more amount of CO_2 production in combustion zone and more amount of N_2 entry along with air flow. Fig. 5.33 and Fig. 5.34 show the comparison of model predicted flow rates of producer gas with those obtained experimentally by Dogru et al. (2002) and those obtained experimentally in the present study respectively. Although the qualitative trends of model predictions are matching with the experimental data, the quantitative values of model predictions of flow rate of producer gas are found to vary widely with the experimental data. Similar inferences are drawn from Fig. 5.35 and Fig. 5.36, which illustrates the comparison of calorific values based on model predicted values of molar fractions and those found experimentally.

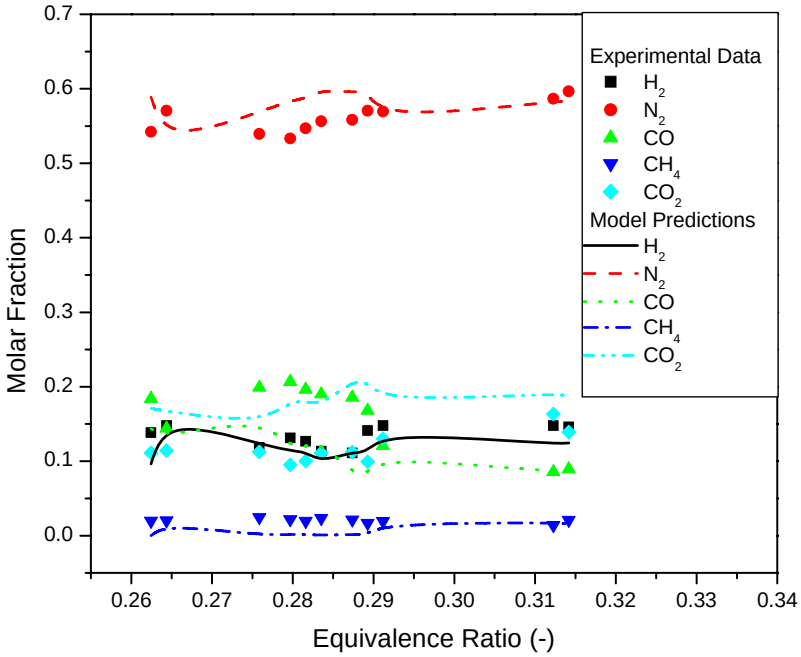

Fig. 5.31 Comparison of experimental data of Dogru et al. (2002) with model predicted composition of producer gas

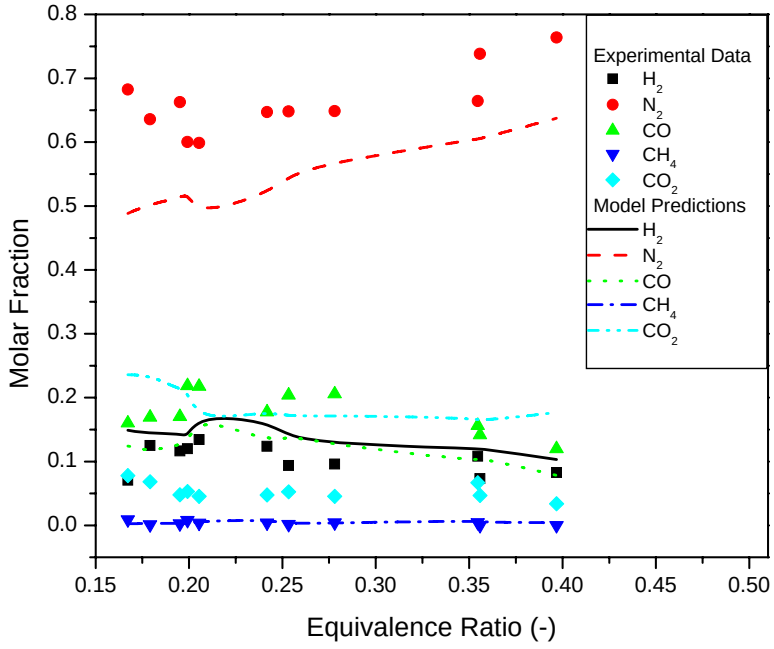

Fig. 5.32 Comparison of experimental data of present study with model predicted composition of producer gas

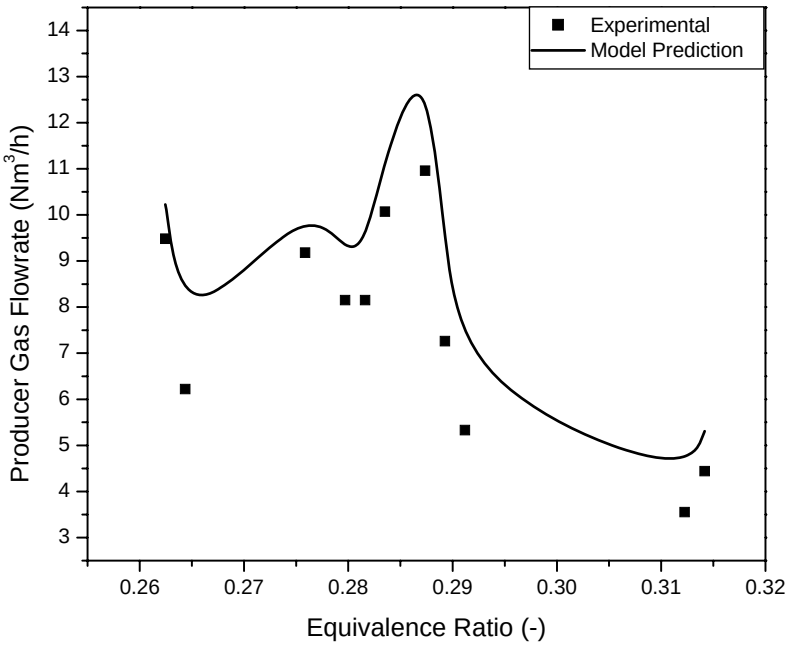

Fig. 5.33 Comparison of experimental data of Dogru et al. (2002) with model predicted flow rate of producer gas

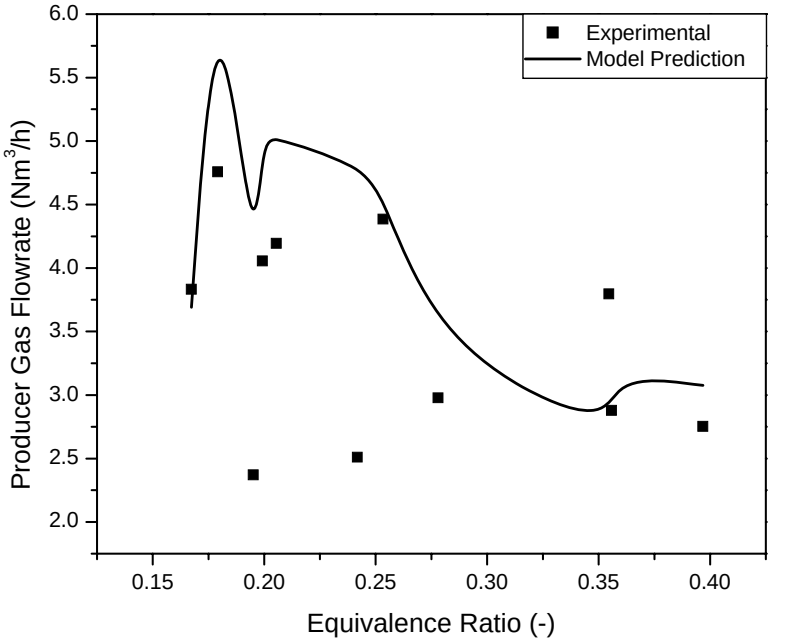

Fig. 5.34 Comparison of experimental data of present study with model predicted flow rate of producer gas

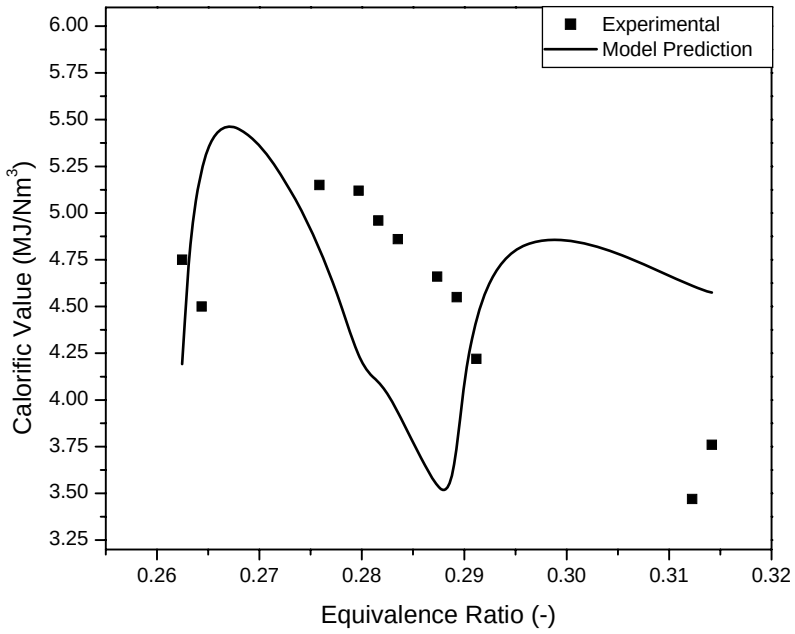

Fig. 5.35 Comparison of experimental data of Dogru et al. (2002) with model predicted calorific value of producer gas

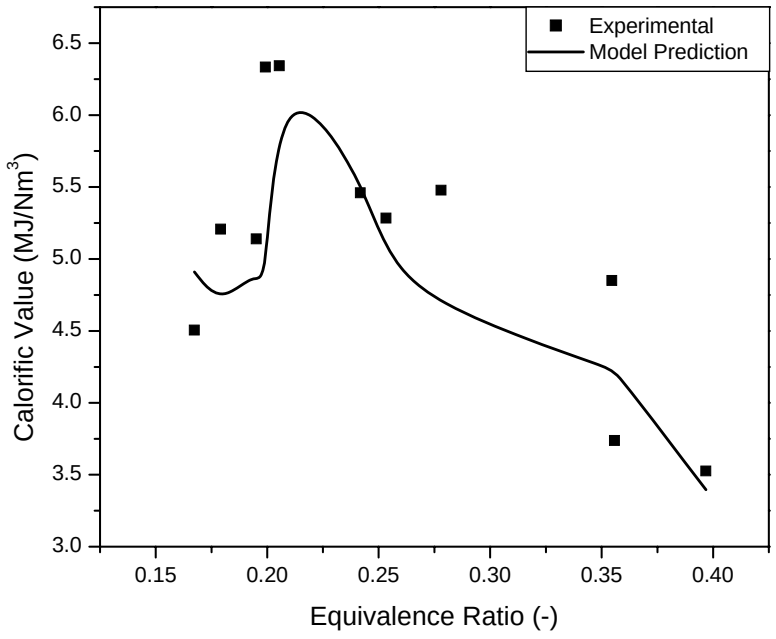

Fig. 5.36 Comparison of experimental data of present study with model predicted calorific value of producer gas

Table-5.5 shows the standard deviations from the experimental data for model predicted composition, flow rate and calorific values. The standard deviation (SD) is calculated using Eq. (5.4).

$$SD = \left[\frac{\sum_{i=1}^{N} \left[\left(Y_{exp} - Y_{cal} \right) / Y_{exp} \right]^2}{N-1} \right]^{\frac{1}{2}} \tag{5.4}$$

5.2.2 Combined Transport and Kinetic Model

A transient one dimensional model is developed for the throated close-top downdraft biomass gasifier in the present study. The developed model takes into account of the pyrolysis, secondary tar reactions, homogeneous gas reactions and heterogeneous combustion/gasification reactions. It was divided into three parts according to three different zones developed: (1) pyrolysis, (2) oxidation, and (3) reduction. The model equations, numerical solution, simulation methodologies and the values of the parameters used were reported in chapter 3. The simulation results of the combined transport and kinetic model are presented in this section. The simulation results of the reduction zone model of the gasifier are validated with the experimental data reported by Jayah et al. (2003) and the findings of the same are described in section 5.2.2.1. The complete model (combined transport and kinetic model) including all the zones of gasifier is validated with the experimental data obtained in the present study and also with those reported in the literature, and the results are presented in section 5.2.2.2.

Table 5.5 Standard deviation of values predicted by equilibrium model

Reference	Variable	Standard Deviation (SD)
Dogru et al. (2002)	Molar fraction of H_2	0.155329
	Molar fraction of N_2	0.065798
	Molar fraction of CO	0.334784
	Molar fraction of CH_4	0.80823
	Molar fraction of CO_2	0.678328
	Flow rate of Gas	0.187555
	Calorific Value of Gas	0.229774
Present Study	Molar fraction of H_2	0.827393
	Molar fraction of N_2	0.201364
	Molar fraction of CO	0.309423
	Molar fraction of CH_4	0.770779
	Molar fraction of CO_2	2.81591
	Flow rate of Gas	0.424568
	Calorific Value of Gas	0.182973

5.2.2.1 Validation of Reduction Zone Model with Experimental Data

The model equations of the reduction zone model proposed in this study were discussed in section 3.2.3. The numerical solution and simulation methodologies were described in section 3.2.4.4. The initial position in the model is the top of reduction zone or the end of oxidation zone. Gases leaving the oxidation zone are a mixture of pyrolysed gas, incombustible CO_2 and inert N_2. The exact proportion of each of these components depends upon the rate of air flowing into the gasifier and the rates of combustion, pyrolysis and cracking reactions. It is assumed that all O_2 from the air is consumed by combustion reactions while N_2 remains inert. The pyrolysis products are assumed to crack into an equivalent amount of CO, CH_4 and H_2O for a typical biomass ($CH_{3.03}O_{1.17}$). Giltrap et al. (2003) introduced a variable 'pyrolysis fraction' (f_p), which can vary from 0 (no pyrolysis products) to 1 (pyrolysis products only). The composition of the gaseous mixture leaving the oxidation zone is calculated from the value of f_p and flow rate of air.

In reduction zone endothermic reactions are carried out and degree of temperature drop depends upon extents of reactions. The extent of reaction depends upon the reactivity of char, which is represented by Char Reactivity Factor (*CRF*) value. *CRF* in turn depends upon thermal history, degree of burn-off, and number of active sites on char and its particle size. As char moves downwards in the reduction zone, the degree of burn-off increases. Due to char-gas reactions and shrinking of particles, char size decreases and porosity increases so gases would come across more active sites and the extent of reaction increases. For higher *CRF* value, the reduction zone temperature drops faster and reaction completion occurs rapidly. Due to this the gas compositions predicted by the model are changed in the initial length of reduction zone only. Above understanding

leads to the fact that *CRF* value must be increased along the length of the reduction zone. Quantitative increment in *CRF* value depends upon the type of biomass and its physical characteristics. Giltrap et al. (2003) simulated for constant *CRF* value for the entire reduction zone. In their work, they varied the *CRF* value from 1 to 10000 and the results of the simulation are compared with the final composition of the producer gas with the data reported in the literature. But temperature and composition profiles are not compared. In the present study, *CRF* value of 1 to 10000 is varied linearly & exponentially and their effects on composition & temperature profiles are observed. The reduction zone model of present study is validated with the experimental data reported by Jayah et al. (2003). Apart from the composition of gas leaving the oxidation zone, other variables such as temperature, pressure and velocity of gas are required as an input to the reduction model. The velocity is approximated from the airflow rate and the throat dimensions reported by Jayah et al. (2003). The operating pressure does not affect the gasification efficiency significantly. Increase of the pressure is limited on two counts: (1) due to the amount of entrained dust (the gas, being denser, exerts a higher thrust on the dust particles), and (2) by the increased cost of manufacturing (Mathieu and Dubuisson, 2002). Due to these limitations and to overcome the pressure drop offered by the bed, the operating pressure should be above the atmospheric pressure. The value has to be found out by approximating the pressure drop in the bed. The value of 1.005 atm is used in simulations and it is ensured that the pressure at the outlet remains always above the atmospheric pressure. Table-5.6 shows the values of parameters used in the model simulations. In Table-5.6, top four quantities, i.e., bed length, velocity, temperature and moisture content are taken from Jayah et al. (2003).

Fig. 5.37 shows the comparison of model predicted temperature profile for different *CRF* values, the experimental data of Jayah et al. (2003), and their model predictions. Experimental data show that the temperature of reduction zone decreases continuously along the length of reduction zone and the trend of profile is concave downwards. Jayah's model predictions are significantly varying from the experimental data and are of convex type. For *CRF* = 1, the temperature drop in reduction zone is very less and much away from the experimental data. As *CRF* values are increased from 1 to 1000, the temperature drop is increased and deviations from the experimental data also increase. For *CRF* = 1000, the final temperature of producer gas reaches close to the experimental data. But when the profile is examined (Fig. 5.37), it indicates that the temperature reduces in the first 2.5 cm from the top of the reduction zone and reaches the final temperature. Significant change is not observed in the remaining part of the reduction zone. This is attributed to the fact that the *CRF* value is increased and kept constant from top of the reduction zone. As *CRF* value is very high, the reactivity of char would also be very high and the reactions would get completed in the initial part only. On increasing *CRF* value, char would be more reactive and the initial length, in which significant temperature drop is observed, also decreases. For linearly increasing *CRF* value from 1 to 10000, temperature profile is also of convex type and deviations from the experimental data are also significant. For exponential increment in the *CRF* value, the temperature profile is matching with the experimental data in a better way than any other profile. The equation used for exponential increment is $CRF = A\,e^{Bx}$ where A = 1 and B = 0.0037. This equation gives an increment from 1 to 8000 for a length of 250 mm.

Table 5.6 Parameters used in the simulation of reduction zone model

Parameter	Value
Bed Length	24.5 cm
v initial	1.175 m/sec
T initial	1400 K
Moisture Content	16% (dry basis)
CRF	1,10,100, 1000, Exponentially varying, Linearly varying
f_p	0.3

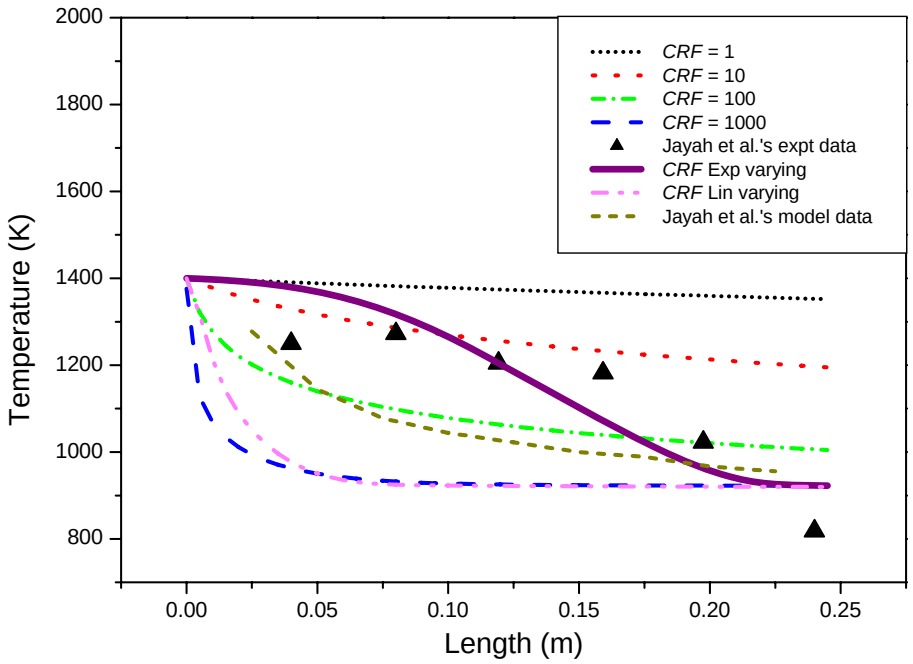

Fig. 5.37 Temperature profile for different *CRF* values

Table-5.7 shows the standard deviations, calculated using Eq. (5.4), from the experimental data for each profile. It shows that for the exponentially varying *CRF* values, the standard variation (SD) is the least, i.e., 0.091151. Fig. 5.38 shows the comparison of product gas compositions leaving the biomass gasifier for different *CRF* values with the experimental data reported by Jayah et al. (2003). It clearly indicates that the simulated data are differing widely from the experimental data when *CRF* value is equal to 1, 10 and 100. The simulated compositions are almost same for the cases of *CRF* = 1000, the linearly varying *CRF*, and the exponentially varying *CRF*. Hence it is difficult to judge which one of the three is better in terms of data fitting. For carbon monoxide, the composition values for *CRF* = 1000 fit well with the experimental data. However, for hydrogen, the composition value for linearly varying *CRF* is matching closely with the experimental data. So to get the quantitative variation from the experimental data standard deviation is found out. Table-5.8 shows the standard deviation of end product composition from the experimental data reported by Jayah et al. (2003).

Table-5.8 shows that the standard deviation is the least for the composition values when linearly varying *CRF* is considered. Based on the standard deviation for temperature profile, the exponentially varying *CRF* value should be considered and based on the standard deviation for end product composition, the linearly varying *CRF* should be chosen. To come out from this dilemma, the composition profiles for *CRF* = 1000, the linearly varying *CRF*, and the exponentially varying *CRF* are simulated and the results are presented in Fig. 5.39, Fig. 5.40, and Fig. 5.41 respectively. Fig. 5.39 shows the composition profile along the normalized length (ratio of actual length to the total length of reduction zone) for *CRF* = 1000.

Table 5.7 Standard deviation of temperature profile from the experimental temperature data for different *CRF*

Profile	*CRF*=1	*CRF*=10	*CRF*=100	*CRF*=1000	Linearly varying *CRF*	Exponentially varying *CRF*	Jayah's model (2003)
SD	0.346302	0.226614	0.145176	0.224383	0.224245	0.091151	0.147922

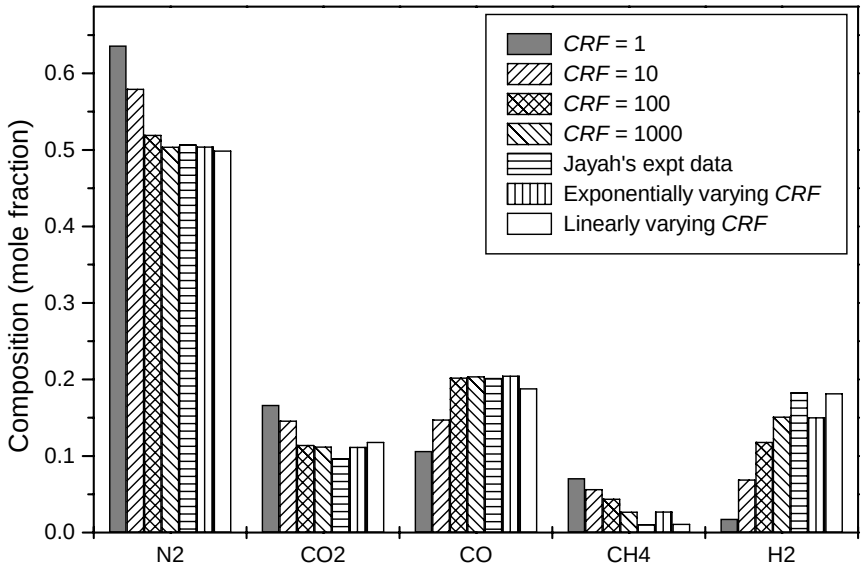

Fig. 5.38 Comparison of product gas composition for different *CRF* values

Table 5.8 Standard deviation of product composition from the experimental data for different *CRF* values

Profile	*CRF*=1	*CRF*=10	*CRF*=100	*CRF*=1000	Linearly varying *CRF*	Exponentially varying *CRF*
SD	2.808762	2.133514	1.533824	0.750679	0.118892	0.765496

Both profiles (Fig. 5.39 and Fig. 5.40) show that the fractions of carbon dioxide, nitrogen and methane continuously decrease and those of carbon monoxide and hydrogen increase. As nitrogen is an inert, its amount does not change. However, the amount of other gases changes due to the generation and depletion and due to the decrease in the fraction of nitrogen. The composition of CO_2 decreases as it is getting converted to CO. The composition of CO increases almost in the same fashion as CO_2 decreases. H_2 composition increases nonlinearly as gas travels through the reduction zone. The change in composition for almost all components is within the initial length of the reduction zone only.

The normalized length from the top of the reduction zone at which 85% of the total change in composition occurs is defined as the initial normalized length, L_{in}. For each component, L_{in} is found out for *CRF* = 1000 and for linearly varying *CRF* which are presented in Table-5.9. Table-5.9 shows that for N_2, CO_2 and CO, the value of L_{in} is less than 0.11 for a *CRF* value of 1000, and less than 0.17 for the values of linearly varying *CRF*. It indicates that only 11% length of the bed is used for the completion of 85% of the reaction, which is highly unrealistic in nature. The same phenomenon is also observed for linearly varying *CRF* where just 17% of the total length of the reduction zone gets used.

It confirms again that the constant *CRF* value should not be used in the simulation as it gives high standard deviation from the experimental data for the temperature profile (Table-5.6). And also it gives highly unrealistic composition profiles. These results also rule out the possibility of usage of linearly varying *CRF* values in the modification of model. For methane and hydrogen, the value of L_{in} is more. This is due to the fact that the

rate of reaction, which is represented by Eq. (3.91), is significantly less and even by increasing *CRF* values, the sudden change in composition is not observed. Fig. 5.41 shows the composition profile for the exponentially varying *CRF* values. Change in composition for all the components is nonlinear in nature. The composition of nitrogen, methane and carbon dioxide decreases and that of carbon monoxide and hydrogen increases. Fig. 5.41 also indicates that the change in composition is spread over the entire length of the reduction zone, which is different from Fig. 5.38 and Fig. 5.39. The results of exponentially varying *CRF* are quite satisfactory and realistic.

Another important observation is made during simulation studies that the rate of Boudouard' reaction, which is represented by Eq. (3.88), becomes negative at a temperature of 933 K. It represents that below this temperature, the reaction occurs in backward direction. The rate of reaction depends upon the equilibrium constant and the relative amount of different reacting species. The concentration of reacting gaseous species depends upon total pressure in the system and the equilibrium constant values. As the total pressure of the system remains constant and the equilibrium constants are functionally dependant on temperature alone, the rate of reaction effectively becomes a function of the bed temperature. As shown in Fig. 5.39, CO decreases and CO_2 increases at an L_n of 0.35. The same phenomenon is also observed in Fig. 5.40 and Fig. 5.41 at an L_n of 0.29 and 0.92 respectively. That is also because of the fact that the temperature of reduction zone falls below 933 K at that point as can be viewed in the Fig. 5.37. The exponentially varying *CRF* is considered for all the estimations in the subsequent studies, based on the positive and encouraging results obtained with this functionality as discussed above.

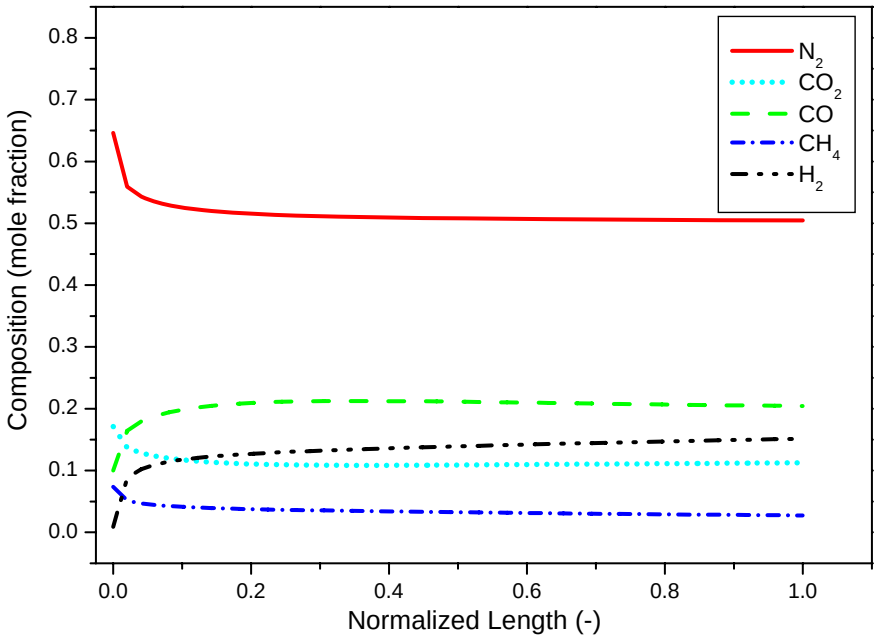

Fig. 5.39 Composition profile for *CRF* = 1000

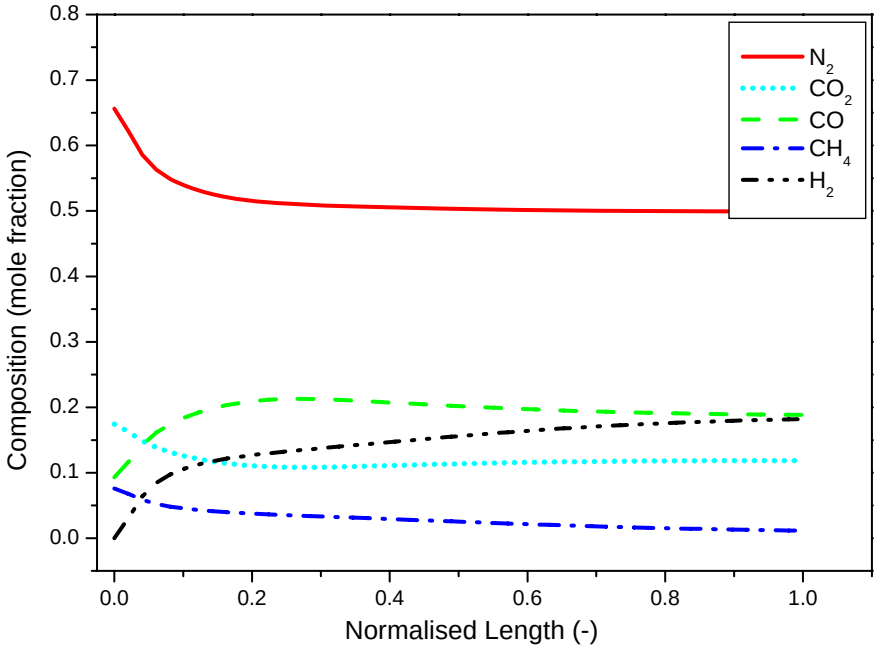

Fig. 5.40 Composition profile for linearly varying *CRF*

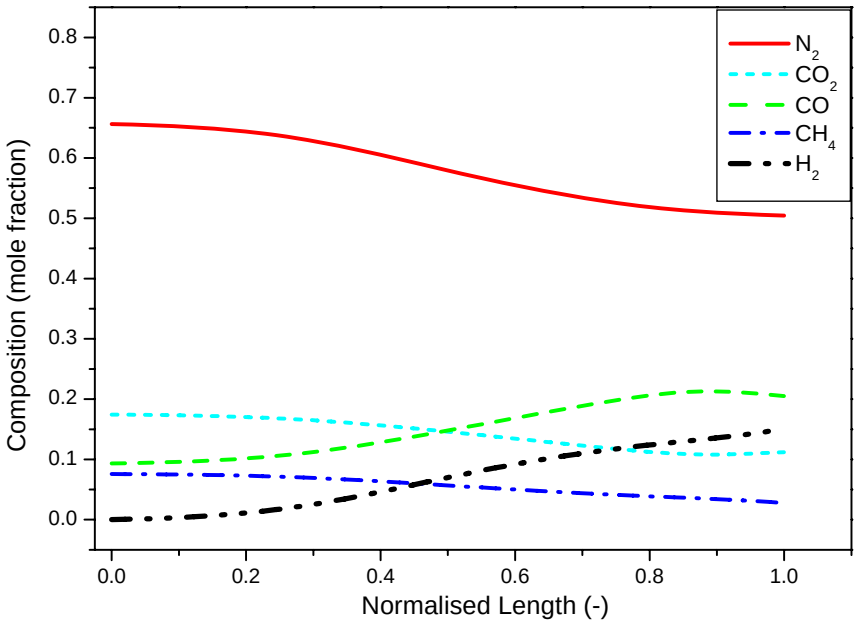

Fig. 5.41 Composition profile for exponentially varying *CRF*

Table 5.9 Initial normalized length L_{in} for different components

Sr No	Component	L_{in} (-)	
		***CRF* = 1000**	**Linearly varying *CRF***
1	N_2	0.1020	0.1633
2	CO_2	0.0612	0.1020
3	CO	0.0735	0.0816
4	CH_4	0.3877	0.4898
5	H_2	0.2653	0.5918

5.2.2.2 Validation of Complete Model with Experimental Data

The experimental data reported by Dogru et al. (2002) and those obtained in the present study are used to validate the simulation results of the complete combined transport and kinetic model. The initial moisture content fraction, air flow rate, temperature of the pyrolysis zone, and chemical composition of the biomass are required as an input data for the model to predict the composition of producer gas. The combined transport and kinetic model is validated using the parametric values as given in Table-4.2. The variation of molar fraction of producer gas components with time is predicted and compared with the experimental data. Figs. 5.42 to 5.52 show the comparison of model predicted molar fractions of producer gas components with those found experimentally. It is found that the model predicted molar fraction of nitrogen decreases first during the few initial minutes (5-10 min) of gasification. After that it increases and attains a steady value (after 10-15 min). The molar amount of nitrogen is constant for a particular flow rate of air as nitrogen acts as an inert but its composition varies due to the changes in molar amount of other components of gaseous mixture. It is found that the model predicted molar fractions of carbon monoxide and hydrogen increase first with time and after that it decreases and attains a steady value. It is observed that the model predicted molar fraction of methane is very less and almost remains constant. It is also found that the model predicted molar fraction of carbon dioxide decreases a little and attains a steady value.

The simulation results of the molar composition of various components of the producer gas match well with the experimental data of 10 minutes or higher from the start of run. For the experimental data of 5 min and 10 min, the simulation results differ more. This is because of the assumption taken in the model that all the gas generated in

pyrolysis or reduction zone travel downwards in the gasifier. However, it is observed while carrying out the experiments that the gas produced in the pyrolysis zone first travels upwards and occupies the empty space above the biomass. After 5 - 10 minutes from the start of the run, the accumulated gas builds up a pressure and the producer gas gets started flowing downwards. Because of this, the model predicts higher concentration of hydrogen and carbon monoxide and lower concentration of nitrogen in comparison to the experimental data for initial 5 -10 minutes from the start of a particular experimental run.

Fig. 5.53 shows the model predicted composition profile of gaseous phase across the gasifier at 5 min from the start of the experiment for the first run of the present study. Figs. 5.54 to 5.57 show the similar profiles at different times from the start of the experiment (run 1). The pyrolysis zone in the gasifier is represented by first 100 mm, oxidation zone by 100 to 140 mm and reduction zone by 140 to 270 mm in Figs. 5.53 to 5.57. It shows the variation of molar fraction of the main components of the producer gas, i.e. nitrogen, carbon monoxide, carbon dioxide, methane, water vapor, hydrogen, and tar, with time in the gasifier. It is found that the composition of water vapor in the gaseous phase is the highest in pyrolysis zone (0-100 mm) and decreases in oxidation zone (100-140 mm) and reduction zone (140-270 mm) of the gasifier, when it travels through these zones (Figs. 5.53 to 5.57). It is also observed that the molar fraction of water vapor decreases with time in all zones of the gasifier. The molar fractions of CO and CH_4 in the gaseous phase increase in the pyrolysis zone as gas travels through it.

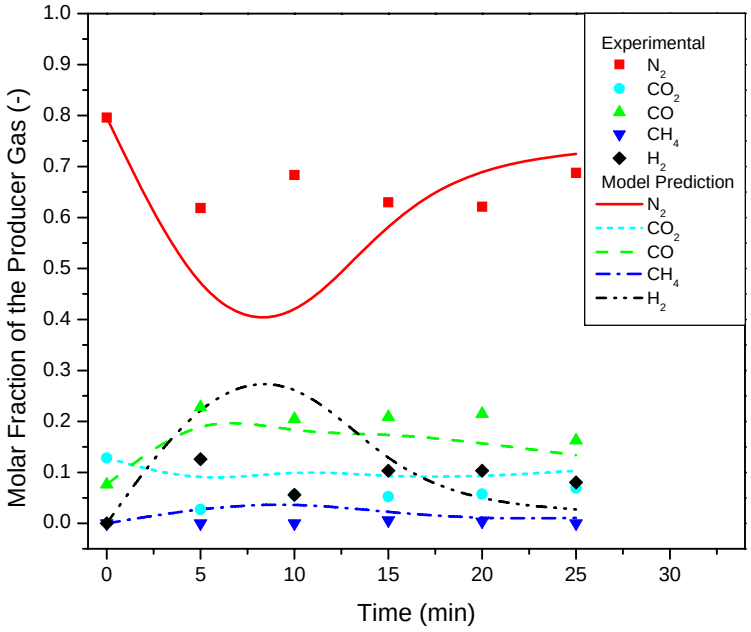

Fig. 5.42 Comparison of model predicted producer gas composition with experimental values of the present study (Φ = 0.2533)

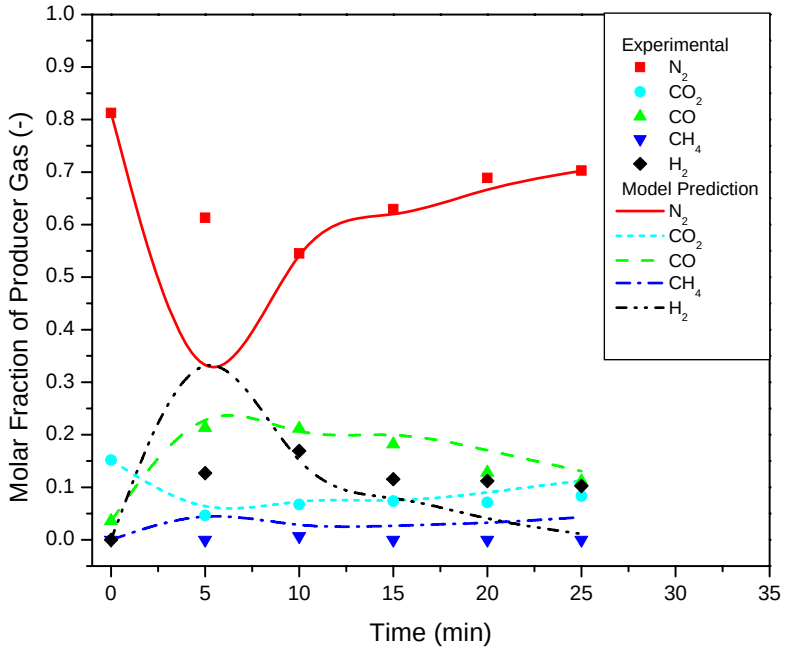

Fig. 5.43 Comparison of model predicted producer gas composition with experimental values of the present study (Φ = 0.1791)

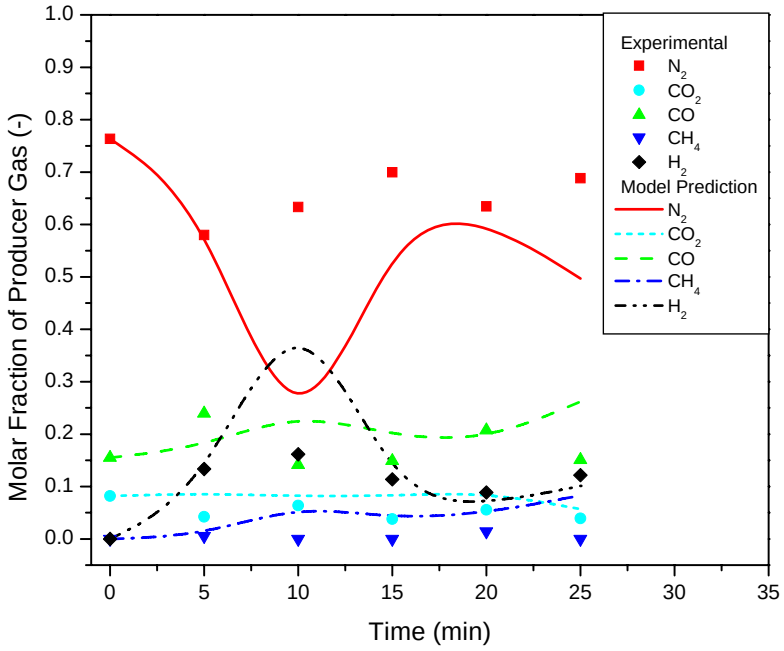

Fig. 5.44 Comparison of model predicted producer gas composition with experimental values of the present study (Φ = 0.1673)

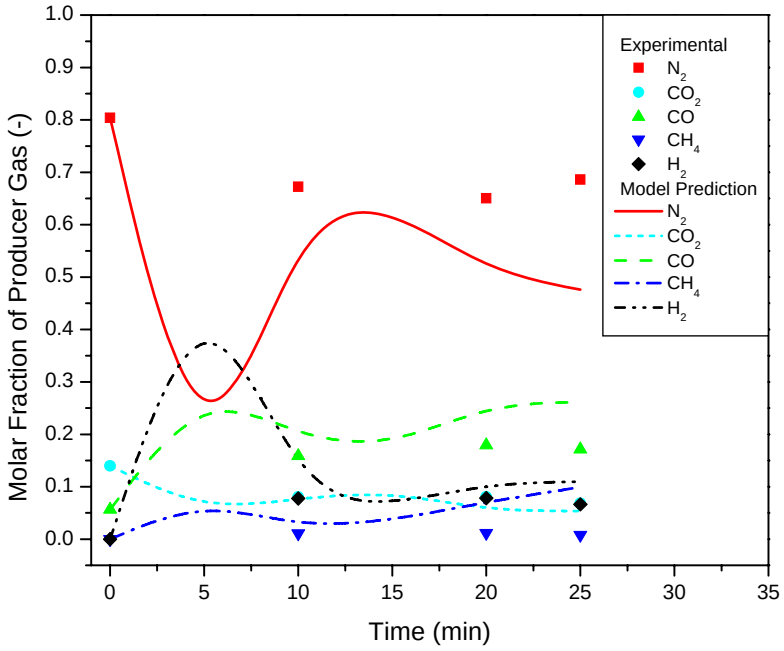

Fig. 5.45 Comparison of model predicted producer gas composition with experimental values of the present study (Φ = 0.1992)

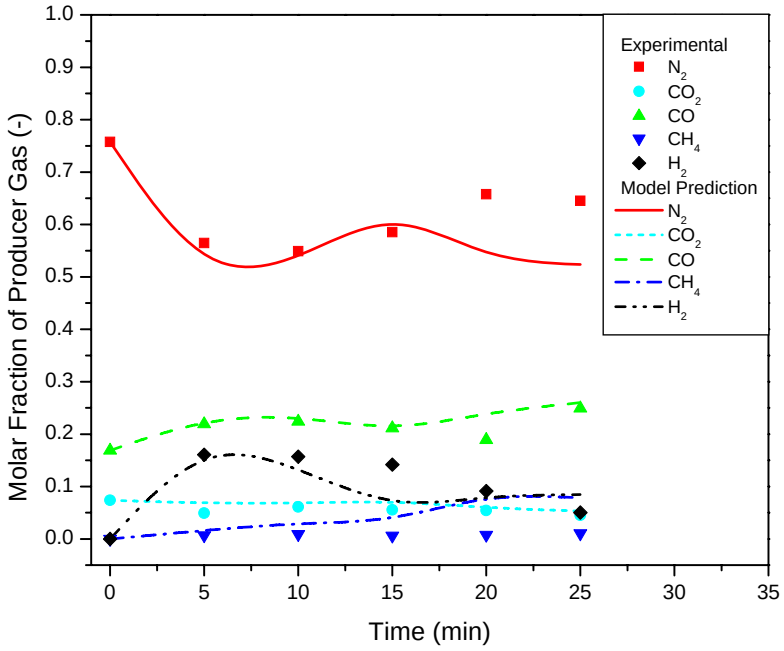

Fig. 5.46 Comparison of model predicted producer gas composition with experimental values of the present study (Φ = 0.2054)

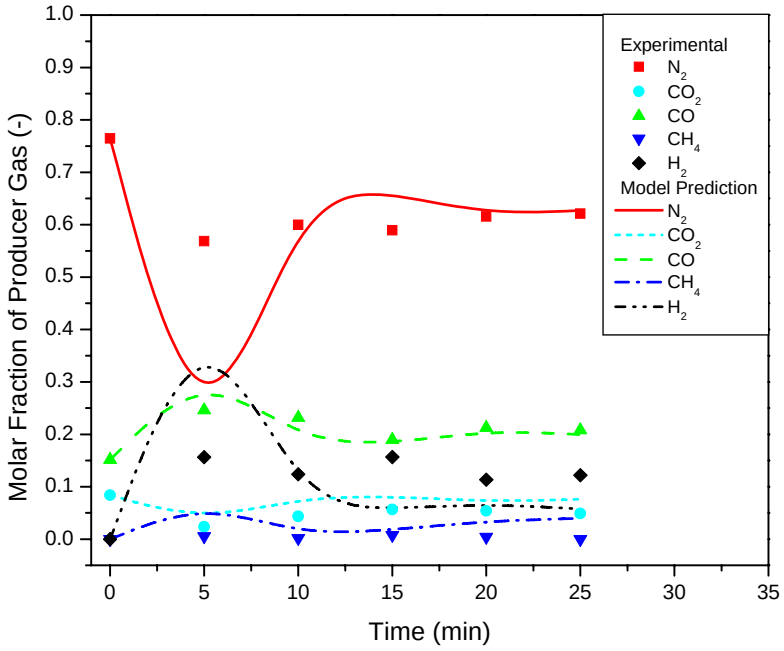

Fig. 5.47 Comparison of model predicted producer gas composition with experimental values of the present study (Φ = 0.3546)

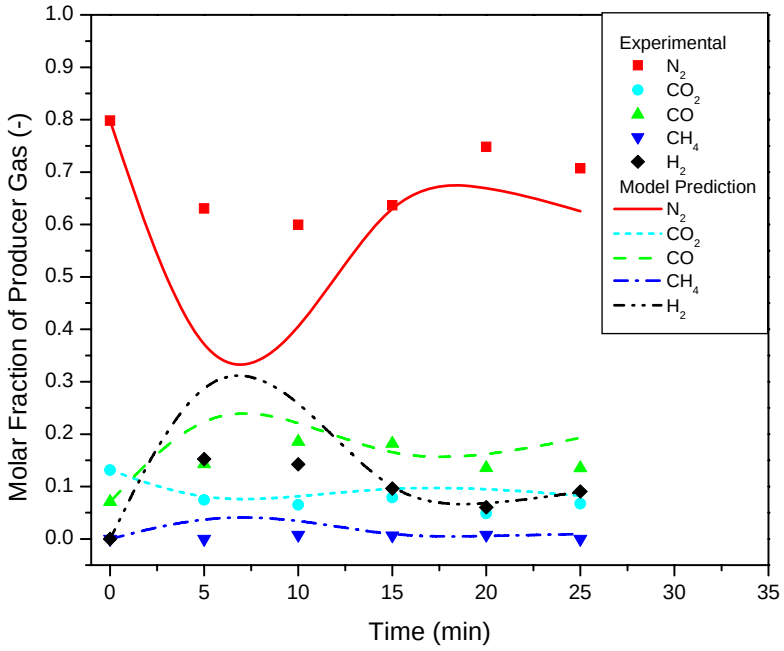

Fig. 5.48 Comparison of model predicted producer gas composition with experimental values of the present study (Φ = 0.2418)

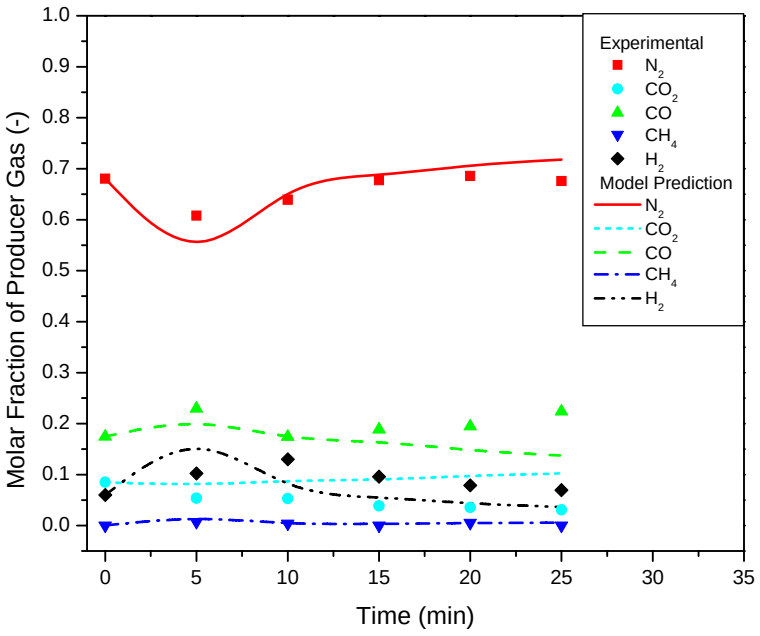

Fig. 5.49 Comparison of model predicted producer gas composition with experimental values of the present study (Φ = 0.278)

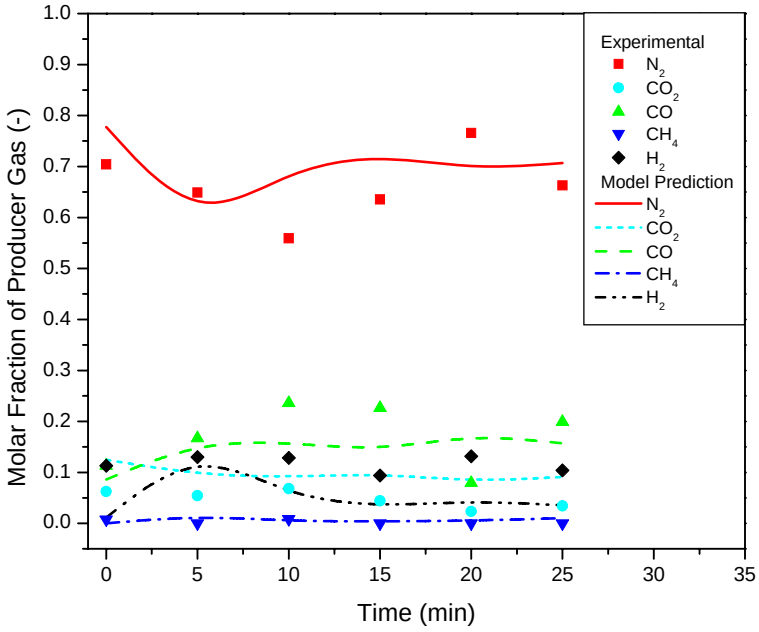

Fig. 5.50 Comparison of model predicted producer gas composition with experimental values of the present study (Φ = 0.1951)

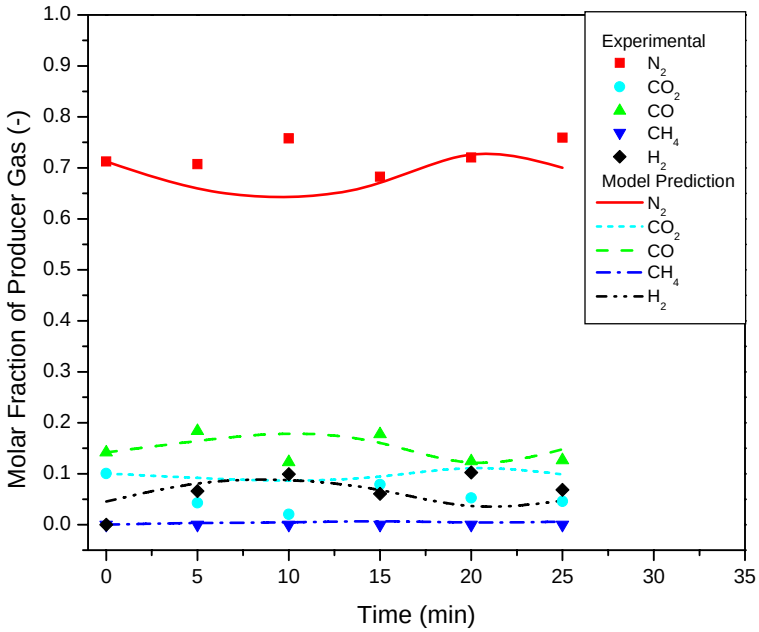

Fig. 5.51 Comparison of model predicted producer gas composition with experimental values of the present study (Φ = 0.3558)

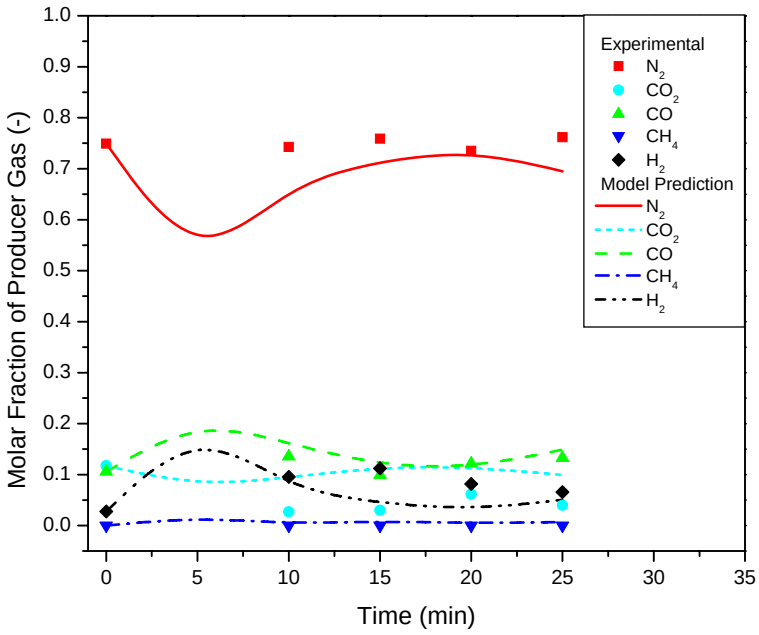

Fig. 5.52 Comparison of model predicted producer gas composition with experimental values of the present study (Φ = 0.3968)

It is found that the molar fractions of CO, H_2, and CH_4 decrease in oxidation zone due to combustion. The molar fraction of CO_2 increases and that of tar decreases due to the high temperature oxidation. The molar fraction of nitrogen almost remains constant in the oxidation zone due to the constant supply of air. In the reduction zone of gasifier, the molar fractions of CO and H_2 increase and those of CO_2 and N_2 decrease. The molar flow rate of nitrogen does not change but due to the water gas reaction, methane formation reaction, and Boudouard reaction, formation of hydrogen and carbon monoxide occurs and the composition of nitrogen decreases in the reduction zone.

It is also found that the composition of carbon monoxide, methane, hydrogen and tar increases and that of water vapor decreases with time in the pyrolysis zone of the gasifier due to successive increase in the temperature of the pyrolysis zone. The simulated composition profiles shown in Figs. 5.53 to 5.57 at different times from the start of the experiment give proper insight of the gasifier. These simulated variations of the molar fraction of gaseous components with time match with the theory of downdraft biomass gasification.

To compare the results generated by simulation of the combined transport and kinetic model with those of equilibrium model, the simulated composition of producer gas is averaged over 25 minutes. Fig. 5.58 shows the comparison of the average composition of producer gas with those found experimentally as a function of equivalence ratio. The simulated predictions using combined transport and kinetic model are matching better than those predicted by equilibrium model (Fig. 3.34).

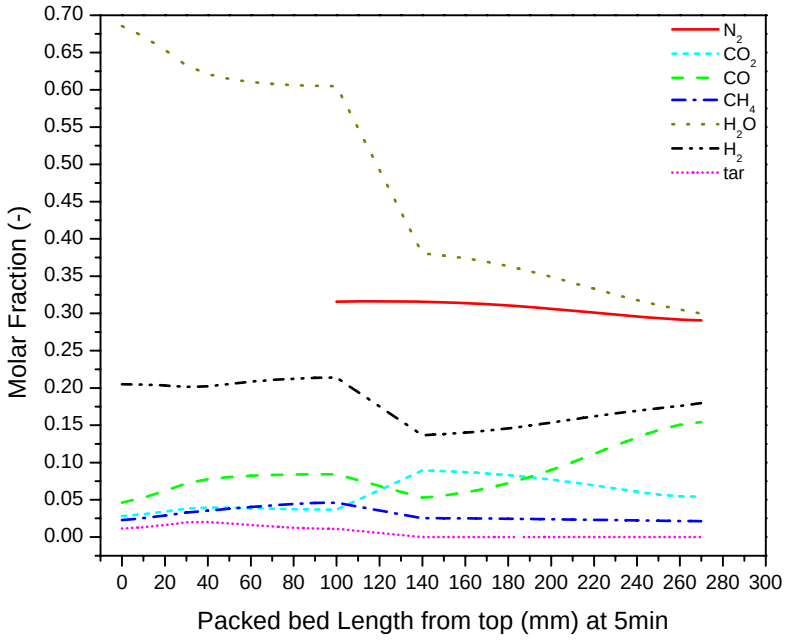

Fig. 5.53 Simulated composition profile across the gasifier at 5 min from the start of the experiment for the present study (Φ = 0.2533)

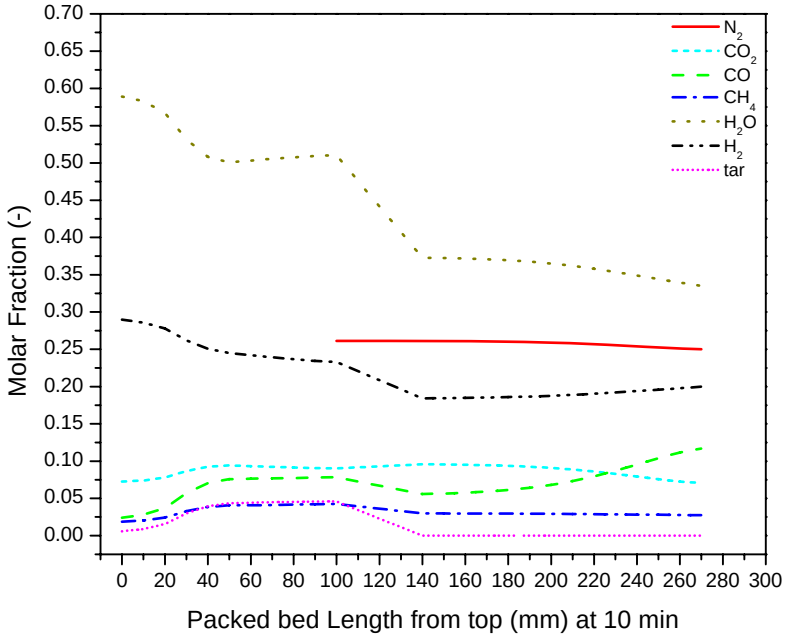

Fig. 5.54 Simulated composition profile across the gasifier at 10 min from the start of the experiment for the present study (Φ = 0.2533)

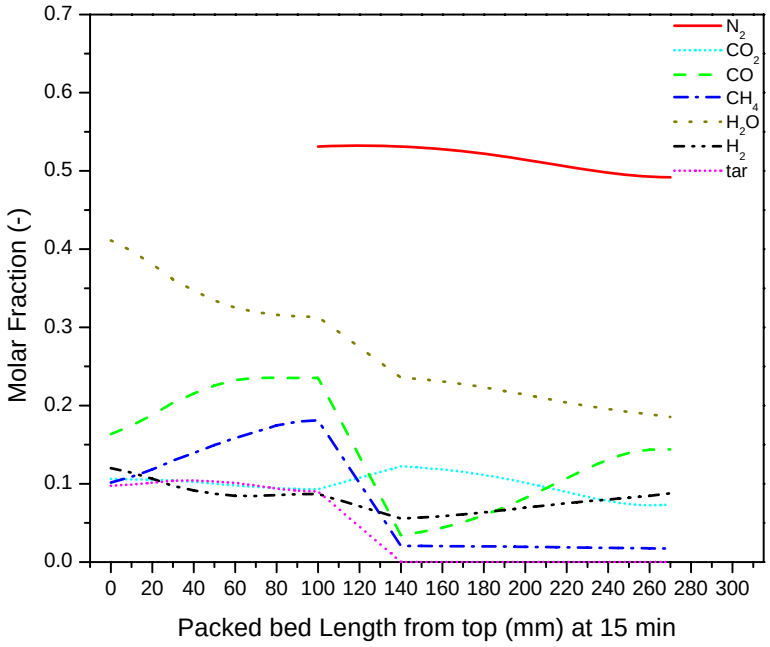

Fig. 5.55 Simulated composition profile across the gasifier at 15 min from the start of the experiment for the present study (Φ = 0.2533)

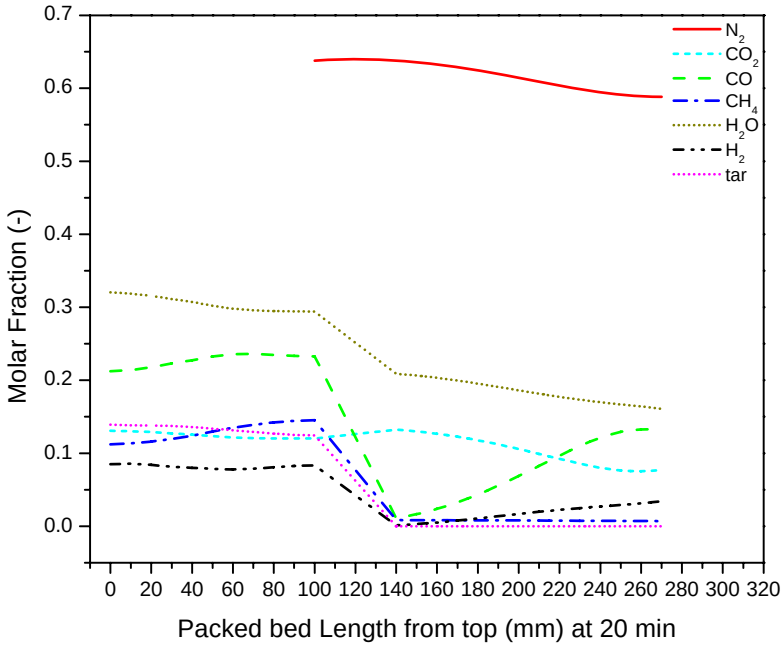

Fig. 5.56 Simulated composition profile across the gasifier at 20 min from the start of the experiment for the present study (Φ = 0.2533)

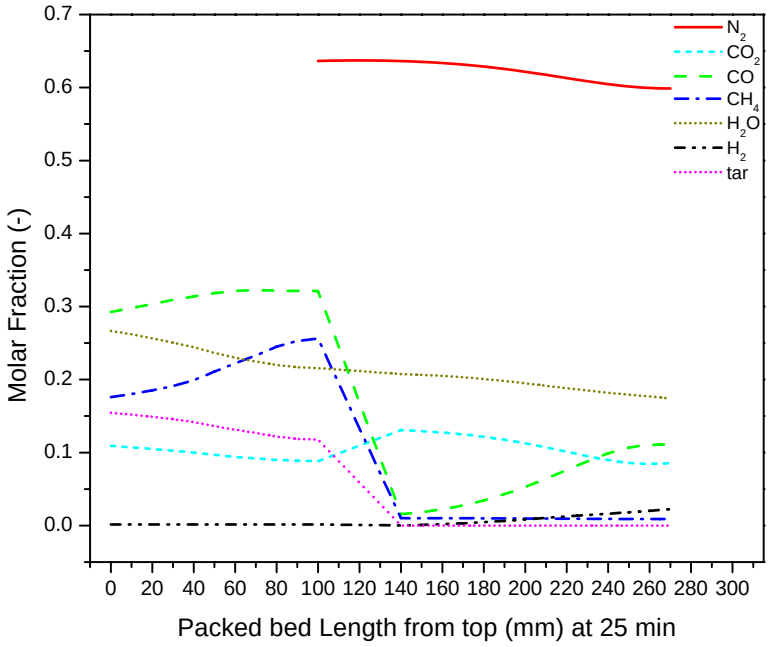

Fig. 5.57 Simulated composition profile across the gasifier at 25 min from the start of the experiment for the present study (Φ = 0.2533)

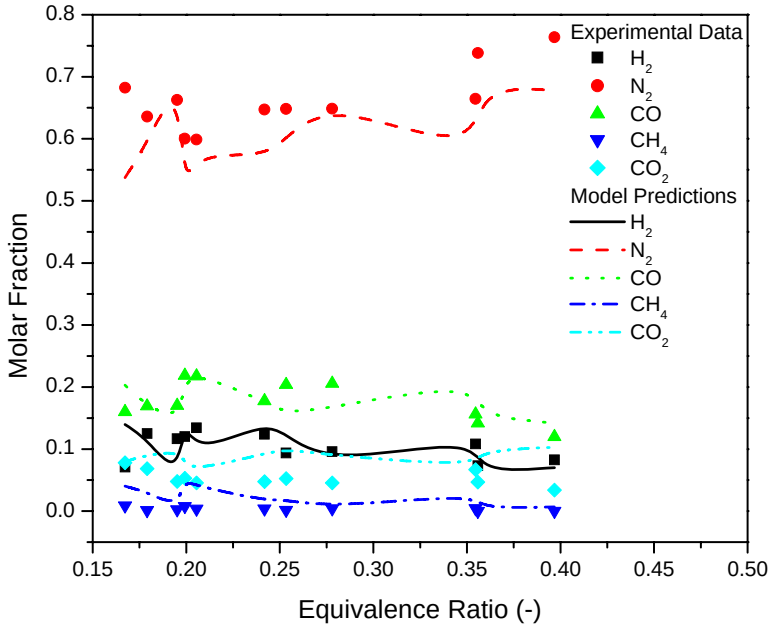

Fig. 5.58 Comparison of experimental data of present study with model predicted composition of producer gas

Table-5.10 shows the standard deviation of model predicted values calculated using Eq. (5.4). It clearly shows that the composition predictions using combined transport and kinetic model yield less standard deviation in comparison to the equilibrium model for all the components except methane. The experimental value of molar fraction of methane in producer gas is found using gas chromatograph. Gas chromatograph does not detect methane, if its concentration is below a certain value (0.25 %) and the molar fraction is considered as zero for a particular sample. Due to this constraint, the averaged value of molar fraction of methane becomes significantly low in comparison to the average value of the model predicted composition of methane.

The model developed in the present study is also validated using the data reported in the literature. Dogru et al. (2002) performed the gasification experiments with hazelnutshell as a biomass and the experimental results reported in their article are used to validate the present model. Table-5.12 shows the details of the experimental runs reported by Dogru et al. (2002) and Table-5.13 shows the details of the gasifier used in their experimental study. Fig. 5.59 shows the comparison of the model predicted composition of the producer gas with those obtained experimentally. It is found that the simulation results match very well with the experimental data. To compare the performance of the developed model with the equilibrium model, standard deviation is found and reported in Table-5.10. It clearly shows that the combined transport and kinetic model predicts much better than the equilibrium model.

Table 5.10 Standard Deviation of model predicted values

Reference	Variable	Standard Deviation	
		Equilibrium model	Combined transport and kinetic model
Present Study	Molar fraction of H_2	0.827393	0.419201
	Molar fraction of N_2	0.201364	0.108755
	Molar fraction of CO	0.309423	0.183082
	Molar fraction of CH_4	0.770779	8.936279
	Molar fraction of CO_2	2.81591	0.967683
Dogru et al. (2002)	Molar fraction of H_2	0.155329	0.130562461
	Molar fraction of N_2	0.065798	0.024335814
	Molar fraction of CO	0.334784	0.116844656
	Molar fraction of CH_4	0.80823	0.274339707
	Molar fraction of CO_2	0.678328	0.114904167

Table 5.11 Experimental data of Dogru et al. (2002) used for the validation of combined transport and kinetic model

Reference	Biomass Species	Run No	Initial Moisture Content (wt fraction, wet basis)	Air to Fuel Ratio (m^3/kg)	Oxidation zone Temperature (°C)	Pyrolysis Zone Temperature (°C)	Feed Rate (kg/h)
Dogru et al. (2002)	Hazelnutshell ($CH_{1.48}O_{0.735}$)	1	0.1245	1.63	821	308	1.73
		2	0.1245	1.64	833	314	2.15
		3	0.1245	1.52	846	362	2.64
		4	0.1245	1.38	869	489	3.19
		5	0.1245	1.51	1025	543	3.69
		6	0.1245	1.46	1015	531	4.02
		7	0.1245	1.47	1020	543	4.06
		8	0.1245	1.44	1130	562	4.48
		9	0.1245	1.37	1206	568	4.7
		10	0.1245	1.48	1110	549	4.93
		11	0.1245	1.50	1021	537	5.4

Table 5.12 The details of gasifier used in the experimental study by Dogru et al. (2002)

Sr. No.	Name of the parameter	Value
1	Pyrolysis zone diameter	375 mm
2	Depth of pyrolysis zone	170 mm
3	Oxidation zone diameter	450 mm
4	Throat diameter	135 mm
5	Reduction zone length	110 mm
6	Reduction zone diameter	135 mm
7	Biomass size	18 mm x 17 mm x 8 mm
8	Biomass absolute density	944.84 kg/m^3

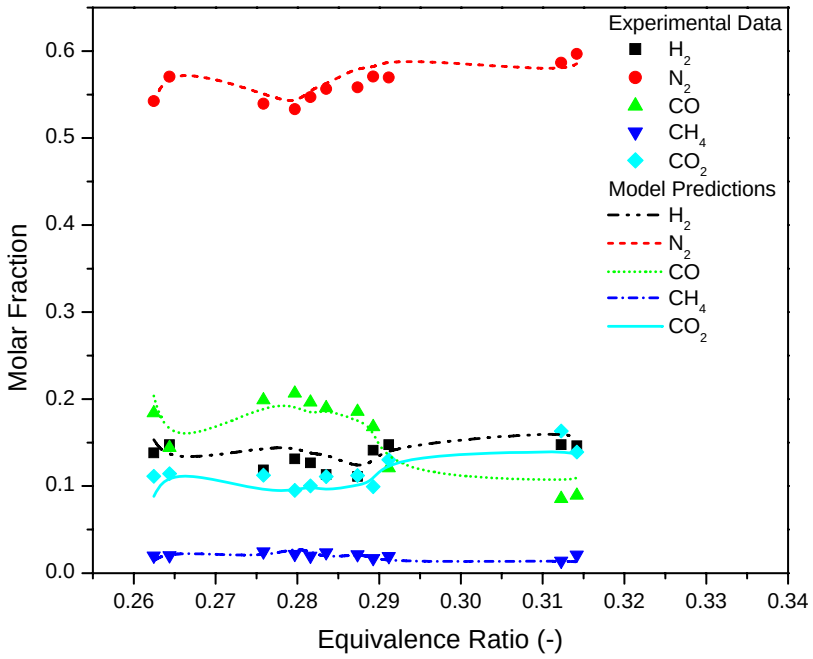

Fig. 5.59 Comparison of experimental data of Dogru et al. (2002) with model predicted composition of producer gas

5.2.3 Kinetic Parameter Estimation

The modeling equations, numerical solution, simulation methodologies and the values of the parameters used were reported in section 3.2.1.3 and section 3.2.4.5 of chapter 3. The objective function is the sum of square of the error between model predicted and experimental value, which is represented by Eq. (3.75) and Eq. (3.85). Differential Evolution (DE), a nontraditional optimization algorithm, is used to find the optimum value of the kinetic parameters. The kinetic parameters for Model-*KPE1* to *KPE4* are obtained using DE and described in section 5.2.3.1. To improve the population distribution, Logarithmic Differential Evolution (LDE) is developed and described in section 5.2.3.2.

5.2.3.1 Optimization using Differential Evolution

Table-5.15 shows the kinetic parameters of reaction 1 (A_1 and E_1) and reaction 2 (A_2 and E_2) of Eq. (3.61) for the heating rates of 10.0, 25.0, and 40.0 K/s for a sample size of 0.180 mm. Kinetic parameters are used to find the residual weight fraction and the results are compared with experimental data as shown in Fig. 5.60. It may be noted that it has not been possible to propose a unified correlation in terms of heating rate and hence separate kinetic parameters are determined for different heating rates (Table-5.15). For the heating rate values of 10, 25 and 40 K/s, model predictions are exactly matching with the experimental values in the temperature range of 600 to 650 K (Fig. 5.60). The rate of pyrolysis is initially very less for all three heating rates. With an increase in temperature, the apparent rate of reaction increases very fast. The rate of reaction remains constant up to a certain residual weight fraction value. This residual weight fraction value is 0.55, 0.47 and 0.35 for the heating rate values of 40, 25 and 10 K/s respectively. It indicates

that during the process of pyrolysis the reactivity of biomass is decreasing with a progress in conversion. To include the effect of variation of biomass activity, four different models are proposed based on different possible relation of activity of biomass with normalized conversion. The proposed models include the rate of change of activity with respect to solid reactant conversion in pyrolysis of hazelnut shell biomass. Reaction rate constant is expressed as a function of extent of reaction, which has replaced the Arrhenius relation of rate constant with temperature. These four developed models were discussed in section 3.2.1.3 of chapter 3.

Table 5.13 Kinetic Parameters of reaction 1 and reaction 2 of Eq. (3.61)

Heating Rates (K/s)		10	25	40
Kinetic Parameters	A_1 **(1/s)**	9.999999870e+014	5.771498789e+014	9.999999870e+014
	E_1 **(J/mol)**	1.830963883e+005	1.780711826e+005	1.789020459e+005
	A_2 **(1/s)**	9.999999870e+014	9.999999870e+014	9.999999870e+014
	E_2 **(J/mol)**	1.860584981e+005	1.818287369e+005	1.784195956e+005
Objective Function Value [Eq. (3.75)]		0.020025030	0.028319044	0.046808721

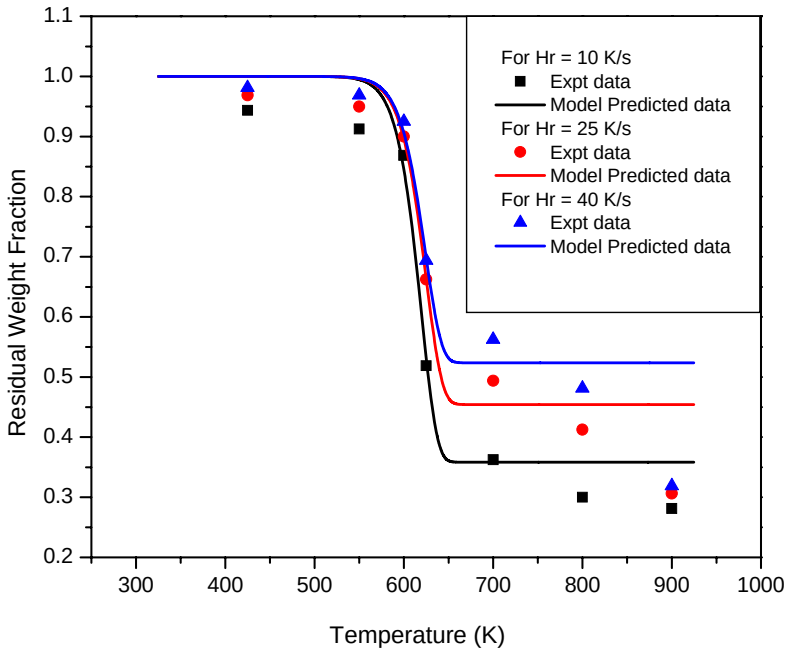

Fig. 5.60 Experimental and theoretical residual weight fraction for different heating rates (*Model-KPE1)*

Simulations are performed to find the kinetic parameters of reaction 1 and reaction 2 (A_1, E_1, A_2, E_2, n, β) of Eq. (3.61) for *Model-KPE1* to *KPE4* for heating rates of 10, 25 and 40 K/s for the ground hazelnut shell biomass sample of 0.180 mm size and reported in Table-5.16. For a heating rate value of 10 K/s, *Model-KPE2* gives the minimum value of objective function amongst various proposed models. But *Model-KPE3* fits better and gives a minimum objective function value for the heating rate of 25 and 40 K/s. It could be deceptive to go totally by objective function value for comparing the performance of various models because of the reasons given below. The values of objective function obtained for *Model-KPE2* and *Model-KPE3* are 0.01949137 and 0.028003858 respectively for heating rate value of 10 K/s (Table-5.16). For the temperature values of 600, 625 and 700K, predicted values of *Model-KPE2* are exactly matching with the experimental data; for the temperature values of 550, 800, and 900 K, the predictions of *Model-KPE3* are much better than the *Model-KPE2* predictions; and for the temperature value of 425 K, both *Model-KPE2* and *Model-KPE3* are predicting the same value (Fig. 5.61). However, *Model-KPE3* predictions and the trends obtained of residual weight fraction better represent the experimental data in the entire temperature range in spite of having a higher objective function value over *Model-KPE2*. Kinetic parameters reported in Table-5.16 are used to find residual weight fraction which is compared with the experimental data as shown in Fig. 5.61, Fig. 5.62 and Fig. 5.63 for the heating rate values of 10, 25 and 40 K/s respectively.

Table 5.14 Kinetic parameters of reaction 1 and reaction 2 of Eq. (3.61) for the pyrolysis of hazelnut shell

Kinetic Parameters								
Heating Rate (K/s)	**MODEL**	A_1 **(1/s)**	E_1 **(J/mol)**	A_2 **(1/s)**	E_2 **(J/mol)**	β	***n***	***Objective Function Value****
10.0	KPE1	9.999999870e+014	1.830963883e+005	9.999999870e+014	1.860584981e+005	-	-	0.020025030
	KPE2	8.101628677e+014	1.820082250e+005	6.525157449e+014	1.839203710e+005	-	8.354	0.019491337
	KPE3	1.631473979e+014	1.687529179e+005	3.817607903e+014	1.770171303e+005	4.000	-	0.028003858
	KPE4	9.998664072e+014	1.830208026e+005	8.531165618e+014	1.849042580e+005	4.000	10.000	0.023827228
25.0	KPE1	5.771498789e+014	1.780711826e+005	9.999999870e+014	1.818287369e+005	-	-	0.028319044
	KPE2	4.802800875e+014	1.771581429e+005	7.671474063e+014	1.805251955e+005	-	6.891	0.027951533
	KPE3	2.826228910e+011	1.348690973e+005	3.820552102e+010	1.273586962e+005	5.504	-	0.016778276
	KPE4	3.466431937e+014	1.755514367e+005	8.786262004e+014	1.812851772e+005	6.831	9.459	0.028126398
40.0	KPE1	9.999999870e+014	1.789020459e+005	9.999999870e+014	1.784195956e+005	-	-	0.046808721
	KPE2	9.928115823e+014	1.789845779e+005	9.928071716e+014	1.785507511e+005	-	7.445	0.111616604
	KPE3	1.354623177e+012	1.375183991e+005	2.255813493e+011	1.320127398e+005	10.000	-	0.017888651
	KPE4	9.999999870e+014	1.788643021e+005	9.999999870e+014	1.783705206e+005	4.000	10.000	0.045454113

*** [Eq. (3.75) for *Model-KPE1* and Eq. (3.85) for *Model-KPE2* to *4*]**

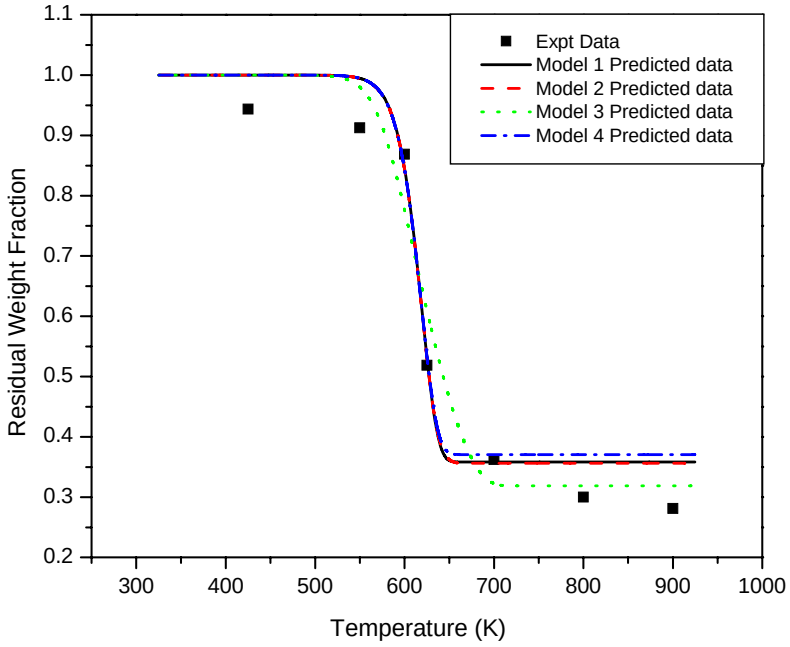

Fig. 5.61 Experimental and theoretical residual weight fraction for various models (heating rate = 10 K/s)

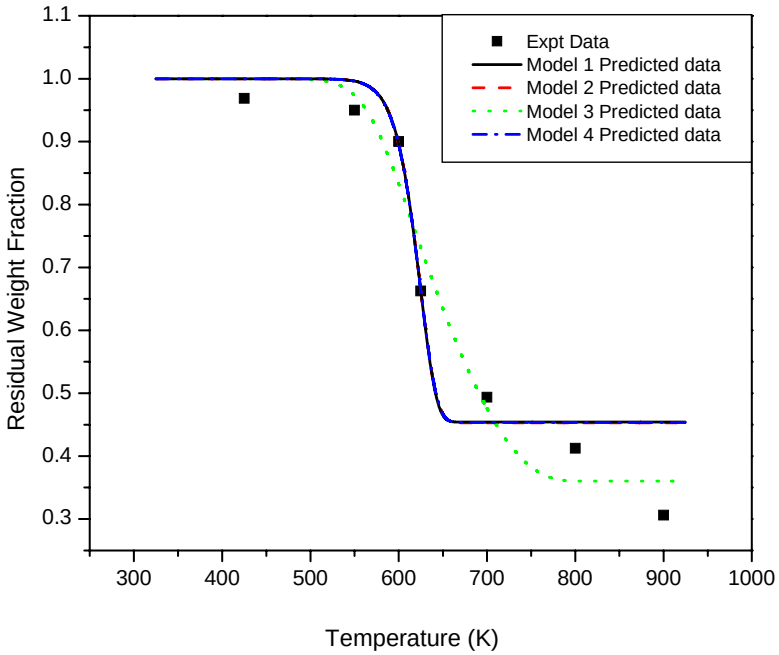

Fig. 5.62 Experimental and theoretical residual weight fraction for various models (heating rate = 25 K/s)

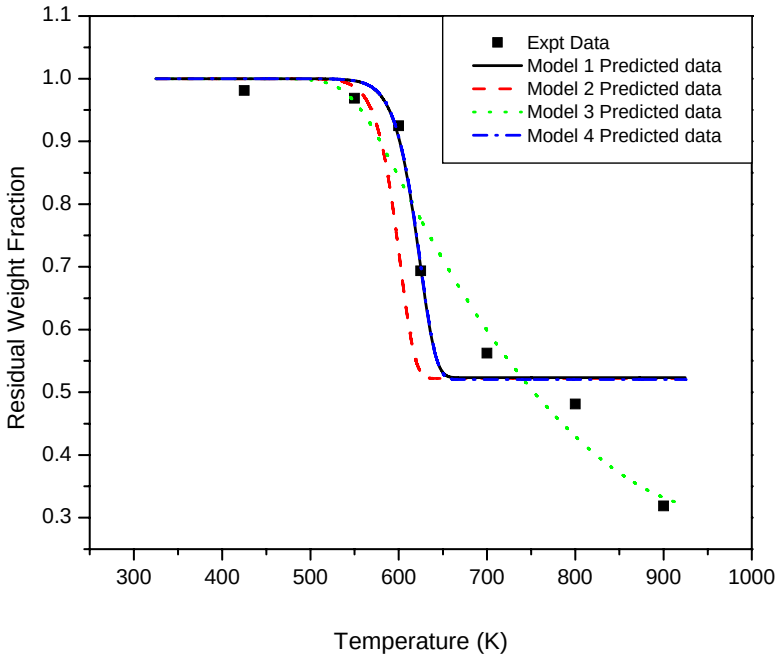

Fig. 5.63 Experimental and theoretical residual weight fraction for various models (Heating Rate = 40 K/s)

In *Model-KPE1*, the change of activity with conversion is neglected. In this model, neither the activation energy nor the frequency factor changes with conversion. As discussed in section 3.2.1.3, this approach gives significant deviations between the experimental and predicted values of the residual weight fraction for the hazelnut shell biomass. This is essentially due to the changes in the chemical composition and the physical properties of solid reactant with the extent of reaction. Fig. 5.62 and Fig. 5.63 show that *Model-KPE3* predictions fit better with the experimental data amongst the simulated results with various models in the entire temperature range for the heating rate values of 25 and 40 K/s. The objective function value is the least for *Model-KPE3* and reported in Table-5.16 for the heating rate values of 25 and 40 K/s.

5.2.3.2 Optimization using Logarithmic Differential Evolution

The key parameters of control in DE are: *NP*-number of population size, *CR*-cross over constant, and *F*-weight applied to random differential (scaling factor). These parameters are problem dependent. However, certain guidelines and heuristics are available for the choice of these parameters (Price and Storn, 1997; Babu, 2004). To study the effect of number of population point (NP) and population distribution on the value of optimized kinetic parameters of Model-*KPE1*, simulations are carried out by varying NP for a heating rate of 25.0 K/s. Table-5.17 shows the kinetic parameters of reaction 1 (A_1 and E_1) and reaction 2 (A_2 and E_2) of Eq. (3.61) for the heating rate of 25.0 K/s. NP value is varied from 10 to 50 times of the dimension of the problem. With an increase in NP value, the objective function value is decreased and a different set of kinetic parameters are found as optimum values. It clearly indicates that the kinetic parameter estimation is a multimodal problem and has a number of local minima. In addition, it also yields the

frequency factors of the order of 10^{17}, whereas the limits cover a wide range from 10^{10} to 10^{18} (i.e. forcibly getting trapped towards the upper limit only). Fig. 5.64 and Fig. 5.65 show the variation of population distribution of frequency factors (A_1 and A_2) and activation energies (E_1 and E_2) with the number of generations for an NP value of 200. For frequency factors (Fig. 5.64) the initial population covers only a part (10^{16} to 10^{18}) of the entire range (10^{10} to 10^{18}). Initial population of activation energies almost covers the entire range from lower to upper limit (Fig. 5.65), but majority of the points lie in the range from 10^5 to $3x10^5$ and a very few points lie near lower limit, i.e., 10^4. This is due to the linear mapping rule used in DE for initialization of normalized population. The mapping rule in the initialization of normalized population is given by Eq. (5.5).

New variable = Minimum value of the variable + Random no. (Maximum value of the variable – Minimum value of the variable) (5.5)

Table-5.18 shows the variable value with different random numbers ranging from 0.1 to 1.0 for a minimum value of 10^{10} and a maximum value of 10^{18}. For a change in the value of random number from 0.1 to 1.0, the change in the variable value is only one order of magnitude ($1.0x10^{17}$ to $1.0x10^{18}$), which is not good enough change taking into account of the possible range of variable value (10^{10} to 10^{18}). By this mathematical operation, the new variable value found in the initialization of DE would have the order of magnitude equal to that of the maximum value. So the optimum value found using simple DE may be a local minimum or maximum and not the global one. To overcome the problem of population distribution, logarithmic mapping rule is proposed for initialization of normalized population as given by Eq. (5.6)

Table 5.15. Kinetic parameters of reaction 1 and reaction 2 found using simple DE for heating rate of 25 K/s

Number of Population (NP)	Kinetic Parameters				Objective Function Value [Eq. (3.75)]
	A_1 (1/s)	E_1 (J/mol)	A_2 (1/s)	E_2 (J/mol)	
40	4.566886671e+017	2.113759061e+005	5.720718806e+017	2.126114848e+005	9.130447823e-003
80	4.558503512e+017	2.113970396e+005	4.765050853e+017	2.117037535e+005	9.128729091e-003
120	3.709092314e+017	2.102901874e+005	3.507645032e+017	2.100792813e+005	9.109103152e-003
160	1.416632742e+017	2.055108395e+005	9.999999843e+017	2.155763135e+005	9.048729762e-003
200	1.337902880e+017	2.052421797e+005	9.999999843e+017	2.156096494e+005	9.041855517e-003

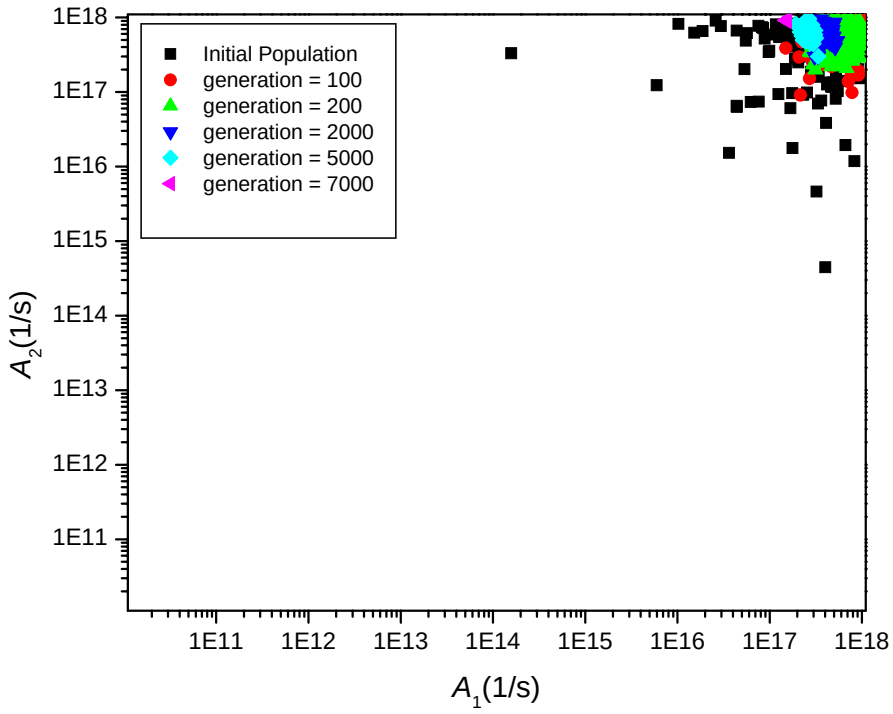

Fig. 5.64 Population distribution of frequency factors for NP = 200 using simple DE

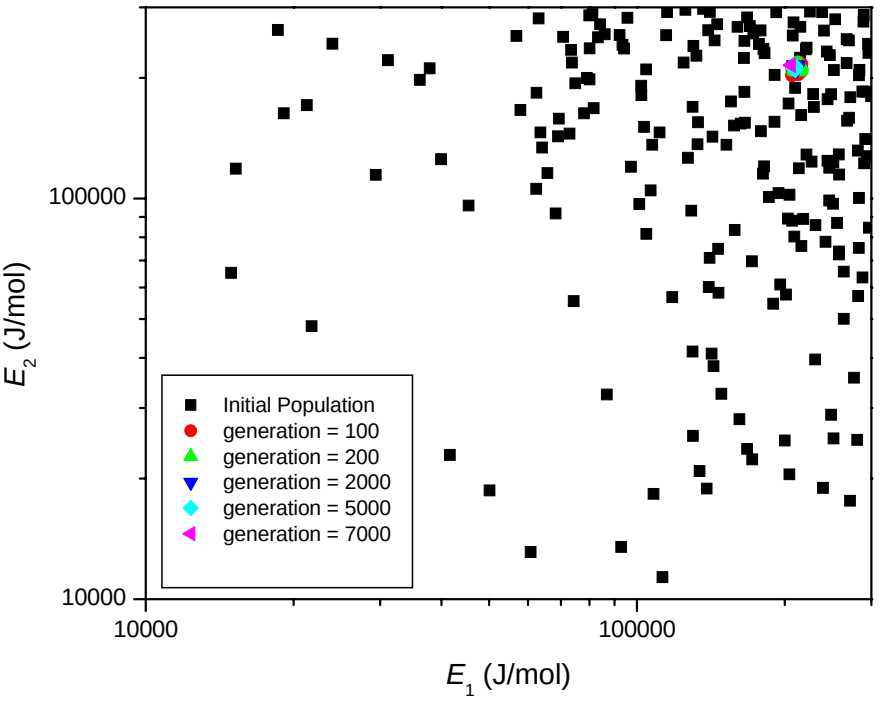

Fig. 5.65 Population distribution of activation energies for NP =200 using simple DE

Table 5.16 Variable value for different random numbers (Min = 10^{10} and Max = 10^{18})

Random Number	Variable Value using simple initialization [Eq. (5.5)]	Variable Value using logarithmic initialization [Eq. (5.6)]
0.1	1.000×10^{17}	6.309×10^{10}
0.2	2.000×10^{17}	3.981×10^{11}
0.3	3.000×10^{17}	2.512×10^{12}
0.4	4.000×10^{17}	1.585×10^{13}
0.5	5.000×10^{17}	1.000×10^{14}
0.6	6.000×10^{17}	6.309×10^{14}
0.7	7.000×10^{17}	3.981×10^{15}
0.8	8.000×10^{17}	2.512×10^{16}
0.9	9.000×10^{17}	1.585×10^{17}
1.0	1.000×10^{18}	1.000×10^{18}

Variable value = AntiLog {Log(minimum value) + (random number) [Log(maximum value) - Log(minimum value)]} (5.6)

New variables are found using Eq. (5.6) with a minimum value of 10^{10} and maximum value of 10^{18} for different values of random numbers ranging from 0.1 to 1.0. A wide distribution of new variable values, which is essential to cover a wide range of the said variable, is obtained and given in Table-5.18.

For the present problem of kinetic parameter estimation for a heating rate of 25 K/s, logarithmic mapping is used to initialize the normalized population vectors and simple differential evolution is applied to find out the global optimum value of kinetic parameters (We call this algorithm, LIDE). Fig. 5.66 and Fig. 5.67 shows the population distribution of frequency factors and activation energies respectively, for NP = 200 with respect to the number of generations in case of LIDE. In comparison with simple DE (Fig. 5.64 and Fig. 5.65), LIDE gives a better population distribution for A_1, A_2, E_1, and E_2. Table-5.19 shows the optimum kinetic parameters and the value of objective function found by using LIDE for different values of NP. Comparison for NP = 40, 120 and 160 from Table-5.17 (simple DE) and Table-5.19 (LIDE) shows that the objective function value is less for simple DE and for NP = 80 and 200 LIDE gives better results in terms of optimum value of objective function. It may be noted that the optimum values of frequency factors are of the order of 10^{17}. Also in Fig. 5.66 and Fig. 5.67, the population distribution just after 20^{th} generation narrows down and all the points lie very close to the upper limit value of the variable. This kind of population distribution change with respect to number of generations in DE is due to the mutation operator.

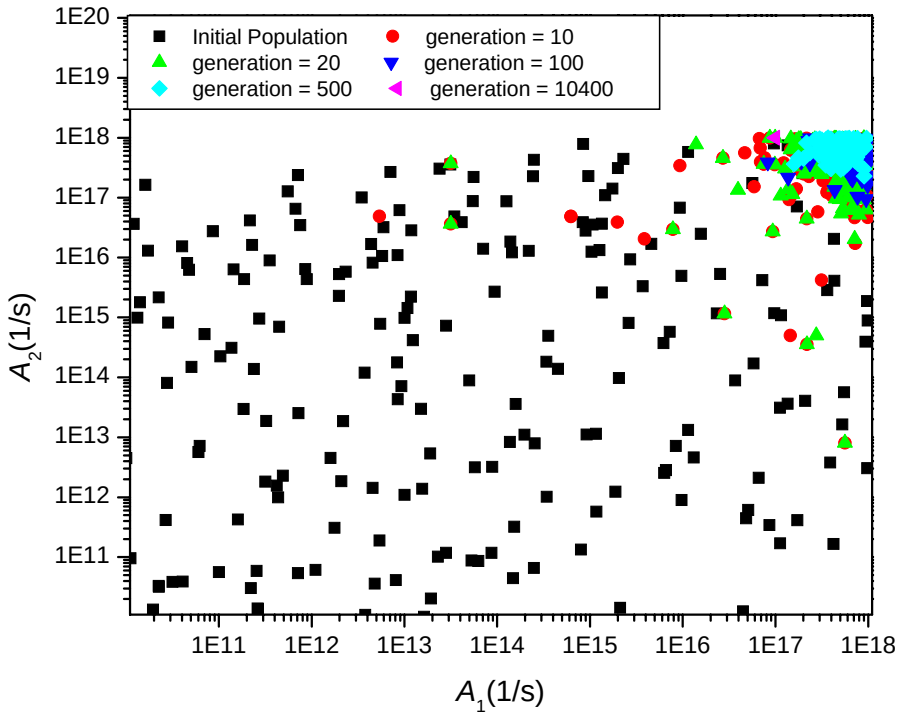

Fig. 5.66 Population distribution of frequency factors for NP =200 using LIDE

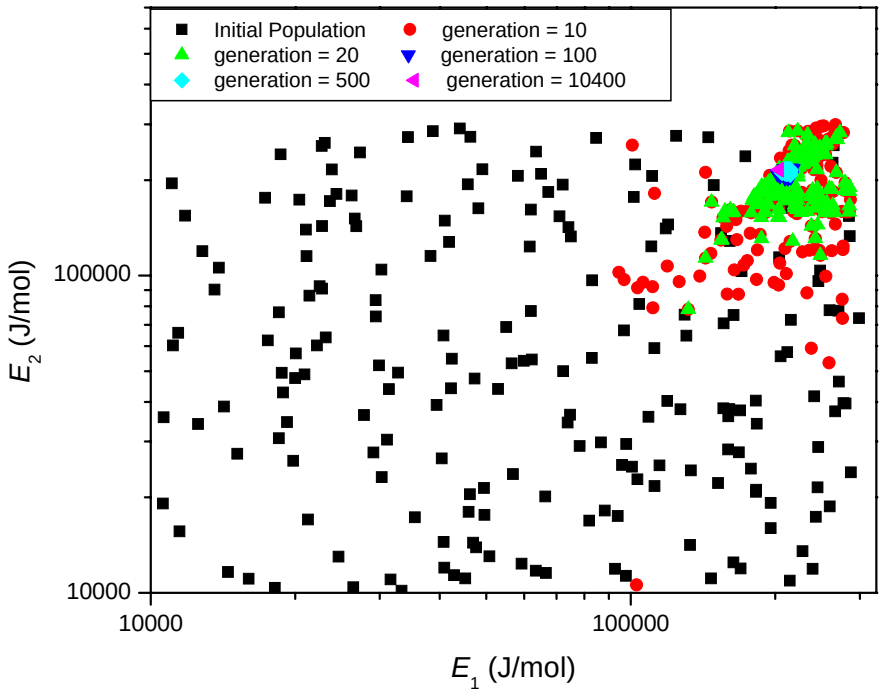

Fig. 5.67 Population distribution of activation energies for NP =200 with LIDE

In the mutation operation of DE, weighted difference vector is generated by taking the difference of two randomly chosen vectors. Noisy random vector is calculated by adding weighted difference vector and the randomly chosen target vector. Mathematically it is written as given by Eq. (5.7).

Noisy Random Vector = Target Vector + Scaling Factor (difference of two randomly chosen vectors) (5.7)

For a scaling factor of 0.5, and the order of three randomly chosen vectors of 10^{10}, 10^{12} and 10^{17} respectively

Noisy Random Vector = $10^{10} + 0.5\ (10^{17} - 10^{15}) = 4.95 \times 10^{16}$

Because of this linear operation, all the members of the mutant population would be of highest order among the three randomly chosen vectors (irrespective of their numerical values) and after few generations, the entire population of points lie near the upper limit of the variable. To overcome the problem of population distribution generation after generation, logarithmic mutation is proposed as given by Eq. (5.8).

Noisy Random Vector = AntiLog {log(variable[c]) + F (log(variable[a]) - log(variable[b]))} (5.8)

where a, b and c are randomly chosen number from the population size. For a Scaling factor of 0.5, and the order of three randomly chosen vectors of 10^{10}, 10^{12} and 10^{17} respectively

Noisy Random Vector = AntiLog $\{\log (10^{10}) + F (\log(10^{17}) - \log(10^{15}))\} = 1.0 \times 10^{11}$

By implementation of logarithmic mutation in DE, a better mutant population in terms of wide population distribution is expected and so a better chance of getting the global

optimum values. We call this logarithmic initialization and logarithmic mutation of DE as Logarithmic DE (LDE).

To compare the performance of LDE with simple DE and LIDE, LDE is applied to the present problem of kinetic parameter estimation for a heating rate of 25 K/s. Table-5.20 shows the optimum kinetic parameters and the value of objective function found by using the LDE for different values of NP. The objective function value is the least using LDE in comparison with simple DE (Table-5.17) or LIDE (Table-5.19) for any NP Value. The optimum values of the kinetic parameters found using LDE are also quite different from those found using simple DE and LIDE. Fig. 5.68 shows the population distribution of the frequency factors with the number of generations using LDE. Initial population is widely spread over the entire range and the population distribution after subsequent generations is also spread over a wide range.

Comparison of Fig 5.68 with Fig. 5.66 and Fig. 5.64 shows that LDE gives a wide spread of population distribution and so could give better values of optimum variables. The lines shown in Fig. 5.68, i.e. the drop lines drawn on to x-axis and y-axis, show the population after 5000 generations, where all the points merge to give the optimum value of frequency factors. Fig. 5.69 shows the variation of population distribution with number of generations for activation energies. Using the optimum kinetic parameters for NP = 200 and found by simple DE (Table-5.17), LIDE (Table-5.19) and LDE (Table-5.20) are used to find the residual weight fraction and the results are compared with the experimental data as shown in Fig. 5.70. It shows that the model predictions for LDE fit better with the model predictions found using simple DE and LIDE.

Table 5.17. Kinetic Parameters of reaction 1 and reaction 2 found using LIDE for heating rate of 25 K/s

Number of Population (NP)	Kinetic Parameters				Objective Function Value [Eq. (3.75)]
	A_1 (1/s)	E_1 (J/mol)	A_2 (1/s)	E_2 (J/mol)	
40	3.625545542e+017	2.101262519e+005	2.405592550e+017	2.080204938e+005	9.135202071e-003
80	1.684361501e+017	2.064137617e+005	6.975696814e+017	2.137319632e+005	9.071062357e-003
120	3.732242417e+017	2.104686034e+005	4.505817354e+017	2.115734744e+005	9.125753720e-003
160	2.426530209e+017	2.082492439e+005	9.999999843e+017	2.155842635e+005	9.085364436e-003
200	9.959812379e+016	2.037569391e+005	9.999999843e+017	2.156303008e+005	9.021881334e-003

Table 5.18. Kinetic Parameters of reaction 1 and reaction 2 found using Logarithmic DE (LDE) for heating rate of 25 K/s

Number of Population (NP)	Kinetic Parameters				Objective Function Value [Eq. (3.75)]
	A_1 (1/s)	E_1 (J/mol)	A_2 (1/s)	E_2 (J/mol)	
40	1.540784554e+014	1.713920488e+005	2.005103335e+013	1.619462097e+005	6.442233304e-003
80	3.885485326e+014	1.758750841e+005	4.551904297e+012	1.541520486e+005	6.441844469e-003
120	2.284807833e+014	1.734125580e+005	1.961720679e+014	1.735975231e+005	6.425304514e-003
160	2.119764183e+014	1.731095826e+005	6.750124424e+014	1.800125476e+005	6.421839787e-003
200	2.106331972e+014	1.730996444e+005	3.014892950e+015	1.876928166e+005	6.294910790e-003

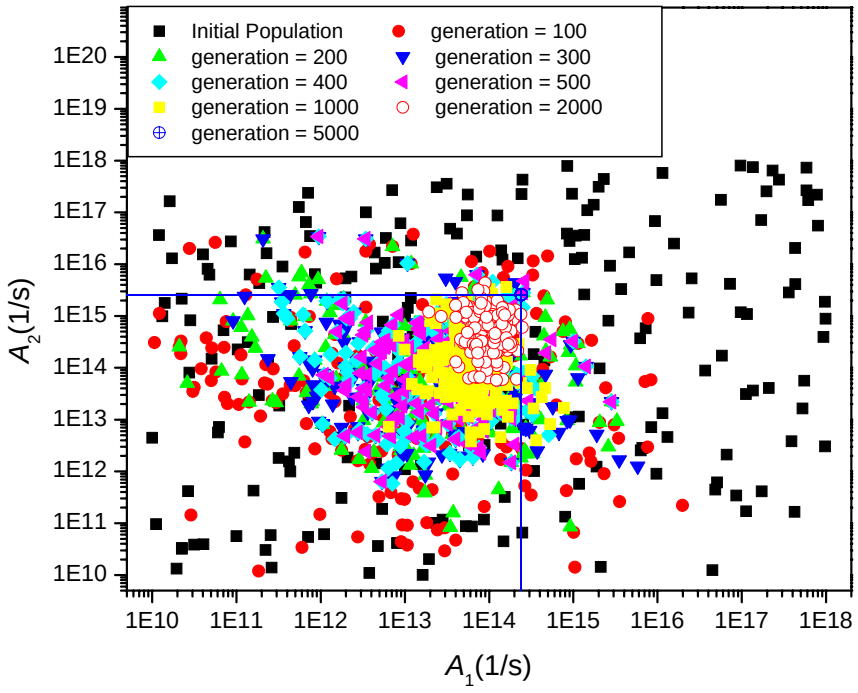

Fig. 5.68 Population distribution of frequency factors for NP =200 with LDE

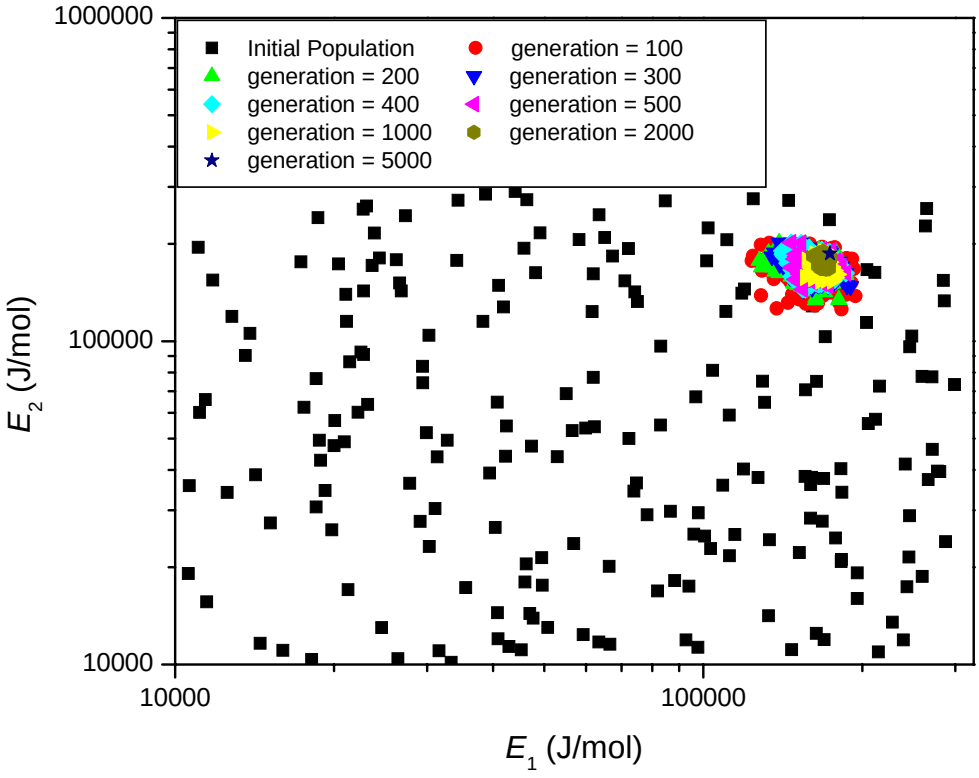

Fig. 5.69 Population distribution of activation energies for NP =200 with LDE

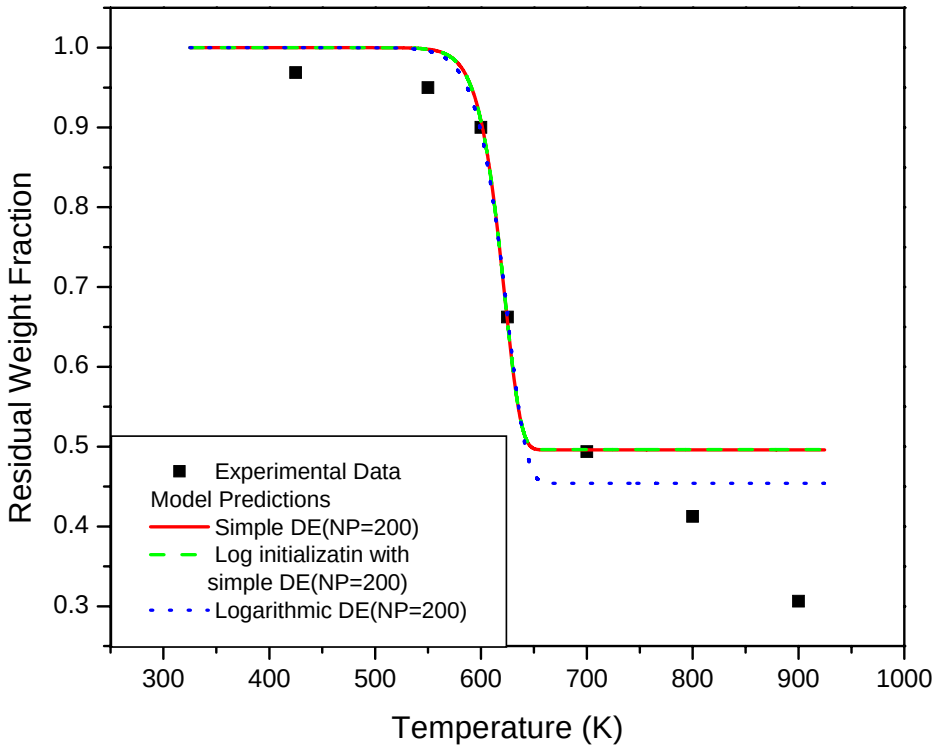

Fig. 5.70 Experimental and theoretical residual weight fraction for heating rate of 25 K/s

CHAPTER – 6

CONCLUDING REMARKS

In the present study, a combined transient single particle and fuel bed model is formulated by incorporating the mass, momentum and energy balances. The developed model takes into account of the kinetics of chemical reactions, heat and mass transfer between solid and gaseous phases and transport of volatiles produced. To validate the combined transport and kinetic model, experimental data is generated covering a wide range of operating parameters. Experimental study is carried out using wood waste as biomass to generate producer gas using a downdraft gasifier. The developed model is also validated with the experimental data reported in the literature. To compare the results predicted by combined transport and kinetic model with those of the equilibrium model, the latter model is also formulated in the present study. This chapter presents a brief summary of the present work followed by conclusions, major contributions and future scope for research in this area.

6.1 Summary

6.1.1. Introduction

All living organisms rely on an external source of energy to grow and to reproduce. The energy resources may be categorized into two groups: finite (e.g. minerals) and perpetual (renewable resources such as solar, wind, tidal, etc.).The major perpetual energy

resources are solar energy, wind energy and bioenergy. The effects on global and environmental air quality of pollutants released into the atmosphere from fossil fuels provide strong arguments for the substitution of these fossil fuels with renewable energy resources. Clean, domestic and renewable energy is commonly accepted as the key for future life. Bioenergy is arguably the one truly renewable energy resource, in that each new crop or harvest represents a partial renewal of its resource base, which itself is subject to constant depletion through its use as a fuel or feedstock. Bioenergy is derived from the plant sources, such as wood from natural forests, waste from agricultural and forestry processes and industrial, human or animal wastes. Due to inherent disadvantage of incomplete and inconsistent combustion in direct combustion of biomass and wastes, biomass is required to be upgraded in terms of more easily handled fuels, namely gases, liquids, and charcoal. Inefficient combustion may produce organic particulate matter, carbon monoxide and other organic gases. The impact on health of air pollution is a serious concern in developing countries, where inefficient combustion of wood is practiced in open fires for domestic cooking and space heating. Thermochemical and biochemical processes are the two categories in which the primary fuel is converted into a secondary fuel (solid, gas and/or liquid form) by processes such as pyrolysis, gasification, carbonization, digestion, fermentation, etc. Although fermentation or digestion is successfully used to produce ethanol, it is feedstock limited, time consuming and low yield process. Biomass gasification is one of the promising routes amongst the renewable energy options of future energy. Gasification is a process of conversion of solid biomass into combustible gas by partial oxidation. The resulting gas is a mixture of carbon monoxide, hydrogen, methane, carbon dioxide and nitrogen, which is known as producer

gas. The producer gas is more versatile than the original solid biomass. It is burnt to produce process heat and steam or used in gas turbines to produce electricity. In view of the considerable interest in the gasification process worldwide, it is necessary to model and predict the performance of a gasifier, *a priori*. There is a need to develop a model, which can predict the composition of producer gas for a specific biomass under particular operating conditions. After developing the mathematical model, it is essential to validate the same using experimental data. To perform the experimental study, down draft biomass gasifier is the best configuration amongst the available gasifiers as it provides almost tar-free gas. For a down draft biomass gasifier, there is a need to find the optimum air flow rate which gives the producer gas with highest calorific value.

6.1.2. Gaps in Literature

Modeling of biomass gasification implies the representation of chemical and physical phenomena constituting pyrolysis, combustion, reduction, and drying in the system of equations which taken together can provide a valuable quantitative information about the process. Downdraft biomass gasification models can be categorized into two groups: (1) Equilibrium models and (2) Combined transport and kinetic models. The equilibrium model assumes that all the reactions are in thermodynamic equilibrium in the biomass gasifier. Kinetics-free equilibrium models can predict the exit gas composition, given the solid composition and the equilibrium temperature, but they cannot be used for reactor design. An equilibrium model can not predict the concentration or temperature profiles across the gasifier axis and hence results generated using an equilibrium model would give the same final composition for different lengths of reduction zone of biomass gasifier. There is a need to develop a model which takes into account of the kinetics of

homogeneous & heterogeneous chemical reactions, transport of volatiles produced, heat & mass transfer between solid & gaseous phase, and pyrolysis reactions. Various models that have been reported for various gasifier configurations include: (1) unsteady one-dimensional model for stratified downdraft gasification, (2) transient single particle and fuel bed model for crosscurrent moving bed furnace, (3) steady state reduction zone model for downdraft gasification, and (4) steady state fluid flow and heat transfer model for open top throat-less downdraft gasification. However, for throated close-top downdraft biomass gasifier, commonly known as an Imbert downdraft gasifier, a complete model including pyrolysis, combustion and reduction zones has not yet been reported in the literature. Taking into account of the importance of downdraft biomass gasifier and its varied applications, it is essential to have a complete model for such a configuration. Furthermore, it should be based on unsteady state modeling of heat and mass transfer, which may allow the prediction of dynamic behavior of the conventional fixed bed biomass gasifier. This would help in understanding different modes of stabilization of the reaction front.

6.1.3. Scope of Work

A generalized mathematical model for throated close-top down draft biomass gasifier is developed which takes into account of the limitations of the earlier studies. The developed model accounts for the pyrolysis, secondary tar reactions, homogeneous gas reactions and heterogeneous combustion/ gasification reactions. In the gas phase, eight species (O_2, N_2, CO_2, CO, H_2O, H_2, CH_4 and tar) are considered. The solid phase is biomass in the pyrolysis & combustion/ oxidation zone, and charcoal in the reduction zone. The pyrolysis model presented here considers gradients both in the bed and inside

single particles. Thus the entire bed is divided into the two subsystems, i.e., gas phase inside the bed and the individual particles. To validate the proposed mathematical model, experiments are carried out covering a wide range of operating parameters. The wood waste is used as a biomass material in the biomass gasification experiments. Various operating parameters such as air flow rate (1.85-3.39 m^3/h), biomass moisture content (0.0254-0.164 wt fraction wet basis), biomass consumption rate (1-3.63 kg/h), etc. are varied to study their effects on the performance of the gasifier.

6.1.4. Mathematical Modeling and Simulation

The mathematical modeling of a downdraft biomass gasifier is carried out by two approaches: (1) developing an equilibrium model which represents the entire gasification process by a single reaction, (2) developing a combined transport and kinetic model which takes into account of the kinetics of chemical reactions, heat & mass transfer between solid & gaseous phases, and transport of volatiles produced. In an equilibrium model, it is expected that the pyrolysis products get burnt and achieve equilibrium in the reduction zone of the gasifier before exiting from the gasifier. This implies that the residence time is long enough to allow the chemical reaction to reach an equilibrium state. The elemental balances and the equilibrium ratio between the species are used to find the composition of the producer gas. In a combined transport and kinetic model, the solid phase is biomass in the pyrolysis & combustion/oxidation zone, and charcoal in the reduction zone. In the gas phase eight species (O_2, N_2, CO_2, CO, H_2O, H_2, CH_4 and tar) are considered. The model takes into account of the pyrolysis, secondary tar reactions, homogeneous gas reactions and heterogeneous combustion/gasification reactions. The developed model is divided into three parts according to three different zones developed:

(1) pyrolysis, (2) oxidation, and (3) reduction. Pyrolysis bed is modeled as a stack of particles in one dimension. The model presented here considers temperature gradient both in the bed and also inside the single particles. Thus the entire bed is divided into two subsystems, i.e., gas phase inside the bed and the individual particles. In the present model, complete combustion of biomass is assumed which can be ensured by supplying excess air (usually around 20%) than stoichiometrical requirement. The volatile products generated in the pyrolysis zone flow downwards and enter into the oxidation zone where a part of volatiles gets oxidized. It is assumed that the tar present in the pyrolysed gas mixture completely gets decomposed due to a very high temperature present in the oxidation zone. In the reduction zone, the gaseous mixture passes through the hot porous charcoal bed resting above the grate. The reduction zone is often referred as gasification zone. Solid carbon in the form of char is assumed to be present throughout the reduction zone. The model assumes a cylindrical gasifier bed of uniform cross-sectional area A with negligible radial variation in the properties of both the bed and gas. The species considered here are nitrogen, carbon dioxide, carbon monoxide, methane, water vapor and hydrogen. In reduction zone endothermic reactions are carried out and degree of temperature drop depends upon extents of reactions. Extent of reaction depends upon the reactivity of char, which is represented by Char Reactivity Factor (*CRF*) value. *CRF* in turn depends upon thermal history, degree of burn-off, and number of active sites on char and its particle size. In the present reduction zone model, the variation of *CRF* along the reduction zone of downdraft biomass gasifier incorporated. It is assumed that *CRF* is exponentially increasing along the bed length of the reduction zone.

The kinetics of pyrolysis plays an important role in the modeling of downdraft biomass gasifier. In the comprehensive model of biomass gasifier, the kinetic scheme based on the two competing reactions is used. This kinetic scheme assumes that biomass decomposes into volatiles, gases and char. The volatiles and gases may further react with char to produce different types of volatiles, gases and char where the compositions are different. Rate constants of kinetic reactions are taken as a function of temperature (Arrhenius relation of kinetic constant with temperature) for *Model-KPE1*. The activity of solid reactant is expected to decrease with the extent of reaction due to the changes in chemical and pore structure of solid. Based on these observations, various other models are proposed in which activity decreases as a function of either conversion or activity itself, which are described by *Model-KPE2 to KPE4.* The kinetic parameters of the proposed models are found by minimizing the sum of the square of errors between model predictions and experimental data using population based search algorithm as optimization routines (Differential Evolution and Logarithmic Differential Evolution algorithms).

6.1.5. Experimental Studies

The main equipment of the experimental set up is an Imbert downdraft biomass gasifier. Biomass is fed from top of the gasifier and air is introduced through a nozzle in the combustion zone. Biomass undergoes pyrolysis and gets oxidized in the combustion zone near the air inlet. The pyrolysed gas mixture and the gases produced due to combustion pass over the charcoal bed resting above the grate and generate producer gas. A rotameter and a pressure gauge are used to measure the flow rate and pressure of air respectively. Thermocouples are placed at various locations along the axial length of the gasifier to

measure the temperature of various zones in the gasifier, and a digital multi channel temperature indicator (Make: Thermotech, Model: TH 046, L3001) with auto-scan facility is used to display the temperature. Five pairs of chromel-alumel thermocouples and one pair of platinum-rhodium thermocouples are used. Each pair is placed at different heights along the axial length of the gasifier (Fig. 4.2b) so as to cover all the zones. In each pair, one thermocouple is placed at the center of the gasifier ($r = 0$) while the other is placed at a half radius distance ($r = R/2$). The producer gas generated in the downdraft biomass gasifier is sampled using airtight syringes (100 ml) and analyzed using a gas chromatograph (NUCON 5765) with thermal conductivity detector (TCD).

6.1.6. Results and Discussion

In the following sections, the experimental results obtained in the present study are summarized. The section also discusses the simulated results which are obtained by validating the proposed mathematical model using the literature data and the obtained experimental data.

6.1.6.1. Experimental Studies

Biomass gasification experiments are carried out with wood waste as biomass covering a wide range of air flow rates and biomass moisture content. The rate of biomass consumption is found to vary from 1.0 to 3.63 kg/h for an air flow rate ranging from 1.85 to 3.39 m^3/h. The moisture content is varied from 0.0254 to 0.164 wt fraction on wet basis. Material balance is carried out to examine the reliability of the results generated. The average mass balance closure, defined as the percentage ratio of the total output mass to that of the total input mass, is found to be 94% in the eleven experimental runs carried out in this study. It is found that with an increase in moisture content fraction, the rate of

biomass consumption decreases. It is also found that with an increase in the air flow rate, the rate of biomass consumption increases for a particular moisture content fraction value.

To study the effect of equivalence ratio on the producer gas composition, the averaged gas composition for each experimental run is considered. The molar fractions of nitrogen and carbon dioxide decrease with an increase in Φ upto a value of $\Phi = 0.205$ and for higher values of Φ, molar fractions of nitrogen and carbon dioxide are found to increase. The fraction of carbon monoxide and hydrogen shows an increasing and decreasing trend just opposite to that of nitrogen and carbon dioxide. A higher value of Φ represents a higher air flow rate for a specific biomass consumption rate which leads to more amount of CO_2 production in combustion zone and more amount of N_2 entry along with air flow. The conversion of CO_2 to CO depends upon the rate of reactions occurring in the reduction zone and length of the reduction zone. With an increase in Φ from 0.16 to 0.205, an increased amount of CO_2 is converted into carbon monoxide and hydrogen, and thereby the fractions of CO and H_2 increase with Φ till a value of $\Phi = 0.205$ and subsequently the values decrease. The increase in CO_2 fraction and decrease in CO & H_2 fractions for an equivalence ratio higher than 0.205 represents that CO_2 produced in combustion zone is in excess to that of the conversion capacity of reduction bed. The increase in N_2 fraction for a Φ value ranging from 0.205 to 0.39 is due to an increased amount of N_2 entry along with the air flow.

. The calorific value is calculated using the composition of the producer gas. Carbon monoxide and hydrogen are the main components of the producer gas and are responsible for higher calorific value. It is found that at an equivalence ratio of 0.17, the

calorific value is 4.5 MJ/Nm^3. With an increase in the equivalence ratio from Φ = 0.17 to Φ = 0.205, the calorific value reaches to a maximum of 6.34 MJ/Nm^3. For the equivalence ratio value higher than 0.205, the calorific value steadily decreases with a further increase in the equivalence ratio. The temperature of oxidation zone varies from 900 °C to 1050 °C and that of pyrolysis zone between 280 °C to 550 °C for an equivalence ratio ranging from 0.17 to 0.39. It is found that both the temperature profiles pass through a maximum at an equivalence ratio of 0.205. It is found that with an increase in the equivalence ratio, production rate of producer gas continuously increases. Cold gas efficiency is at a lowest value of 0.25 for an equivalence ratio value of 0.17. The value of cold gas efficiency becomes almost double with a small increase in the equivalence ratio at Φ = 0.205.

6.1.6.2 Mathematical Modeling and Simulation

The experimental data reported in the literature and those obtained in the present study are used to validate the simulation results of the complete combined transport and kinetic model. The initial moisture content fraction, air flow rate, temperature of the pyrolysis zone, and chemical composition of the biomass are required as an input data for the model to predict the composition of producer gas. The developed model is solved and simulated to predict the composition of producer gas across the axial length of the gasifier.

It is found that the composition of water vapor in the gaseous phase is the highest in pyrolysis zone and decreases as it travels through the oxidation and reduction zones of the gasifier. The molar fractions of CO and CH_4 in the gaseous phase increase in the pyrolysis zone as gas travels through it. However, the molar fractions of CO, H_2, tar, and

CH_4 decrease in the oxidation zone due to high temperature oxidation and that of CO_2 increases. In the reduction zone of the gasifier, the molar fractions of CO and H_2 increase and those of CO_2 and N_2 decrease. It is also found that the composition of CO, CH_4 and tar increases and that of water vapor decreases with time in the pyrolysis zone of the gasifier due to the subsequent increase in the temperature of the pyrolysis zone. Results generated by simulation of the combined transport and kinetic model are compared with those obtained from the equilibrium model. It is found that the simulated predictions using the combined transport and kinetic model are matching better than those predicted by the equilibrium model.

6.1.6.3 Kinetic Parameter Estimation

Simulations are performed to find the kinetic parameters of *Model-KPE1* to *KPE4* for heating rates of 10, 25 and 40 K/s for the ground hazelnut shell biomass sample of 0.180 mm size. For a heating rate value of 10 K/s, *Model-KPE2* gives the minimum value of objective function amongst various proposed models. But *Model-KPE3* fits better and gives a minimum value of objective function for the heating rates of 25 and 40 K/s. Moreover, *Model-KPE3* predictions and the trends obtained of residual weight fraction better represent the experimental data in the entire temperature range in spite of having a higher objective function value over *Model-KPE2*. The proposed kinetic model, which considers the kinetic scheme of biomass decomposition by two competing reactions giving volatile gaseous and solid charcoal products, better represent the thermogravimetry results than apparent decomposition rate expression.

NP (Number of population points used in DE) value is varied from 10 to 50 times of the dimension of the problem. With an increase in NP value, the objective function

value is decreased and different set of kinetic parameters are found as optimum values. It clearly indicates that the kinetic parameter estimation is a multimodal problem and has a number of local minima. To improve the population distribution, logarithmic mapping rule is used to initialize the normalized population vectors and simple differential evolution is applied to find the global optimum value of kinetic parameters (We call it the LIDE). To overcome the problem of population distribution generation after generation, logarithmic mutation is proposed. By implementation of logarithmic mutation in DE, better mutant population in terms of wide population distribution is obtained and hence could converge to near solutions. We call this logarithmic initialization and logarithmic mutation of DE as Logarithmic DE (LDE). The objective function value is the least using LDE in comparison with simple DE or LIDE for any NP Value.

6.2. Conclusions

Based on the results obtained in the present study, the following conclusions are drawn:

1. Wood waste can be successfully converted to generate the combustible gas, known as producer gas, using an Imbert downdraft biomass gasifier.
2. With an increase in the moisture content, biomass consumption rate decreases and with an increase in the air flow rate biomass consumption rate increases.
3. Optimum operating conditions are found by varying the equivalence ratio, which gives the producer gas having the highest calorific value.
4. Molar fraction of N_2 and CO_2 decrease with an increase in equivalence ratio (Φ) till $\Phi = 0.205$, and they increase subsequently for higher values of Φ. The fraction

of CO and H_2 shows an increasing and decreasing trend exactly opposite to that of N_2 and CO_2.

5. The calorific value, pyrolysis zone temperature and the oxidation zone temperature are maximum at Φ = 0.205. However, the calorific value decreases for an equivalence ratio ranging from 0.205 to 0.39.
6. With an increase in Φ, the production rate of producer gas continuously increases.
7. The value of cold gas efficiency is 0.25 for Φ = 0.17. It becomes almost double with a small increase of 0.035 in the value of Φ. The effect of Φ on cold gas efficiency is comparatively less for higher values of Φ.
8. The optimum equivalence ratio is 0.205 for the Imbert downdraft biomass gasifier studied.
9. The proposed combined transport and kinetic model is successfully validated with the experimental data reported in the literature and those obtained in the present experimental study.
10. The model predicted composition of producer gas matches very well with the experimental data reported in the literature and those obtained in the present study in comparison to the equilibrium model predictions.
11. The value of char reactivity factor (*CRF*), which represents the reactivity of char must be varied along the reduction zone of the down draft biomass gasifier.
12. The simulated results obtained from the reduction zone model developed in the present study are in very good agreement with the experimental data reported in the literature, in comparison with the mathematical models developed by other researchers, when exponentially varying CRF value is considered.

13. The rate of Boudouard reaction becomes negative and the reaction occurs in backward direction below a temperature of 933 K when the pressure is slightly above the atmospheric pressure.
14. The molar fractions of CO, CH_4 and tar increase and that of water vapor decreases with time in the pyrolysis zone of the gasifier due to a subsequent increase in the temperature of pyrolysis zone.
15. The molar fraction of water vapor in the gaseous phase is the highest in the pyrolysis zone and decreases as it travels through the oxidation and reduction zones of the gasifier.
16. The molar fractions of CO and CH_4 in the gaseous phase increase in the pyrolysis zone as gas travels through it. However, the molar fractions of CO, H_2, tar, and CH_4 decrease in the oxidation zone due to high temperature oxidation and hence the molar fraction of CO_2 increases.
17. The proposed kinetic model, which considers the kinetic scheme of biomass decomposition by two competing reactions giving volatile gaseous and solid charcoal products, better represent the thermogravimetry results than apparent decomposition rate expression.
18. Kinetic parameters (frequency factors and activation energies) for the two competing reactions, found using simple differential evolution (DE) are not the global values and the optimum value of frequency factors are biased towards the upper limit of the range chosen using simple DE.

19. Logarithmic DE (LDE) which is a combination of logarithmic initialization and logarithmic mutation with simple DE yields kinetic parameters which give a better value of objective function.
20. Kinetic parameters found using LDE gives global optimum set when compared with the experimental data.

6.3 Major Contributions

1. A combined transport and kinetic model considering all four zones of biomass gasifier is developed for an Imbert downdraft biomass gasifier to predict the composition of the producer gas.
2. The developed model is successfully simulated and the results are validated with the experimental data obtained in the present study and also with those reported in literature.
3. An important parameter ‘char reactivity factor’ is identified and its exponential variation along the bed of reduction zone is proposed, which provides simulation results very close to the experimental values.
4. Experiments are performed successfully with wood waste as a biomass in a down draft biomass gasifier covering a wide range of air flow rate and biomass moisture content.
5. An optimum operating condition in terms of equivalence ratio is found for the downdraft biomass gasifier used in the present study.
6. The kinetic model based on biomass decomposition by two competing reactions giving volatile gaseous and solid charcoal products, is proposed, which represents

the thermogravimetry results better than the apparent decomposition rate expression.

7. Logarithmic DE (LDE) which is a combination of logarithmic initialization and logarithmic mutation with simple DE is proposed, and kinetic parameters found using LDE gave the global optimum set.

6.4 Future Scope of Research

The future scope of this work is enumerated below:

1. The developed mathematical model can be modified for the updraft configuration of the biomass gasifier.
2. It is assumed in the model that all the volatiles produced in the pyrolysis zone flow downwards in the gasifier. It can be relaxed by incorporating the momentum balance equations.
3. The developed model can be modified to incorporate the effect of radial variation by proposing two dimensional model.
4. The kinetic scheme based on the decomposition of its components (cellulose, hemicelllose and lignin) can be proposed for the biomass pyrolysis.
5. The experimental study carried out in the present work can also pave the way for implementing the biomass gasifier on commercial scale for gasification of wood waste.
6. The producer gas can be utilized to run an engine or to drive turbine to produce electricity.

REFERENCES

Altafini, R.P., Wnader, R., Barreto, M., 2003. Prediction of the Working Parameters of a Wood Waste Gasifier through an Equilibrium Model. Energy Conversion and Management, 44, 459-469.

Angira, R., Babu, B.V., 2006. Optimization of Process Synthesis and Design Problems: A Modified Differential Evolution Approach. Chemical Engineering Science, 61, 4707-4721.

Anthony, D.B., Howard, J.B., 1976. Coal Devolatilization and Hydrogasification. American Institute of Chemical Engineers Journal, 22, 625-656.

Babu, B.V., 2008a. Biomass Pyrolysis: A State-of-the-art Review. Biofuels Bioproducts and Biorefining, 2, 393-414.

Babu, B.V., 2008b. Biohydrogen-A Clean and Green Energy: Economic Perspective & Optimization Strategies. Proceedings of Indo-French Workshop on 'Biohydrogen: from Basic Concepts to Technology' under the aegis of Indo French Center for Promotion of Advanced Research, organized by The Energy and Resources Institute (TERI)-New Delhi, Jaypee Residency Manor, Mussoorie, November 6-8, 2008.

Babu, B.V., 2004. Process Plant Simulation, Oxford University Press, India.

Babu, B.V., Angira, R., 2005. Optimal Design of an Auto-thermal Ammonia Synthesis Reactor. Computers and Chemical Engineering, 29, 1041-1045.

Babu, B.V., Angira, R. 2006. Modified Differential Evolution (MDE) for Optimization of Non-Linear Chemical Processes. Computers and Chemical Engineering, 30, 989-1002.

Babu, B.V., Chaurasia A.S., 2002a. Modeling & Simulation of Pyrolysis: Effect of Convective Heat Transfer & Orders of Reactions. Proceedings of International Symposium & 55th Annual Session of IIChE (CHEMCON-2002), OU, Hyderabad, December 19-22, 2002.

Babu, B.V., Chaurasia A.S., 2002b. Modeling & Simulation of Pyrolysis: Influence of Particle Size and Temperature. Proceedings of International Conference on Multimedia and Design, Organized by Arena Multimedia-India & IIT-Bombay, Mumbai, September 23-25, 2002, Volume-IV, Track-IV: Design, pp. 103-128.

Babu, B.V., Chaurasia A.S., 2003a. Modeling, Simulation, and Estimation of Optimum Parameters in Pyrolysis of Biomass. Energy Conversion and Management, 44, 2135-2158.

Babu, B.V., Chaurasia A.S., 2003b. Modeling for Pyrolysis of Solid Particle: Kinetics and Heat Transfer Effects. Energy Conversion and Management, 44, 2251-2275.

Babu, B.V., Chaurasia A.S., 2003c. Modeling & Simulation of Pyrolysis of Biomass: Effect of Heat of Reaction. Proceedings of International Symposium on Process Systems Engineering and Control (ISPSEC'03) - For Productivity Enhancement through Design and Optimization, IIT-Bombay, Mumbai, January 3-4, 2003, Paper No. FAB1, pp. 181-186.

Babu, B.V., Chaurasia A.S., 2003d. Pyrolysis of Shrinking Cylindrical Biomass Pellet. Proceedings of International Symposium & 56th Annual Session of IIChE (CHEMCON-2003), Bhubaneswar, December 19-22, 2003.

Babu, B.V., Chaurasia A.S., 2003e. Optimization of Pyrolysis of Biomass Using Differential Evolution Approach, Proceedings of The Second International Conference on Computational Intelligence, Robotics, and Autonomous Systems (CIRAS-2003), Singapore, December 15-18, 2003.

Babu, B.V., Chaurasia A.S., 2004a. Parametric Study of Thermal and Thermodynamic Properties on Pyrolysis of Biomass in Thermally Thick Regime. Energy Conversion and Management, 45, 53-72.

Babu, B.V., Chaurasia A.S., 2004b. Dominant Design Variables in Pyrolysis of Biomass Particles of Different Geometries in Thermally Thick Regime. Chemical Engineering Science, 59, 611-622.

Babu, B.V., Chaurasia A.S., 2004c. Pyrolysis of Biomass: Improved Models for Simultaneous Kinetics & Transport of Heat, Mass, and Momentum. Energy Conversion and Management, 45, 1297-1327.

Babu, B.V., Chaurasia A.S., 2004d. Heat Transfer and Kinetics in the Pyrolysis of Shrinking Biomass Particle, Chemical Engineering Science, 59, 1999-2012.

Babu, B.V., Munawar, S.A. 2007. Differential Evolution Strategies for Optimal Design of Shell-and-Tube Heat Exchangers. Chemical Engineering Science, 62, 3720-3739.

Babu, B.V., Chakole, P.G., Mubeen, J.H.S., 2005. Differential Evolution Strategy for Optimal Design of Gas Transmission Network. Journal of Multidisciplinary Modeling in Materials and Structures, 1, 315-328.

Babu, B.V., Sastry, K.K.N., 1999. Estimation of Heat Transfer Parameters in a Trickle Bed Reactor using Differential Evolution and Orthogonal Collocation. Computers and Chemical Engineering, 23, 327-339.

Bamford, C.H., Crank, J., Malan, D.H., 1946. The Combustion of Wood Part I. Proceedings of the Cambridge Philosophical Society, 42, 166-182.

Barth, T., 1999. Similarities and Differences in Hydrous Pyrolysis and Source Rocks. Organic Geochemistry, 30, 1495-1507.

Bhave, A.G., 2001. Technical Notes in the Proceedings of Intensive workshop on - Testing Evaluation of Biomass Gasifier Systems and Related Laboratory Investigation. Held at Saradar Patel Renewable Energy Research Institute (SPRERI), Vallabh Vidhyanagar, Gujarat, (April, 2001).

Bilbao, R., Millera, A., Murillo, M.B., 1993. Temperature Profiles and Weight Loss in the Thermal Decomposition of Large Spherical Wood Particles. Industrial Engineering and Chemistry Research, 32, 1811-1817.

Bilbao, R., Mastral, J.F., Ceamanos, J., Aldea, M.E., 1996. Modeling of the Pyrolysis of Wet Wood. Journal of Analytical and Applied Pyrolysis, 36, 81-97.

Boroson, M.L., Howard, J.B., Longwell, J.P., Peters, W.A., 1989. Product Yields and Kinetics from the Vapor Phase Cracking of Wood Pyrolysis Tars. American Institute of Chemical Engineers Journal, 35, 120-128.

Branca, C., Di Blasi, C., 2003. Kinetics of the Isothermal Degradation of Wood in the Temperature Range 528–708 K. Journal of Analytical and Applied Pyrolysis, 67, 207-219.

Bridgwater, A.V., Meier, D., Radlein, D. 1999. An Overview of Fast Pyrolysis of Biomass. Organic Geochemistry, 30, 1479-1493.

Bridgwater, A.V., 2002. Bio-Energy Research Group, Aston University, Birmingham B47ET, UK,(2002). http://www.icheme.org/.../conferences/gasi/Gasification% 20Conf%20Papers/ Session%202%20presentation-Bridgewater.

Bryden, K.M., Ragland, K.W., Rutland, C.J., 2002. Modeling Thermally Thick Pyrolysis of Wood, Biomass and Bioenergy, 22, 41-53.

Bryden, K.M., Hagge, M.J., 2003. Modeling the Combined Impact of Moisture and Char Shrinkage on the Pyrolysis of a Biomass Particle. Fuel, 82, 1633-1644.

Caillé, A., 2007. Survey of Energy Resources. World Energy council, London, U.K.

Carnahan, B., Luther, H.A., James, O.W., 1969. Applied Numerical Methods. Wiley Publications, New York.

Chaurasia, A.S., Babu, B.V., 2003a. Modeling & Simulation of Pyrolysis of Biomass: Effect of Thermal Conductivity, Reactor Temperature and Particle Size on Product Concentrations. Proceedings of International Conference on Energy and Environmental Technologies for Sustainable Development (ICEET-2003) Jaipur, October 8-10, 2003, Eds. Upendra Pandel& M.P.Poonia, 151-156.

Chaurasia, A.S., Babu, B.V., 2003b. Influence of Product Yields, Density, Heating Conditions, and Conversion on Pyrolysis of Biomass. Proceedings of International Conference on Desert Technology–7 (DT-7), Jodhpur, November 9-14, 2003, 111.

Chaurasia, A.S., Babu, B.V., 2004. Influence of Product Yields, Density, Heating Conditions, and Conversion on Pyrolysis of Biomass. Journal of Arid Land Studies, 14S, 159-162.

Chaurasia, A.S., Babu, B.V., Kaur, A., Thiruchitrambalam, V., 2005. Convective and Radiative Heat Transfer in Pyrolysis of a Biomass Particle, Indian Chemical Engineer, 47, 75-80.

Chaurasia, A.S., Kulkarni, B.D., 2007. Most Sensitive Parameters in Pyrolysis of Shrinking Biomass Particle. Energy Conversion and Management, 48, 836-849.

Chern, S., Walawender, W.P., Fan, L.T. 1991a. Equilibrium Modeling of a Downdraft Gasifier – I Overall Gasifier. Chemical Engineering Communications, 108, 243-265.

Chern, S., Walawender, W.P., Fan, L.T. 1991b. Equilibrium Modeling of a Downdraft Gasifier II – Flaming Pyrolysis Zone. Chemical Engineering Communications, 108, 267-287.

Chowdhury, R., Bhattacharya, P., Chakravarty, M. 1994. Modelling and Simulation of a Downdraft Rice Husk Gasifier. International Journal of Energy Research, 18, 581-594.

Curtis, L.J., Miller, D.J. 1988. Transport Model with Radiative Heat Transfer for Rapid Cellulose Pyrolysis. Industrial and Engineering Chemistry Research, 27, 1775-1783.

Demirbas, A., 1998. Kinetics for Non-isothermal Flash Pyrolysis of Hazelnut Shell. Bioresource Technology, 66, 247-252.

Demirbas, A., Küçük, M.M., 1999. Delignification of Ailanthus Altissima and Spruce Orientalis with Glycerol or Alkaline Glycerol at Atmospheric Pressure. Cellulose Chemical Technology, 27, 679-686.

Demirbas, A., 2000. Biomass Resources for Energy and Chemical Industry. Energy Education and Science Technology, 5, 21-45.

Demirbas, A., 2001. Bioresource Facilities and Biomass Conversion Processing for Fuels and Chemicals. Energy Conversion and Management, 42, 357-1378.

Demirbas, A., Arin, G., 2002. An Overview of Biomass Pyrolysis, Energy Sources, 24, 471-482.

Di Blasi, C., 1993. Analysis of Convection and Secondary Reaction Effects Within Porous Solid Fuels Undergoing Pyrolysis. Combustion Science and Technology, 90, 315-340.

Di Blasi, C., 1996a. Kinetic and Heat Transfer Control in the Slow and Flash Pyrolysis of Solids, Industrial Engineering and Chemistry Research, 35, 37-47.

Di Blasi, C., 1996b. Influence of Model Assumptions on the Predictions of Cellulose Pyrolysis in the Transfer Controlled Regime, Fuel, 75, 58-66.

Di Blasi, C., 1996c. Heat, Momentum and Mass Transport through a Shrinking Biomass Particle Exposed to Thermal Radiation. Chemical Engineering Science, 51, 1121-1132.

Di Blasi, C., 1997. Influence of Physical Properties on Biomass Devolatilization Characteristics. Fuel, 76, 957-964.

Di Blasi, C., 1998a. Multi-phase Moisture in the High Temperature Drying of Wood Particles. Chemical Engineering Science, 53, 353-366.

Di Blasi, C., 1998b. Physico-chemical Processes Occurring inside a Degrading Two-dimensional Anisotropic Porous Medium. International Journal of Heat and Mass Transfer, 41, 4139-4150.

Di Blasi, C., 2000. Dynamic Behaviour of the Stratified Downdraft Gasifiers. Chemical Engineering Science, 55, 2931-2944.

Dogru, M., Howrath, C.R., Akay, G., Keskinler, B., Malik, A.A., 2002. Gasification of Hazelnut Shells in a Downdraft Gasifier. Energy, 27, 415-427.

Fan, L.T., Fan, L.S., Miyanami, K., Chen, T.Y., Walawender, W.P., 1977. Mathematical Model for Pyrolysis of a Solid Particle Effects of Lewis Number. Canadian Journal of Chemical Engineering, 55, 47-53.

Fiaschi, D., Michelini, M., 2001. A Two-phase One-dimensional Biomass Gasification Kinetics Model. Biomass and Bioenergy, 21, 121–132.

Fridleifsson, I.B., 2003. Status of Geothermal Energy Amongst the World's Energy Sources. Geothermics, 32, 379-388.

Galgano, A., Di Blasi, C., 2004. Modeling the Propagation of Drying and Decomposition Fronts in Wood. Combustion and Flame, 139, 16–27.

Ghoshdastidar, P.S., 1998. Computer Simulation of Flow and Heat Transfer. Tata McGraw Hill Publishing Company Limited, New Delhi.

Gerald, C.F., Wheatley, P.O., 1994. Applied Numerical Analysis, Addison-Wesley Publication, MA.

Giltrap, D.L., McKibbin, R.; Barnes, G.R.G., 2003. A Steady State Model of Gas-Char Reactions in a Down Draft Biomass Gasifier. Solar Energy, 74, 85-91.

Ghoshdastidar, P.S., 1998. Computer Simulation of Flow and Heat Transfer. Tata McGraw-Hill Publishing Company Limited, New Delhi.

Goldberg, D.E., 1989. Genetic algorithms in search, optimization, and machine learning, reading, Addision-Wesley Publication, MA.

Green, A.E.S., Zanardi, M A., Mullin, J.P., 1997. Phenomenological Models of Cellulose Pyrolysis. Biomass and Bioenergy, 13, 15-24.

Grobski, M., Bain, R., 1981. Properties of Biomass Relevant to Gasification. Biomass Gasification: Principles & Technology: Energy Technology, edited by Reed, T. B., Solar Energy Research Institute (SERI), Golden, Colorado.

Hagge, M.J., Bryden, K.M., 2002. Modeling the Impact of Shrinkage on the Pyrolysis of Dry Biomass. Chemical Engineering Science, 57, 2811-2823.

Hanaoka, T., Inoue, S., Uno, S., Ogi, T, Minowa, T., 2005. Effect of Woody Biomass Components on Air-Steam Gasification. Biomass and Bioenergy, 28, 69-76.

Jalan, R.K., Srivastava, V.K., 1999. Studies on Pyrolysis of a Single Biomass Cylindrical Pellet-Kinetic and Heat Transfer Effects. Energy Conversion and Management, 40, 467-494.

Janse, A.M.C., Westerhout, R.W.J., Pinrs, W., 2000. Modeling of Flash Pyrolysis of a Single Wood Particle. Chemical Engineering and Processing, 39, 239-252.

Jayah, T.H., Aye, Lu, Fuller, R.J., Stewart, D.F., 2003. Computer Simulation of a Downdraft Wood Gasifier for Tea Drying. Biomass and Bioenergy, 25, 459-469.

Jorapur, R.M., Rajvanshi, A.K., 1995. Development of a Sugarcane Leaf Gasifier for Electricity Generation. Biomass and Bioenergy, 8, 91-98.

Jorapur, R.M., Rajvanshi, A.K., 1997. Sugarcane Leaf-bagasse Gasifiers for Industrial Heating Applications. Biomass and Bioenergy, 13, 141-146.

Koufopanos, C.A., Maschio, G., Lucchesi, A., 1989. Kinetic Modeling of the Pyrolysis of Biomass and Biomass Components. The Canadian Journal of Chemical Engineering, 67, 75-83.

Koufopanos, C.A., Papayannakos, N., Maschio, G., Lucchesi, A., 1991. Modeling of the Pyrolysis of Biomass Particles, Studies on Kinetics, Thermal and Heat Transfer Effects. The Canadian Journal of Chemical Engineering, 69, 907-915.

Liliedahl, T., Sjöström, K., 1998. Heat Transfer Controlled Pyrolysis Kinetics of a Biomass Slab, Rod or Sphere. Biomass and Bioenergy, 15, 503-509.

Maschio, G., Lucchesi, A., Stoppato, G., 1994. Production of Syngas from Biomass. Bioresource Technology, 48, 119-126.

Matheiu, P., Dubuisson, R., 2002. Performance Analysis of a Biomass gasifier. Energy Conversion and Management, 43, 1291-1299.

Melgar, A., Pe´rez, J.F., Laget, H., Horillo, A. 2007. Thermochemical Equilibrium Modelling of a Gasifying Process. Energy Conversion Management, 48, 59-67.

Mousqués, P., Dirion, J.L., Grouset, D., 2001. Modeling of Solid Particles Pyrolysis. Journal of Analytical and Applied Pyrolysis, 58, 733-745.

Ningbo, G., Aimin, L., 2008. Modeling and Simulation of Combined Pyrolysis and Reduction Zone for a Downdraft Biomass Gasifier. Energy Conversion and Management, 49, 3483-3490.

Ownubolu, G.C., Babu, B.V., 2004. New Optimization Techniques in Engineering; Springer-Verilag, Heidelberg, Germany.

Parikh, J., Channiwala, S.A., Ghosal, G.K., 2005. A Correlation for Calculating HHV from Proximate Analysis of Solid Fuels. Fuel, 84, 487-494.

Pellistor, K., 2008. Application Note 5 - Thermal Conductivity Sensors. e2v technologies ltd, England, UK

Peters, B., Bruch, C., 2003. Drying and Pyrolysis of Wood Particles: Experiments and Simulation. Journal of Analytical and Applied Pyrolysis, 70, 233-250.

Price, K.V., Storn, R., 1997. Differential Evolution – a Simple Evolution Strategy for Fast Optimization. Dr. Dobb's Journal, 22**,** 18–24.

Pyle, D.L., Zaror, C.A., 1984. Heat Transfer and Kinetics in the Low Temperature Pyrolysis of Solids. Chemical Engineering Science, 39, 147-158.

Radmanesh, R., Courbariaux, Y., Chaouki, J., Guy, C., 2006. A Unified Lumped Approach in Kinetic Modeling of Biomass Pyrolysis. Fuel, 85, 1211-1220.

Rao, T.R., Sharma, A., 1998. Pyrolysis Rates of Biomass Materials. Energy, 23, 973-978.

Reed, T.B., Das, A., 1988. Handbook of Biomass Downdraft Gasifier Engine Systems. The Biomass Energy Foundation Press, Colorado.

Ruggiero, M., Manfrida, G., 1999. An Equilibrium Model for Biomass Gasification Processes. Renewable Energy, 16, 1106-1109.

Sadhukhan, A., Gupta, P., Saha, R., 2008. Modeling and Experimental Studies on Pyrolysis of Biomass Particles. Journal of Analytical and Applied Pyrolysis, 81, 183-192.

Sand, U, Sandberg, J., Larfeldt, J., Bel Fdhila, R., 2008. Numerical Prediction of the Transport and Pyrolysis in the Interior and Surrounding of Dry and Wet Wood Log. Applied Energy, 85, 1208-1224.

Schuster, G., Löffler, G., Weigl, K., Hofbauer, H., 2001. Biomass Steam Gasification – an Extensive Parametric Modeling Study. Bioresource Technology, 77, 71-79 .

Shafizadeh, F., Chin, P.S., 1977. Thermal Deterioration of Wood. In Wood Technology: Chemical Aspects, Americal Chemical Society Symposium Series, 43, ed. Goldstein, I.S., American Chemical Society, Washington, 57.

Shafizadeh, F., 1982. Introduction to Pyrolysis of Biomass. Journal of Analytical and Applied Pyrolysis, 3, 283-305.

Sharma, A.K., Ravi, M.R., Kohli, S., 2006. Modelling Product Composition in Slow Pyrolysis of Wood. Solar Energy Society of India Journal, 16, 1-11.

Sharma, A.K., 2007. Modeling Fluid and Heat Transport in the Reactive, Porous Bed of Downdraft (Biomass) Gasifier. International Journal of Heat and Fluid Flow, 28, 1518–1530.

Sharma, A.K., 2008. Equilibrium Modeling of Global Reduction Reactions for a Downdraft (Biomass) Gasifier, Energy Conversion and Management, 49, 832-842.

Sheng, G.X., 1989. Biomass Gasifiers: from Waste to Energy Production. Biomass, 20, 3-12.

Shen, D.K., Fang, M.X., Luo, Z.Y., Cena, K.F., 2007. Modeling Pyrolysis of Wet Wood Under External Heat Flux. Fire Safety Journal, 42, 210-217.

Singer, C.J., 1958. History of Technology, IV, 252, Claderon Press, Oxford.

Song, H., Andreas, J., Minhou, X., 2007. Kinetic Study of Chinese Biomass Slow Pyrolysis: Comparison of Different Kinetic Models. Fuel, 86, 2778-2788.

Srivastava, V.K., Sushil, Jalan, R.K., 1996. Predictions of Concentration in the Pyrolysis of Biomass Material-II. Energy Conversion and Management, 37, 473-483.

Stucley, C.R., Schuck, S.M., Sims, R.E.H., Larsen, P.L., Turvey, N.D., Marino, B.E., 2004. Biomass Energy Production in Australia, A report for the Joint Venture Agroforestry Program (in conjunction with the Australian Greenhouse Office).

Thunman, H., Niklasson, F., Johnson, F., Leckner, B., 2001. Composition of Volatile Gases and Thermochemical Properties of Wood for Modeling of Fixed or Fluidized Beds. Energy and Fuel, 15, 1488-1497.

Tillman, D.A., Rossi, A.M., Kitto, W.A., 1981. Wood Combustion, Academic Press Inc., New York.

Twidell, J., 1998. Biomass Energy. Renewable Energy World, 3, 38-39.

Varhegyi, G., Antal, M.J., Jakab, E., Szabo, P., 1997. Kinetic Modeling of Biomass Pyrolysis. Journal of Analytical and Applied Pyrolysis, 42, 73-87.

Wander, P.R., Altafini, C.R., Barreto, R.M., 2004. Assessment of a Small Sawdust Gasification Unit, Biomass and Bioenergy, 27, 467–476.

Wang, Y., Kinoshita, C.M., 1993. Kinetic Model of Biomass Gasification. Solar Energy, 51, 19-25.

Wurzenberger, J.C., Wallner, S., Raupenstrauch, H., Khinst, J.G., 2002. Thermal Conversion of Biomass: Comprehensive Reactor and Particle Modeling, American Institute of Chemical Engineers Journal, 48, 2398-2411.

Yuen, R.K.K., Yeoh, G.H., Davis, G.D., Leonardi, E., 2007. Modelling the Pyrolysis of Wet Wood – I. Three-dimensional Formulation and Analysis. International Journal of Heat and Mass Transfer, 50, 4371-4386.

Zabaniotou, A., Damartzis, T., 2007. Modelling the Intra-particle Transport Phenomena and Chemical Reactions of Olive Kernel Fast Pyrolysis. Journal of Analytical and Applied Pyrolysis, 80, 187-194.

Zainal, Z.A., Ali, R., Lean, C.H., Seetharamu, K.N., 2001. Prediciton of a Performance of a Downdraft Gasifier using Equilibrium Modeling for Different Biomass Materials. Energy Conversion and Management, 42, 1499-1515.

Zainal, Z.A., Ali, R., Quadir, G.A., Seetharamu, K.N., 2002. Experimental Investigation of a Downdraft Biomass Gasifier. Biomass and Bioenergy, 23, 283-289.

Zhengqi, L., Wei, Z., Baihong, M., Chunlong, L., Qunyi, Z., Guangbo, Z., 2008. Kinetic Study of Corn Straw Pyrolysis: Comparison of Two Different Three-pseudocomponent Models. Bioresource Technology, 99, 7616-7622.

LIST OF PUBLICATIONS

International Journals

1. Babu, B.V. and Pratik N Sheth, "Modeling and Simulation of Reduction Zone of Downdraft Biomass Gasifier: Effect of Char Reactivity Factor", Energy Conversion and Management, Vol. 47 (No. 15-16), pp. 2602-2611, 2006.
2. Babu, B.V. and Pratik N.Sheth, " Modeling and Simulation of Reduction Zone of Downdraft Biomass Gasifier: Effect of Air to Fuel Ratio". Journal on Engineering and Technology, Vol. 2 (No. 3), pp. 35-40, 2007.
3. Sheth, P. N. and B.V.Babu, "Differential Evolution Approach for obtaining Kinetic Parameters in Non isothermal Pyrolysis of Biomass". Materials and Manufacturing Processes. Vol. 24 (No. 1), pp. 47-52, 2009.
4. Sheth, P. N. and B.V.Babu, "Experimental studies on producer gas generation from wood waste in a downdraft biomass gasifier". Bioresource Technology, Vol. 100 (No. 12), pp. 3127-3133, 2009.
5. Sheth, P. N. and B.V.Babu, “Biohydrogen Production through biomass (waste wood) gasification”. To be communicated to International Journal of Hydrogen Energy.
6. Sheth, P. N. and B.V.Babu, “Combined Transport and Kinetic Modeling of Downdraft Biomass Gasifier” To be Communicated.

International Conference Proceedings

1. Babu, B.V. and Pratik N.Sheth, "Modeling and Simulation of Downdraft Biomass Gasifier", Proceedings of International Symposium & 57th Annual Session of IIChE in association with AIChE (CHEMCON-2004), Mumbai, December 27-30, 2004.
2. Babu, B.V. and Pratik N. Sheth, “Modeling & Simulation of Biomass Gasifier: Effect of Oxygen Enrichment and Steam-to-air Ratio”, Presented at International Congress on Renewable Energy (ICORE-2005), Pune, January 20-22, 2005.
3. Sheth, P.N. and B.V.Babu, "Parametric Study of Factors affecting the Composition of Producer Gas", Proceedings of International Symposium & 58th Annual Session of IIChE in association with International Partners (CHEMCON-2005), New Delhi, December 14-17, 2005.
4. Sheth, P.N. and B.V.Babu, "Effect of Moisture Content on Composition Profiles of Producer Gas in Downdraft Biomass Gasifier", Proceedings of International Congress Chemistry and Environment (ICCE-2005), Indore , December 24-26, 2005, pp. 356-360, 2005.
5. Sheth, P.N. and B.V.Babu , "Pyrolysis of Hazelnut Shell: Kinetic Modeling and Simulation". Proceedings of International Symposium & 59th Annual Session of

IIChE in association with International Partners (CHEMCON-2006), GNFC Complex, Bharuch, December 27-30, 2006.

6. Sheth, P.N. and B.V.Babu , " Kinetic Modeling for Pyrolysis of Hazelnut Shell: Optimal Parameter Estimation using Differential Evolution (DE)". Proceedings of International Symposium & 60th Annual Session of IIChE in association with International Partners (CHEMCON-2007), The Diamond Jubilee Conference of IIChE, Heritage Institute of Technology, Kolkata, December 27-30, 2007, pp. 33, 2007.
7. Sheth, P.N. and B.V.Babu , "Optimization of Kinetic Parameters in Pyrolysis of Biomass Using Differential Evolution (DE)". Proceedings of International Conference on Neural Network and Genetic Algorithm in Materials Science and Engineering (NGMS-2008), Kolkata, January 9-11, 2008.
8. Sheth, P.N. and B.V.Babu , "Optimization of Kinetic Parameters in Pyrolysis of Biomass Using Logarithmic Differential Evolution (LDE)". Proceedings of Genetic and Evolutionary Computation Conference (GECCO-2008), Atlanta, Georgia, USA, July 12-16, 2008.
9. Sheth, P.N. and B.V.Babu , "Kinetic Modeling, Simulation and Optimization of Pyrolysis". Proceedings of International Symposium & 61st Annual Session of IIChE in association with International Partners (CHEMCON-2008), Panjab University, Chandigarh, December 27-30, 2008.

National Conference Proceedings

1. Sheth, P.N. and B.V.Babu , "Kinetic Modeling of the Pyrolysis of Biomass". Proceedings of National Conference on Environmental Conservation (NCEC-2006), BITS-Pilani, September 1-3, 2006, pp. 453-458, 2006.

BIOGRAPHIES

Biography of the Candidate

Pratik N Sheth completed his B.E. Degree in Chemical Engineering from Govt. Engg. College, Gandhinagar in the year 2001. He obtained his masters degree in Chemical Engineering from BITS, PILANI in the year 2002. He joined BITS Pilani as an Assistant Lecturer in Chemical Engineering Group in December 2002 and currently he is working as a Lecturer in this institute. He has 6 years of teaching experience and has guided 2 Professional Practice –II students and around 70 project students. He taught courses such as Heat Transfer Operations, Chemical Process Technology, Advanced Mass Transfer, Advanced Heat Transfer, Thermodynamics, Structure and Properties of Materials, Process Equipment Design, and Measurement Techniques-II and involved in the tutorials of Selected Chemical Engineering Operations and Mass Transfer Operations. His research interests include biomass gasification, pyrolysis, modeling and simulation, and computational fluid dynamics.

Biography of Supervisor

Dr B V Babu is Professor of Chemical Engineering and Dean of Educational Hardware Division (EHD) at Birla Institute of Technology and Science (BITS), Pilani. He did his PhD from IIT-Bombay. His biography is included in 2005, 2006 & 2007 editions of Marquis Who's Who in the World, in Thirty-Third Edition of the Dictionary of International Biography in September 2006, in 2000 Outstanding Intellectuals of the 21st Century in 2006, and in First Edition of Marquis Who's Who in Asia in 2007. He is the Coordinator for PETROTECH Society at BITS-Pilani. He is on various academic and administrative committees at BITS Pilani. He is the member of project planning & implementation committees of BITS-Pilani Dubai Campus, BITS-Pilani Goa Campus, and BITS-Pilani Hyderabad Campus. He is external expert member of Board of Studies at Banasthali University and MNIT-Jaipur. He is expert peer committee member of National Assessment and Accreditation Council (NAAC), Bangalore, India.

He has 23 years of Teaching, Research, Consultancy, and Administrative experience. He guided 4 PhD students, 36 ME Dissertation students and 33 Thesis students and around 200 Project students. He is currently guiding 5 PhD candidates, 2 Thesis students. He is on doctoral advisory committee for 10 PhD students. He currently has 4 research and sponsored projects from UGC, DST & KK Birla Academy. He is PhD Examiner for 5 candidates and PhD Thesis Reviewer for 5 Candidates.

His research interests include Evolutionary Computation (Population-based search algorithms for optimization of highly complex and non-linear engineering problems), Environmental Engineering, Biomass Gasification, Energy Integration, Artificial Neural Networks, Nano Technology, and Modeling & Simulation.

He is the recipient of National Technology Day (11th May, 2003) Award given by CSIR, obtained in recognition of the research work done in the area of 'A New Concept in Differential Evolution (DE) – Nested DE'. His paper entitled "Convective and Radiative Heat Transfer in Pyrolysis of a Biomass Particle" authored by A S Chaurasia, B V Babu, Amanpreet Kaur, and V Thiruchitrambalam, published in Indian Chemical Engineer Journal, Vol. 47 (No. 2), pp. 75-80, April-June, 2005 earned the Kuloor Memorial Award, 2006 awarded for the Best Technical Paper published in the Institute's Journal "Indian Chemical Engineer" in its issues for 2005.

He is the Life member of Indian Institute of Chemical Engineers (IIChE), Life member of Indian Society for Technical Education (ISTE), Life member of Institution of Engineers (IE), Fellow of International Congress of Chemistry and Environment (ICCE), Life member of Indian Environmental Association (IEA), Life member of Society of Operations Management (SOM), Associate Member of International Society for Structural and Multidisciplinary Optimization (ISSMO), Member of International Institute of Informatics and Systemics (IIIS), Member of International Association of Engineers (IAENG). Nine of his technical papers have been included as successful applications of Differential Evolution (DE: a population based search algorithm for optimization) on their Homepage at http://www.icsi.berkeley.edu/~storn/code.html#appl.

He has around 170 research publications (International & National Journals & Conference Proceedings) to his credit. He completed three consultancy projects successfully and he has been Technical Consultant for Maharashtra Electricity Regulatory Commission (MERC), Mumbai and offering Advisory Services in the "Study relating to Bagasse Based Co-generation". He also has been invited as a consultant by a Bahrain (Middle East) based company for making a complex of chemical factories. He is a Panel Expert for www.chemicalhouse.com.

He has published five books (1) "Process Plant Simulation", EDD, BITS-Pilani, 2002, (2)"New Optimization Techniques in Engineering", Springer-Verlag, Germany, 2004, and (3)"Process Plant Simulation", Oxford University Press, India, 2004, (4) "Environmental Management Systems", EDD, BITS-Pilani, 2005, (5) "Chemical Engineering Laboratory Manual", EDD, BITS-Pilani, 2006. In addition he has written several chapters and invited articles in various books, lecture notes, and International Journals. He was invited to write an editorial and for cover design on Conservation of Natural Resources, for December 2006 Issue of International Research Journal of Chemistry & Environment.

He was the Invited Chief Guest and delivered the Keynote addresses at five international conferences and workshops (Desert Technology–7, Jodhpur; Life Cycle Assessment, Kaula Lumpur; Indo-US Workshop, IIT-Kanpur; Indo-French Workshop, TERI-New

Delhi; Indo-US Workshop, Kolkata) and three national seminars. He organized many Seminars & Conferences at BITS-Pilani. He also chaired 19 Technical Sessions at various International & National Conferences. He delivered 38 invited lectures at various IITs and Universities abroad.

He is Editorial Board Member of five International Journals 'Energy Education Science & Technology', 'Research Journal of Chemistry and Environment', 'International Journal of Computer, Mathematical Sciences and Applications', 'Journal on Future Engineering and Technology', and 'International Journal of Applied Evolutionary Computation'. He is the referee & expert reviewer of 42 International Journals. He is also on the Programme Committees as an expert reviewer at many International Conferences. He reviewed five books of McGraw Hill, John Wiley & Science, Elsevier, Oxford University Press, and Tata McGraw Hill publishers.

He is the Organizing Secretary for "National Conference on Environmental Conservation (NCEC-2006)" held at BITSPilani during September 1-3, 2006. He is also the Organizing Committee Member (Publicity Chair), and Session Organizer for the Special Session on "Evolutionary Computation" at The Second International Conference on "Computational Intelligence, Robotics, and Autonomous Systems (CIRAS-2003)", National University of Singapore, Singapore, December 15-17, 2003. He is the Session Chair and organized an Invited Session on "Engineering Applications of Evolutionary Computation Techniques" at "The Eighth World Multi-Conference on Systemics, Cybernetics, and Informatics (SCI-2004)", Orlando, Florida, USA, July 18-21, 2004.

APPENDIX I

Code in MatLab for the Equilibrium Model

```
% The Program developed for finding out the outlet composition of the gas from
downdraft %   gasifier using equilibrium modeling
clear all
clc
% CHaOb
ac = 1.48 % for hazelnutshell
bc = 0.735 % for hazelnutshell
   %C H 1.531 O 0.693 for dalbergia sisoo

MC =0.16
%for ij= 1:10
% molar fraction of water per kmol of wood calculation
w = (24 * MC) /(18*(1-MC));
x1 = 0.35;    x2 = 0.35;    x3=  0.35; % initial guess

m1 = 0.46099  % the kmol of oxygen per kmol of wood

T = 973.0; % first guess
%    N2 CO2  CO CH4 H2O(v)  H2  H2O(l) wood respectively  1 2 3 4 5 6 7 8.
 %for ii =1:10
% Heat of formation of vaious components
   H0f = [0.0,-393509.0,-110525.0,-74520.0,-241818.0,0.0,-285830.0];
% Heat of formation of wood
   H0fw =  -118050.0;
% Heat of vaporization
   Hvap = 40609.8;
% Constants for specific heat calculation
   CA = [3.280,5.457,3.376,1.702,3.47,3.249];
   CB = [ 0.000593,0.001047,0.000557,0.009081,0.00145,0.000422];
   CC = [ 0.0,0.0,0.0,-0.000002164,0.0,0.0];
   CD = [40000.0,-115700.0,-3100.0,0.0,12100.0,8300.0];
% Constants for Equilibrium Constant Calculation
   deltaA=[1.86000,-6.567000,7.951000];
   deltaB=[-5.379999e-004,7.466001e-003,-8.708000e-003];
   deltaC=[0.000000e+000,-2.164000e-006,2.164000e-006];
   deltaD=[-1.164000e+005,7.010000e+004,9.700000e+003];
   J=[-48823.644531,-58886.800781,189433.312500];
   I=[-18.013929,32.541370,-24.899353];
% Universal Gas Constant
```

```
  Rconst= 8.314;
   Tavg =( T + 298.15)/2.0;
% Specific Heat Calcualation
  for k=1:6
       Cp(k) = Rconst * ( CA(k) + CB(k) * Tavg + (CC(k)/3.0) * (4 * Tavg * Tavg -
       T*298.15 ) + CD(k) * (1/(T*298.15)));
  end
% Equilibrium Constant Calculation
   for j=1:3
       lnK(j) = (-J(j)/(Rconst * T)) + ( deltaA(j) * log(T)) + ( ( deltaB(j)/2)*T) +
       ((deltaC(j)/6)* T * T) + ((deltaD(j)/2)*(1/ (T * T))) + I(j) ;
    K(j) = exp(lnK(j));
  end

 k1 = K(1);
 k0 = K(2);
  for j=1:50
    for i=1:10000
     f1 = k0 * x1 * x1 + x2 + x3 -1;
          g1 = -k1 * x1 * x2 + (w - 1.28)*k1*x2 + 2 *k1*x2 *x2 -x1 *x3 + 2 * k1*x2 *x3;
     fx1 = 2.0 * x1 * k0;
     fx2 = 1.0;
     gx1 = -k1* x2 - x3;
     gx2 = k1 * ( -x1 + w - 1.28 + 4 * x2 + 2 * x3);

     if ( (abs(f1) < 0.0000000000001) & (abs(g1)<0.0000000000001))
     % disp('pratik');
         break;
     end
     m= [ fx1 fx2; gx1 gx2];
     n= inv(m);
     delx1 = n(1,1) * f1 + n(1,2) * g1;
     delx2 = n(2,1) * f1 + n(2,2) * g1;
     x1new = x1 - ( delx1);
     x2new = x2 - ( delx2);

     if ( x1 < 0)
        x1 = x1 * (-1.0);
     end
     if (x1>0.50)
        for q = 1:10054
           x1 = x1 * 0.5;
           if x1<0.50
              break;
           end
        end
```

```
      end

      if (x2new<0.0)
         x2new = x2new * (-1.0);
      end

      if (x2new>0.50)
         for q = 1:100
            x2new = x2new * 0.5;
            if (x2new<0.50)
               break;
            end
         end
      end
      x1 = x1new;
      x2 = x2new;
   end
    f1 = k0 * x1 * x1 + x2 + x3 -1;
        g1 = -k1 * x1 * x2 + (w- 1.28)*k1*x2 + 2 *k1*x2 *x2 -x1 *x3 + 2 * k1*x2 *x3;

     x3 = [2 * m1 + 1.94 + x1 - 3 * x2] * 0.25;

      fid = fopen('tempa.txt','a+');
   fprintf(fid,'%f\t%f\t%f\t%f\t%f\n',x1,x2,x3,f1,g1);
      fclose(fid);
   end
   x4 = (x1 * x3)/(k1*x2);
   x5 = k0 *  x1 * x1;

   A1 = H0fw + w *(H0f(7) + Hvap);
   B1 = x2 * H0f(3) + x3 * H0f(2) + x4 * H0f(5)  + x5 * H0f(4) ;
   C1 = x1 * Cp(6) + x2 * Cp(3) + x3 * Cp(2) + x4 * Cp(5) + x5 *
      Cp(4)+ 3.76 * m1 * Cp(1);

 %   Tnew =   298.15 +  (( A1 -B1)/C1) ;

  %  disp('pratik, new temperature is ');
   % T = Tnew

%end
      fid = fopen('result.txt','a+');
   %if ( ij==1)
      fprintf(fid,'comp_H2 comp_N2 comp_CO comp_CH4 comp_CO2 CV\n');
    %   end
 % composition Calculation
   su = x1 + x2 + x3 + x5 + 3.76 *m1;
```

```
    su1 = x1 + x2 + x3 + x4 +  x5 + 3.76 *m1;
    comp_H2 = x1/su;
    comp_CO= x2/su;
    comp_CO2 = x3/su;
    comp_H2O = x4/su1;
    comp_CH4 = x5/su;
    comp_N2 = 3.76 * m1/su;

    % Calorific Value Calculation
    CV = (x1* 285.84) + (x5* 890.4) + (x2* 282.99);
    CV = (CV * 11.3565)/su1;
    fprintf(fid,'%f %f %f %f %f %f
\n',comp_H2,comp_N2,comp_CO,comp_CH4,comp_CO2,CV);
    fclose(fid);

    fid1 = fopen('allx.txt','a+');
    fprintf(fid1,'MC T H2 CO CO2 H2O CH4 N2 Total\n');

fprintf(fid1,'%f\t%f\t%f\t%f\t%f\t%f\t%f\t%f\t%f\n',MC,T,x1,x2,x3,x4,x5,3.76*m1,su1);
    fclose(fid1);
       %MC = MC + 0.1
    %end
```

APPENDIX II

Code in 'C' Language for Combined Transport and Kinetic Model

```
// for the pyrolysis and combustion model
#include <stdio.h>
#include <math.h>
#include <ctype.h>
#define M 150
#define maxt 65
#define Mbed 100
float densitygas(float fraction[],float Temp,float Pressure);
FILE *fp;
FILE *fp1;
main()
{
        int i,j,l,counter;
long double t,alpha,R,Rc,tau,dtau,dx,Tf,T0,bgf,Le,Bim,Bimc,h,emico,stboco,Sh,htime,
time[M+2],Vf0, constant;
long double CB[maxt][M+2],T[maxt][M+2],TC[maxt][M+2],CG1[maxt][M+2],
CC1[maxt][M+2],CG2[maxt][M+2],CC2[maxt][M+2],theta[maxt][M+2],thetac[maxt][M
+2],kw[M+2];
long double kc[M+2],Cpw[M+2],Cpc[M+2],ro[M+2],Qdp[M+2],Qdpc[M+2],k1[M+2],
k2[M+2],k3[M+2],Dbar[M+2],Cbarpg1[M+2],Vf[M+2],x[M+2],beta[M+2],gamma[M+2
],Cb[M+2];
long double a[M+2],b[M+2],c[M+2],d[M+2],bc[M+2],dc[M+2],aa[M+2],bb[M+2],
cc[M+2], dd[M+2],betacg[M+2],gammacg[M+2],betac[M+2],gammac[M+2];
long double roin,n1,n2,n3,dH,A1,D1,L1,A2,D2,L2,A3,E3,dumCB,dumCC1,dumCC2,
dumCG2,dumCG1;

//for packed bed
long double Tbed[5][maxt],mtotal[5][maxt],Dzero,nchar[5][maxt],sum,sumcc,sum1,
rototal[Mbed+2],vbed[Mbed+2],sumCB[maxt];
long double nco2[5][maxt],nco[5][maxt],nh2[5][maxt],nh2o[5][maxt],nch4[5][maxt],
ntar[5][maxt];
long double robed[6][Mbed+2],m[6][Mbed+2],Temp1[M+2],finalavgCB[5][maxt];
float density;

//robed 0,1,2,3,4,5 - CH4, CO, CO2, H2,H20,tar respectively

float fraction[5],Temp,Pressure;
long double dtbed,dy,ebed,apar,Deffbed,molarflow,massflow,volpyrozone,absdensity,
molarflowrate[6][6],molwt,Bmassini,Bmassfin,mcini,mcfin,otime;
```

```
int z,y,p,q;

long double airflowrate,AmtCO2,AmtCO2bm,AmtCO2tar,AmtH2O,AmtH2Obm,
AmtH2Otar,AmtH2Odrying,AmtN2,AmtO2,AmtO2bm,AmtO2tar;
volpyrozone = 0.0041548; // m3
absdensity = 1170.0;  //kg/m3
ebed = 2.5/(volpyrozone*absdensity);
//ebed = 0.2;
Deffbed = 0.2e-04;// as tkaen by DiBlasi (2001)
apar =6.0; //m2/m3
dy = 0.001; // m
dtbed = 30.0;  //second
Dzero = 0.01e-04;  //     m2/sec
fp = fopen("G:\\Pratik_Sheth\\programs\\pyrolysisbed\\temp1.txt","a+");
fp1 = fopen("G:\\Pratik_Sheth\\programs\\pyrolysisbed\\temp2.txt","a+");
constant = 0.3;
Vf0 = 0.5;
n1 = 1.0;
n2 =1.5;
n3 = 1.5;
t = 30.0;  // sec
dH = -255000.0;
alpha=1.79e-07;
R=0.0127; // 1 inch = 2.54 cm size so half of that is taken as R
Rc=8.314;
bgf=1.0; // as the material is a cube so bgf is taken as 1.0..... if it is cylinder bgf = 2.0 and
if it is sphere bgf = 3.0
//roin = 650.0;
roin = 1170.0; //kg/m3
tau =(alpha*t)/(R*R);
dtau = tau;
dx = (1.0/M);
htime =dtau/1000.0;

printf ("dx = %f",dx);
Le = 2.0;
emico = 0.95;
stboco = 5.67e-08;

T0 = 303.0;
A1 = 9.973e-05; D1 = 17254.4;L1 = -9061227.0;A2 = 1.068e-03; D2 = 10224.4;L2 = -
6123081.0;
A3 = 5.7e+5;E3 = 81000.0;
printf("dtau=%e\n",dtau);
getchar();
 for(j=0;j<51;j=j+1)
```

```
 {
  z=0;
  if (z==0)
  {
   if(j<=10)
    Tbed[z][j] = 4*0.5*j + 130.0;
   else if (j>10 && j<=40)
    Tbed[z][j] = 0.0184*pow(0.5*j,4.0)  -0.938*pow(0.5*j,3.0) +13.913*pow(0.5*j,2.0)-
45.014* 0.5*j + 130.5;
   else
    Tbed[z][j] = 1.4 * (0.5*j) + 210.0;

   Tbed[z][j] =  Tbed[z][j] + 273.15;
  }

  z=4;
  if (z==4)
   {
   if(j<=10)
    Tbed[z][j] = 48.8*0.5*j + 727.0;
   else if (j>10 && j<=40)
    Tbed[z][j] =  0.0042*pow(0.5*j,5.0) -0.2863*pow(0.5*j,4.0) +6.9107*pow(0.5*j,3.0) -
69.642*pow(0.5*j,2.0) + 257.4* 0.5*j + 727.0;
   else
    Tbed[z][j] = -19.2* (0.5*j) + 1340.0;


    Tbed[z][j] =  Tbed[z][j] + 273.15;
   }
 }


for (z=1;z<=3;z=z+1)
{
for(j=0;j<51;j=j+1)
{
Tbed[z][j] = Tbed[0][j] + (z*25.0)*0.01*(Tbed[4][j] - Tbed[0][j]);
}
}

for (z=0;z<=4;z=z+1)
                {
                        for(j=0;j<51;j=j+1)
                        {
                        printf("Tbed[%d][%d]=%f\n",z,j,Tbed[z][j]);
                        }
```

```
                        getchar();
        }

for (z=0;z<=4;z=z+1)
        {
// intial conditions
        for (i=0;i<=M;i=i+1)
        {
                T[0][i] = T0;
                TC[0][i] = T0;
                CB[0][i] = 1.0;
                Cb[i]  = roin;
                CG1[0][i] = 0.0;
                CC1[0][i] = 0.0;
                CG2[0][i] = 0.0;
                CC2[0][i] = 0.0;
                theta[0][i] =1.0;
                thetac[0][i] =1.0;
        //printf("%f\n",TC[0][i]);
        }
        x[0]=0;
        //getchar();

        kw[M] =0.13 + 0.0003*(T[0][M]-273.0);
        kc[M] =0.08 - 0.0001 * (TC[0][M]-273.0);
        //printf("pratik%f\n",kw[M]);
        //getchar();

        nchar[z][0] = 0.0;
mtotal[z][0] = 0.0;
        for(j=0;j<51;j=j+1)
        {

                Tf = Tbed[z][j];


                if(T[j][M]>673.0)
                        h = 20.0;
                else
                        h = 8.4;
        //      printf("h=%f",h);
        //      getchar();

                Bim = (R/kw[M])*(h + emico*stboco*((pow(T[j][M],3.0)+
T[j][M]*T[j][M]*Tf+Tf*Tf*T[j][M]+Tf*Tf*Tf)));
```

```
		Bimc =(R/kc[M])*(h + emico*stboco*((pow(TC[j][M],3.0)+
TC[j][M]*TC[j][M]*Tf+Tf*Tf*TC[j][M]+Tf*Tf*Tf)));
		Sh = 50000.0*pow(theta[j][M],0.75);
	//	printf("Bimc=%f and Sh = %f",Bimc,Sh);
	//	getchar();
		for (i=0;i<=M;i=i+1)
			{
			kw[i] =0.13 + 0.0003 * (T[j][i]-273.0);
			kc[i] =0.08 - 0.0001 * (TC[j][i]-273.0);
			Cpw[i] =112.0 + 4.85 * (T[j][i]-273.0);
			Cpc[i] =1003.2 + 2.09 * (T[j][i]-273.0);
			ro[i] = roin * (CB[j][i] + CC1[j][i]+CC2[j][i]);
			k1[i] =A1 * exp((D1/T[j][i])+(L1/(T[j][i] * T[j][i])));
			k2[i] =A2 * exp((D2/TC[j][i])+(L2/(TC[j][i] * TC[j][i])));
			k3[i] = A3*exp(-E3/(Rc*TC[j][i]));
			Cb[i] = CB[j][i] * roin;
			Qdp[i] = ((-dH + Cpw[i] * T[j][i])/(ro[i] * Cpw[i] * (T0-
Tf)))*pow(Cb[i],n1);
			Qdpc[i] =((-dH + Cpc[i] * TC[j][i])/(ro[i] * Cpc[i] * (T0-
Tf)))*pow(Cb[i],n1);
		Dbar[i] =pow(theta[j][i],1.5)* exp(1.0-CB[j][i]);
			Cbarpg1[i] = 1.0 + 0.001 * (theta[j][i]-1.0);
			Vf[i] =Vf0 + constant*(1-CB[j][i]);
			x[i] = x[i] + dx ;
//	if((i%10)==0)
//	printf("k1[%d] = %e\tk2[%d] = %e\n",i,k1[i],i,k2[i]);
	//getchar();
			if(i==0)
			{
				a[i] = 0.0;
				b[i] = 1.0 + (2 * bgf * dtau/(dx * dx));
				bc[i] = 1.0 + (2 * bgf * dtau/(dx * dx));
				c[i] = -2.0 * bgf * dtau /(dx * dx);
				d[i] = theta[j][i] + (dtau/alpha)*Qdp[i]* R * R * k1[i];
				dc[i] = thetac[j][i] + (dtau/alpha)*Qdpc[i]* R * R * k1[i];
			}
			else if (i==M)
			{
				a[i] =   -2.0 * dtau /(dx*dx);
				b[i] = (2.0*dtau * Bim/dx)+(2.0*dtau/(dx*dx))+1.0+((bgf-
1.0)/x[i])*Bim*dtau + (Sh/Le)*(-CG1[j][i])*Cbarpg1[i]*dtau*Bim;
				bc[i] = (2.0*dtau *
Bimc/dx)+(2.0*dtau/(dx*dx))+1.0+((bgf-1.0)/x[i])*Bimc*dtau + (Sh/Le)*(-
CG1[j][i])*Cbarpg1[i]*dtau*Bimc;
				c[i] = 0.0;
				d[i] = theta[j][i]+ (dtau/alpha)*Qdp[i]*R*R*k1[i];
```

```
                        dc[i] = thetac[j][i] + (dtau/alpha)*Qdpc[i]* R * R * k1[i];
                }
                else
                {
                        a[i] = (dtau /(dx*dx))*(-1.0+ ((bgf-1.0)/(2.0*x[i]))*dx +
(Dbar[i]/(4.0*Le))*Cbarpg1[i]*(CG1[j][i+1]-CG1[j][i-1]));
                        b[i] = 2.0*(dtau /(dx*dx)) + 1.0;
                        bc[i] = 2.0*(dtau /(dx*dx)) + 1.0;
                        c[i] = (dtau /(dx*dx))*(-1.0- ((bgf-1.0)/(2.0*x[i]))*dx +
(Dbar[i]/(4.0*Le))*Cbarpg1[i]*(-CG1[j][i+1]+CG1[j][i-1]));
                        d[i] = theta[j][i]+ (dtau/alpha)*Qdp[i]*R*R*k1[i];
                        dc[i] = thetac[j][i] + (dtau/alpha)*Qdpc[i]* R * R * k1[i];
                }
        //      if((i%10)==0)
//      printf("thetac%f %f %f %f\n",b[i],bc[i],d[i],dc[i]);

        }
//getchar();
        for (i=0;i<=M;i=i+1)
                {
                        if(i==0)
                        {
                                beta[i] = b[i];
                                gamma[i] = (d[i]/beta[i]);

                                betac[i] = bc[i];
                                gammac[i] = (dc[i]/betac[i]);
                        }
                        else
                        {
                                beta[i] = b[i] - ((a[i]*c[i-1])/beta[i-1]);
                                gamma[i] =(d[i] - a[i]* gamma[i-1])/beta[i];

                                betac[i] = bc[i] - ((a[i]*c[i-1])/betac[i-1]);
                                gammac[i] =(dc[i] - a[i]* gammac[i-1])/betac[i];

                        }
                }
                for (i=M;i>=0;i=i-1)
                {
                if (i==M)
                        theta[j+1][i] = gamma[i];
                else
                        theta[j+1][i] = gamma[i] - (c[i]/beta[i])*theta[j+1][i+1];
                if (theta[j+1][i] <0.0)
                        theta[j+1][i] = 0.00001;
```

```
                        }

                        for (i=M;i>=0;i=i-1)
                        {
                        if (i==M)
                                thetac[j+1][i] = gammac[i];
                        else
                                thetac[j+1][i] = gammac[i] -
(c[i]/betac[i])*thetac[j+1][i+1];
                        if (thetac[j+1][i] <0.0)
                                thetac[j+1][i] = 0.00001;
                        }
                        for (i=0;i<=M;i=i+1)
                        {
                        //      if((i%10)==0)
        //      printf("%d\ttheta = %f\t thetac = %f\n",i,theta[j+1][i],thetac[j+1][i]);
                        }
        //      getchar();
                        for (i=0;i<=M;i=i+1)
                        {
                        T[j+1][i] = Tf - (theta[j+1][i] *(Tf-T0));

                        TC[j+1][i] = Tf - (thetac[j+1][i] *(Tf-T0));
        //if((i%10)==0)
        //              printf("%d\tTemperature=%f\t%f\n",i,T[j+1][i],TC[j+1][i]);
                        }
        //      getchar();
                        for (i=0;i<=M;i=i+1)
                        {
                                if(i==0)
                                {
                                aa[i] = 0.0;
                                bb[i] = 1.0 + (2 * bgf * dtau*Dbar[i]/(dx * dx* Le*Vf[i]));
                                cc[i] = -2.0 * bgf * (dtau *Dbar[i]/(dx * dx*Le*Vf[i]));
                                dd[i] = CG1[j][i] + (dtau/(alpha*Vf[i]))*pow(CB[j][i],n1)*
R * R * k1[i] - (dtau/alpha)*R*R*k3[i]*pow(CG1[j][i],n2)*pow(CC1[j][i],n3);
                                }
                                else if (i==M)
                                {
                                aa[i] = -2.0 * dtau *Dbar[i]/(dx*dx*Le*Vf[i]);
                                bb[i] = (dtau/(Le*Vf[i]*dx*dx))*(2*Dbar[i] + 2*dx*Sh +
(bgf-1.0)*Sh*dx*dx*(1.0/x[i]) +   (Le*Vf[i]*dx*dx)/dtau  );
                                cc[i] = 0.0;
                                dd[i] = CG1[j][i] +  (  (R*R*dtau/alpha)*
((k1[i]/Vf[i])*pow(CB[j][i],n1) - k3[i] *pow(CG1[j][i],n2)*pow(CC1[j][i],n3)));
```

```
                                }
                                else
                                {
                                aa[i] = (dtau /Vf[i])*(((bgf-1.0)*Dbar[i]/(2.0*x[i]*dx*Le))-
(Dbar[i]/(dx*dx*Le)));
                                bb[i] = 2.0*(dtau*Dbar[i]/(dx*dx*Le*Vf[i])) + 1.0;
                                cc[i] = (-1.0)*(dtau*Dbar[i]/(Le*Vf[i]))*(((bgf-
1.0)/(2.0*x[i]*dx)) + (1/(dx*dx)));
                                dd[i] = CG1[j][i]+
(dtau/(alpha*Vf[i]))*pow(CB[j][i],n1)*R*R*k1[i]  -  (dtau/alpha)*
R*R*k3[i]*pow(CG1[j][i],n2)*pow(CC1[j][i],n3);
                                }
                        /*      if((i%10)==0)
                                {
                                printf("cgcalcn%e %e %e %e %e
\n",aa[i],bb[i],cc[i],dd[i],(dtau/alpha)* R*R*k3[i]*pow(CG1[j][i],n2)*pow(CC1[j][i],n3)
);
                }*/
                }
                        for (i=0;i<=M;i=i+1)
                        {

                                if(i==0)
                                {
                                        betacg[i] = bb[i];
                                        gammacg[i] = (dd[i]/betacg[i]);
                                }
                                else
                                {
                                betacg[i] = bb[i] - ((aa[i]*cc[i-1])/betacg[i-1]);
                                gammacg[i] =(dd[i] - aa[i]* gammacg[i-1])/betacg[i];
                                }
                        //if((i%10)==0)
                        //
        printf("cgcalcn\tgammacg%e\tbetacg%e\n",gammacg[i],betacg[i]);
                }
                for (i=M;i>=0;i=i-1)
                {
                        if (i==M)
                        CG1[j+1][i] = gammacg[i];
                        else
                        CG1[j+1][i] = gammacg[i] - (cc[i]/betacg[i])*CG1[j+1][i+1];
                }

//calculation of CB,CC1,CG2,CC2 by finite diff explicit method
                        sum = 0.0;
```

```
                sumcc = 0.0;
            for (i=0;i<=M;i=i+1)
                {
                dumCB = CB[j][i];
                dumCC1 = CC1[j][i];
                dumCG1 = CG1[j][i];
                dumCG2 = CG2[j][i];
                dumCC2 = CC2[j][i];
                for (l=0;l<1000;l=l+1)
                        {
                        dumCB = dumCB +  htime* (-k1[i]*pow(dumCB,n1) -
k2[i]*pow(dumCB,n1));
                        dumCC1= dumCC1 +  htime* (k2[i]*pow(dumCB,n1) -
k3[i]*pow(dumCG1,n2)*pow(dumCC1,n3));
                        dumCG2 = dumCG2 +  htime*
(k3[i]*pow(dumCG1,n2)*pow(dumCC1,n3));
                        dumCC2 = dumCC2+  htime*
(k3[i]*pow(dumCG1,n2)*pow(dumCC1,n3));

                        if(dumCC1<0)
                                dumCC1 =0.0;

                        if(dumCG1<0)
                                dumCG1 =0.0;
                    /*  CB[j+1][i] = CB[j][i] +  dtau* (-k1[i]*pow(CB[j][i],n1) -
k2[i]*pow(CB[j][i],n1));
                        CC1[j+1][i] = CC1[j][i] +  dtau* (k2[i]*pow(CB[j][i],n1) -
k3[i]*pow(CG1[j][i],n2)*pow(CC1[j][i],n3));
                        CG2[j+1][i] = CG2[j][i] +  dtau*
(k3[i]*pow(CG1[j][i],n2)*pow(CC1[j][i],n3));
                        CC2[j+1][i] = CC2[j][i] +  dtau*
(k3[i]*pow(CG1[j][i],n2)*pow(CC1[j][i],n3));*/
                        }
                        sumcc = sumcc +       ((k2[i]*pow(dumCB,n1) -
k3[i]*pow(dumCG1,n2)*pow(dumCC1,n3))/(k1[i]*pow(dumCB,n1) +
k2[i]*pow(dumCB,n1)));
                        CB[j+1][i]  = dumCB;
                        CC1[j+1][i]     = dumCC1;
                        CG2[j+1][i] = dumCG2;
                        CC2[j+1][i] = dumCC2;
                        if(CC1[j+1][i]<0)
                                CC1[j+1][i] =0.0;

                        if(CG1[j+1][i]<0)
                                CG1[j+1][i] =0.0;
```

```
                        }
                        fprintf(fp1,"z=%d\n",z);
                        sumCB[j] = 0.0;
                        for (i=0;i<=M;i=i+1)
                        {
                                sumCB[j] = sumCB[j] + CB[j][i];
                        }


                        finalavgCB[z][j] = sumCB[j]/(M+1);

                        printf("finalavgCB[%d][%d] = %f\n",z,j,finalavgCB[z][j]);
        //      nchar[z][j+1] = (sumcc*131.3049)/(151.0*12.0);
        nchar[z][j+1] = (sumcc*131.3049)/(151.0*22.0);
                if (nchar[z][j+1] < 0.0)
                        nchar[z][j+1] = 0.0;
mtotal[z][j+1] = roin*(Dzero*Dbar[M])*((CG1[j+1][M-1]-CG1[j+1][M])/(dx*R));
printf("\nDbar[%d] = %e\tCG1[%d][%d] =
%e\nCG1[%d][%d])=%e\n",M,Dbar[M],j+1,M-1,CG1[j+1][M-1],j+1,M,CG1[j+1][M]);
if(mtotal[z][j+1] < 0.0)
{
getchar();
}
nco2[z][j] = (90.39 + nchar[z][j])/(45.57142857* pow(2.718281828,(-1.845 +
(7730.3/Tbed[z][j])  - (5019898.0/(Tbed[z][j]*Tbed[z][j])))) + 132.33333 - 13.75e-16 *
pow(Tbed[z][j],5.06));
nh2o[z][j] = 2.444444 * nco2[z][j] ;
nch4[z][j] =  13.75e-16 * pow(Tbed[z][j],5.06)*nco2[z][j];
nco[z][j] = 1.571428 * pow(2.718281828,(-1.845 + (7730.3/Tbed[z][j])  -
(5019898.0/(Tbed[z][j]*Tbed[z][j])))) * nco2[z][j];
ntar[z][j] = (1.0/6.0)*(6.0 - nchar[z][j] - nco[z][j] - nco2[z][j] - nch4[z][j]);
nh2[z][j] = 0.5 * (7.8965 - 2.0 * nh2o[z][j] - 4.0* nch4[z][j] - 6.2* ntar[z][j] );
if (ntar[z][j] < 0.0)
{
        printf(" ntar[%d][%d] is negative",z,j);
ntar[z][j] = 0.0;
nco2[z][j] = (6.0 - nchar[z][j])/( 1+ 1.571428 * pow(2.718281828,(-1.845 +
(7730.3/Tbed[z][j])  - (5019898.0/(Tbed[z][j]*Tbed[z][j])))) +  13.75e-16 *
pow(Tbed[z][j],5.06));
nch4[z][j] =  13.75e-16 * pow(Tbed[z][j],5.06)*nco2[z][j];
nco[z][j] = 1.571428*pow(2.718281828,(-1.845 + (7730.3/Tbed[z][j])  -
(5019898.0/(Tbed[z][j]*Tbed[z][j])))) * nco2[z][j];
nh2o[z][j]= 3.213 - nco[z][j]- 2.0 * nco2[z][j];
nh2[z][j] = 0.5 * (7.8965 - 2.0 * nh2o[z][j] - 4.0 * nch4[z][j]);
```

```
}

if (nh2[z][j] < 0.0)
                nh2[z][j] = 0.0;
        printf("\nmtotal[%d][%d] =
%e\tnchar[%d][%d]=%e\n",z,j+1,mtotal[z][j+1],z,j,nchar[z][j+1]);
        printf("\nnco2[%d][%d] = %e\tnco[%d][%d]=%e\n",z,j,nco2[z][j],z,j,nco[z][j]);
        printf("\nnh2o[%d][%d] =
%e\tnch4[%d][%d]=%e\n",z,j,nh2o[z][j],z,j,nch4[z][j]);
        printf("\nntar[%d][%d] = %e\tnh2[%d][%d]=%e\n",z,j,ntar[z][j],z,j,nh2[z][j]);
        } //loop of time (j) ends here
//printf("\n");
//      for (i=0;i<=M;i=i+1)
//              printf("%f\n",T[60][i]);
}//loop of z ends here
// packed bed program starts here.
//intial conditions
for (l=0;l<6;l=l+1)
{
        for (i=0;i<=Mbed;i++)
        {
                robed[l][i] = 0.0;

        }
}
//robed 0,1,2,3,4,5 - CH4, CO, CO2, H2,H20,tar respectively
        counter = 0;
for(j=0;j<51;j++)
        {
                fprintf(fp,"time = %f minute\n",0.5*j);
                printf("j=%d\n",j);
//velocity calculation  //  CO2  CO CH4 H2O  H2
        for (i=0;i<=Mbed;i=i+1)
        {
                if(i<25)
                                {
                                        l=0;     p = 0;q =1;
                                }
                                else if(i>=25 && i<50)
                                {
                                        l = 1;p = 1;q =2;
                                }
                                else if(i>=50 && i<75)
                                {
                                        l = 2;p = 2;q =3;
                                }
```

```
                    else if(i>=75 && i<101)
                    {
                            l = 3;    p = 3;q =4;
                    }

        Temp = Tbed[l][j];//K
        Pressure =  151987.5;// N/m2
        Temp1[i] = Temp;
                    rototal[i] =0.0;
                    for(l=0;l<5;l++)
                    {
                            if(l==0)
                                    molarflow = nco2[p][j] + nco2[q][j];
                                    else if(l==1)
                                    molarflow = nco[p][j] + nco[q][j];
                                    else if(l==2)
                                    molarflow = nch4[p][j] + nch4[q][j];
                                    else if(l==3)
                                    molarflow = nh2o[p][j] + nh2o[q][j];
                                    else
                                            molarflow = nh2[p][j] + nh2[q][j];

                    fraction[l] = (molarflow)/(nco2[p][j]+ nco2[q][j] + nco[p][j]+
nco[q][j] + nch4[p][j]+ nch4[q][j]+  nh2o[p][j]+ nh2o[q][j] +  nh2[p][j]+ nh2[q][j]);

                    rototal[i] = rototal[i] + robed[l][i] ;

                    }
                    rototal[i] = rototal[i] + robed[5][i] ;
                    density = densitygas(fraction,Temp,Pressure);
        vbed[i] = (rototal[i] * dy)/(dtbed * density);
        if((j%10 == 0) &&  (i == Mbed))
        {
                    for(l=0;l<6;l++)
                    {
                                    if(l==0)
                                    molwt = 16.0;
                                    else if(l==1)
                                    molwt = 28.0;
                                    else if(l==2)
                                    molwt = 44.0;
                                    else if(l==3)
                                    molwt = 2.0;
                                    else if(l==4)
                                    molwt = 18.0;
```

```
                                        else
                                        molwt = 81.4;
                                molarflowrate[counter][l] =
robed[l][i]*vbed[i]*(3.141592654/4.0)*(0.15*0.15)*(3600.0/molwt); //kmole/hr
        fprintf(fp1,"\nmolarflowrate[%d][%d] = %f",counter,l,molarflowrate[counter][l]);
                                }
                        counter = counter + 1;
                        getchar();
                }
        }
        for (i=0;i<=Mbed;i=i+1)
                        {
                                if((i%10)==0)
                                        fprintf(fp,"\n%d\t%e\t%e\t",i,vbed[i],Temp1[i]);
                        for(l=0;l<6;l=l+1)
                        {

                        if((i%10)==0)
                                fprintf(fp,"%e\t",robed[l][i]);

                }
        }

for(l=0;l<6;l=l+1)
{
//getchar();
        for (i=0;i<=Mbed;i=i+1)
                        {

                                if(i<25)
                                {
                                        p = 0;q =1;

                                }
                                else if(i>=25 && i<50)
                                {
                                        p = 1;q =2;
                                }
                                else if(i>=50 && i<75)
                                {
                                        p = 2;q =3;
                                }

                                else if(i>=75 && i<101)
                                {
                                        p = 3;q =4;
```

```
                                        }


                                                if(l==0)
                                                        massflow = (nch4[p][j] + nch4[q][j]) * 16.0;
                                                        else if(l==1)
                                                        massflow = (nco[p][j] + nco[q][j]) * 28.0;
                                                        else if(l==2)
                                                        massflow = (nco2[p][j] + nco2[q][j]) * 44.0;
                                                        else if(l==3)
                                                        massflow = (nh2[p][j] + nh2[q][j])*2.0;
                                                        else if(l==4)
                                                        massflow = (nh2o[p][j] + nh2o[q][j]) * 18.0;
                                                        else
                                                        massflow = (ntar[p][j] + ntar[q][j]) * 81.4;

                                                m[l][i] = 0.5 * (mtotal[p][j] + mtotal[q][j])*
(massflow)/((nco2[p][j]+ nco2[q][j])*44.0 + (nco[p][j]+ nco[q][j]) *28.0 + (nch4[p][j]+
nch4[q][j]) *16.0+ (ntar[p][j]+ ntar[q][j])*81.4 + (nh2o[p][j]+ nh2o[q][j])*18.0 +
(nh2[p][j]+ nh2[q][j]) *2.0);
                //          printf("\tm[%d][%d] = %f\n",l,i,m[l][i]);
                                        if(i==0)
                                        {
                                        aa[i] = 0.0;
                                        bb[i] = 1 + (dtbed*vbed[i])/(2*dy) +
(2*dtbed*Deffbed)/(dy*dy);
                                        cc[i] = (dtbed*vbed[i])/(2*dy) - (dtbed*Deffbed)/(dy*dy);
                                        dd[i] = robed[l][i] + (apar*dtbed/ebed)*m[l][i];
                                        }
                                        else if (i==Mbed)
                                        {
                                        aa[i] = - (2*dtbed*Deffbed)/(dy*dy);
                                        bb[i] = 1 + (dtbed*(vbed[i]- vbed[i-1]))/(dy) +
(2*dtbed*Deffbed)/(dy*dy);
                                        cc[i] = 0.0;
                                        dd[i] = robed[l][i] + (apar*dtbed/ebed)*m[l][i];
                                        }
                                        else
                                        {
                                aa[i] = - (dtbed*Deffbed)/(dy*dy) - (dtbed*vbed[i])/(2*dy) ;
                                        bb[i] = 1 + (dtbed*(vbed[i]- vbed[i-1]))/(2*dy) +
(2*dtbed*Deffbed)/(dy*dy);
                                        cc[i] = (dtbed*vbed[i])/(2*dy) - (dtbed*Deffbed)/(dy*dy);
                                        dd[i] = robed[l][i] + (apar*dtbed/ebed)*m[l][i];
                                        }
                                        /*if((i%10)==0)
```

```
                        {
                        printf("cgcalcn%e %e %e %e \n",aa[i],bb[i],cc[i],dd[i]);
                        }*/
                }
        for (i=0;i<=Mbed;i=i+1)
                {
                        if(i==0)
                        {
                                betacg[i] = bb[i];
                                gammacg[i] = (dd[i]/betacg[i]);
                        }
                        else
                        {
                        betacg[i] = bb[i] - ((aa[i]*cc[i-1])/betacg[i-1]);
                        gammacg[i] =(dd[i] - aa[i]* gammacg[i-1])/betacg[i];
                        }
        }
        for (i=Mbed;i>=0;i=i-1)
        {
                if (i==Mbed)
                        robed[l][i] = gammacg[i];
                else
                        robed[l][i] = gammacg[i] - (cc[i]/betacg[i])*robed[l][i+1];

                //if((i%10)==0)
                //      fprintf(fp"%e\n",robed[l][i]);

        }
}
}

//oxidation and drying  calulations
// for oxidation zone calculations biomass ( C6 H7.8965 O3.213), MW = 131.3045 kg/kmole
        // 1 mole of biomass require 6.367625 mole of oxygen to completely burn it into CO2 and H20 according to the following chemical reaction

//C6 H7.8965 O3.213   +   6.367625 O2  --->   6 CO2   +   3.94825  H2O

 airflowrate =2.7765; //m3/hr
//(lest consider 20 % extra air is coming to complete the combustion
 //so stoichiometrically only 1/1.2 = 0.8333 is only available)

AmtO2 = ((airflowrate * 1.1854)/29.0)*0.21 *0.8333;       //kmole/hr
AmtN2 = ((airflowrate * 1.1854)/29.0)*0.79;                       //kmole/hr
```

```
Bmassini = 2.7 ;  //kg
Bmassfin  = 1.7; // kg
otime = 25.0 ;  //min
mcini =  0.1145;  // wet basis moisture content
mcfin=   0.1083 ; //    wet basis moisture content
AmtH2Odrying = ((Bmassini * mcini) -  (Bmassfin*mcfin))* (60.0/otime)*(1.0/18.0);
//kmole/hr

// tar oxidation
//C6 H6.2 O0.2   +   7.45 O2  --->   6 CO2   +   3.1  H2
fprintf(fp1,"\n\n");
for(i=0;i<6;i=i+1)
{
        AmtO2tar = molarflowrate[i][5] * 7.45;
        AmtCO2tar =  molarflowrate[i][5] * 6.0;
        AmtH2Otar  = molarflowrate[i][5] * 3.1;
        AmtO2bm = AmtO2 - AmtO2tar;
        AmtCO2bm = AmtO2bm*(6.0/6.367625);              //kmole/hr
        AmtH2Obm = AmtO2bm*(3.94825/6.367625);                  //kmole/hr
        AmtCO2 = AmtCO2bm + AmtCO2tar;
        AmtH2O = AmtH2Obm + AmtH2Otar + AmtH2Odrying;
        fprintf(fp1,"%d\t",i*5);
        for(l=0;l<6;l=l+1)
        {
                if(l==0 || l==1 || l==3)
                        fprintf(fp1,"%e\t",molarflowrate[i][l]);
                else if(l==2)
                        fprintf(fp1,"%e\t",molarflowrate[i][l] + AmtCO2);
                else if(l==4)
                        fprintf(fp1,"%e\t",molarflowrate[i][l] + AmtH2O);
                else
                        fprintf(fp1,"%e\t",AmtN2);
                //0,1,2,3,4,5 - CH4, CO, CO2, H2,H20,N2 respectively
        }
fprintf(fp1,"\n");
}
fclose(fp);
}// main loop ends here
float densitygas(float fraction[5],float Temp,float Pressure)
{
        int j,k;
        float v,v1=1.0,v2;//v1 is in  m^3/mole
        float a,b,alfa,kappa,p_omega,p_PC,p_TC,Rconst=8.314;
        float sum,F_v,Fprime_v,density1,density2,avgMolwt;
        //  CO2  CO CH4 H2O  H2
        float Molwt[5]= {44.01,28.01,16.04,18.02,2.02};
```

```
	float omega[5]= { 0.225,0.049,0.008,0.344,-0.22};
float PC[5]=	{7380000,3500000,4600000,22120000,1300000};//all values in N/m^2
	float TC[5]=	{304.4,133.1,190.6,647.3,33.2};//all vaues are in K
	p_omega=0.0;p_PC=0.0;p_TC=0.0;
		avgMolwt = 0.0;
	for(j=0;j<5;j++)
	{
		p_omega=p_omega + fraction[j]*omega[j];
		p_TC=p_TC + fraction[j]*TC[j];
		p_PC=p_PC + fraction[j]*PC[j];
		avgMolwt = avgMolwt + fraction[j] * Molwt[j];
	}
	kappa = 0.37464 + 1.54226 * p_omega - 0.26992 * pow(p_omega,2);
	alfa = pow((1+kappa*(1-pow((Temp/p_TC),0.5))),2);
	a = 0.45724 * pow((Rconst*p_TC),2)/p_PC;
	b=0.0778 * Rconst * p_TC /p_PC;
	for (j=0;j<100;j++)
	{
		v=v1;
		F_v= -(Pressure * pow(v,3)) + ((Rconst * Temp - Pressure * b ) *
pow(v,2)) + ((2 * b * Rconst * Temp + 3* Pressure * pow(b,2) - a * alfa)* v) - (Rconst *
Temp * b * b) - ( Pressure* pow(b,3)) + ( a * b);
		Fprime_v= -(3 * Pressure * pow(v,2))+ (2 * (Rconst * Temp - Pressure *
b ) * v) + (2 * b * Rconst * Temp + 3* Pressure * pow(b,2) - a * alfa);
		//getch();
		v2 = v1 - ( F_v/Fprime_v);
			density1 = (avgMolwt * 0.001)/v1;
			density2 = (avgMolwt * 0.001)/v2;
		if (j > 50)
		{
			density1 = (avgMolwt * 0.001)/v1;
			density2 = (avgMolwt * 0.001)/v2;
			if ( abs(density2-density1) < 0.01 )
			goto b1;
		else
			v1=v2;
		}
		else
			v1=v2;
		//if (j<9)
		//	printf("\ndensity=%f\t volume = %f",density2,v2);
//		if (j%10==0)
//			printf("\ndensity=%f\t volume = %f",density2,v2);
	}
	b1 :
```

```
        return(density2);
}
// for the reduction model

#include<stdio.h>
#include<math.h>
#include<ctype.h>
FILE *fp;
FILE *fp1;
float densitygas(float n[10000][6],float Temp,float Pressure,int i);
 main()
{
        int       i,j,k,time;
        float deltaz=0.0001,z,v[10000];
        double P[10000],ydry[1500][6],ywet[1500][6],kmolrate[1500];
        float n[10000][6];
        float c[6],T[10000],EA,EB,EC,ED,Rconst,rA,rB,rC,rD,CRF,CRF1,AA,AB,AC,
AD, lnK[4],K[4],p[6],deltaH[4],sum,sum1,sum2,sum3;
        float    R[6],sumrdeltaH,part1,sum4;
        float rho_gas,rho_air;
        float Temp,Pressure,Feedrate,Airtofuelratio,AirF,Gasflowrate[6],molardensity[6];
        float DTDZ,DVDZ,DPDZ,fpyro;
        // deltaA,B,C,D for all rxns
        static float deltaA[4]={-0.476000,1.384000,-6.567000,7.951000};
        static float deltaB[4]={-7.040001e-004,-1.240e-003,7.466001e-003,-8.708000e-
003};
        static float deltaC[4]={0.000000e+000,0.000000e+000,-2.164000e-
006,2.164000e-006};
        static float
deltaD[4]={1.962000e+005,7.980000e+004,7.010000e+004,9.700000e+003};
        static float J[4]={179370.156250,130546.515625,-
58886.800781,189433.312500};
        static float I[4]={25.655949,7.642021,32.541370,-24.899353};
        fp =fopen("G:\\Pratik_Sheth\\programs\\sskinetic\\results_ssmodel\\pns_sesame1
inch\\test1.txt","a+");
        fp1 =fopen("G:\\Pratik_Sheth\\programs\\sskinetic\\results_ssmodel\\pns_
sesame1inch\\wettest1.txt","a+");
                //fp =fopen("G:\\Pratik_Sheth\\pns_sesame1inch\\test1.txt","a+");
        //array of [6] corresponds to properties of N2 CO2  CO CH4 H2O  H2
respectively

//array of [6] corresponds to properties of N2, CO2,  CO, CH4, H2O,  H2 respectively
// initial data of case 1 27 june 45 rota
static float composition[6][6] =
{{0.65273,0.13624,0,0,0.21103,0},{0.49679,0.11233,0.02787,0.01398,0.29124,0.05779}
,{0.63384,0.13375,0.00345,0.00175,0.21918,0.00803},{0.6507,0.13598,4.78577E-
```

```
4,2.70643E-4,0.21171,8.67321E-4},{0.65242,0.13618,1.45083E-4,1.06374E-
4,0.21106,8.68368E-5},{0.65255,0.13619,1.37868E-4,9.44272E-5,0.21101,1.69978E-
5}};              // 6 times and 6 variables
static float temparature[6] = {747.0,971.0,805.0,942.0,956.0,860.0}; // deg C
static float Actualflowrate[6]= {0.13736,0.18048,0.14145,0.13779,0.13743,0.1374}; //
kmol/hr
for (time = 0;time<6;time = time +1 )
{
        //intial conditions
P[0]= 151987.5;// 1.5 atm abs
        T[0]= temparature[time] + 273.15;   // in    deg K
                Rconst = 8.314; //  in   Joules / (mole K)
                molardensity[time] = P[0] /(T[0]*Rconst);// mol/m3
n[0][0] = composition[time][0]*molardensity[time];
n[0][1] = composition[time][1]*molardensity[time];
n[0][2] = composition[time][2]*molardensity[time];
n[0][3] = composition[time][3]*molardensity[time];
n[0][4] = composition[time][4]*molardensity[time];
n[0][5] = composition[time][5]*molardensity[time];
for(j=0;j<6;j++)
        printf("n[0][%d] = %f",j,n[0][j]);
Gasflowrate[time] = Actualflowrate[time] * 1000.0 /molardensity[time] ;
v[0] = Gasflowrate[time] * 4.0 / (3.141592654*0.15*0.15*3600.0); //m/s
        // values of the constants EA in the unit of kJ/mole and A in the unit of (1/sec)
        EA=77390.0;EB=121620.0;EC=19210.0;ED=36150.0;
        AA=36.16l;AB=15170.0;AC=0.004189;AD=0.07301;
//      CRF=10000.0;          // Char reactivity factor
// heat  capacities constants for the gaseous components N2 CO2  CO CH4 H2O  H2
respectively
        static float CA[6] = { 3.280,5.457,3.376,1.702,3.47,3.249};
        static float CB[6] = { 0.000593,0.001047,0.000557,0.009081,0.00145,0.000422};
        static float CC[6] = { 0.0,0.0,0.0,-0.000002164,0.0,0.0};
        static float CD[6] = { 40000.0,-115700.0,-3100.0,0.0,12100.0,8300.0};

        /*      dP/dz = -1183 * density of gas * v^2/(density of air at room temperature)
                -388.19*v + 79.896 */
        rho_air=1.1854;/* Kg/m^3*/
        for(i=0;i<1310;i++)
                {
                //printf("\n\niteration no =%d",i);

        /*      if(i<1000)
                        CRF=10;
                else if (i<1500 && i>= 1000)
                        CRF= 100;
                else if (i<2000 && i>= 1500)
```

```
                        CRF = 1000;
                else
                        CRF = 10000;*/
//CRF = 1.0;
                if(time == 0)
                                CRF = exp(i * 0.004);
                else if (time == 1)
                        CRF = exp(i * 0.004);
                else if (time == 2)
                        CRF = exp(i * 0.004);
                else if (time == 3)
                        CRF = exp(i *0.004);
                else if (time == 4)
                        CRF = exp(i * 0.004);
                else if (time == 5)
                        CRF = exp(i * 0.004);
CRF1 = CRF * 10.0;
                printf("\nCRF=%f\t CRF1 = %f\n",CRF,CRF1);
                Temp=T[i];
                Pressure=P[i];
                rho_gas = densitygas(n,Temp,Pressure,i);
                P[i+1]=P[i] - deltaz *((1183 * rho_gas * pow(v[i],2)/rho_air) + (388.19 *
v[i]) + 79.896);

                for(j=0;j<4;j++)
                {
                        lnK[j] = (-J[j]/(Rconst * T[i])) + ( deltaA[j] * log(T[i])) + ( (
deltaB[j]/2)*T[i]) + ((deltaC[j]/6)*pow(T[i],2)) + ((deltaD[j]/2)*pow(T[i],-2)) + I[j] ;
                        K[j] = exp(lnK[j]);
                        deltaH[j] = J[j] + Rconst * (( deltaA[j] * T[i])+(deltaB[j] *
pow(T[i],2)/2) +(deltaC[j] * pow(T[i],3)/3)-(deltaD[j]/T[i]));
                }

                sum=0.0; sum1=0.0;sum2=0.0;sum3=0.0;
                for(j=0;j<6;j++)
                        sum1 = sum1 + n[i][j];
                for(j=0;j<6;j++)
                        p[j]= (n[i][j]/sum1);
rA= sum1 * CRF1 * AA * exp(-EA/(Rconst * T[i])) * (p[1]-(pow(p[2],2)/K[0]));
rB= sum1 * CRF * AB * exp(-EB/(Rconst * T[i])) * (p[4]-(p[2] * p[5]/K[1]));
rC= sum1 * CRF * AC * exp(-EC/(Rconst * T[i])) * (pow(p[5],2)-(p[3]/K[2]));
rD= sum1 * CRF * AD * exp(-ED/(Rconst * T[i])) * ((p[3] * p[4])-(p[2] *
pow(p[5],3)/K[3]));

R[0]=0;R[1]=-rA;R[2]=(2 * rA + rB + rD);R[3] = rC-rD;R[4]=-rB-rD;R[5]= rB - (2 * rC)
+ (3 * rD);
```

```
sumrdeltaH     = (rA * deltaH[0])      + (rB * deltaH[1]) + ( rC * deltaH[2]) + (rD *
deltaH[3]);
for(k=0;k<6;k++)
        {
        c[k] = Rconst * ( CA[k] + CB[k] * T[i] + CC[k] * pow(T[i],2) + CD[k] *
pow(T[i],-2));
                }
                for(j=0;j<6;j++)
                {
                        sum  = sum + (n[i][j] * c[j]);
                        sum2 = sum2 + R[j];
                        sum3 = sum3 + ( R[j] * c[j]);
                }
                        part1=((P[i+1]-P[i])/deltaz) * ((v[i] * sum/P[i])+(v[i]/T[i]));
v[i+1] = v[i] + deltaz * (1/(sum + sum1 * Rconst)) * ((sum*sum2/sum1)-
(sumrdeltaH/T[i])-part1-sum3);
T[i+1]=T[i] + deltaz * (1/(v[i]*sum)) * ( -sumrdeltaH-v[i] * ((P[i+1]-P[i])/deltaz)-
P[i]*((v[i+1]-v[i])/deltaz)-(sum3*T[i]));
DTDZ = (1/(v[i]*sum)) * ( -sumrdeltaH-v[i] * ((P[i+1]-P[i])/deltaz)-P[i]*((v[i+1]-
v[i])/deltaz)-(sum3*T[i]));
DVDZ =          (1/(sum + sum1 * Rconst)) * ((sum*sum2/sum1)-(sumrdeltaH/T[i])-part1-
sum3);
DPDZ = ((1183 * rho_gas * pow(v[i],2)/rho_air) + (388.19 * v[i]) + 79.896);
        if(i==0)
        {
        fprintf(fp,"Temp(K)\t\tLength(m)\tN2\t\tCO2\t\tCO\t\tCH4\t\tH2\n");
        fprintf(fp1,"Temp(K)\t\tLength(m)\tN2\t\tCO2\t\tCO\t\tCH4\t\tH2O\t\tH2\t\trate(
kmol/hr)\n");
                        }
                fprintf(fp,"%f\t %f\t",T[i+1],(i * 0.0001));
                fprintf(fp1,"%f\t %f\t",T[i+1],(i * 0.0001));
        //      fprintf(fp,"%e\t%e\t%e\t%e\t",rA,rB,rC,rD);
                }
                sum4=0;
                for(j=0;j<6;j++)
                {
        n[i+1][j] = n[i][j] + deltaz * (1/v[i]) * ( R[j] - n[i][j] * ((v[i+1]-v[i])/deltaz));
                        sum4 = sum4 + n[i+1][j];
                }

                kmolrate[i+1] = sum4*v[i+1]
*(3.141592654*0.15*0.15*3600.0)/(4.0*1000.0);
                        for(j=0;j<6;j++)
                                ydry[i+1][j] = n[i+1][j]/(sum4 - n[i+1][4]);
                        for(j=0;j<6;j++)
                                ywet[i+1][j] = n[i+1][j]/sum4;
```

```
                if ( (i%50)==0)
                {

                        for(j=0;j<6;j++)
                        {
                        if(j !=4)
                        fprintf(fp,"%f\t",ydry[i+1][j]);
                        }
                        for(j=0;j<6;j++)
                        {
                        fprintf(fp1,"%f\t",ywet[i+1][j]);
                        }
                        fprintf(fp1,"%f\t",kmolrate[i+1]);
                fprintf(fp,"\n");
                        fprintf(fp1,"\n");
                }
        if ( (i%50)==0)
                {
                for(j=0;j<6;j++)
                {
                        printf("  n[%d][%d]=%f \n ",i+1,j,n[i+1][j]);

                }
                }

        }
        }
        fclose(fp);
        fclose(fp1);
        printf("hello\nhi  ");
        getchar();
        return(0);
}
float densitygas(float n[10000][6],float Temp,float Pressure,int i)
{
        int j,k;
        float v,v1=1.0,v2;//v1 is in  m^3/mole
        float a,b,alfa,kappa,p_omega,p_PC,p_TC,Rconst=8.314;
        float y[10000][6],sum,F_v,Fprime_v,density1,density2,avgMolwt;
        sum =0 ;
        for (j=0;j<6;j++)
                sum = sum + n[i][j];
        for (j=0;j<6;j++)
        {
                y[i][j]=n[i][j]/sum;
//              printf("\n%f",y[i][j]);
```

```
        }
        //  N2 CO2  CO CH4 H2O  H2
        float Molwt[6]= {28.01,44.01,28.01,16.04,18.02,2.02};
        float omega[6]= { 0.04,0.225,0.049,0.008,0.344,-0.22};
        float PC[6]=    {3400000,7380000,3500000,4600000,22120000,1300000};//all
values are in N/m^2
        float TC[6]=    {126.2,304.4,133.1,190.6,647.3,33.2};//all vaues are in K
        p_omega=0.0;p_PC=0.0;p_TC=0.0;
        avgMolwt = 0.0;
        for(j=0;j<6;j++)
        {
                p_omega=p_omega + y[i][j]*omega[j];
                p_TC=p_TC + y[i][j]*TC[j];
                p_PC=p_PC + y[i][j]*PC[j];
                avgMolwt = avgMolwt + y[i][j] * Molwt[j];
        }
        kappa = 0.37464 + 1.54226 * p_omega - 0.26992 * pow(p_omega,2);
        alfa = pow((1+kappa*(1-pow((Temp/p_TC),0.5))),2);
        a = 0.45724 * pow((Rconst*p_TC),2)/p_PC;
        b=0.0778 * Rconst * p_TC /p_PC;
        for (j=0;j<100;j++)
        {
                v=v1;
                F_v= -(Pressure * pow(v,3)) + ((Rconst * Temp - Pressure * b ) *
pow(v,2)) + ((2 * b * Rconst * Temp + 3* Pressure * pow(b,2) - a * alfa)* v) - (Rconst *
Temp * b * b) - ( Pressure* pow(b,3)) + ( a * b);
                Fprime_v= -(3 * Pressure * pow(v,2))+ (2 * (Rconst * Temp - Pressure *
b ) * v) + (2 * b * Rconst * Temp + 3* Pressure * pow(b,2) - a * alfa);
                        v2 = v1 - ( F_v/Fprime_v);
                        density1 = (avgMolwt * 0.001)/v1;
                        density2 = (avgMolwt * 0.001)/v2;
                if (j > 50)
                {
                        density1 = (avgMolwt * 0.001)/v1;
                        density2 = (avgMolwt * 0.001)/v2;
                        if ( abs(density2-density1) < 0.01 )
                        goto b1;
                else
                        v1=v2;
                }
                else
                        v1=v2;
                        b1 :

        return(density2);
}
```

APPENDIX III

Code in 'C' Language for the kinetic parameter estimation

```
#include<conio.h>
#include<iostream.h>
#include<math.h>
#include<ctype.h>
#include<time.h>
#include<stdlib.h>
#include<stdio.h>
#define NP 160
#define D 4
#define genmax 100000
#define F 0.5
#define CR 0.9
FILE *fp;
double funvalue(double aef[],double hr,float Wexp[],int k);
#define IM1 2147483563
#define IM2 2147483399
#define AM (1.0/IM1)
#define IMM1 (IM1-1)
#define IA1 40014
#define IA2 40692
#define IQ1 53668
#define IQ2 52774
#define IR1 12211
#define IR2 3791
#define NTAB 32
#define NDIV (1+ IMM1/NTAB)
#define EPS1 1.2e-7
int q,q11;
#define RNMX (1.0-EPS1)
//Random Number Generator Function
double rand_uni(double * );
double rand_uni(long *idum)
{
  long j,k;
  static long idum2=123456789;
  static long iy=0;
  static long iv[NTAB];
  double temp;
  if(*idum<=0)
    {
```

```
        if(-(*idum)<1)
                *idum=1;
        else
        *idum=-(*idum);
        idum2=(*idum);

        for (j=NTAB+7;j>=0;j--)
        {
          k=(*idum)/IQ1;
          *idum=IA1 * (*idum-k*IQ1)-k*IR1;
          if (*idum<0)
            *idum+=IM1;
          if(j<NTAB)
          iv[j]=*idum;
        }          //End of For loop for j
        iy=iv[0];

}       //End of if
k=(*idum)/IQ1;
*idum=IA1*(*idum-k-IQ1)-k*IR1;
if(*idum<0)
  *idum+=IM1;
  k=idum2/IQ2;
  idum2=IA2*(idum2-k*IQ2)-k*IR2;
  if(idum2<0)
  idum2+=IM2;
  j=iy/NDIV;
  iy=iv[j]-idum2;
  iv[j]=*idum;
//printf(" The Random Number is %4.4f \n %4.4f",temp,RNMX);
        //getch();
  if(iy<1)
    iy+=IMM1;
  if((temp=AM*iy)>RNMX)  {
          return RNMX;
  printf(" The Random Number is RNMX %4.4f \n ",RNMX); getchar();}
  else
  {
  return temp;
  printf(" The Random Number is %4.4f \n ",temp); getchar();
  } //getch();
} //End Rand Function
main()
{
double ae[NP][D],ae1[NP],aet[NP],aeo[NP],check,aef[NP],newae[NP][D];
int     i,j,k,a,b,c,seed;
```

```
double
sbv,hr,sbvhr,R,w1,w2,w3,w4,w5,w6,w7,y1,Ft,Fi,logmini,logmaxi,temp,l,LS=0.5,temp1;

//static double Wexp[7] = {0.8687,0.7875,0.6000,0.3125,0.2937,0.275,0.2687};//for  hr =
0.5 K/s
//static double Wexp[7] = {0.9437,0.9125,0.8687,0.5187,0.3625,0.3,0.2812};//for  hr =
10 K/s
static double Wexp[7] = {0.9687,0.95,0.9,0.6625,0.4937,0.4125,0.3062}; //for  hr = 25
K/s
static float ael[4] = {1.0e+3,1.0e+3,1.0e+3,1.0e+3};
static float aeu[4] = {1.0e+5,1.0e+5,1.0e+5,1.0e+5};
hr =25.0;
R = 8.3140;//J/ mol K

fp = fopen("G:\\Pratik_Sheth\\Simple model 1\\10to18NP160totalLDEhalf.txt","a+");
printf("Enter the seed for random number\n");
scanf("%d",&seed);
long rand_uni_init=seed;
for(i=0;i<NP;i++)
        {
                for(j=0;j<D;j++)
                        {
                        ae[i][j] = 0.0;
                        logmini = log10(ael[j]); logmaxi = log10(aeu[j]);
                        temp = logmini + (rand_uni(&rand_uni_init))*(logmaxi-logmini);
                        ae[i][j] = pow(10.0,temp);
                        printf("ae[%d][%d]=%e\n",i,j,ae[i][j]);
                        }
                }
        for(k=0;k<genmax;k++)
                {
                if ((k%100)==0)
                        {
                                printf("k=%d\n",k);
                                fprintf(fp,"k=%d\n",k);
                        }
                for(i=0;i<NP;i++)
                        {
                        do a=(int)((NP)*rand_uni(&rand_uni_init));
                                while(a==i);
                        do b=(int)((NP)*rand_uni(&rand_uni_init));
                                while(b==i || b==a);
                        do c=(int)((NP)*rand_uni(&rand_uni_init));
                                while( c==i || c==a || c==b);
                        for(j=0;j<D;j++)
                                {
```

```
                                        ae1[j] = 0.0;
                                        aet[j] = 0.0;

                                        l = rand_uni(&rand_uni_init);

                ae1[j] = pow(10.0,temp1);
                //Cross over
                y1 = (rand_uni(&rand_uni_init));
                if ((ae1[j] > aeu[j]) || (ae1[j] < ael[j]))
                {
                        logmini = log10(ael[j]); logmaxi = log10(aeu[j]);
                        temp = logmini + (rand_uni(&rand_uni_init))*(logmaxi-logmini);
                        ae1[j] = pow(10.0,temp);
                }

                        if(y1>CR)
                                        aet[j] = ae[i][j];
                        else
                                        aet[j] = ae1[j];
                        if ((k%100)==0)
                                        {
                                        fprintf(fp,"%12.9le ",ae[i][j]);
                                        }
                                        if(aet[j] <0.0)
                                                        aet[j] = aet[j] * (-1.0);
                                }
        for(j=0;j<D;j++)
                aef[j] = ae[i][j];
        Fi = funvalue(aef,hr,Wexp,k);
        Ft = funvalue(aef,hr,Wexp,k);
                if ((k%100)==0)
                        {
                                fprintf(fp,"Fi = %12.9le\n",Fi);
                        }
                        if (Ft<Fi)
                        {
                        for (j=0;j<D;j++)
                        newae[i][j]=aet[j];
                        }
                }
for(i=0;i<NP;i++)
                        {
                                for(j=0;j<D;j++)
                                        ae[i][j]=newae[i][j];
                        }
                }
```

```
}
double funvalue(double aef[],double hr,double Wexp[],int k)
{
        int j;
        double B[6000],C[6000],W[6000],T[6000],ti,R,Fun;
        ti = 0.10;
        R = 8.314;
        T[0] = 325.0;
        B[0] = 1.0;
        C[0] = 0.0;
        W[0] = 1.0;
for(j=0;j<5800;j++)
        {
        T[j+1] = ti + T[j];
        B[j+1]  = B[j] - ti * ( aef[0] * exp((-1.0)*aef[1]/(R * T[j]))+ aef[2] * exp((-
1.0)*aef[3]/(R * T[j]))) * B[j] * (1.0/hr);

        //      C[j+1]  = C[j] + ti * aef[2] * exp(-aef[3]/(R * T[j])) * sbvhr * B[j];

        W[j+1]  = W[j] - ti * aef[0] * exp((-1.0)*aef[1]/(R * T[j])) * B[j] * (1.0/hr);

        if (W[j+1] < 0.0)
                        W[j+1] = W[j];
        if (W[j+1] > 1.0)
                        W[j+1] = W[j];

        //      W[j+1] = B[j+1] + C[j+1];
        }

Fun = pow((Wexp[0]-W[1000]),2) + pow((Wexp[1]-W[2250]),2) + pow((Wexp[2]-
W[2750]),2) + pow((Wexp[3]-W[3000]),2) + pow((Wexp[4]-W[3750]),2) +
pow((Wexp[5]-W[4750]),2) + pow((Wexp[6]-W[5750]),2);
return(Fun);

}
```

Errata

Changes in Thesis:

1. **Page 11, Line 2:** The sentence "In the updraft **gasifiers**, biomass moves down vertically and comes in contact with an upward moving product gas stream counter-currently." is to be replaced with "In the updraft **gasifier**, biomass moves down vertically and comes in contact with an upward moving product gas stream counter-currently."

2. **Page 48, Line 6 from bottom:** The sentence "Di Blasi (2000) formulated a one-dimensional unsteady model for biomass gasification in a stratified concurrent (downdraft) **reactor**." is to be replaced with "Di Blasi (2000) formulated a one-dimensional unsteady model for biomass gasification in a stratified concurrent (downdraft) **gasifier**."

3. **Page 138, Last Line:** The sentence "Figs. 5.5-5.14 show the temperature profile at the centre and at a half radial distance for different values of equivalence ratio ranging **between 0.1673 and 0.3968.**" is to be replaced with "Figs. 5.5-5.14 show the temperature profile at the centre and at a half radial distance for different values of equivalence ratio ranging **from 0.1673 to 0.3968**."

4. **Page 131 line 1:** The sentence "The stoichiometric ratio of air flow rate to the rate of biomass consumption is 5.22 m^3 air/kg of wood (Zainal et al., 2002)." is to be replaced with "The stoichiometric ratio of air flow rate to the rate of biomass consumption is 5.22 m^3 air/kg of wood **(equivalent to 6.33 kg of air/kg of biomass)** (Zainal et al., 2002).

5. **Table 3.8 (page 91):** n_1**= 0** is to be replaced with n_1**=1.0**.

6. **Page 86, line 1:** The following sentence is added "**As gasification proceeds, the char developed in the pyrolysis zone moves downwards into the oxidation and reduction zones and facilitates the gasification reactions.**"

7. **Page 169, line 12:** The following sentence is added: "**The value of 0.3 for the f_p is chosen based on the amount of nitrogen present in the producer gas. It is observed that the more the value of f_p, lesser the concentration of nitrogen in the producer gas.**"

8. **Page 82: Equation 3.68:** $\frac{dC_1}{dt} = \boldsymbol{k_1} B$ is to be replaced with $\frac{dC_1}{dt} = \boldsymbol{k_2} B$

9. **Page 191, Last Line:** The sentence "The simulated predictions using combined transport and kinetic model are matching better than those predicted by equilibrium model (**Fig. 3.34**)." is to be replaced with "The simulated predictions using combined transport and kinetic model are matching better than those predicted by equilibrium model (**Fig. 5.34**)."

10. **Page 195, Para 2, line 5:** The sentence "**Table-5.12** shows the details of the experimental runs reported by Dogru et al. (2002) and **Table-5.13** shows the details of the gasifier used in their experimental study." is to be replaced with "**Table-5.11** shows the details of the experimental runs reported by Dogru et al. (2002) and **Table-5.12** shows the details of the gasifier used in their experimental study."

11. **Page 199, section 5.2.3.1, line 1:** The sentence "**Table-5.15** shows the kinetic parameters of reaction 1 (A_1 and E_1) and reaction 2 (A_2 and E_2) of Eq. (3.61) for the heating rates of 10.0, 25.0, and 40.0 K/s for a sample size of 0.180 mm." is to be replaced with "**Table-5.13** shows the kinetic parameters of reaction 1 (A_1 and E_1) and reaction 2 (A_2 and E_2) of Eq. (3.61) for the heating rates of 10.0, 25.0, and 40.0 K/s for a sample size of 0.180 mm."

12. **Page 203, para.1, line 1:** The sentence "Simulations are performed to find the kinetic parameters of reaction 1 and reaction 2 (A_1, E_1, A_2, E_2, n, β) of Eq. (3.61) for Model-KPE1 to KPE4 for heating rates of 10, 25 and 40 K/s for the ground hazelnut shell biomass sample of 0.180 mm size and reported in **Table-5.16**." is to be replaced with "Simulations are performed to find the kinetic parameters of reaction 1 and reaction 2 (A_1, E_1, A_2, E_2, n, β) of Eq. (3.61) for Model-KPE1 to KPE4 for heating rates of 10, 25 and 40 K/s for the ground hazelnut shell biomass sample of 0.180 mm size and reported in **Table-5.14**."

13. **Page 203, para.1, line 9:** The sentence "The values of objective function obtained for Model-KPE2 and Model-KPE3 are 0.01949137 and 0.028003858 respectively for heating rate value of 10 K/s (**Table-5.16**)." is to be replaced with "The values of objective function obtained for Model-KPE2 and Model-KPE3 are 0.01949137 and 0.028003858 respectively for heating rate value of 10 K/s (**Table-5.14**)."

14. **Page 203, para 2, line 17:** The sentence "Kinetic parameters reported in **Table-5.16** are used to find residual weight fraction which is compared with the experimental data as shown in Fig. 5.61, Fig. 5.62 and Fig. 5.63 for the heating rate values of 10, 25 and 40 K/s respectively." is to be replaced with "Kinetic parameters reported in **Table-5.14** are used to find residual weight fraction which is compared with the experimental data as shown in Fig. 5.61, Fig. 5.62 and Fig. 5.63 for the heating rate values of 10, 25 and 40 K/s respectively."

15. **Page 207, para 1, line 9:** The sentence "The objective function value is the least for Model-KPE3 and reported in **Table-5.16** for the heating rate values of 25 and 40 K/s." is to be replaced with "The objective function value is the least for Model-KPE3 and reported in **Table-5.14** for the heating rate values of 25 and 40 K/s."

16. **Page 207, para 2, line 7:** The sentence "**Table-5.17** shows the kinetic parameters of reaction 1 (A_1 and E_1) and reaction 2 (A_2 and E_2) of Eq. (3.61) for the heating rate of 25.0 K/s. NP value is varied from 10 to 50 times of the dimension of the problem." is to be replaced with "**Table-5.15** shows the kinetic parameters of reaction 1 (A_1 and

E_1) and reaction 2 (A_2 and E_2) of Eq. (3.61) for the heating rate of 25.0 K/s. NP value is varied from 10 to 50 times of the dimension of the problem."

17. **Page 208, para 2, line 1:** The sentence "**Table-5.18** shows the variable value with different random numbers ranging from 0.1 to 1.0 for a minimum value of 10^{10} and a maximum value of 10^{18}." is to be replaced with "**Table-5.16** shows the variable value with different random numbers ranging from 0.1 to 1.0 for a minimum value of 10^{10} and a maximum value of 10^{18}."

18. **Page 212, para 2, line 2:** The sentence "A wide distribution of new variable values, which is essential to cover a wide range of the said variable, is obtained and given in **Table-5.18**." is to be replaced with "A wide distribution of new variable values, which is essential to cover a wide range of the said variable, is obtained and given in **Table-5.16**."

19. **Page 212, para 3, line 8:** The sentence "**Table-5.19** shows the optimum kinetic parameters and the value of objective function found by using LIDE for different values of NP. Comparison for NP = 40, 120 and 160 from **Table-5.17** (simple DE) and **Table-5.19** (LIDE) shows that the objective function value is less for simple DE and for NP = 80 and 200 LIDE gives better results in terms of optimum value of objective function." is to be replaced with "**Table-5.17** shows the optimum kinetic parameters and the value of objective function found by using LIDE for different values of NP. Comparison for NP = 40, 120 and 160 from **Table-5.15** (simple DE) and **Table-5.17** (LIDE) shows that the objective function value is less for simple DE and for NP = 80 and 200 LIDE gives better results in terms of optimum value of objective function."

20. **Page 215, para 2, line 4:** The sentence "The objective function value is the least using LDE in comparison with simple DE (**Table-5.17**) or LIDE (**Table-5.19**) for any NP Value." is to be replaced with "The objective function value is the least using LDE in comparison with simple DE (**Table-5.15**) or LIDE (**Table-5.17**) for any NP Value."

21. **Page 218, para 3, line 3:** The sentence "Using the optimum kinetic parameters for NP = 200 and found by simple DE (**Table-5.17**), LIDE (**Table-5.19**) and LDE (**Table-5.20**) are used to find the residual weight fraction and the results are compared with the experimental data as shown in Fig. 5.70." is to be replaced with "Using the optimum kinetic parameters for NP = 200 and found by simple DE (**Table-5.15**), LIDE (**Table-5.17**) and LDE (**Table-5.18**) are used to find the residual weight fraction and the results are compared with the experimental data as shown in Fig. 5.70."